NASA CR-168137
PWA-5594-231

223p.

#304592

NASA

ENERGY EFFICIENT ENGINE

INTEGRATED CORE/LOW SPOOL TEST HARDWARE DESIGN REPORT

J. W. Bisset and D. C. Howe

UNITED TECHNOLOGIES CORPORATION
Pratt & Whitney Aircraft Group
Engineering Division - Connecticut Operation

Prepared for

NATIONAL AERONAUTICS AND SPACE ADMINISTRATION
Lewis Research Center
Cleveland, Ohio 44135
Contract NAS3-20646

TABLE OF CONTENTS

I, II

TABLE OF CONTENTS (Cont'd)

TABLE OF CONTENTS (Cont'd)

TABLE OF CONTENTS (Cont'd)

LIST OF ILLUSTRATIONS

LIST OF ILLUSTRATIONS (Continued)

LIST OF ILLUSTRATIONS (Continued)

LIST OF ILLUSTRATIONS (Continued)

LIST OF ILLUSTRATIONS (Continued)

LIST OF ILLUSTRATIONS (Continued)

LIST OF ILLUSTRATIONS (Continued)

LIST OF TABLES

LIST OF TABLES (Continued)

LIST OF TABLES (Continued)

SECTION 1.0
SUMMARY

The National Aeronautics and Space Administration is sponsoring the Energy Efficient Engine Program to identify and verify the technology required to significantly lower fuel consumption and operating costs for future commercial gas-turbine engines. This program focuses on demonstrating the benefits that can be derived from mid-1980 technology advancements in the areas of aerodynamics, materials/cooling and structure-mechanics.

A major task that has been completed under this program is the design and analysis of test hardware for the integrated core/low spool. The integrated core/low spool is a simulation of the flight propulsion system -- the conceptual study engine that has been defined to meet the performance, economic and environmental goals of the Energy Efficient Engine Program. It is intended to permit evaluation and verification of critical technologies in a full engine operating environment.

The design and analysis of test hardware for the integrated core/low spool involved nearly a 24-month effort. The scope of work included establishing the design of major components, engine systems, test instrumentation, and analyzing component and engine performance.

The major engine components have essentially the same aerodynamics as those in the flight propulsion system. The mechanical design is also similar, although the design reflects the use of existing hardware and conventional materials, whenever feasible, to lower program costs and meet fabrication schedules. Such changes, however, have not compromised goals for structural integrity.

The integrated core/low spool incorporates nearly 1500 sensors to monitor aerodynamic performance, structural integrity and test conditions. The design of components includes provisions for installing the various types of sensors.

Engine ancillary systems such as external accessories and test ducting have been designed. To meet test requirements, external ducting for two test configurations has been defined. For the first test, a bifurcated duct is used with a nonmixed configuration to assess component and system performance. The second configuration is a mixed system, using a full nacelle and an internal exhaust mixer, to evaluate aero-acoustic performance.

A series of analyses was performed to estimate the performance of the two test configurations both on a component and system basis. Analyses were conducted to assess compressor system stability, determine effects of test instrumentation, define component operating maps and performance, and review starting requirements. On the basis of these analyses, the performance of the integrated core/low spool is predicted to be very close to the design intent. In addition, no serious limiting conditions have been identified throughout the planned operating range.

Overall, the integrated core/low spool closely simulates the flight propulsion system in terms of both aerothermal-mechanical design and predicted performance.

SECTION 2.0
INTRODUCTION

The Energy Efficient Engine Component Development and Integration Program, sponsored by the National Aeronautics and Space Administration, is directed toward developing the technology to achieve greater fuel efficiency and lower operating costs for future commercial gas-turbine engines. The main program goals are a reduction in fuel consumption of at least 12 percent, a reduction in direct operating cost of at least 5 percent and 50 percent less performance deterioration relative to the Pratt & Whitney Aircraft JT9D-7A base engine. Also of major importance are meeting the Federal Aviation Regulation Part 36 noise rules for 1978 and the proposed Environmental Protection Agency emissions standards for 1981.

To verify the technology to attain these goals, the Energy Efficient Engine Program is organized into three technical tasks:

Task 1	Propulsion System Analysis, Design and Integration
Task 2	Component Analysis, Design and Development
Task 4	Integrated Core/Low Spool Design, Fabrication and Test

Under Task 4, the preliminary design and analysis of test hardware for the integrated core/low spool has been completed. The integrated core/low spool is the test vehicle used to evaluate the technology that has evolved from the Energy Efficient Engine Program to lower fuel consumption and operating costs. Its design simulates the flight propulsion system, the conceptual study engine with a 1988 certification date, that has been defined to meet the goals of the program. Like the flight propulsion system, the integrated core/low spool is a dual spool, direct drive, mixed exhaust configuration. A short stiff high-pressure rotor and a single-stage high-pressure turbine are among the major features to improve performance retention and lower operating economics. Improved active clearance control in the high-pressure compressor and the turbines, advanced single crystal materials for the turbine blades and vanes, and low loss aerodynamic concepts are among the many performance improvement features.

The work in Task 4 proceeded for approximately 24 months, as indicated by the overall program schedule in Figure 2-1, before being terminated on 5 March 1982 for the convenience of the Government. At this point, the design of all major components and nearly all ancillary systems of the integrated core/low spool was complete, and effort to procur test hardware and organize the test program plan was in progress.

This report describes the design and results of related analyses for the integrated core/low spool and its subsystems. The design effort included a definition of the engine, major components, internal and external systems, test ducting, and test instrumentation. Various analytical representations, in addition to results acquired from supporting component rig and subscale model tests, have been used to verify aerodynamic and structural design concepts as well as to predict performance.

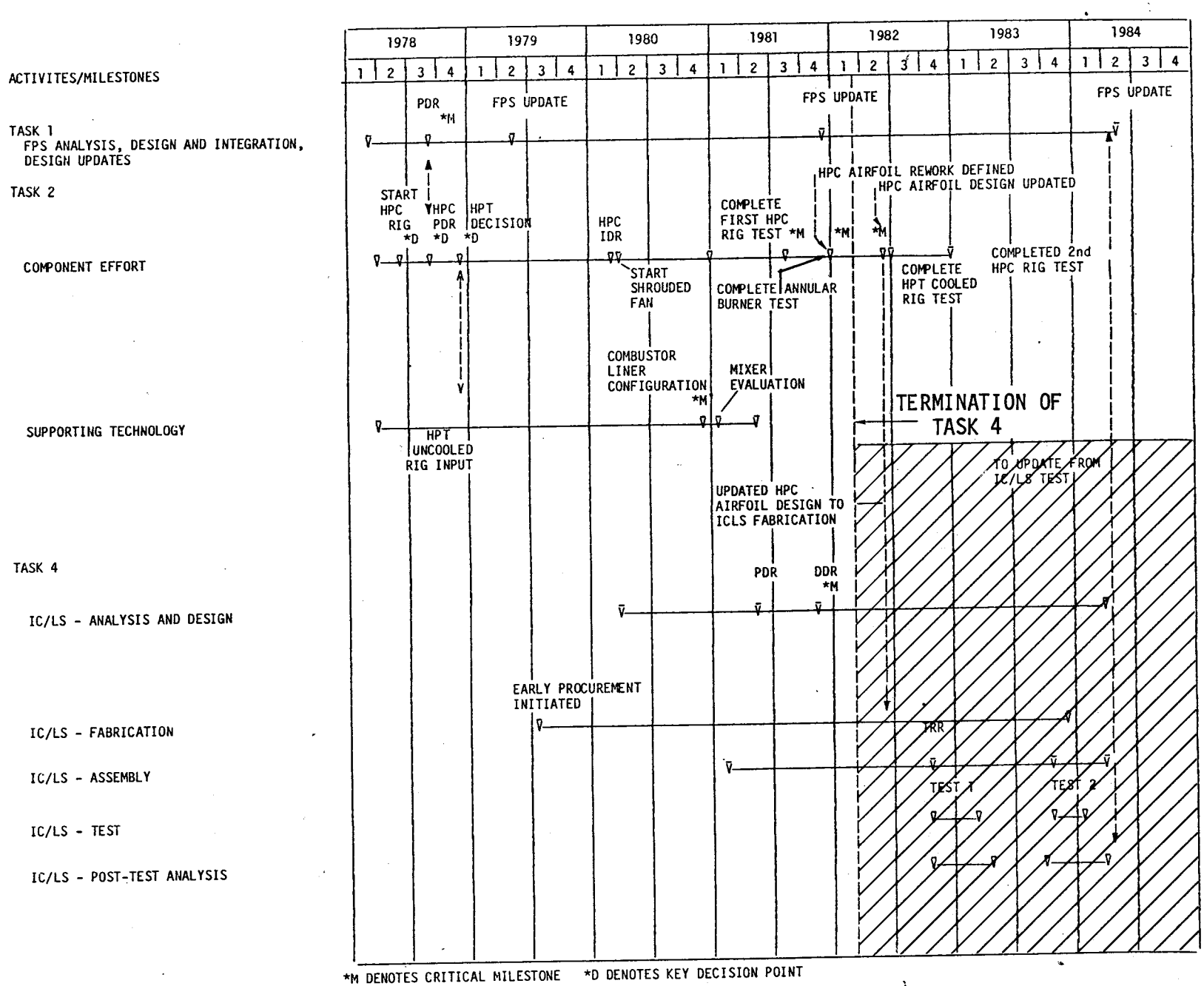

Figure 2-1 Schedule For the Energy Efficient Engine Program

In the following section of this report, Section 3, an overall description of the integrated core/low spool is presented, along with a complete analysis of predicted performance. Section 4 contains a discussion of the aerodynamic and mechanical designs of the major engine components. Similar design information pertaining to the engine systems is presented in Section 5. Section 6 summarizes the test instrumentation requirements. Concluding remarks are presented in Section 7.

SECTION 3.0
INTEGRATED CORE/LOW SPOOL DESIGN DEFINITION

3.1 INTRODUCTION

The design of the integrated core/low spool simulates the aerothermal-mechanical definition of the Energy Efficient Engine's flight propulsion system -- the study engine concept designed to meet the program goals. The flight propulsion system is configured for a balance in fuel efficiency, lower operating economics and environmental acceptability using advances in aerodynamics, materials/cooling techniques and structure-mechanics. Demonstrating the merits of these technology advances in an actual engine operating environment is accomplished with the integrated core/low spool. It serves as a test vehicle to evaluate component and subsystem performance, verify the structural integrity of the mechanical design, and demonstrate the goals established for the flight propulsion system.

As a technology demonstration vehicle, the integrated core/low spool is designed to Pratt & Whitney Aircraft's standards for experimental hardware. Existing components such as bearings and external accessories are used whenever feasible to reduce program costs. Also, alternate materials and fabrication techniques are sometimes used for economic reasons when the substitution does not impact program objectives.

Figure 3.1-1 presents a comparative cross-sectional view of the integrated core/low spool and the flight propulsion system. The integrated core/low spool maintains the same aerodynamics as the flight engine concept. Also, the mechanical design is generally duplicated. Specific differences are discussed in detail in Sections 4 and 5.

3.2 GENERAL DESCRIPTION

The integrated core/low spool, like the flight engine concept, is a five bearing design with two main support frames and two main bearing compartments. The dual spool configuration has a high-pressure spool with a ten-stage compressor powered by a single-stage turbine. The counterrotating low-pressure spool has a single-stage fan and a four-stage low-pressure compressor driven by a four-stage turbine. The combustor is a two-stage annular design. Salient design features of the components are summarized in the following paragraph.

Both the fan and low-pressure compressor employ features such as recessed blade tip seals and low volume interstage cavities to minimize endwall losses. The use of controlled diffusion airfoils also contributes to higher efficiency and better aerodynamic stability. These same concepts, in addition to active clearance control and variable-geometry stators, are used in the high-pressure compressor. The combustor is a two-stage system for low emissions at all flight conditions. A prominant feature is the segmented liner with a unique cooling technique. The single-stage high-pressure turbine contributes substantially to a large reduction in initial cost and on-going maintenance cost. Airfoil cooling requirements are reduced by using a single crystal alloy, and improved sealing techniques as well as active clearance control contribute to a higher efficiency. The low-pressure turbine incorporates low loss airfoil concepts, high temperature capability materials to eliminate airfoil cooling, and active clearance control. The fuel system features a dual channel, full authority electronic control.

ORIGINAL PAGE IS
OF POOR QUALITY

ORIGINAL PAGE IS
OF POOR QUALITY

FLIGHT PROPULSION SYSTEM

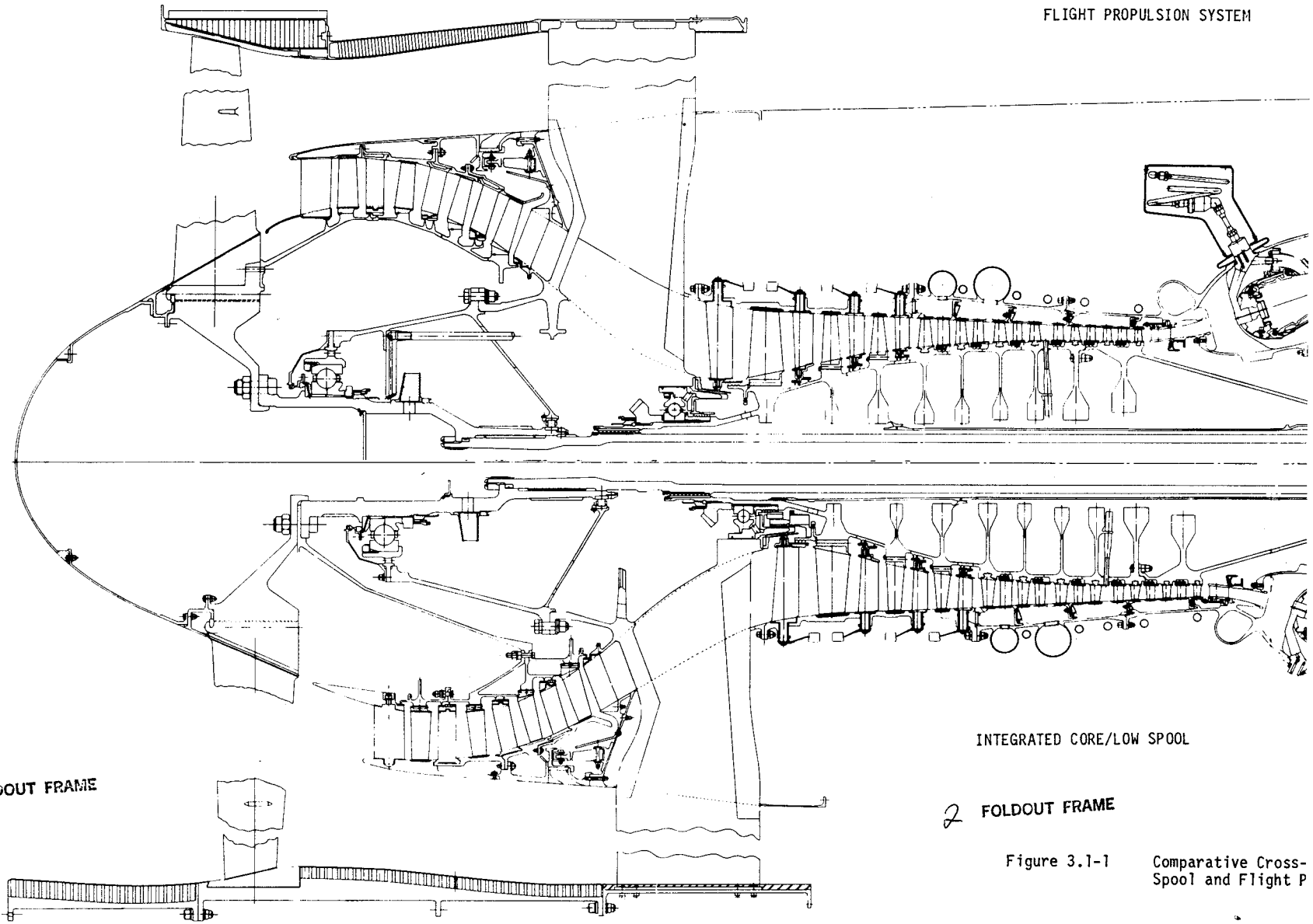

INTEGRATED CORE/LOW SPOOL

FOLDOUT FRAME

2 FOLDOUT FRAME

Figure 3.1-1 Comparative Cross-Spool and Flight P

ORIGINAL PAGE IS
OF POOR QUALITY

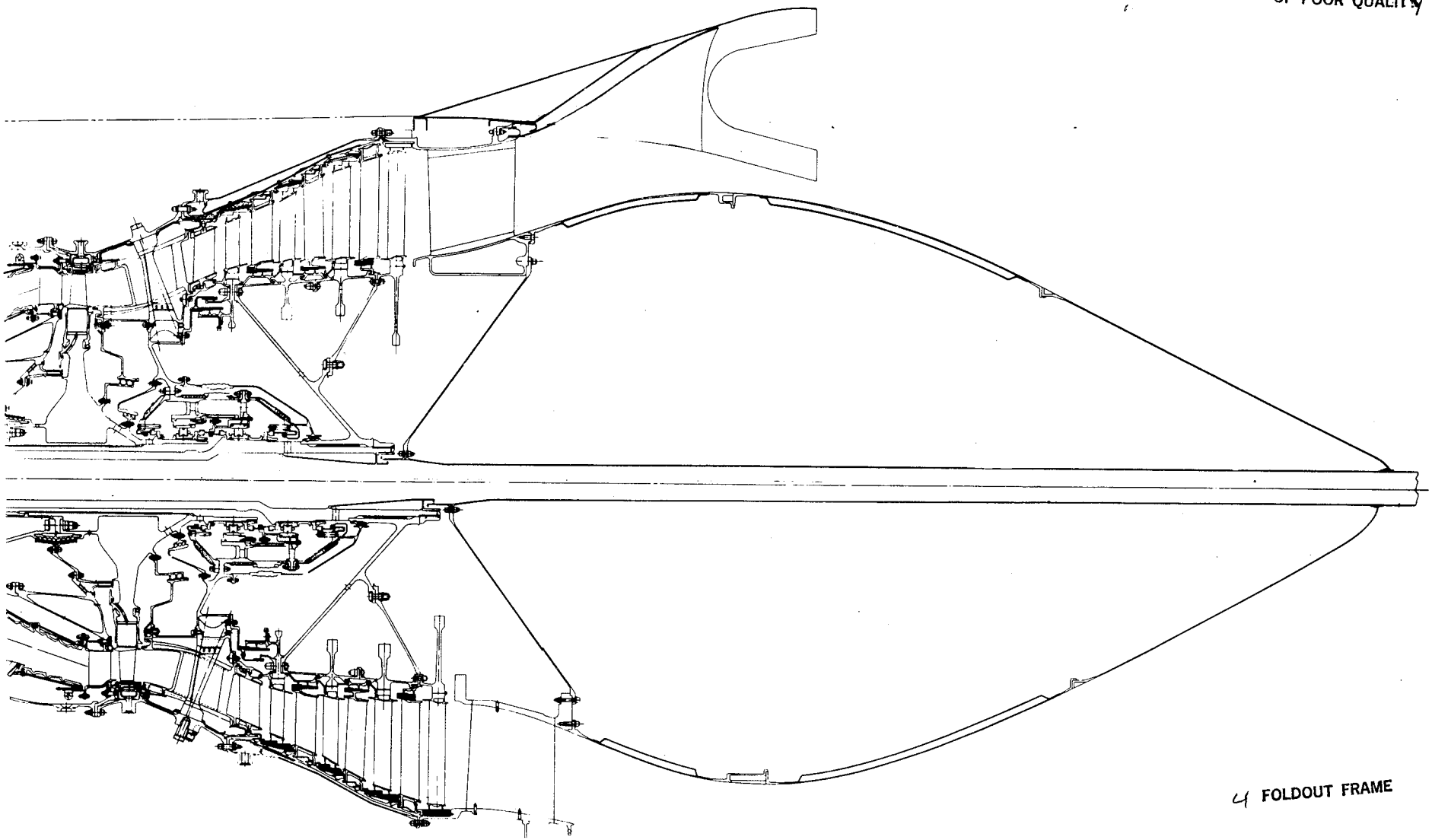

ɔnal View of the Integrated Core/Low
ɜion System

3 FOLDOUT FRAME

4 FOLDOUT FRAME

Two test configurations of the integrated core/low spool are used in the planned test program. The first test, oriented toward assessing component and system performance, requires a nonmixed or separate exhaust configuration. The second test configuration is more representative of the flight engine. It is a mixed flow system containing an exhaust mixer and an experimental-type full nacelle to assess aero-acoustic performance.

3.3 PREDICTED PERFORMANCE

3.3.1 Matching

The general approach used to predict performance of the integrated core/low spool is based on establishing a unique component system match at the aerodynamic design point (10,668 m (35,000 feet altitude, 0.8 Mach number, standard day)) that duplicates the cycle of the flight propulsion system. Since component efficiencies for the integrated core/low spool are lower than those projected for the flight engine, the design combustor exit temperature is higher in order to hold the flight propulsion system cycle at the design point. Initial design turbine throat areas, and then exhaust nozzle areas, were adjusted to maintain operating lines and compression system surge margins.

Unlike the "rubber engine" hardware approach used for predicting the performance of the flight propulsion system, a "fixed" hardware approach is employed for the integrated core/low spool. The differences between these approaches are summarized in Table 3.3.1-I.

TABLE 3.3.1-I

HARDWARE DIFFERENCES - APPROACH

o Flight Propulsion System	- "Rubber Engine". Turbine and nozzle areas float as components are updated to hold cycle fan pressure ratio/bypass ratio/overall pressure ratio, flows and operating lines at aerodynamic design point. Turbine temperature set to hold mixing plane pressure split.
o IC/LS Mixed	- Fixed geometry. Turbine and jet areas are integrated core/low spool design table, reflecting lower component efficiences and higher combustor exit temperatures to hold cycle.
o IC/LS Separate	- Same high-pressure turbine and low-pressure turbine as integrated core/low spool mixed. Jet areas initially set to hold integrated core/low spool mixed cycle, flows and operating lines at aerodynamic design point. This resulted in higher fan operating line at takeoff for the separate exhaust configuration. Consequently, duct jet area for this configuration was opened to hold integrated core/low spool mixed fan operating line at takeoff.

The procedure for updating integrated core/low spool data starts with holding the cycle constant at the aerodynamic design point by a combustor exit temperature rematch and varying all controlling areas to account for the effects of component performance changes. The aerodynamic design point is then redefined at that combustor exit temperature using the actual design controlling turbine and mixing plane areas to establish the rematch. In addition, the fan (duct portion) operating point is adjusted to maximize stability, as required, to be coincident with the flight propulsion system operating line at the takeoff condition. This adjustment is accomplished for the separate exhaust configuration by adjusting the duct exhaust nozzle area and for the mixed configuration by adjusting the mixed exhaust nozzle area.

Results derived from using these approaches are shown in Table 3.3.1-II. This information depicts the hardware differences between flight propulsion system and integrated core/low spool status levels, along with the original design tables. The high-pressure turbine flow parameter difference between the status and design table versions of the mixed exhaust configuration is caused by a design restagger to provide a better aerodynamic relationship with the low-pressure turbine design.

3.3.2 Ratings

Ratings for the integrated core/low spool were initially established using the same thrust ratios as the flight propulsion system. These are the rating definitions in the design table. For subsequent status performance updates, the combustor exit temperature at the initial rating was kept constant. Resulting combustor exit temperatures at the integrated core/low spool ratings are:

- Maximum Climb -- 1469°C (2676°F) (Standard 28°C (84°F) Day)
- Maximum Cruise -- 1339°C (2443°F) (Standard Day)
- Takeoff -- 1519°C (2767°F) (Standard 32°C (91°F) Day)

Status thrust at the rating then varies as performance is updated.

3.3.3 Cycle

A comparison of cycle parameters for the status integrated core/low spool configurations and the flight propulsion system at the maximum cruise ratings is presented in Table 3.3.3-I. Also included are the operating line differences of the integrated core/low spool compression system relative to the flight propulsion system. Cycle differences are not considered to be large, and the increased combustor exit temperature level for the integrated core/low spool is recognized in the design. Only the low-pressure compressor in mixed exhaust configuration shows a higher operating line, but this amount of loss in surge margin is not considered a problem if the system operates at simulated altitude conditions. Thrust and thrust specific fuel consumption for the mixed exhaust configuration were defined with the flight propulsion system inlet and exhaust nozzle for purposes of comparison. Status thrust specific fuel consumption improvements relative to the JT9D-7A reference engine are 15 percent for the flight propulsion system and 10 percent for the integrated core/low spool.

TABLE 3.3.1-II

HARDWARE DIFFERENCES
(AERODYNAMIC DESIGN POINTS)

	Flight Propulsion System		Integrated Core/Low Spool		
	Des. Table	Status	Mixed Des. Table	Mixed Status	Separate Status
Fan	Shroudless	Shrouded	Shroudless	Shrouded	Shrouded
LPC	Base	Base	Base	Base	Base
HPC	Base	Base	Base	Base	Base
HPT % ΔA_{Throat}	Base	-0.7	+1.0	+1.4	+1.4
HPT % $\Delta W\sqrt{T}/P$					
% $\Delta N_2/\sqrt{T}$	Base	-0.1	-1.8	-1.2	-1.4
LPT % ΔA_{Throat}	Base	-2.5	+3.3	+3.4	+3.4
LPT % $\Delta W\sqrt{T}/P$					
% $\Delta N_2/\sqrt{T}$	Base	-0.1	-1.8	-1.2	-1.4
% $\Delta N_1/\sqrt{T}$	Base	Base	-2.2	-2.4	-2.2
Mixer % Δ Area Core	Base	-0.3	Base	+.1	--
% Δ Area Duct	Base	-0.1	Base	-1.1	--
Exhaust Area:					
Core, cm^2 (in^2)	--	--	--	-- 4168 (646.2)	
Duct, cm^2 (in^2)	--	--	--	-- 14,673 (2275*)	
% Δ Area Mixed	Base	-0.1	+1.4	+5.6*	--

*Defined to place takeoff fan match on flight propulsion system operating line at sea level static

TABLE 3.3.3.-I

STATUS CYCLE COMPARISON
10,668 M (35,000 FT)/0.8 MN/STD. DAY/MAX. CRUISE
ISOLATED POD/NO BLEED OR POWER EXTRACTION

	Flight Propulsion System	Integrated Core/Low Spool Mixed	Integrated Core/Low Spool Separate
FPR Rotor/Stage	1.74/1.71	1.74/1.71	1.74/1.71
BPR	6.60	6.57	6.55
OPR	37.33	38.46	37.59
CET/RIT, °C (°F)	1268 /1201 (2315)/(2195)	1339 /1265 (2443)/(2308)	1339 /1264 (2443)/(2308)
Wat $\sqrt{\theta}/\delta$, kg/sec (lb/sec)	615 (1356)	632 (1395)	616 (1360)
Installed Thrust, N (lb)	37742 (8485)	39531 (8887)*	--
TSFC Inst, lb/hr/lb	0.576	0.609*	--
% Δ Fan Operating Line	Base	-5.3	0.0
% Δ LPC Operating Line	Base	+1.1	-2.2
% Δ HPC Operating Line	Base	-1.9	-2.1

*Defined with flight propulsion system nozzle and inlet

Similar data are presented in Table 3.3.3-II for the takeoff rating. The conclusions reached on the basis of this information are the same as those for the maximum cruise rating, except no adverse operating line shifts occur for the integrated core/low spool compression system. Thrust and thrust specific fuel consumption are defined with the inlets and nozzles used for each configuration.

TABLE 3.3.3-II

STATUS CYCLE COMPARISON
SEA LEVEL STATIC/STD. +13.8°C (+25°F)/TAKEOFF
ISOLATED POD/NO BLEED OR POWER EXTRACTION

	Flight Propulsion System	Integrated Core/Low Spool Mixed	Integrated Core/Low Spool Separate
FPR Rotor/Stage	1.60/1.58	1.63/1.61	1.62/1.60
BPR	6.83	6.71	6.72
OPR	31.05	32.03	31.77
CET/RIT, °C (°F)	1435 /1363 (2616)/(2486)	1519 /1438 (2767)/(2621)	1519 /1438 (2767)/(2621)
Wat $\sqrt{\theta}/\delta$	1214	1235	1226
Fn Inst, N (lb)	162047 (36430)	169307 (38062)	166616 (37457)
TSFC Inst, lb/hr/lb	0.330	0.352	0.355
% Δ Fan Operating Line	Base	0	0
% Δ LPC Operating Line	Base	-0.7	-1.3
% Δ HPC Operating Line	Base	-2.2	-2.5

3.3.4 System/Component Performance

A detailed comparison of system and component performance is presented for the maximum cruise rating in Tables 3.3.4-I through -II. The status system summary, Table 3.3.4-I, shows a higher thrust for the integrated core/low spool because it matches the flight propulsion system cycle at the aerodynamic design point by using higher combustor exit temperatures to compensate for components that are not completely developed.

Component performance shown for the flight propulsion system is that predicted for the fully developed flight engine. The levels indicated for both configurations of the integrated core/low spool (Table 3.3.4-II) are those expected (50 percent probability of achievement) for a first test of the component systems. The comparison shows relatively small differences in performance despite the fact that components in the integrated core/low spool are not fully developed.

In general, integrated core/low spool airflows and rotor speeds are higher than flight propulsion system levels. However, none of the data indicates any reason to preclude operating the integrated core/low spool at simulated altitude conditions, if desired.

A similar comparison of system and component performance is presented for the takeoff rating in Tables 3.3.4-III through -IV. The results are quite similar to those for the maximum cruise rating. Thus, the conclusions are the same for the flight propulsion system and both configurations of the integrated core/low spool at the two ratings.

TABLE 3.3.4-I

STATUS SYSTEM SUMMARY
MAXIMUM CRUISE

	Flight Propulsion System	Integrated Core/Low Spool	
		Mixed	Separate
Altitude, m (ft)	10,668 (35000)	10,668 (35000)	10,668 (35000)
Mach No.	0.8	0.8	0.8
Ambient Temp, °C (°F)	28 (84)	28 (84)	28 (84)
Inlet Ram Recovery	0.9965	0.9965	0.9965
Thrust (Excl. Drag), N (lb)	39455 (8870)	41243 (9272)*	--
Nacelle Drag, N (lb)	1712 (385)	1712 (385)	--
Fuel Flow, kg/hr (lb/hr)	2215 (4884)	2456 (5415)	2412 (5319)

*Defined with flight propulsion system nozzle and inlet

TABLE 3.3.4-II

STATUS COMPONENT SUMMARY
MAXIMUM CRUISE

	Flight Propulsion System	Integrated Core/Low Spool Mixed	Integrated Core/Low Spool Separate
Fan			
$W\sqrt{\theta}/\delta$, kg/sec (lb/sec)	615 (1356)	632 (1395)	616 (1360)
BPR	6.60	6.57	6.55
N rpm	3846	3931	3854
Pressure Ratio			
Duct	1.710	1.712	1.713
Core	1.544	1.570	1.547
Efficiency			
Duct	0.867	0.842	0.849
Core	0.904	0.874	0.877
Low-Pressure Compressor			
$W\sqrt{\theta}/\delta$, kg/sec (lb/sec)	56.0 (123.6)	57.3 (126.4)	56.6 (125.0)
Pressure Ratio	1.748	1.783	1.733
Efficiency	0.904	0.875	0.873
High-Pressure Compressor			
$W\sqrt{\theta}/\delta$, kg/sec (lb/sec)	34.9 (77.0)	35.1 (77.6)	35.6 (78.7)
N rpm	13092	13247	13219
Pressure Ratio	13.83	13.74	14.02
Efficiency	0.884	0.865	0.862
Combustor			
Efficiency	0.9995	0.9995	0.9995
High-Pressure Turbine			
$W\sqrt{T}/P \left[\frac{lb\sqrt{°R}\ in^2}{sec\ lb}\right]$	16.7	17.0	17.0
Rotor Inlet Temperature, °C (°F)	1201 (2195)	1265 (2309)	1265 (2309)
Pressure Ratio	3.99	4.08	4.09
Efficiency	0.891	0.879	0.878
Total Cooling Air and Secondary Airflow (% Core Airflow)	17.24	17.99	17.99
Low-Pressure Turbine			
$W\sqrt{T}/P \left[\frac{lb\sqrt{°R}\ in^2}{sec\ lb}\right]$	65.5	69.3	69.4
Pressure Ratio	5.66	5.69	5.50
Efficiency	0.913	0.903	0.902
Exhaust Mixer			
Efficiency	0.85	0.85	--
Pressure Losses			
Combustor	0.0553	0.0563	0.0560
Turbine Transition Duct	0.0070	0.0155	0.0155
Turbine Exhaust Case	0.0087	0.0098	0.0090
Core Mixer	0.0023	0.0092	--
Fan Duct	0.0061	0.0081	0.0124
Duct Mixer	0.0018	0.0063	--
Tailpipe	0.0034	0.0039	Duct 0.0021 Core 0.0094
Nozzle			
Gross Thrust Coefficient	0.9960	0.9950	Duct 0.9955 Core 0.9942

TABLE 3.3.4-III

STATUS SYSTEM SUMMARY
TAKEOFF

	Flight Propulsion System	Integrated Core/Low Spool	
		Mixed	Separate
Altitude, m (ft)	0	0	0
Mach No.	0	0	0
Ambient Temperature, °C(°F)	28 (84)	28 (84)	28 (84)
Inlet Ram Recovery	0.9925	0.9925	0.9925
Thrust (Excl. Drag), N (lb)	162,047 (36430)	169,307 (38062)	166,616 (37457)
Nacelle Drag, N (lb)	0	0	0
Fuel Flow, kg/hr (lb/hr)	5448 (12012)	6069 (13382)	6032 (13300)

TABLE 3.3.4-IV

STATUS COMPONENT SUMMARY
TAKEOFF

	Flight Propulsion System	Integrated Core/Low Spool	
		Mixed	Separate
Fan			
$W\sqrt{\theta}/\delta$, kg/sec (lb/sec)	550 (1214)	560 (1235)	556 (1226)
BPR	6.83	6.71	6.72
N rpm	3905	3966	3941
Pressure Ratio			
Duct	1.581	1.607	1.596
Core	1.454	1.470	1.463
Efficiency			
Duct	0.869	0.851	0.851
Core	0.914	0.886	0.886
Low-Pressure Compressor			
$W\sqrt{\theta}/\delta$, kg/sec (lb/sec)	51.2 (113.0)	52.5 (115.9)	52.3 (115.4)
Pressure Ratio	1.640	1.654	1.639
Efficiency	0.922	0.986	0.985
High-Pressure Compressor			
$W\sqrt{\theta}/\delta$, kg/sec (lb/sec)	33.6 (74.2)	34.3 (75.7)	34.4 (75.9)
N rpm	13969	14132	14119
Pressure Ratio	13.03	13.18	13.25
Efficiency	0.894	0.873	0.872
Combustor			
Efficiency	0.9995	0.9995	0.9995

TABLE 3.3.4-IV (Cont'd)

	Flight Propulsion System	Integrated Core/Low Spool Mixed	Integrated Core/Low Spool Separate
High-Pressure Turbine			
$W\sqrt{T}/P \left[\frac{lb\sqrt{°R}\ in^2}{sec\ lb}\right]$	16.7	17.0	17.0
Rotor Inlet Temperature, °C (°F)	1363 (2486)	1438 (2621)	1438 (2621)
Pressure Ratio	3.98	4.07	4.07
Efficiency	0.892	0.879	0.879
Total Cooling Air and Secondary Airflow (% Core Airflow)	17.24	17.99	17.99
Low-Pressure Turbine			
$W\sqrt{T}/P \left[\frac{lb\sqrt{°R}\ in^2}{sec\ lb}\right]$	65.4	69.2	69.2
Pressure Ratio	5.09	5.01	4.88
Efficiency	0.905	0.907	0.906
Mixer			
Efficiency	0.85	0.85	--
Pressure Losses			
Combustor	0.0558	0.0565	0.0564
Turbine Transition Duct	0.0070	0.0154	0.0154
Turbine Exhaust Case	0.0069	0.0070	0.0066
Core Mixer	0.0010	0.0071	--
Fan Duct	0.0054	0.0067	0.0112
Duct Mixer	0.0017	0.0053	--
Tailpipe	0.0029	0.0030	Duct 0.0019 Core 0.0094
Nozzle			
Gross Thrust Coefficient	0.9907	0.9945	Duct 0.9942 Core 0.9948

3.3.5 Instrumentation Effects

The performance predicted for the integrated core/low spool, as discussed in the preceding section, does not include the impact of test instrumentation. The separate exhaust configuration is fully instrumented so that the performance of the individual components can be assessed. In the mixed configuration, the quantity of instrumentation is reduced significantly to obtain the best possible measurement for a representation of propulsion system performance.

The impact of instrumentation was estimated in terms of pressure loss at each pertinent performance station. Tables 3.3.5-I and -II show the estimated pressure losses for the two test configurations. As expected, losses for the mixed configuration are substantially lower.

TABLE 3.3.5-I

INSTRUMENTATION - INTEGRATED CORE/LOW SPOOL SEPARATE EXHAUST
INSTRUMENTATION PRESSURE LOSSES AT AERODYNAMIC DESIGN POINT

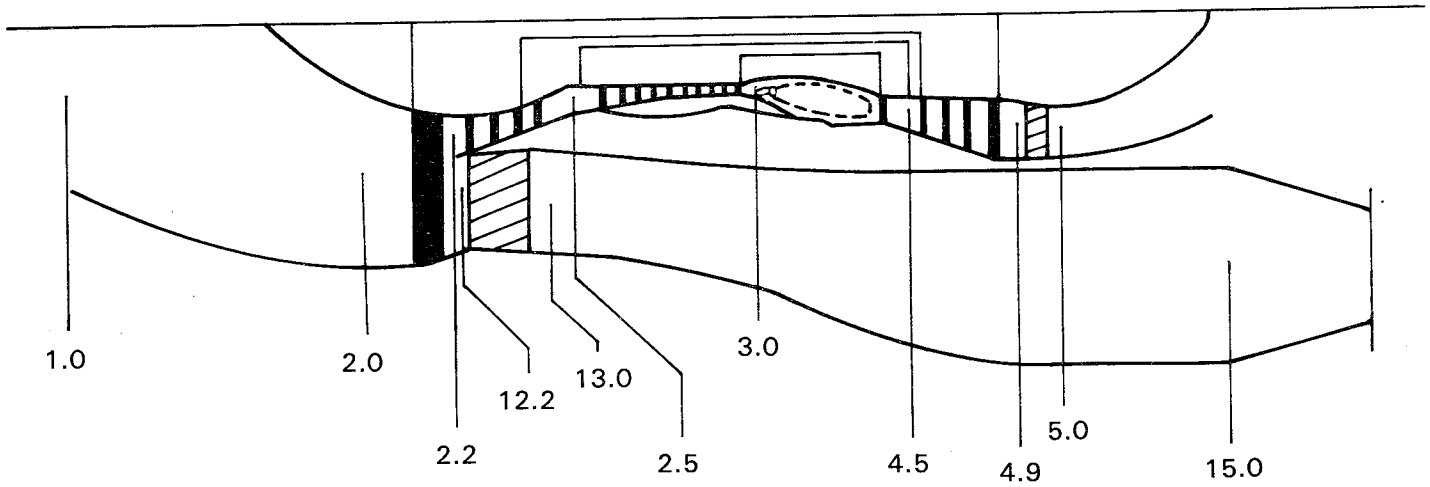

Station	ΔP/P	Station	ΔP/P
1.0	0.0089	4.5	0.010
2.0		4.9	0.0055
2.2	0.0015	5.0	0.0015
2.5	0.005	12.2	0.0015
3.0	0.004	13.0	0.001
		15.0	0.0013

TABLE 3.3.5-II

INSTRUMENTATION - INTEGRATED CORE/LOW SPOOL MIXED EXHAUST
INSTRUMENTATION PRESSURE LOSSES AT AERODYNAMIC DESIGN POINT

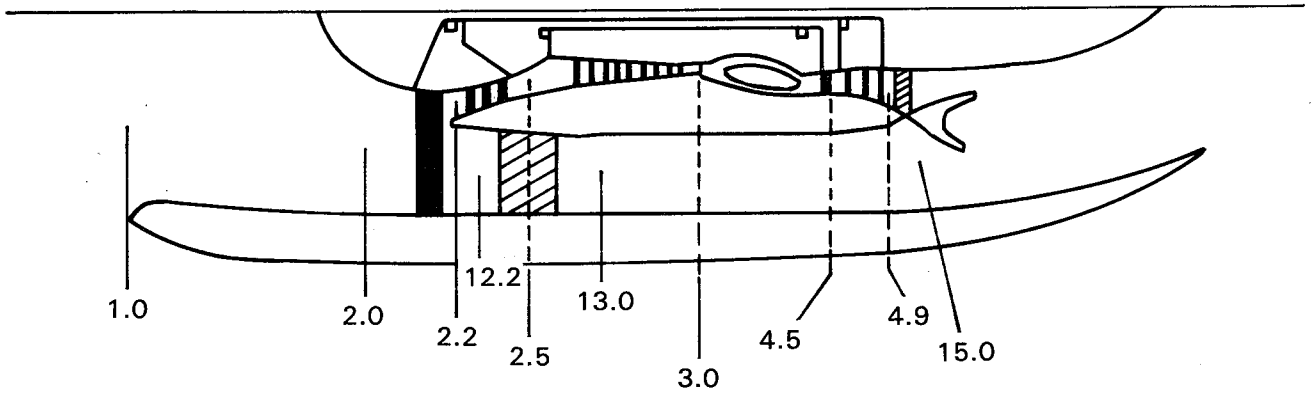

Station	ΔP/P	Station	ΔP/P
1.0	0.0089	4.5	0.0038
2.0		4.9	0.0017
2.2	0.0006	12.2	0.0015
2.5	0.0025	13.0	0.001
3.0	0.0015	15.0	0.0013

The general procedure used to predict performance with engine instrumentation is the same as that described in Table 3.3.1-I to obtain integrated core/low spool performance without instrumentation. The influence of instrumentation on the performance of the separate exhaust configuration is summarized in Tables 3.3.5-III and -IV. Table 3.3.5-III gives a synopsis of parameters at the maximum cruise rating to show the effect of instrumentation if the configuration is tested at altitude conditions. The results indicate relatively small changes in performance with instrumentation. The compression system incurs the largest impact, with both low- and high-pressure compressors showing operating line shifts toward the surge line. However, the loss in surge margin is not considered a limitation for testing.

TABLE 3.3.5-III

ANTICIPATED EFFECT OF INSTRUMENTATION
ON STATUS PERFORMANCE
SEPARATE EXHAUST
10,668 M (35,000 FT)/0.8 MN/STD. DAY/MAX. CRUISE

	Integrated Core/Low Spool Without Instrumentation	Integrated Core/Low Spool With Instrumentation
Wat $\sqrt{\theta}/\delta$, kg/sec (lb/sec)	616 (1360)	616 (1360)
FPR Rotor/Stage	1.742/1.713	1.727/1.691
BPR	6.55	6.64
OPR	37.59	37.27
CET/RIT, °C (°F)	1339 /1264 (2443)/(2308)	1339 /2308 (2443)/(1264)
PTD/PTE	1.11	1.10
% Δ Fan Operating Line	Base	-1.1
% Δ LPC Operating Line	Base	+1.1
% Δ HPC Operating Line	Base	+1.0

*(1) Isolated nacelle, no bleed or power extraction
(2) Takeoff fan match on flight propulsion system operating line at sea level static

Table 3.3.5-IV provides a more complete summary to indicate the impact of instrumentation during sea level testing of the separate exhaust configuration. The effects at takeoff are quite small, with the largest being the effect on thrust, thrust specific fuel consumption and compression system operating line shifts. Again, losses in surge margin and the other parameter changes are not an impediment to successful testing at sea level conditions.

The influence of instrumentation on the performance of the mixed exhaust configuration is presented in Tables 3.3.5-V and -VI for maximum cruise and takeoff ratings, respectively. At both conditions, the results are quite similar to those shown for the separate exhaust configuration. Thus, none of the data indicates any reason why operation of the mixed exhaust version would not be successful at either flight condition.

TABLE 3.3.5-IV

ANTICIPATED EFFECT OF INSTRUMENTATION
ON STATUS PERFORMANCE
SEPARATE EXHAUST*
SEA LEVEL STATIC/STD. 13.8°C (+25°F)/TAKEOFF

	Integrated Core/Low Spool Without Instrumentation	Integrated Core/Low Spool With Instrumentation
Wat $\sqrt{\theta}/\delta$, kg/sec (lb/sec)	556 (1226)	551 (1216)
FPR Rotor/Stage	1.616/1.596	1.602/1.575
BPR	6.72	6.81
OPR	31.77	31.25
CET/RIT, °C (°F)	1519 /1438 (2767)/(2621)	1519 /1437) (2767)/(2620)
N_1 rpm	3941	3908
$W\sqrt{\theta}/\delta$ HPC, kg/sec (lb/sec)	34.45 (75.95)	34.17 (75.35)
Pressure ratio HPC	13.25	13.21
Pressure Ratio HPT	4.07	4.03
N_2 rpm	14119	14065
FN Inst., N (lb)	166,616 (37457)	159,801 (35925)
TSFC Inst. lb/hr/lb	0.3551	0.3616
% Δ Fan Operating Line	Base	0
% Δ LPC Operating Line	Base	+.7
% Δ HPC Operating Line	Base	+1.1

*(1) Isolated nacelle, no bleed or power extraction
(2) Takeoff fan match on flight propulsion system operating line at sea level static

TABLE 3.3.5-V

ANTICIPATED EFFECT OF INSTRUMENTATION
ON STATUS PERFORMANCE
MIXED EXHAUST*
10,668 m (35,000 FT)/0.8 MN/STD. DAY/MAX. CRUISE

	Integrated Core/Low Spool Without Instrumentation	Integrated Core/Low Spool With Instrumentation
Wat $\sqrt{\theta}/\delta$, kg/sec (lb/sec)	632 (1395)	636 (1404)
FPR Rotor/Stage	1.742/1.712	1.737/1.703
BPR	6.57	6.60
OPR	38.46	38.61
CET/RIT, °C (°F)	1339 /1265 (2443)/(2309)	1339 /1265 (2443)/(2309)
PTD/PTE	1.12	1.12
FN Inst., N (lb)	39531 (8887)	37747 (8486)
TSFC Inst. lb/hr/lb	0.609	0.6267
% Δ TSFC Relative to JT9D	Base (-10.0)	-7.4
% Δ Fan Operating Line	Base	-1.3
% Δ LPC Operating Line	Base	+1.3
% Δ HPC Operating Line	Base	+ .6

*Isolated nacelle, no bleed or power extraction, flight propulsion system nozzles and inlet

TABLE 3.3.5-VI

ANTICIPATED EFFECT OF INSTRUMENTATION
ON STATUS PERFORMANCE
MIXED EXHAUST*
SEA LEVEL STATIC/STD. 13.8°C (+25°F)/TAKEOFF

	Integrated Core/Low Spool Without Instrumentation	Integrated Core/Low Spool With Instrumentation
Wat $\sqrt{\theta}/\delta$, kg/sec (lb/sec)	560 (1235)	560 (1235)
FPR Rotor/Stage	1.627/1.607	1.621/1.598
BPR	6.71	6.77
OPR	32.03	31.83
CET/RIT, °C (°F)	1519/1438 (2767)/(2621)	1519/1438 (2767)/(2621)
N_1 rpm	3077	3057
$W\sqrt{\theta}/\delta$ HPC, kg/sec (lb/sec)	34.33 (75.70)	34.20 (75.41)
Pressure ratio HPC	13.18	13.15
Pressure Ratio HPT	4.07	4.06
N_2 rpm	14132	14112
FN Inst., N (lb)	169,307 (38062)	165,415 (37187)
TSFC Inst. lb/hr/lb	0.3516	0.3549
% Δ Fan Operating Line	Base	0
% Δ LPC Operating Line	Base	+.3
% Δ HPC Operating Line	Base	+.7

*Isolated nacelle, no bleed or power extraction, flight propulsion system nozzles and inlet

3.3.6 Operating Lines

Influence coefficients were derived to estimate operating line sensitivity (stability margin) to component performance changes from expected test levels. The data are used to update the stability assessments of the fan, low-pressure compressor, and high-pressure compressor components as results are acquired from analyses, designs, and experimental tests.

Compression system stability was analyzed for both steady state and transient conditions. In Figures 3.3.6-1 through 4, steady state operating lines and surge lines are shown for sea level hot day conditions. The predicted nominal operating lines show acceptable stability margins, although the outer fan surge margin in the idle region for the separate exhaust configuration (Figure 3.3.6-1) is only slightly greater than the requirement (2.3 percent versus 1.9 percent). A similar analysis at altitude shows that sufficient surge margins are available.

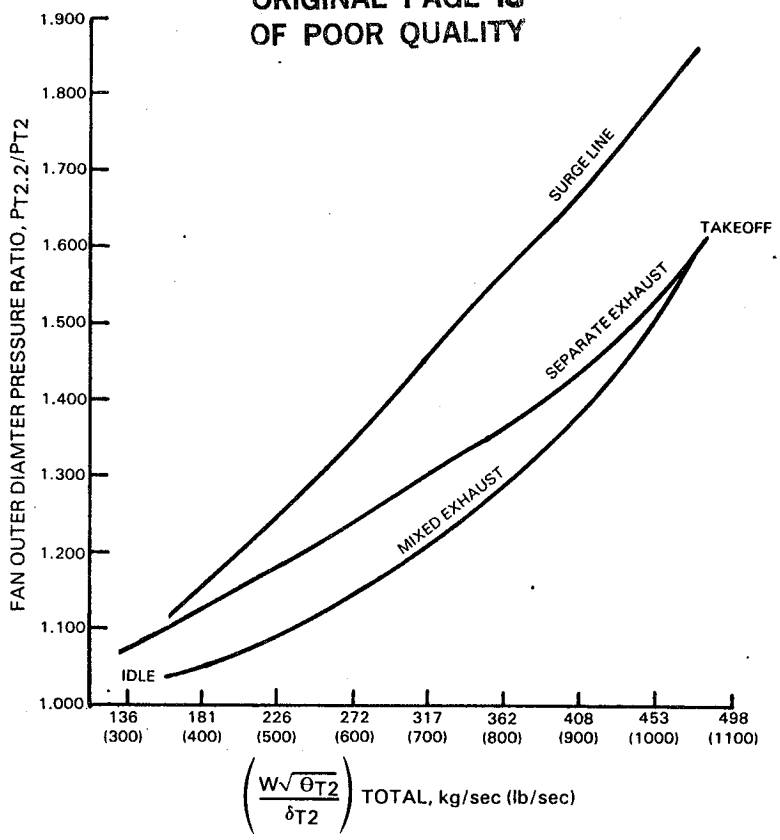

Figure 3.3.6-1 Fan Outer Diameter Operating Line Comparison

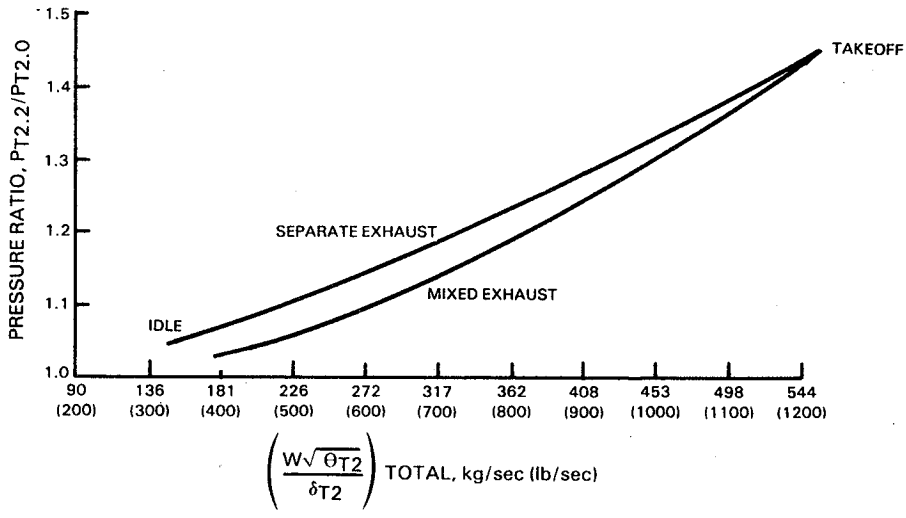

Figure 3.3.6-2 Fan Inner Diameter Operating Line Comparison

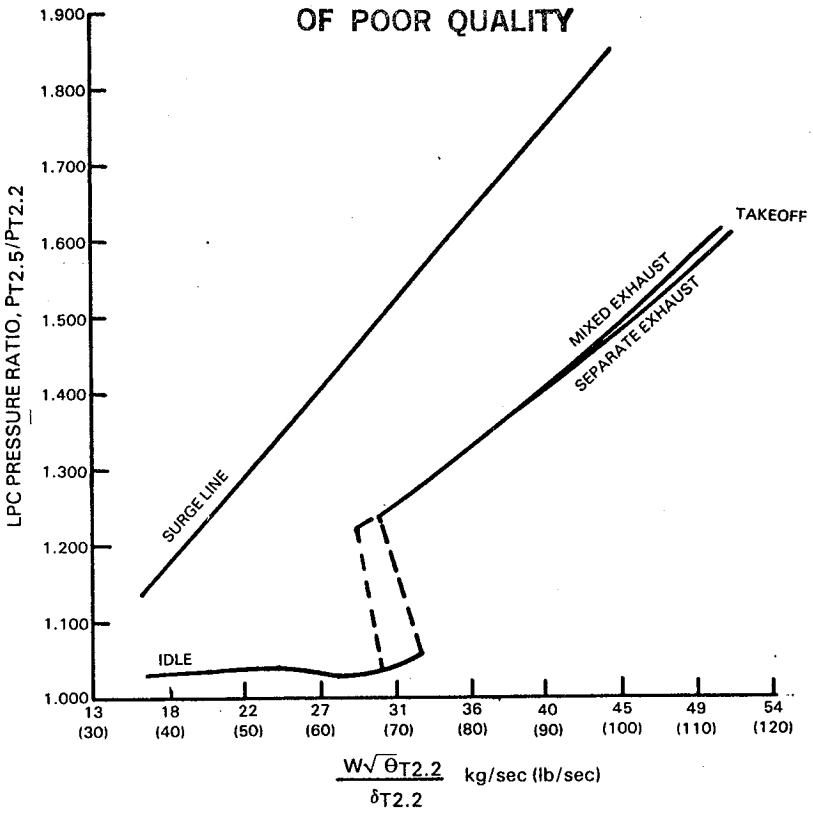

Figure 3.3.6-3 Low-Pressure Compressor Operating Line Comparison

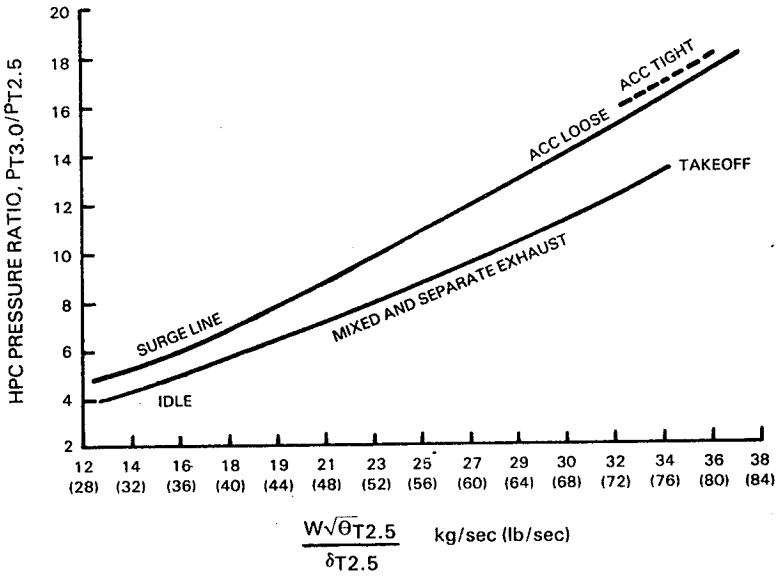

Figure 3.3.6-4 High-Pressure Compressor Operating Line Comparison

In a stability analysis for transient conditions, the separate exhaust configuration was evaluated at sea level and the mixed version was evaluated at both sea level and altitude. The simulation used in these analyses included the effects of instrumentation. Also, preliminary surge margin requirements for the flight propulsion system were used to measure stability adequacy. Evaluations were made for the three transient modes planned for the integrated core/low spool control system during testing. These include a rate-limited deceleration, snap (emergency) deceleration and rate-limited acceleration. (Rate-limited power lever movements are on the order of 20 seconds at sea level and 16.7 seconds at altitude. Sea level transients are between takeoff and ground idle, while altitude transients are between maximum climb and flight idle (minimum fuel flow).

Results showed that fan stability is adequate. Transient and steady state operating lines are essentially the same for the different configurations and conditions. However, the analyses did indicate some potential problems in the low- and high-pressure compressors. Figures 3.3.6-5 through 3.3.6-7 present typical operating characteristics of the low-pressure compressor. Similar information is shown in Figures 3.3.6-8 through 3.3.6-10 for the high-pressure compressor. Although these results are for a mixed configuration at sea level conditions, they are indicative of the operating trends at sea level with the separate exhaust configuration and at altitude with the mixed configuration.

As indicated in Figure 3.3.6-5, there is a potential deficiency in low-pressure compressor surge margin in the region above idle during rate-limited deceleration. However, actuating the surge bleed in the high-pressure rotor speed appears to provide sufficient margin.

Also, the analyses indicate that bleed should be based on mechanical rather than corrected high-pressure rotor speed to provide adequate surge margin during rate-limited deceleration at altitude. As shown in Figure 3.3.6-6, immediate opening of the surge bleed provides protection for the low-pressure compressor during a snap deceleration.

A potential deficiency in high-pressure compressor surge margin exists in the region above idle during a rate-limited acceleration. This condition is shown in Figure 3.3.6-10, where surge margin twice falls below the idle stability requirement before the takeoff or maximum climb (or maximum cruise) condition is reached. However, surge margin is always greater than the takeoff and maximum climb requirements. A slower power lever movement, therefore, should be used during rate-limited acceleration to provide an adequate surge margin for the high-pressure compressor, if high-pressure compressor rig testing indicates stability to be less than the analytical results shown in Figure 3.3.6-10.

No other potential stability problems are anticipated for the compression system.

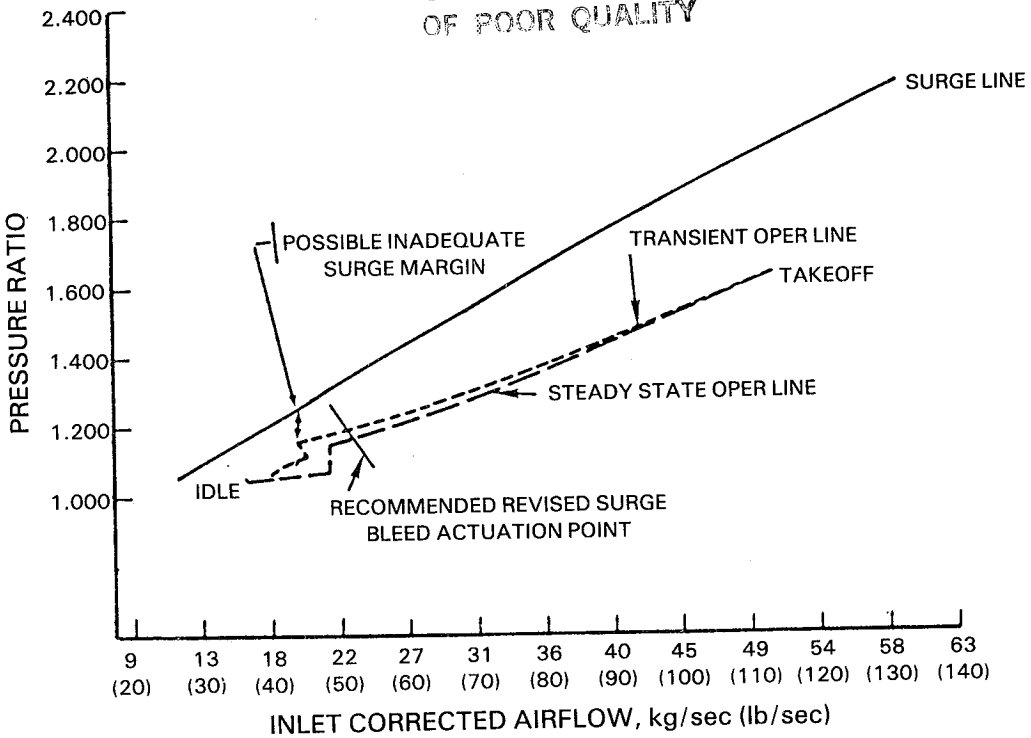

Figure 3.3.6-5 Low-Pressure Compressor Rate-Limited Deceleration Operating Characteristics for a Mixed Exhaust Configuration at Sea Level Static Conditions

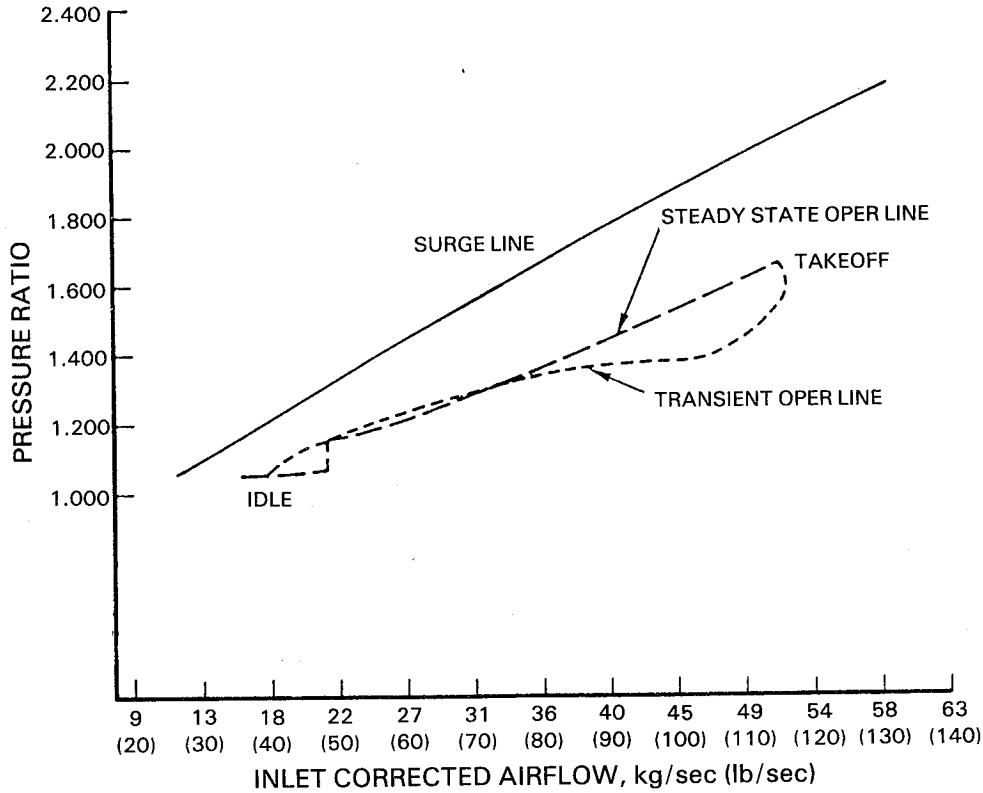

Figure 3.3.6-6 Low-Pressure Compressor Snap Deceleration Operating Characteristics for a Mixed Exhaust Configuration at Sea Level Static Conditions

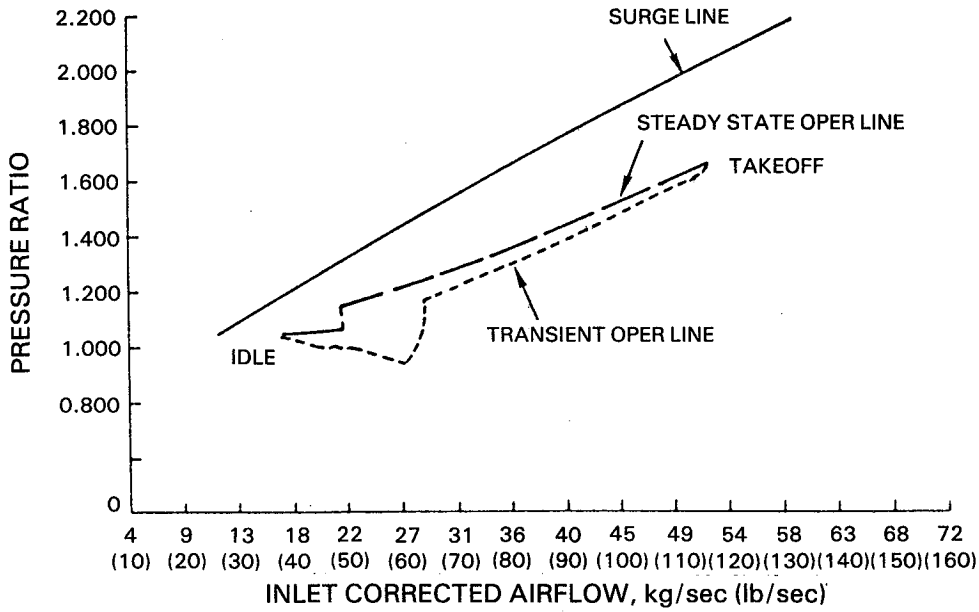

Figure 3.3.6-7 Low-Pressure Compressor Rate-Limited Acceleration Operating Characteristics for a Mixed Exhaust Configuration at Sea Level Static Conditions

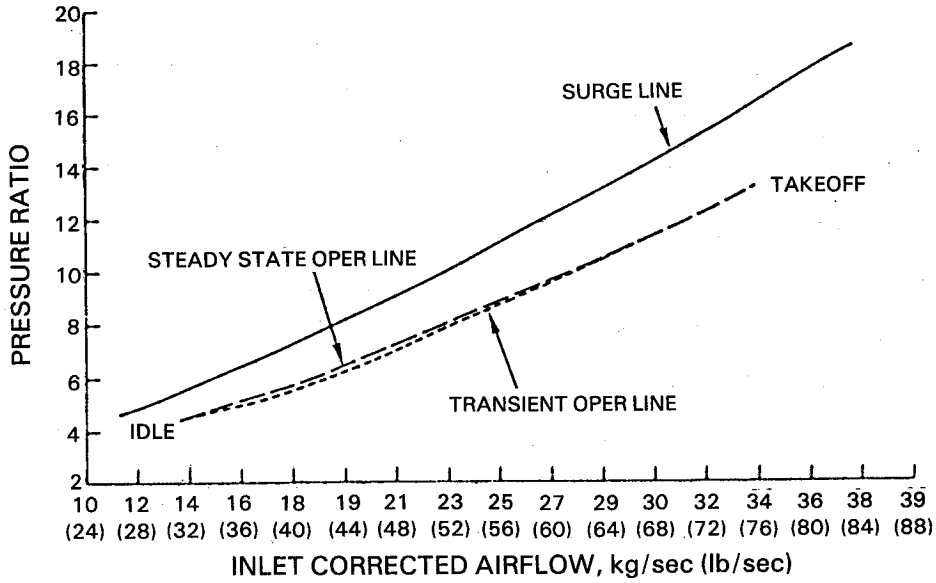

Figure 3.3.6-8 High-Pressure Compressor Rate-Limited Deceleration Operating Characteristics for a Mixed Exhaust Configuration at Sea Level Static Conditions

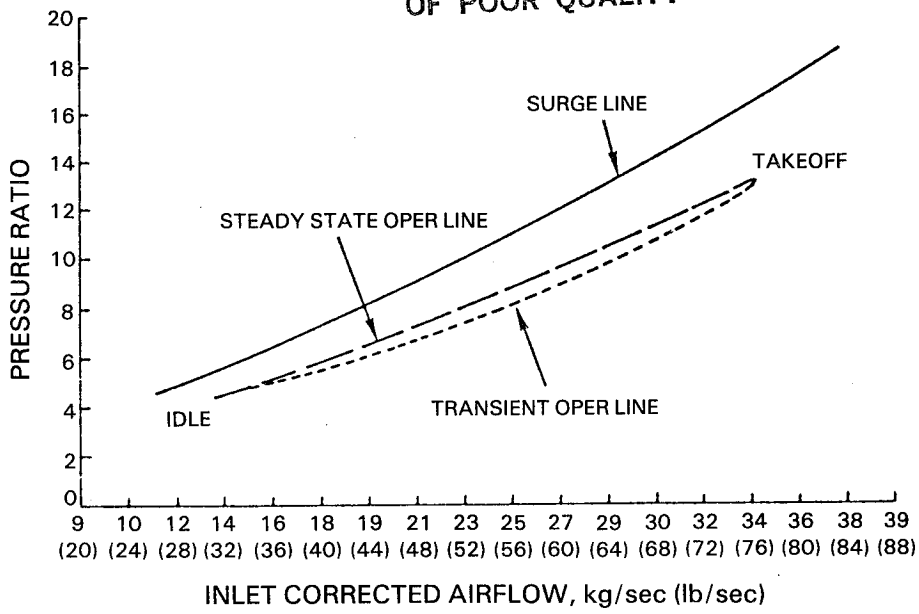

Figure 3.3.6-9 High-Pressure Compressor Snap Deceleration Operating Characteristics for a Mixed Exhaust Configuration at Sea Level Static Conditions

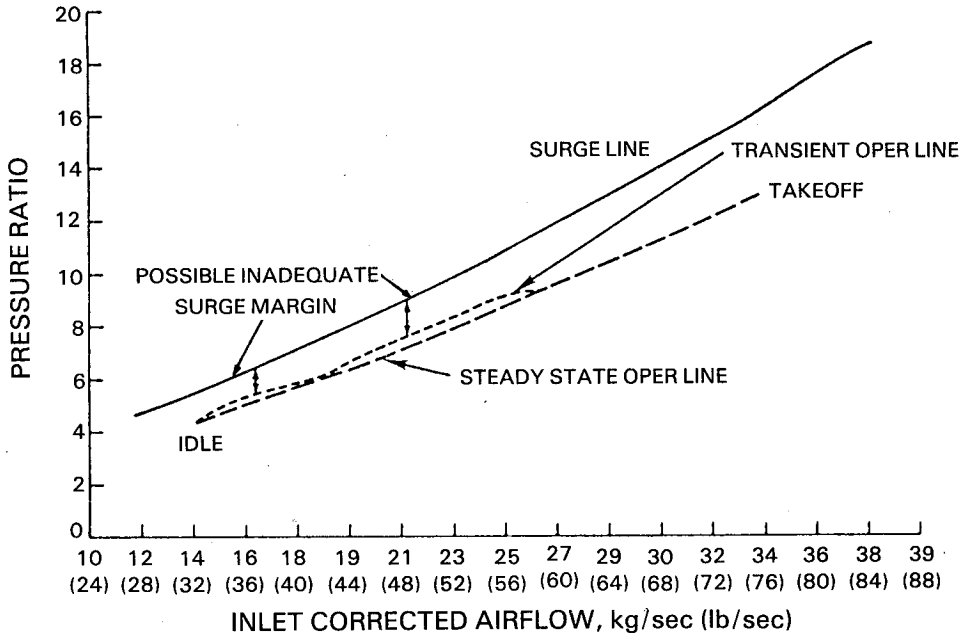

Figure 3.3.6-10 High-Pressure Compressor Rate-Limited Acceleration Operating Characteristics for a Mixed Exhaust Configuration at Sea Level Static Conditions

3.3.7 Starting

An estimate of motoring torque was made for the integrated core/low spool to determine starter sizing requirements. Figure 3.3.7-1 shows that substantial torque is obtainable using a currently available ATS 200-11 starter relative to the estimated motoring torque requirement of the integrated core/low spool.

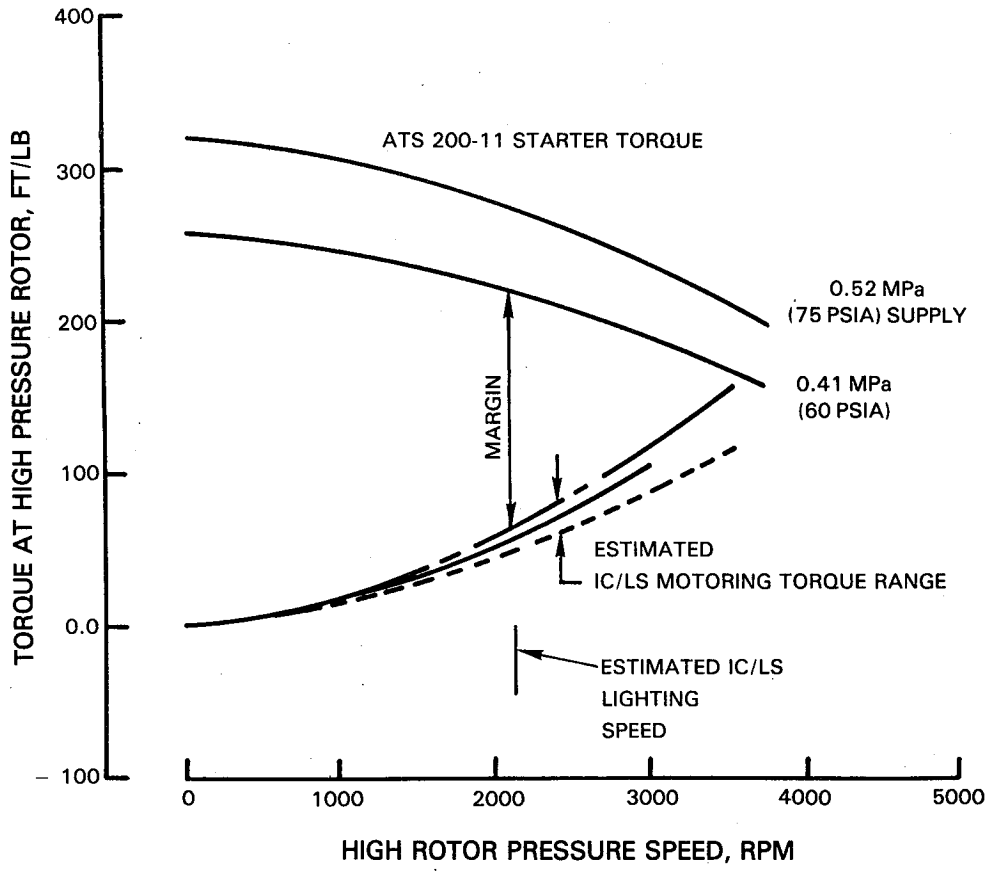

Figure 3.3.7-1 Integrated Core/Low Spool Torque Estimate and Starter Torque Capability (Standard Day)

A general review of the factors affecting the starting capability of the integrated core/low spool was also made. The different areas investigated with respect to their impact on starting included knowledge gained from combustor rig lighting and high-pressure compressor rig testing as well as high-pressure turbine operating line predictions, stability airbleed capabilities, and other Pratt & Whitney Aircraft engine experience. These are discussed in the following paragraphs.

Combustor lighting characteristics were assessed by analyzing sector combustor rig test results. Performance simulation parameters were extrapolated into the region below idle and combined with relight test results. A combustor lighting speed estimate of 2050 rpm high-pressure rotor speed was determined for standard day operation. At this speed, adequate torque margin is available with the ATS 200-11 starter. Furthermore, the speed is low enough so that additional torque is available to help accelerate the spool to idle. Combustor rig testing also demonstrated that lighting will be "soft" and accomplished at low fuel flow rates. Therefore, combustor ignition should not significantly influence high-pressure compressor operation during starting.

High-pressure compressor rig testing indicated that regions of rotating stall exist in the vicinity of the predicted bleeds closed operating line, as shown in Figure 3.3.7-2. However, since the operating line is very difficult to locate accurately in the starting region, other factors were examined to determine the direction and magnitude of their impact. The influence of fifteenth-stage compressor bleed was evaluated analytically since rig testing showed that the tenth-stage bleed was not effective in improving surge margin in the starting region. The bleed capability from the fifteenth stage for the integrated core/low spool was estimated at 7.4 percent of core airflow in the starting region. Influence coefficients indicated the effect of this quantity on improving surge margin to be relatively small. Consequently, the bleed flow was increased to 15 percent. The effect of these quantities on the operating line is shown in Figure 3.3.7-3. As indicated in Figure 3.3.7-3 a 15 percent bleed flow results in a 1.6 percent lower operating line in the starting region.

A re-assessment of high-pressure turbine operation at low power conditions indicated that the effective controlling vane area is larger than that assumed in the performance simulation. In the starting region (about 25 percent of design corrected rotor speed), the turbine flow capacity is increased 7.5 percent. An additional high pressure compressor surge margin benefit of at least 1.2 percent should result.

A comparison of integrated core/low spool starting analysis results was made with other Pratt & Whitney Aircraft engine starting experience. Conclusions reached are that the analytical predictions of starting capability have proven to be rather pessimistic in the past and that the integrated core/low spool predictions appear to be comparable to those for engines that have not experienced starting difficulties.

On the basis of this review, the following recommendations have been made. First, provisions should be made to extract the maximum possible airbleed from the fifteenth stage of the high-pressure compressor. Second, high-pressure turbine rig testing should include operation in the starting region to confirm the flow capacity levels predicted analytically. Finally, The starter should be kept engaged to the highest possible rotor speed to help accelerate the spool to idle.

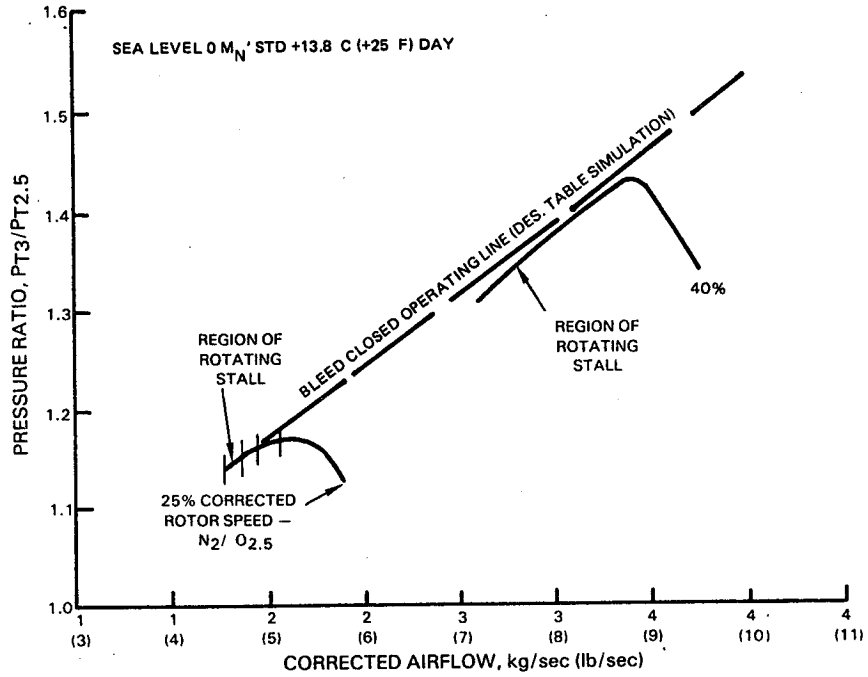

Figure 3.3.7-2 High Pressure Compressor Rig Performance Results in Starting Region

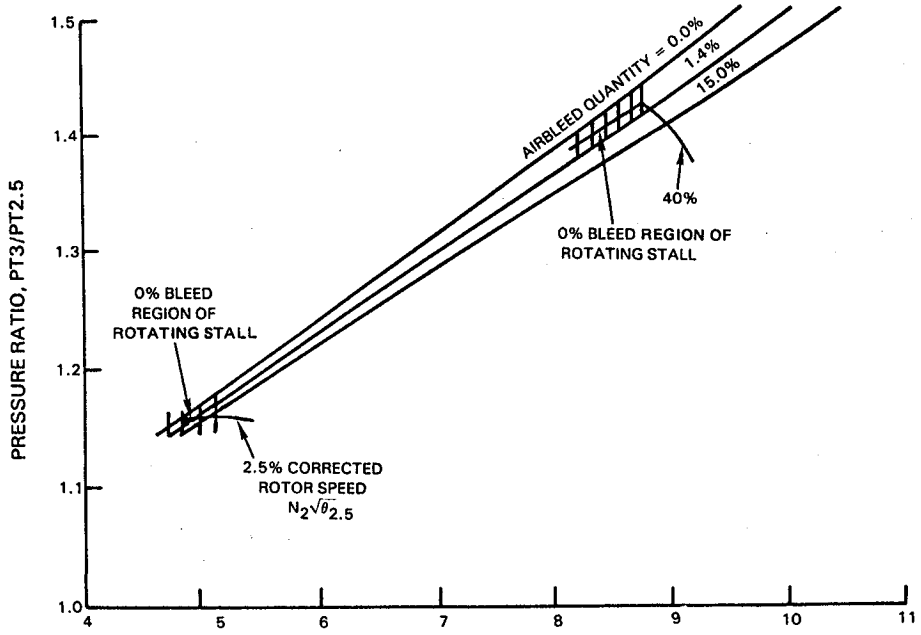

Figure 3.3.7-3 High-Pressure Compressor Design Table Simulation

3.4 PERFORMANCE BOOKKEEPING

At the completion of component and integrated core/low spool testing, the test data will be used to project the maximum cruise thrust specific fuel consumption of the flight propulsion system. The procedure diagramed in Figure 3.4-1 has been developed to provide this information.

The cycle and analysis computer program simulation developed for both the flight propulsion system and integrated core/low spool is used in making the projection. Results from high-pressure compressor, combustor and high-pressure turbine component rig tests, and exhaust mixer model tests are used to update the maps in the simulation that had been defined during the design process. Results from the integrated core/low spool test program will furnish additional data. Fan, low-pressure compressor, low-pressure turbine, and internal nacelle test results will be available for the first time. These data will be used to update their respective component maps in the simulation.

The effects of instrumentation will be removed from component and integrated core/low spool systems data. The data will also be adjusted for differences between test and flight propulsion system radial clearances and Reynolds numbers. Component performance and flow capacity inaccuracies will be compensated for, as necessary, using test data from similar programs to adjust operating lines and points to achieve compatibility with turbine and exhaust nozzle area changes and airfoil restaggers and recambers. Additional observed improvements to component performance not predicted by the design system will be compensated for by applying traceable results from existing test data.

Fan, low-pressure compressor and low-pressure turbine performance measured at sea level conditions will be extrapolated to cruise conditions using test data from components with similar aerodynamic parameters. Mixer performance from integrated core/low spool testing with a convergent exhaust nozzle will be adjusted to the convergent-divergent configuration in the flight propulsion system using mixer model test results. Techniques developed in coordination with the airframe manufacturers will be used to analytically estimate external nacelle performance so that installed performance, without nacelle-to-wing interference effects, can be determined. The final revised computer program simulation will then be used to define flight propulsion system cruise performance predictions.

3.5 DESIGN LIFE REQUIREMENTS

The minimum design life for the integrated core/low spool experimental hardware was defined as the more limiting of (1) 50 hours of operation at hot day sea level static takeoff power or (2) 1000 cycles. A cycle is defined as beginning at a steady state idle condition, followed by a slow (rate limited) acceleration to a steady state hot day takeoff condition, and then a slow (rate limited) deceleration to steady state idle. In addition, the experimental hardware is designed for operating at any sea level static steady state or transient point throughout the range from idle to hot day takeoff thrust. It is also designed for operation at steady state altitude cruise to provide additional test capability, should that be required. These minimum requirements were set to permit substitution of low cost materials, where feasible, in the experimental hardware.

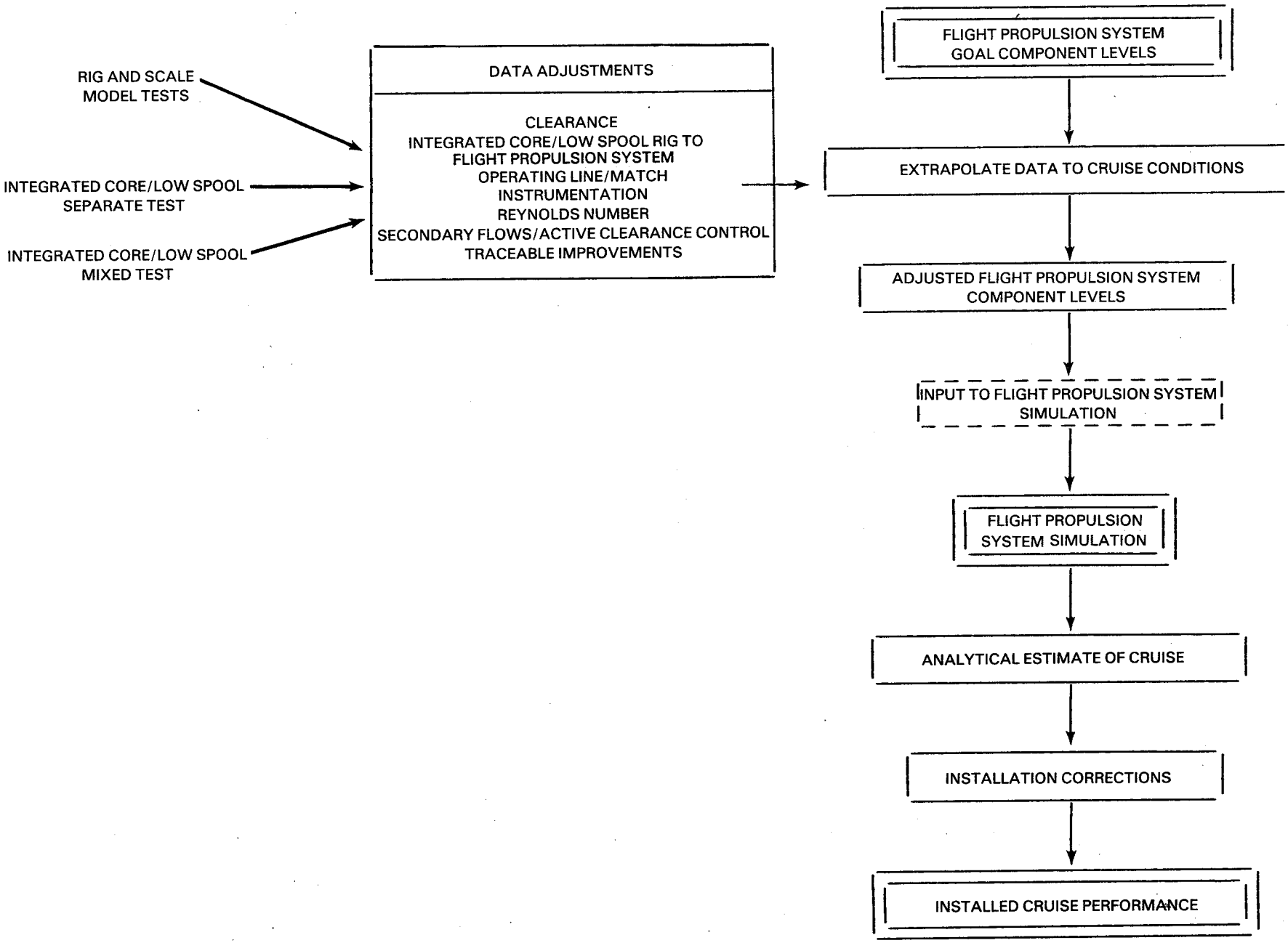

Figure 3.4-1 Procedure for Projecting Cruise Performance of Flight Propulsion System

SECTION 4.0
INTEGRATED CORE/LOW SPOOL COMPONENT DESIGN

4.1 INTRODUCTION

The components in the integrated core/low spool include the fan, low-pressure compressor, high-pressure compressor, combustor, high-pressure turbine, low-pressure turbine, and exhaust/mixer. Three of the components -- the high-pressure compressor, combustor, and high-pressure turbine -- were tested in full-scale component rig test programs to verify performance and structural integrity prior to assembly into the full engine. In addition, a mixer model test program and a turbine transition duct model test program were conducted to establish the aerodynamic designs of these components. Rig programs were not required for the fan, low-pressure compressor, and low-pressure turbine since these components are high confidence designs. Salient characteristics of the components in the integrated core/low spool are described in the following sections.

4.2 FAN

4.2.1 General Description

The fan is a high performance, single-stage configuration similar to those currently in service in Pratt & Whitney Aircraft high bypass ratio engines. The blades are designed with a single part-span shroud and the rotor is an integral disk/hub arrangement to reduce weight. Blade tip leakage is reduced by the use of a recessed abradable tip seal. Figure 4.2.1-1 shows a cross-sectional view of the fan component. A summary of the component aerodynamic and mechanical designs is presented in the following section. Details pertaining to the fan design are contained in Reference 1.

4.2.2 Aerodynamic Design

The aerodynamic design of the fan is based on the aerodynamics of current high performance, single-stage shrouded configurations. The aerodynamic design point was set at an altitude of 10,668 m (35,000 ft) and a cruise Mach number of 0.8.

Figure 4.2.2-1 shows the fan flowpath. The fan contains 36 blades and an array of both structural and nonstructural exit guide vanes in the duct stream.

Design characteristics of the fan blade are presented in Table 4.2.2-I. The blade is a combination of multiple circular arc and design-contoured sections. Multiple circular arc sections are retained in the inner 50 percent span, whereas design-contoured sections are used in the outer 50 percent span because of the higher flow field Mach numbers. Incidence, choke margin and delta deviation are consistent with current shrouded fan design practice. Deviation is similar to that of the NASA 1800 ft/sec tip speed fan, except in the tip region where the airfoil has been modified to maintain a smooth contour. The shroud is located at 71.5 percent span and positioned rearward on the blade. Rearward positioning minimizes the incident flow velocity on the shroud and positions the shroud in the region of maximum blade-to-blade distance normal to the flow, thereby reducing losses.

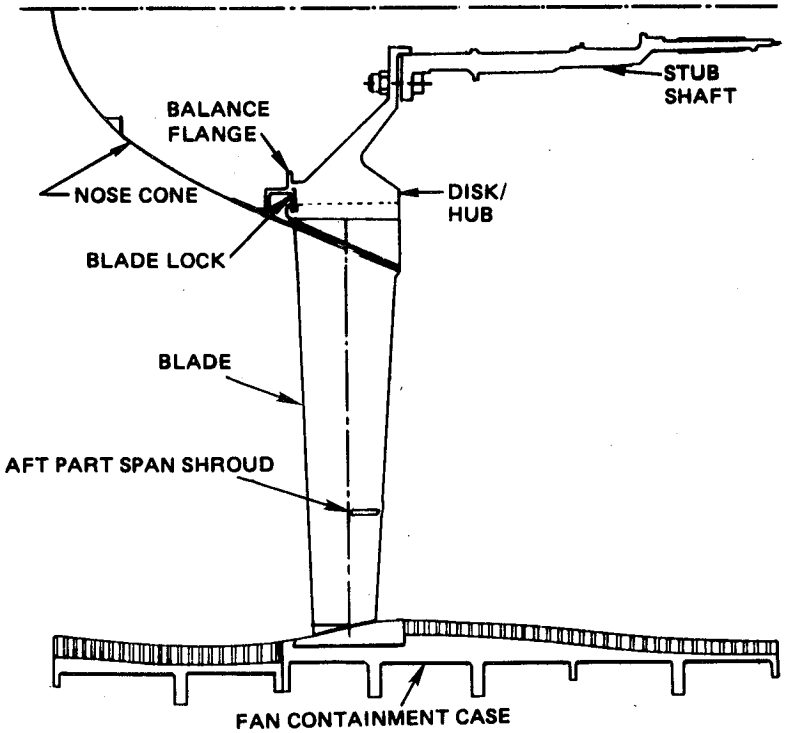

Figure 4.2.1-1 Energy Efficient Engine Fan Component

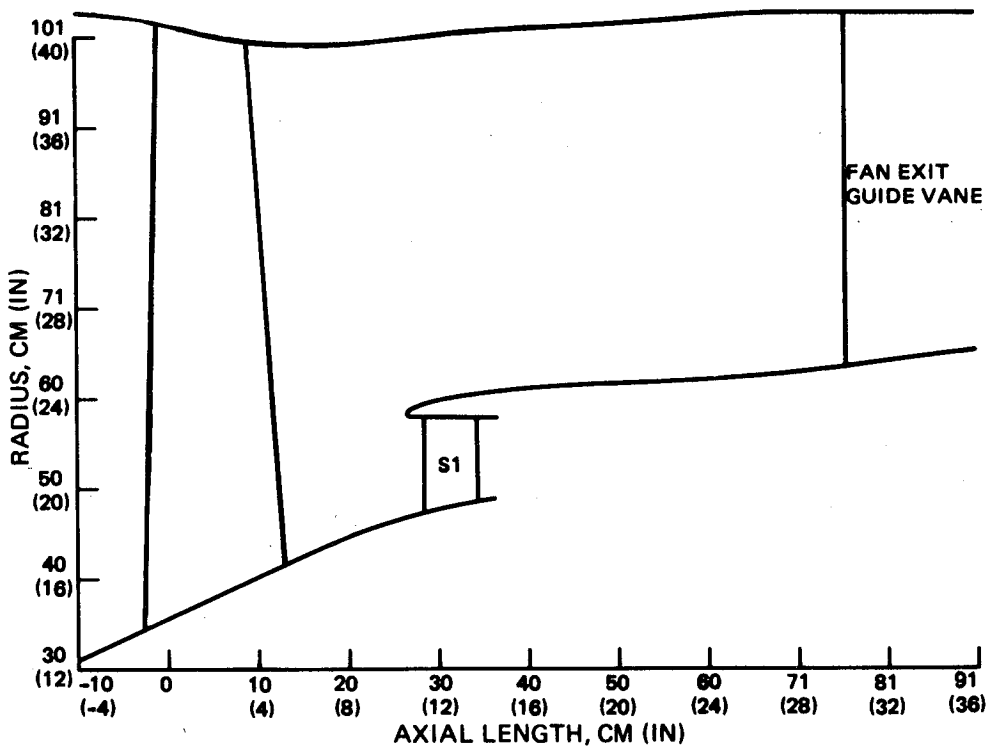

Figure 4.2.2-1 Fan Flowpath Definition

TABLE 4.2.2-I

FAN BLADE DESIGN FEATURES

Hub/Tip Ratio	0.34
Taper Ratio	1.45
Bypass Ratio	6.51
Aspect Ratio	4.0
Average Root Chord, cm (in)	15 (6.219)
Average Tip Chord, cm (in)	23 (9.059)
Shroud Location, % span	71.5
Airfoil Length at stacking line, cm (in)	63.304 (24.923) (hot with 0.254 (0.100) in tip gap)
Z Plane Radius, cm (in)	32 (12.835) (cold)

The fan exit duct section is designed to remove blade exit swirl through an array of 29 exit guide vanes. Ten of these vanes are structural struts, with the top dead center strut serving as the leading edge fairing for the engine support pylon. The structural and nonstructural struts have the same surface contours and both employ controlled diffusion shapes for improved incidence range and loading capability. Sufficient choke margin is provided to accommodate part power flow requirements. The exit guide vane array is pylon matched to minimize blockage and back pressure distortion on the rotor. The effect of pylon matching is shown in Figure 4.2.2-2.

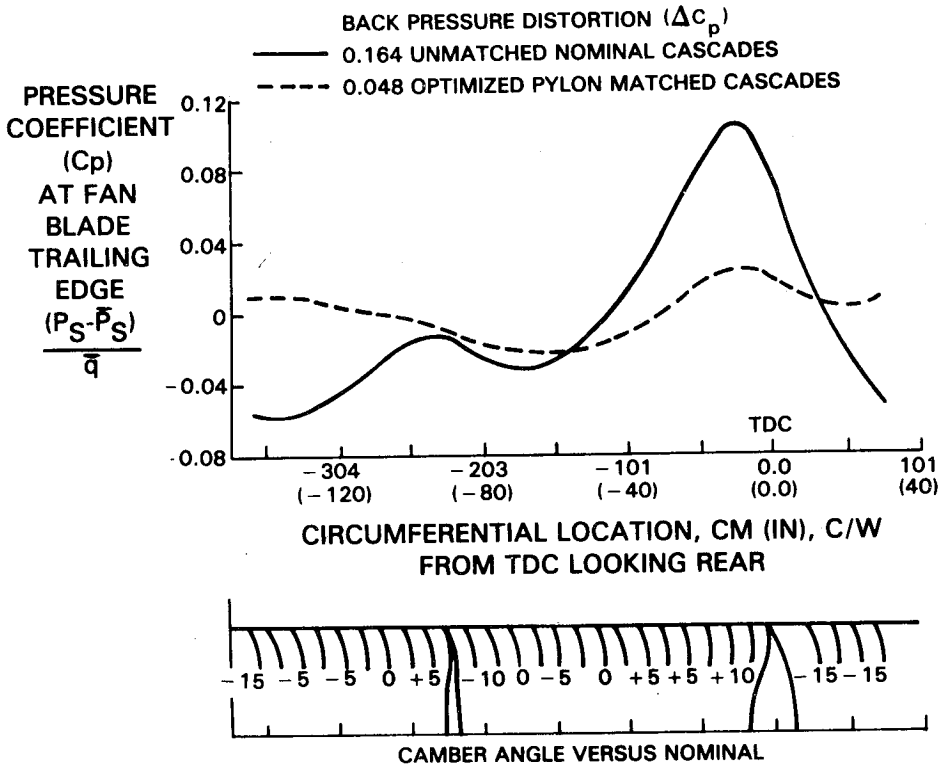

Figure 4.2.2-2 Calculated Back Pressure Distortion with Nominal and Pylon Matched Fan Exit Guide Vanes

4.2.3 Mechanical Design

Rotor System

The fan rotor is a cantilevered configuration, supported by two main shaft bearings (Nos. 1 and 2). Both bearings are housed in a common bearing support in the compressor intermediate case and are existing designs. The No. 1 bearing is an unflanged ball type with a split inner race and the No. 2 bearing is an unflanged roller type with a double shouldered outer race. Design details of these bearings are presented in Section 5.4.

The fan blade is made of solid titanium (AMS 4928) with an aspect ratio of 4.0. A 65-degree shroud-to-shroud contact angle is used and the shroud is defined as a tipped cylinder to simplify manufacturing. The blade attachment is an existing broach design.

Besides the blades, the major components in the fan rotor are the hub and stub shaft. The rotor hub is fabricated from AMS 4928 titanium and bolted to a stub shaft with 15 2.54-cm (1.0-in) diameter steel tiebolts. Bolted to the front of the rotor is the nose cone and end cap. These components are constructed from AMS 4135 aluminum and are based on an existing design used in the JT9D engine. The nose cone incorporates a stainless steel blade retention ring that locks the blades into the rotor to prevent any axial movement. It also serves to brace the hub against dynamic loads imposed by the blades.

The stub shaft is fabricated from steel and is splined to the mating low-pressure rotor drive shaft. It is designed to satisfy blade loss moment loads at the centerline of the No. 1 bearing, torque loads and bearing axial load requirements. Mounted on the stub shaft is the de-oiler, which separates oil from breather air for all engine main bearing compartments.

Case

For the integrated core/low spool, the fan containment case is designed principally for cost considerations and experimental test purposes. Consequently, the case does not meet weight requirements for a flight engine, although it does meet the requirements for containment and structural integrity. The assembly, as illustrated in Figure 4.2.3-1, consists of two ring sections machined from AMS 5062 low carbon steel forgings and bolted together at a flange just forward of the blade. Stiffening rings are integral to the case and two of these are located where the accessory drive gearbox can be bolted to this structure. Acoustic liners, both in the front and rear cases, are constructed of aluminum honeycomb and bonded to the steel case. A perforated aluminum sheet is bonded to the honeycomb, which, in turn, is covered with a stainless steel mesh for lower pressure loss.

The blade tip rubstrip is an abradable material with tip trenches to reduce leakage. The rubstrip consists of 25 abradable Kevlar®/epoxy segments that are bonded to the case. The segments are machined after installation to form the trench.

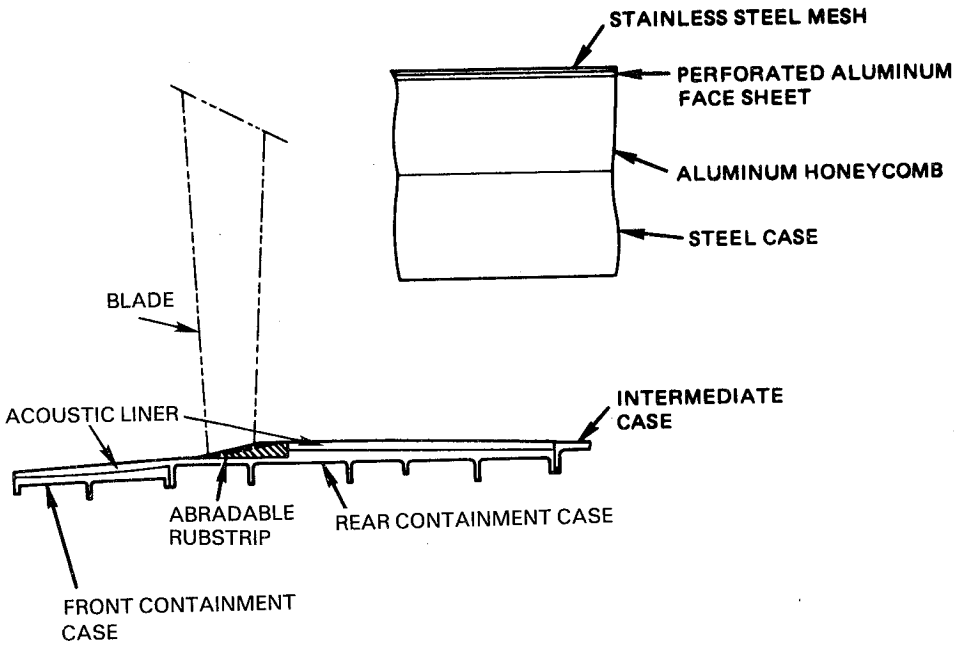

Figure 4.2.3-1 Integrated Core/Low Spool Fan Containment Case

4.2.4 Design Substantiation and Supporting Analyses

4.2.4.1 Predicted Performance

Predicted performance at the aerodynamic design point is summarized in Table 4.2.4-I. As indicated, the integrated core/low spool fan is predicted to meet or exceed all its design goals, including the efficiency goal of 84.5 percent.

TABLE 4.2.4-I

PREDICTED FAN PERFORMANCE
AT AERODYNAMIC DESIGN POINT

Parameter	Design Goal	Predicted
Corrected total airflow, kg/sec (lbm/sec)	622.7 (1372.8)	622.7 (1372.8)
Corrected rotor speed, rpm	4215	4215
Fan tip speed, m/sec (ft/sec)	456.0 (1496)	456.9 (1499)
Corrected flow/unit area, kg/sec-m^2 (lbm/sec-ft^2)	209.9 (43.0)	209.9 (43.0)
Duct pressure ratio	1.740	1.740
Fan hub pressure ratio	1.61	1.61
Efficiency, %	84.5	84.7
Surge margin goal, %	15	15

Preliminary fan surge margin requirements were established by a stability audit taken for the flight propulsion system at the major operating points in the flight envelope. Results showed a 15 percent design point surge margin also provides sufficient margin at takeoff, climb, cruise, idle, and reverse power settings, (Table 4.2.4-II).

TABLE 4.2.4-II

FAN STABILITY AUDIT RESULTS AT MAJOR OPERATING POINTS

Flight Condition	Flow (%)	Surge Margin (%) Required	Available
Aerodynamic Design Point*	100	4.5	15.0
Idle (sea level static)	29.7	1.9	7.4
Takeoff	89.7	7.5	16.2
Reverse	88.9	9.5	16.7

*Representative of maximum climb and cruise operation

4.2.4.2 Structural/Life Analyses

All major structural elements have been designed to ensure structural integrity as well as adequate life for experimental testing.

Blades

Bending stresses at the blade root are designed to be zero at the low cycle fatigue limiting condition of 3879 rpm and sea level takeoff thrust gas bending load. The blade is also balanced about the root with a slight offset between the airfoil stacking line and the blade root centerline. This not only accounts for the centrifugal load of the blade and shroud and the gas loads, but also for platform and neck pulls to yield a zero moment about the "Z" plane. Blade steady stresses are summarized in Table 4.2.4-III. Root and under shroud stresses meet the low cycle fatigue life requirement. The maximum trailing edge stress is 482.6 MPa (70 ksi) and occurs just below the shroud.

TABLE 4.2.4-III

BLADE LOW CYCLE FATIGUE LIFE SUMMARY

Location	Concentrated Stress, MPa (ksi)	Low Cycle Fatigue Stage Life, (cycles)
Airfoil root 30% chord convex	503.3 (73)	10^5
Undershroud 85% chord convex	730.8 (106)	58,000
Undershroud 40% chord concave	620.5 (90)	10^5

An analysis of blade resonant and natural frequencies was performed using a beam vibration analysis. The resultant frequency margins are shown in Figure 4.2.4-1. Critical harmonic orders, which are 2E, 3E, 4E, and 10E (the intermediate case strut order), are outside the normal engine operating range. Margins for critical frequencies near the blade tip, where vibration is caused by chordwise bending modes, are shown in Table 4.2.4-IV. Adequate margins exist for all of these resonances.

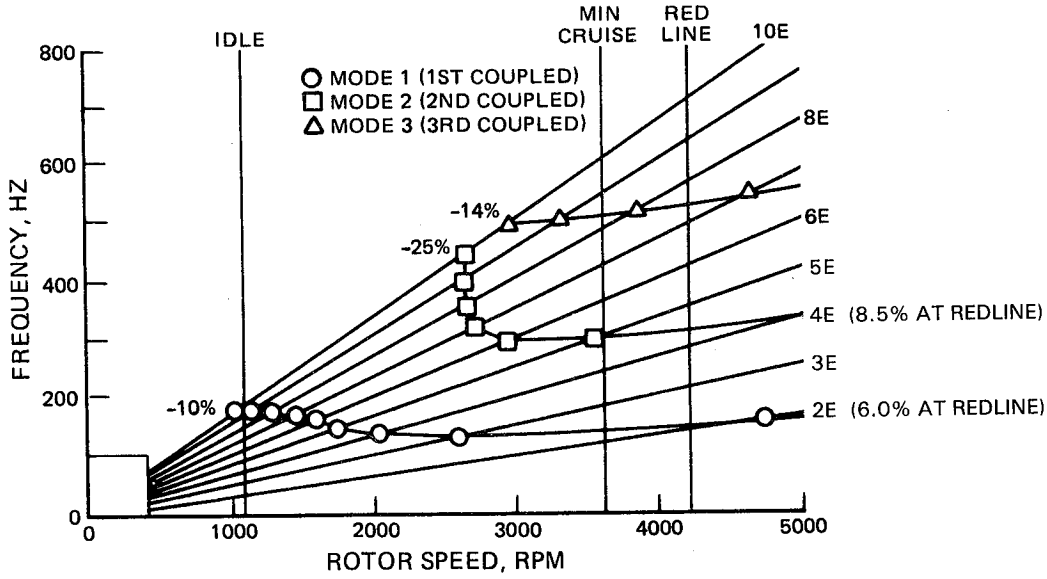

Figure 4.2.4-1 Fan Blade Resonance Diagram

TABLE 4.2.4-IV

BLADE TIP MODE FREQUENCY MARGINS

	10E	20E	30E
First Tip Mode (%)	54 at Min. Cruise	-9.6 at Min. Cruise	-40 at Min. Cruise
Second Tip Mode (%)	236 at Redline	68 at Redline	12 at Redline

The final airfoil design was analyzed for supersonic unstalled flutter and stalled flutter. Supersonic unstalled flutter is based on sea level takeoff aerodynamic conditions, since this is the only critical operating point the integrated core/low spool will encounter. Analysis indicates that neither form of flutter will occur.

Although the integrated core/low spool is not scheduled for bird ingestion testing, the fan blade was analyzed for resistance to bird strikes. Results showed that the blade design satisfies the criteria for both parameters.

Fan Disk Hub and Blade Attachment

The fan disk hub is sized to keep the coupled blade/disk vibratory mode out of the engine operating speed range. Burst margin and maximum stresses were calculated at the redline speed of 3902 rpm. Blade attachment and snap ring stresses are well within design limits. Principal stresses and lives are summarized in Table 4.2.4-V. Analysis indicated that a single fan blade failure would not lead to multiple blade failures (i.e., the following blade could absorb the energy of the failed blade without, in turn, failing).

TABLE 4.2.4-V

DISK STRESS AND LIFE SUMMARY

	Shrouded Blade
Average Tangential Stress, MPa (ksi)	339.2 (49.2)
Rim	
Tangential Stress, MPa (ksi)	305.4 (44.3)
Radial Stress, MPa (ksi)	56.5 (8.2)
Low Cycle Fatigue Life, Cycles	10^5
Inner Bolt Circle	
Tangential Stress, MPa (ksi)	151.6 (22)
Radial Stress, MPa (ksi)	8.2 (1.2)
Low Cycle Fatigue Life, Cycles	10^5
Outer Bolt Circle	
Tangential Stress, MPa (ksi)	89.6 (13.0)
Radial Stress, MPa (ksi)	200.6 (29.1)
Low Cycle Fatigue Life, Cycles	10^5
SNAP - Concentrated Stress, MPa (ksi)	187.5 (27.2)
Low Cycle Fatigue Life, Cycles	10^5
Hub - Bending Stress, MPa (ksi)	389.5 (56.5)
Low Cycle Fatigue Life, Cycles	10^5

Stub shaft and Bearing Support

The stub shaft and bearing support are designed to satisfy a blade loss moment load at the No. 1 bearing location. In addition, the stub shaft accommodates a torque load and an axial load forward and rearward of the No. 1 bearing.

Case

The fan case meets buckling and bending load requirements at a 3902 rpm redline speed and a blade loss moment in the plane of the blades. Four coincidence rings are included on the case to provide a coincidence frequency margin at the redline speed.

4.2.5 Differences Relative to the Flight Propulsion System

Only minor differences exist between the fan configuration in the integrated core/low spool and the flight propulsion system. These differences are essentially all mechanical or materials substitution in nature and have no impact on the basic aerodynamic definition.

In the flight engine, an advanced titanium alloy (PWA 1215) is used for the hub material. Fiberglas® is also specified for the nose cone and end cap for an additional weight savings. Also, to meet the life requirements for the flight engine, both the Nos. 1 and 2 bearings require a larger diameter. This would, in turn, necessitate a redesign of the fan hub to stub shaft bolted joint.

The containment case for the flight propulsion system case is constructed of a Kevlar®-wrapped AMS 4150 aluminum base alloy to provide lightweight containment. Since the gearbox is core mounted on the flight propulsion system, the containment case does not have mount rings for the assessory drive gearbox.

Finally, the axial spacing behind the fan blade is greater than required. This spacing was set to accommodate the requirements of the shroudless fan blade, which was originally planned for the fan design.

4.3 LOW-PRESSURE COMPRESSOR

4.3.1 General Description

The low-pressure compressor in the integrated core/low spool is based largely on the technology in current Pratt & Whitney Aircraft commercial engines. The design of this component is shown in Figure 4.3.1-1, and the key design goals are presented in Table 4.3.1-I. The compressor consists of a four-stage, bolted rotor configuration. It is designed with recessed abradable rubstrips to reduce the sensitivity of compressor efficiency to blade tip clearance and mini-cavities to minimize recirculation losses. Aerodynamic losses are further reduced by the use of controlled diffusion airfoils. Finally, a modulated bleed is incorporated near the compressor exit to avoid surge during starting and reverser operation. Details of of the low-pressure compressor component design are contained in Reference 2.

TABLE 4.3.1-I

LOW-PRESSURE COMPRESSOR KEY DESIGN GOALS

Pressure Ratio	1.77
Adiabatic Efficiency, %	87.5
Inlet Corrected Flow, kg/sec (lb/sec)	56.97 (125.6)
Surge Margin, %	20
Low Cycle Fatigue Life, missions	1000

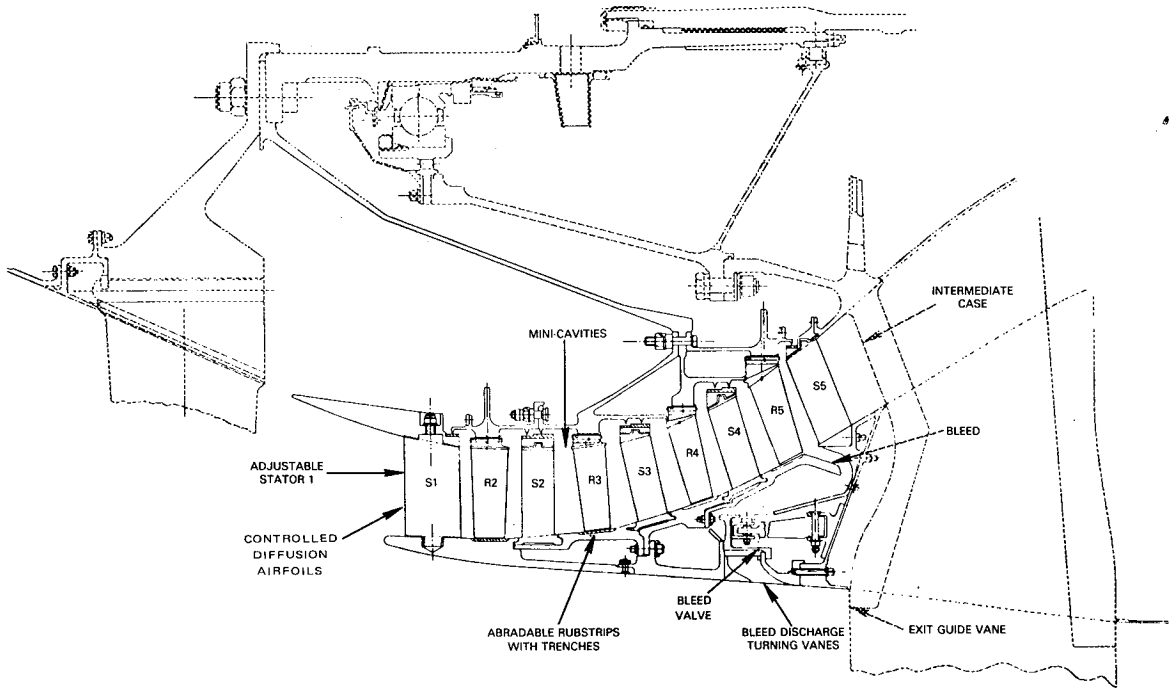

Figure 4.3.1-1 Low-Pressure Compressor Design

4.3.2 Aerodynamic Design

The low-pressure compressor aerodynamic design point is the same as for the fan component (altitude of 10,668 m (35,000 ft) and cruise Mach number of 0.8). General design parameters governing the aerodynamic design are listed in Table 4.3.2-I.

The various concepts for efficiency improvement have been verified in related technology programs. Consequently, a separate technology program was not required to substantiate the low-pressure compressor design. However, since the first test of this component is in the integrated core/low spool, an adjustable first-stage stator is included to provide flow capacity flexibility.

The compressor flowpath and the number of stages were determined from studies to optimize the compressor/intermediate case length and loading levels. The four compressor stages contain a total of 820 airfoils with an average blade aspect ratio of 2.24 and an average gap to chord ratio of 0.9. Aerodynamically, a principal benefit is derived from the low axial velocity (0.72 average flow coefficient) and the relatively high gap to chord ratio. This results in a somewhat higher aerodynamic speed and lower specific weight flow than the low-pressure compressor in the JT9D-7A reference engine.

TABLE 4.3.2-I

GENERAL DESIGN PARAMETERS
(100 Percent Speed)

Parameter	Design Point	
Inlet airflow*, kg/sec (lb/sec)	55.3	(121.9)
Rotor speed*, rpm	3921	
Pressure Ratio	1.713	
Rotor 2 tip speed*, m/sec (ft/sec)	242.3	(795)
Inlet Hub/Tip (Stator 1)	0.83	
Exit Hub/Tip (Stator 5)	0.81	
Solidity (Avg.)	1.19	
Aspect Ratio (Avg.)	2.24	
Flow Coefficient, $C_{X/U}$ (Avg.)	0.72	
Work Coefficient, E	0.65	
Reaction (Avg.)	0.60	
D-Factor (Avg.)	0.38	
$\Delta P/Po-P$ (Avg.)	0.33	

* Corrected to first-stage stator inlet conditions.

Since the low- and high-pressure spools are counterrotating, the flow at the low-pressure compressor exit is designed to be axial. This results in an increasing reaction through the compressor. The high stage reaction causes the stators to load up faster than the rotors when approaching surge. As a result, the mean solidity of the stators is larger (1.27) than that of the rotors (1.01) to achieve a loading balance at surge.

Controlled diffusion airfoils are used in all stages because of their inherent lower loss and greater incidence range capability in comparison to circular arc airfoils. The blade design, which is canted to match the contour of the flowpath, provides an increase in the root loading capability. A summary of vane and blade design characteristics is provided in Table 4.3.2-II.

Low power surge protection and reverse thrust stability are provided by a fifth-stage annular bleed. This bleed is sized to extract a maximum of 15 percent of the core flow.

4.3.3 Mechanical Design

Rotor System

The low-pressure compressor mechanical design is very similar to a JT9D design with only slight differences in size and the geometry of the interstage seals. Figure 4.3.3-1 presents a cross-sectional view of the rotor system. The major components are the disks, interstage seals and blades.

TABLE 4.3.2-II

FINAL AIRFOIL GEOMETRY SUMMARY

	Stator 1	Rotor 2	Stator 2	Rotor 3	Stator 3	Rotor 4	Stator 4	Rotor 5	Stator 5
Airfoil Series	CDA	CDA	CDA	CDA	CDA	CDA	CDA	CDA	CDA
Number of Airfoils	76	82	102	88	110	90	108	74	90
Length, cm	10.13	9.49	9.14	8.79	8.64	8.71	8.76	9.27	9.78
(in)	(3.99)	(3.74)	(3.60)	(3.46)	(3.40)	(3.43)	(3.45)	(3.65)	(3.85)
Hub/tip Ratio	0.83	0.84	0.84	0.85	0.85	0.85	0.84	0.83	0.81
Aspect Ratio	1.54	2.28	2.20	2.29	2.29	2.40	2.44	2.24	2.50
Root Radius, cm	48.52	49.58	49.75	49.50	48.65	46.91	45.00	42.16	39.32
(in)	(19.10)	(19.52)	(19.59)	(19.49)	(19.15)	(18.47)	(17.72)	(16.60)	(15.48)
Mean Radius, cm	53.80	54.51	54.33	53.84	52.73	51.16	49.15	46.79	43.99
(in)	(21.18)	(21.46)	(21.39)	(21.20	(20.76)	(20.14)	(19.35)	(18.42)	(17.32)
Tip Radius, cm	58.84	59.08	58.95	58.24	57.09	55.42	53.51	51.10	48.39
(in)	(23.17)	(23.26)	(23.21)	(22.93)	(22.48)	(21.82)	(21.07)	(20.12)	(19.05)
Root Chord, cm	6.70	4.17	4.18	3.84	3.78	3.63	3.62	4.14	3.91
(in)	(2.64)	(1.64)	(1.65)	(1.51)	(1.49)	(1.43)	(1.43)	(1.63)	(1.54)
Mean Chord, cm	6.68	4.19	4.19	3.84	3.76	3.61	3.63	4.11	3.94
(in)	(2.63)	(1.65)	(1.65)	(1.51)	(1.48)	(1.42)	(1.43)	(1.62)	(1.55)
Tip Chord, cm	6.68	4.50	4.19	3.84	3.78	3.61	3.63	4.06	3.94
(in)	(2.63)	(1.77)	(1.65)	(1.51)	(1.49)	(1.42)	(1.43)	(1.60)	(1.55)
Root Thickness/Chord	0.050	0.085	0.070	0.083	0.070	0.085	0.069	0.064	0.068
Mean Thickness/Chord	0.061	0.057	0.070	0.064	0.070	0.065	0.069	0.045	0.068
Tip Thickness/Chord	0.070	0.030	0.070	0.045	0.070	0.045	0.069	0.036	0.069
Root Camber Angle deg	39.4	43.4	40.8	35.6	34.5	43.9	47.4	43.2	58.6
Mean Camber Angle deg	22.7	18.4	22.9	20.3	27.0	22.2	36.3	18.0	42.9
Tip Camber Angle deg	22.4	27.9	36.2	25.8	39.5	28.7	50.3	26.2	56.3
Root Chord Angle deg	35.4	20.0	34.8	22.5	28.4	25.1	26.3	31.6	17.5
Mean Chord Angle deg	30.5	31.3	27.5	34.4	25.6	35.7	23.1	39.1	12.1
Tip Chord Angle deg (from axial)	30.2	42.6	32.7	45.4	31.2	47.4	29.2	47.9	15.9
Root Solidity	1.659	1.096	1.363	1.086	1.360	1.108	1.386	1.184	1.426
Mean Solidity	1.493	1.002	1.248	0.999	1.252	1.011	1.266	1.034	1.278
Tip Solidity	1.371	0.993	1.156	0.923	1.160	0.930	1.171	0.938	1.168

CDA = Controlled Diffusion Airfoil.

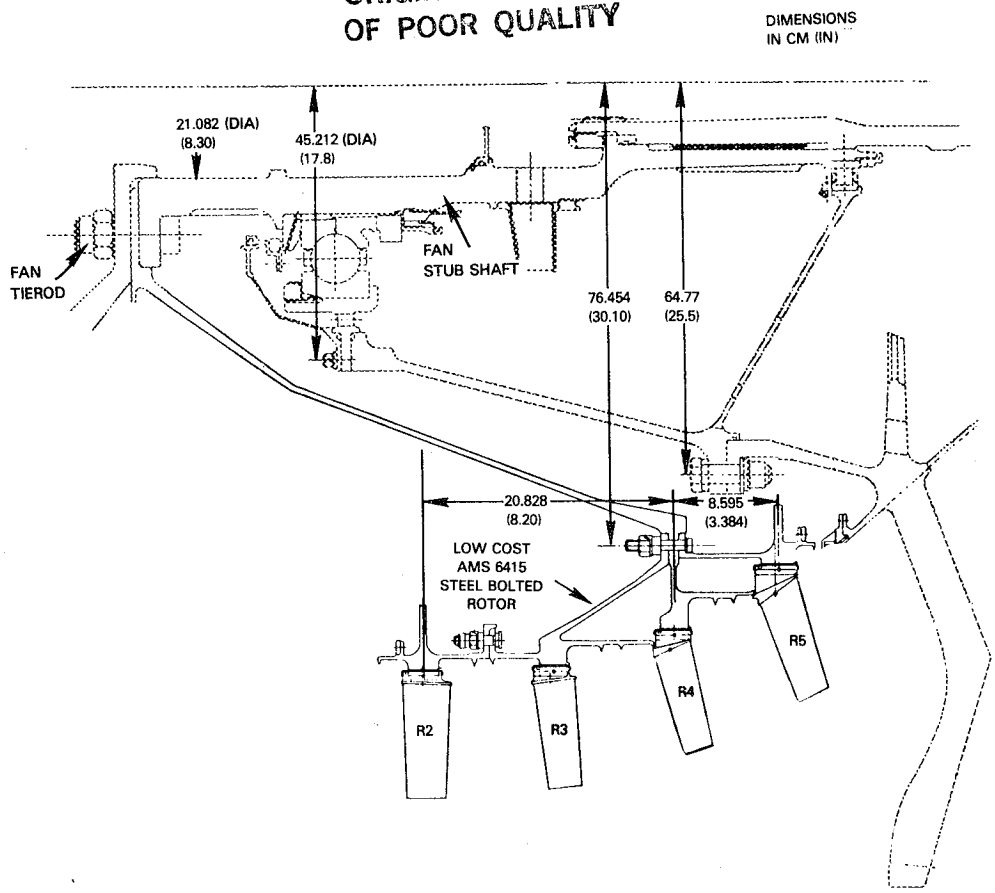

Figure 4.3.3-1 Low-Pressure Compressor Rotor System

Disk Assembly -- The rotor consists of four disks bolted together. The disk material is AMS 6415, a low alloy steel with excellent low temperature properties. As indicated in Figure 4.3.3-1, the rotor has an integral hub and disk geometry. A bolt circle is provided in the disk portion for coupling the third- and fifth-stage disks to the fourth stage. The forward section of the hub is flanged and attaches to the fan and low-pressure rotor with the fan tierods. To complete the rotor assembly, the second-stage disk is bolted to the third-stage disk at a flange located between the two stages.

The fifth-stage rotor disk contains oil drain holes. These holes allow oil to drain from the No. 1 bearing into the flowpath, thus eliminating the necessity to disassemble the rotor during the program to remove any residual oil. The rotor interstage seals are designed to minimize the cavity volume and thereby reduce recirculation losses. To lower cost, the seals are designed with the intent of reducing the number of forgings. The knife edges have a thicker cross section and are tapered radially for greater durability.

Blades -- All blades are fabricated from titanium (AMS 4928) material. To reduce bending stresses, the blades are canted and tilted towards the suction surface. The use of an existing dovetail design made it possible to use a blade lock design similar to that in JT9D engines. The locks are a two-piece construction, consisting of a retainer and lock. A rubber strip is bonded to the under side of the platform to provide a seal between adjacent blade platforms and minimize leakage. Silicone rubber is also used when the blades are being installed to seal between the disk lugs and platforms and to seal around the dovetails.

Vane and Case Assembly

The main components in the vane and case assembly are shown in Figure 4.3.3-2. These include the outer case, the vanes and the bleed system.

Case Assembly -- As indicated in Figure 4.3.3-2, the compressor case consists of six separate full rings. The case as well as the inlet splitter are fabricated from aluminum (AMS 4312). Case thicknesses are not representative of a flight weight configuration in order to minimize design and fabrication costs of the test hardware.

The case contains abradable silicone rubber rubstrips to allow the blade tips to run on line with the flowpath wall at the aerodynamic design point. These rubstrips also have shallow trenches to allow for normal operating excursions of rotor whirl, maneuver and cowl loading, although rub-in from hardware tolerances and case ovalization is permitted.

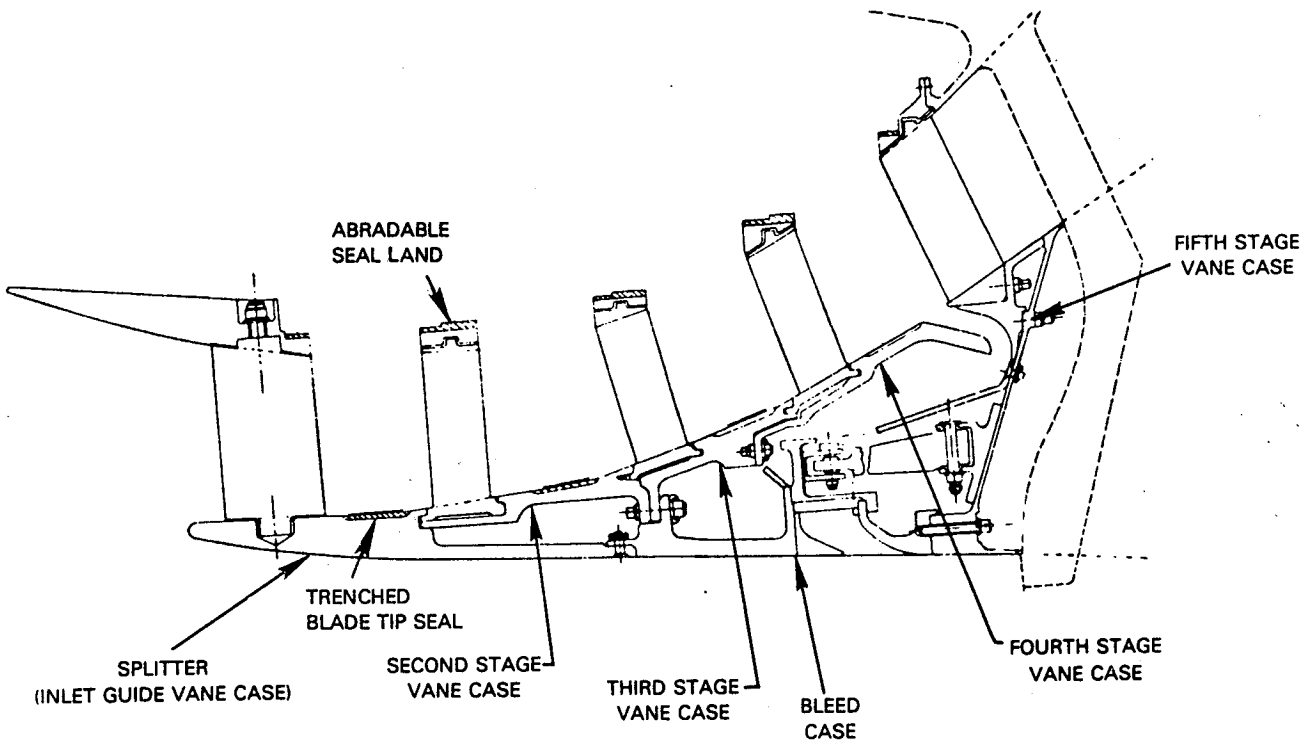

Figure 4.3.3-2 Low-Pressure Compressor Vane and Case Assembly

Vanes -- With the exception of the inlet guide vane, the typical design of the low-pressure compressor vanes is shown in Figure 4.3.3-3. The vane assemblies have individual footed vanes that are bonded in rubber to the inner shroud ring. The second-, third and fourth-stage assemblies are split into 180-degree segments to facilitate assembly, while the fifth-stage is a full ring structure. The vanes are fabricated from AMS 4312 aluminum. Silicon rubber (PWA 407) is used on the inner case surface to provide an abradable seal land for the rotor interstage knife edge seals.

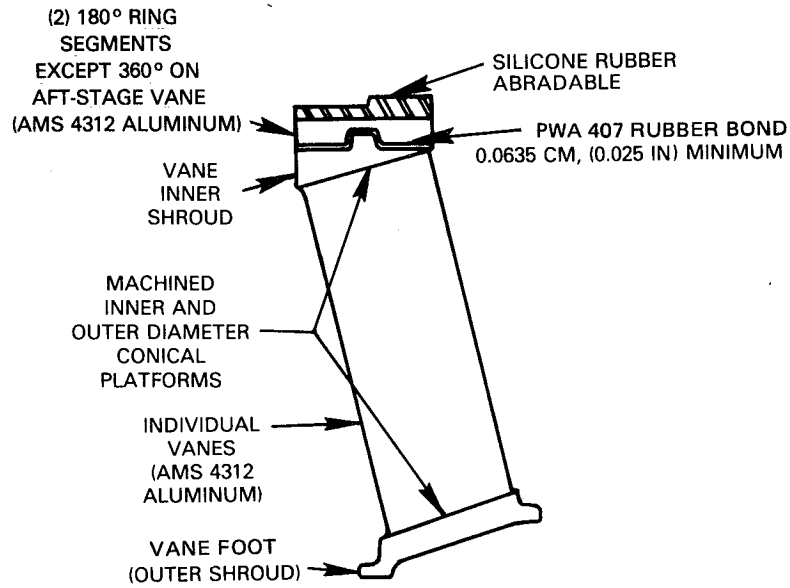

Figure 4.3.3-3 Typical Low-Pressure Compressor Vane Construction

The design of the inlet guide vane is unique to the integrated core/low spool. These vanes are individually resetable, with a 10-degree range of variability. This provides the capability to compensate for improper incidence and surge margin during the initial testing of the integrated core/low spool. The vane is designed with a redundant locking scheme for positive retention as well as with provisions for leading edge instrumentation. The airfoils are constructed from AMS 5613 steel, and both the inner and outer shrouds are AMS 4312 aluminum. Silicon rubber is also used for the abradable seal land.

Bleed System -- The low-pressure compressor bleed system design is based on the mature JT9D-7 engine station 3.0 bleed system, and uses the actuator, bearings, levers, bushings, pins, seals, and valve brackets from that engine. A circumferential gap in the outer flowpath wall ahead of the fifth-stage vane provides airflow to an annular bleed ring which translates rearward via a linkage system to allow bleed air to exit from the compressor and dump into the fan duct forward of the fan exit vanes. The bleed system is sized to extract a nominal 15 percent of the core engine flow.

4.3.4 Design Substantiation and Supporting Analyses

4.3.4.1 Predicted Performance

The predicted performance of the low-pressure compressor is summarized in Table 4.3.4-I. As indicated, the component is predicted to meet or exceed all design goals with the exception of surge margin, which is 2 percent below the goal.

TABLE 4.3.4-I

PREDICTED PERFORMANCE OF THE LOW-PRESSURE COMPRESSOR COMPONENT

	Goal	Predicted
Pressure Ratio	1.77	1.77
Adiabatic Efficiency, %	87.5	87.5
Inlet Corrected Flow, kg/sec (lb/sec)	56.97 (125.6)	56.97 (125.6)
Surge Margin, %	20	18
Low Cycle Fatigue Life, missions	1000	8000

A preliminary stability audit was conducted to evaluate the effects of destabilizing influences on surge margin. The effect of both surge line and operating line change were accounted for as functions of the stability threats. Results of a typical audit at takeoff power are shown in Table 4.3.4-II and indicate that the major destabilizing influence is engine power transients.

TABLE 4.3.4-II

TYPICAL LOW-PRESSURE SURGE MARGIN AUDIT FOR COMPRESSOR AT TAKEOFF

	Fixed Quantity (%)	Random Quantity (%)
Surge Line Degradation		
Engine Deterioration	1	$\pm$0.5
Distortion	2	0
Engine Production Clearance	0	$\pm$1.0
Operating Line Degradation		
Engine Power Transients	4	0
Control Production Tolerance	0	$\pm$1.1
Control Deterioration	0	$\pm$0.6
Engine Deterioration	2	$\pm$1.1
Engine Production Tolerance	0	$\pm$1.0
Sum of Fixed	9	---
Sum of Random	---	$\pm$2.2
Required Margin	11.2	
Available Surge Margin	16.3	

4.3.4.2 Structural/Life Analyses

All major structural elements were designed to ensure structural integrity and adequate life for experimental purposes.

Blades

The blades are balanced to minimize bending stress at the root for the low cycle fatigue limiting condition of sea level takeoff power. This stress is minimized by the tangential tilt of the airfoil. Analysis indicated that a maximum stress of only 124 MPa (18 ksi) (pressure/area plus bending) occurs at the trailing edge of the fifth-stage blade. Along with airfoil balancing accomplished by tangential tilt, the blades are balanced about the attachment. This not only accounts for centrifugal and gas loads, but also for platform, dovetail and blade lock pulls to yield a zero moment at the intersection of the "Z" plane and disk centerline.

Blade resonance diagrams are shown in Figures 4.3.4-1 through 4.3.4-4. Critical engine order resonances include the low orders (2E, 3E, and 4E), vane passing order in each stage and the 10th (10E) and 20th (20E) in the fifth stage for the intermediate case strut order. As shown, all stages have adequate resonance margin at both redline and minimum cruise speeds, and all critical resonances are out of the idle speed regime. Flutter margin is also adequate for all blades. An analysis of the blade attachment design verified that stresses are acceptable, as indicated in Table 4.3.4-III.

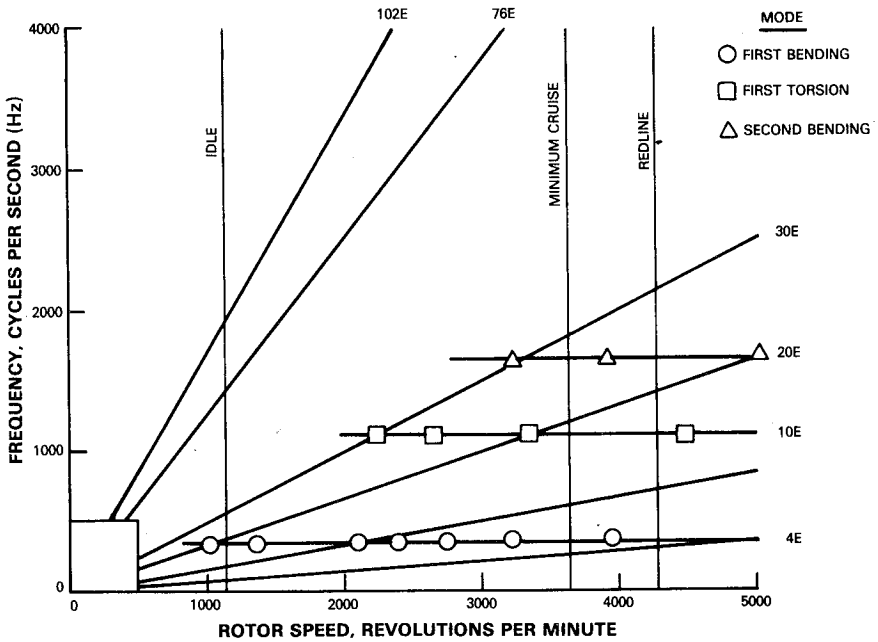

Figure 4.3.4-1 Second Stage Blade Resonance Diagram

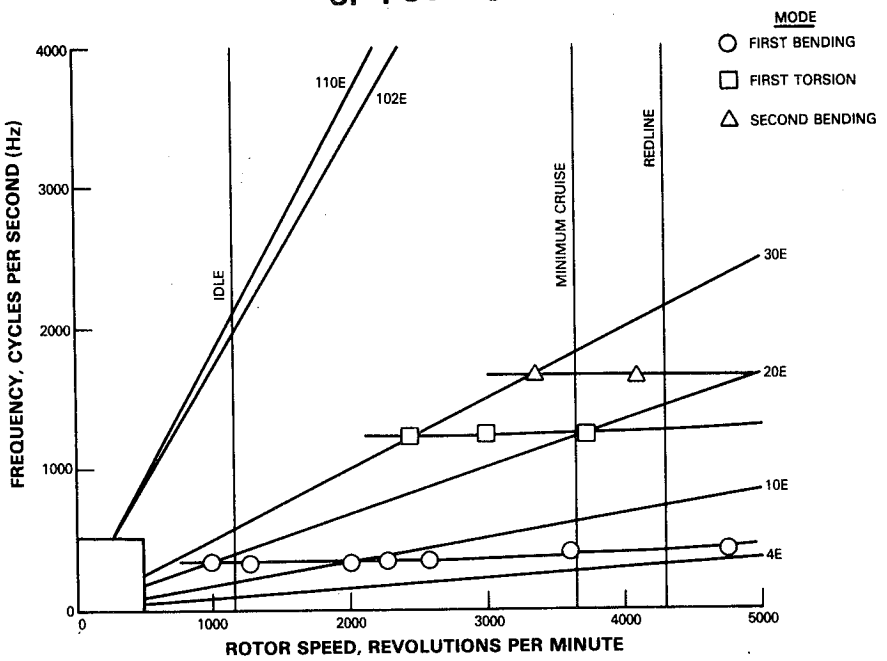

Figure 4.3.4-2 Third Stage Blade Resonance Diagram

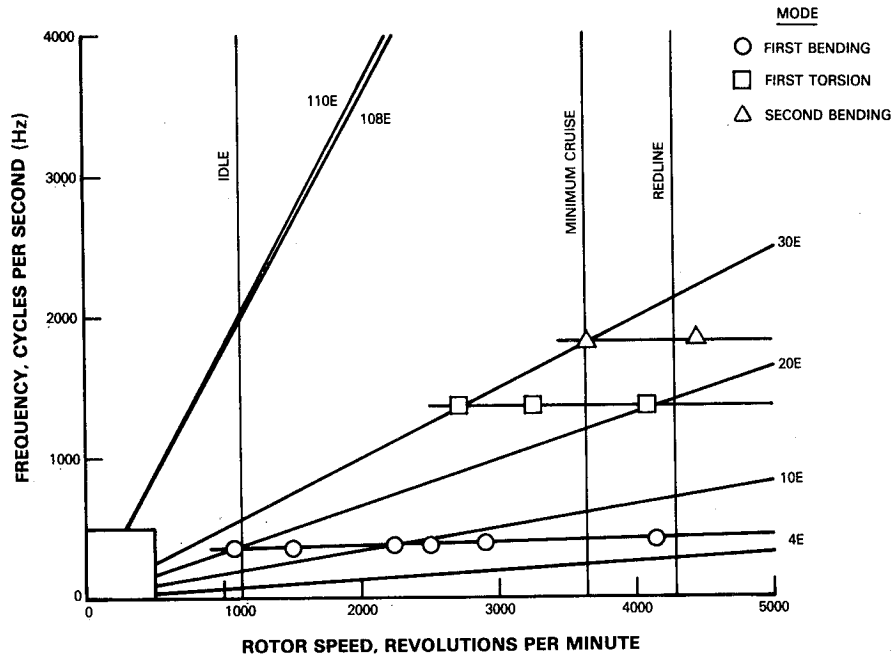

Figure 4.3.4-3 Fourth Stage Blade Resonance Diagram

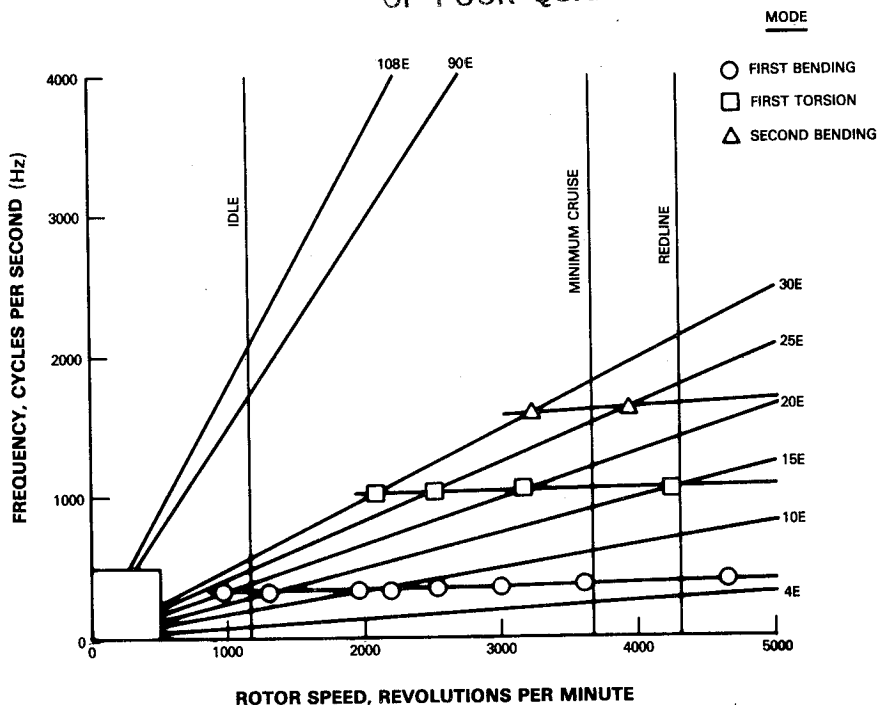

Figure 4.3.4-4 Fifth Stage Blade Resonance Diagram

TABLE 4.3.4-III

ATTACHMENT STRESS SUMMARY
MPa (ksi)

	Rotor 2	Rotor 3	Rotor 4	Rotor 5
Blade Neck Tensile	24.1 (3.5)	24.8 (3.6)	25.5 (3.7)	23.4 (3.4)
Lug Neck Tensile	13.8 (2.0)	15.9 (2.3)	20.7 (2.3)	16.5 (2.4)
Blade Bending	42.7 (6.2)	26.2 (3.8)	26.9 (3.9)	41.4 (6.0)
Lug Bending	23.4 (3.4)	27.6 (4.0)	28.3 (4.1)	25.5 (3.7)
Blade Combined	67.6 (9.8)	51.0 (7.4)	52.4 (7.6)	64.1 (9.3)
Lug Combined	52.4 (7.6)	59.3 (8.6)	60.7 (8.8)	49.6 (7 2)
Blade-Lug Bearing	82.1 (11.9)	67.6 (9.8)	69.6 (10.1)	78.6 (11.4)
Blade Shear	25.5 (3.7)	18.6 (2.7)	19.3 (2.8)	24.1 (3.5)
Lug Shear	15.9 (2.3)	17.9 (2.6)	18.6 (2.7)	17.9 (2.6)

Rotor

Rotor stresses were calculated for conditions at: (1) sea level takeoff on a 28°C (84°F) day, (2) the aerodynamic design point, (3) single blade loss in the second-stage rotor at takeoff, and (4) single blade loss in the fifth-stage rotor at takeoff. These analyses were directed towards identifying stress levels as well as deflection patterns, axial and radial growths of disk rims, snap diameter compatibilities, effects of blade loss on rotor stresses, and low cycle fatigue lives of the disks. A summary of the calculated stresses and lives is presented in Table 4.3.4-IV. Figure 4.3.4-5 shows representative bending stresses, including the maximum rotor stress at 198 MPa (28.8 ksi). All stresses and lives meet integrated core/low spool test requirements.

TABLE 4.3.4-IV

SUMMARY OF DISK STRESSES AND LIVES

Rotor	Average Tangential Stress MPa (ksi)	Radial Stress, MPa (ksi) Bore	Bolt Circle	Rim	Low Cycle Fatigue, Cycles Bore	Bolt Circle	Rim
2	344 (49.9)	40.9 (5.9)	-----	9.41 (1.4)	10,000	-----	10,000
3	338 (49)	19.1 (2.8)	-----	10.2 (1.5)	10,000	-----	10,000
4	267 (38.7)	14.5 (2.1)	28.6 (4150)	11.1 (1.6)	100,000	80,000	100,000
5	296 (42.9)	8.75 (1.3)	-----	10.5 (1.5)	100,000	-----	100,000
2-3	391 (56.9)	-----	37.7 24.4 (5.5) (3.6)	-----	-----	8000	-----

Notes:

Stress levels are based on takeoff condition.
At bolt circle locations, the most limiting design stresses are accounted for.

A blade loss analysis indicated only a slight increase in the rotor stress level. Analysis showed a maximum bending stress of 276 MPa (40 ksi) when blade loss was assumed in either the second or fifth-stage rotor. The maximum stress in the rotor tie bolts was 13.8 MPa (2 ksi).

Stress levels in the disk lug attachments from blade pulling forces are low and consistent with the conservative nature of the rotor design. A vibration analysis of the rotor interstage seals indicated that all seals have frequency margins in excess of 200 percent.

Cases

The calculated maximum bending stress and hoop stress in any of the cases is 68.9 MPa (10 ksi) and 165 MPa (24 ksi), respectively. These levels are well within the design limits. Stresses resulting from reaction loads in the vane hook are also low and well within allowable limits. Analysis showed that all four vane cases have acceptable blade containment capability. The effect of second-stage blade loss was an increase in stress at the bleed case/intermediate case junction. However, stress levels remained well within design allowables.

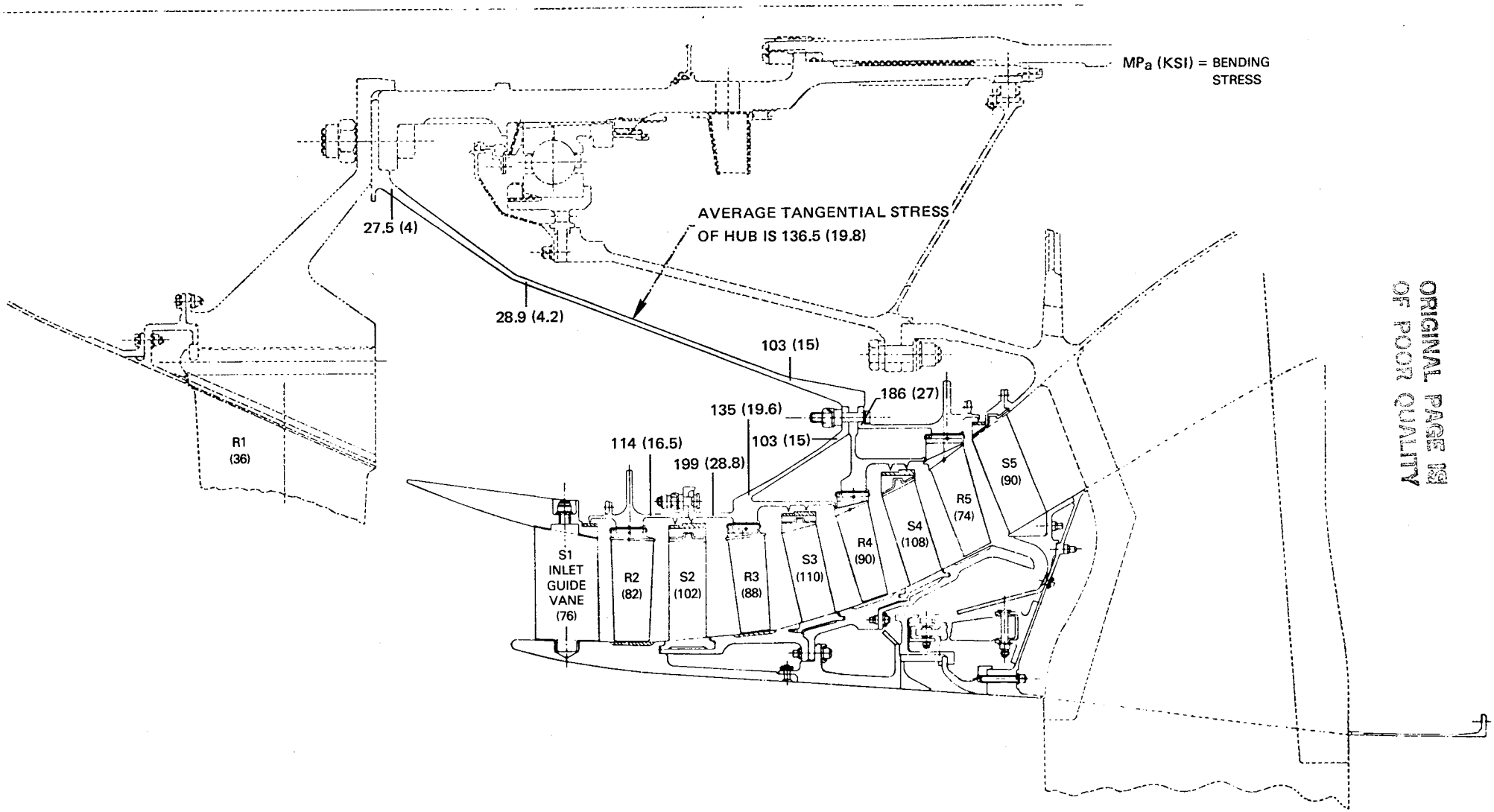

Figure 4.3.4-5 Low-Pressure Rotor Bending Stresses

Vanes

The inlet guide vane was analyzed for resonance to ensure that fan blade passing order frequencies (36E) would be out of the integrated core/low spool operating range. The resonance diagram in Figure 4.3.4-6 shows that an adequate margin of 7 percent exists in the first coupled mode at the redline speed with a 20 percent margin in the first bending mode at idle. First torsion and bending mode resonances occur between idle and minimum cruise and the first coupled mode has sufficient margin above the redline speed. The maximum calculated stress is 14.3 MPa (2.1 ksi) at the leading edge at sea level takeoff, which is well within allowables. Neither bending nor torsional flutter is predicted to occur in this vane.

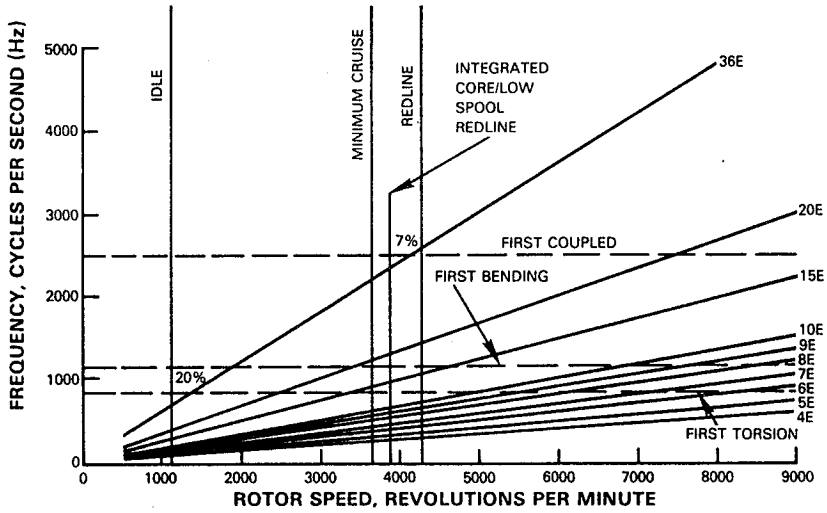

Figure 4.3.4-6 Low-Pressure Compressor Inlet Guide Vane Resonance Diagram

The vanes in the remaining stages were analyzed for stress and axial deflection resulting from gas loads. The results are summarized in Table 4.3.4-V. Both stress levels and deflections are well within the design limits. Also, on the basis of a flutter analysis, neither bending nor torsion flutter is predicted to occur at any engine operating condition.

TABLE 4.3.4-V

LOW-PRESSURE COMPRESSOR STATOR STRESSES AND DEFLECTIONS

Stator	Maximum Stress, MPa (ksi)	Edge	Axial Deflection, cm (in)
2	108 (15.7)	Trailing	0.086 (0.034)
3	54 (7.9)	Leading	0.028 (0.011)
4	31 (4.5)	Leading	0.003 (0.001)
5	32 (4.7)	Leading	0.005 (0.002)

4.3.5 Differences Relative to the Flight Propulsion System

The low-pressure compressor in the flight propulsion system retains the same aerodynamics, although certain changes are required to the mechanical configuration. The rotor system in the flight engine is a drum configuration, as opposed to the bolted design in the integrated core/low spool. The material is AMS 4928, which is a titanium alloy. The rotor drum does not contain the oil drain holes in the bolted rotor design.

In the static structure, the cases are optimized for weight. Also, the inlet guide vane is a fixed rather than a variable geometry airfoil, and the material is AMS 4312 aluminum for lighter weight. Because of the anti-icing requirements for the flight engine, the inlet guide vanes are a hollow construction. The hollow construction necessitates a low aspect ratio airfoil design.

4.4 COMPRESSOR INTERMEDIATE CASE

4.4.1 General Description

The compressor intermediate case supports the fan and high-pressure compressor rotors, forms the low- to high-pressure compressor flowpath and provides the front mount locations. In addition, it contains the provisions and plumbing for the towershaft and accessory drive components.

The intermediate case, integrated between the low- and high-pressure compressors, is shown in Figure 4.4.1-1. The case assembly consists of three concentric annular cases with an array of both structural and nonstructural fan exit guide vanes.

4.4.2 Aerodynamic Design

The intermediate case comprises two distinct flowpath sections. These include the fan duct and the core sections.

The fan duct flowpath is designed to decelerate the fan discharge flow from a Mach number of 0.67 to 0.49 within a constant diameter outer wall annular passage. It is also designed to remove the swirl, minimize the upstream influence of pylon blockage and provide sufficient choke margin to pass the part power flow requirement. The case has an array of 10 structural struts and 19 nonstructural exit guide vanes, all of which are controlled diffusion airfoil sections to provide greater incidence range and loading capability. Both structural and nonstructural vanes have identical aerodynamic contours. As discussed in Section 4.2.2, the vane array is pylon matched to minimize backpressurizing effects on the fan rotor.

The core section provides the transition between the low- and high-pressure compressor flowpaths while maintaining a nonseparated flow field. This is accomplished by designing the flowpath with a curvature that controls the wall static pressure gradient plus the use of 10 nonturning struts. A cross section of the flowpath is shown in Figure 4.4.2-1 along with the corresponding wall diffusion loadings. The maximum diffusion occurs on the inner wall and is well within Pratt & Whitney Aircraft experience. The outer wall has continual acceleration over the entire length.

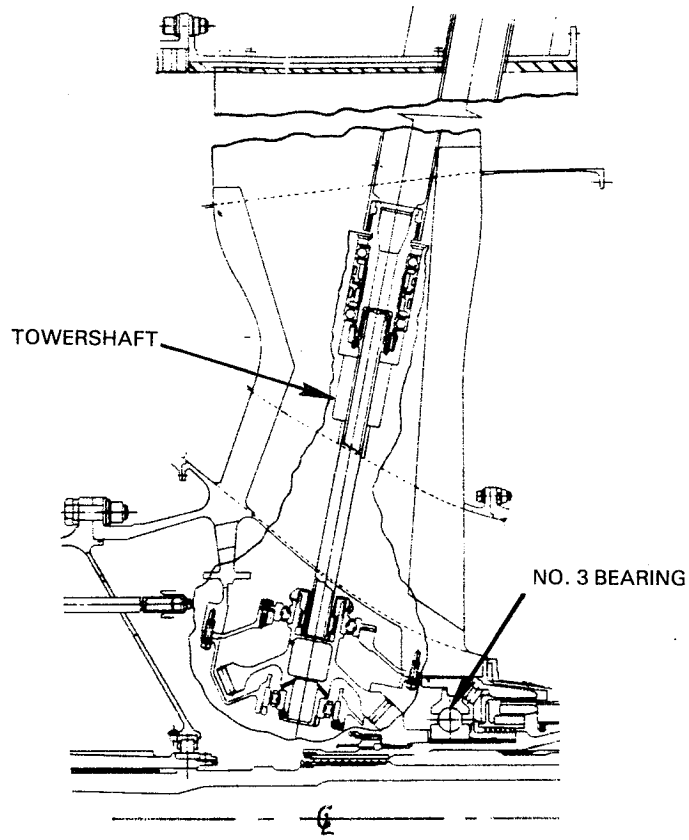

Figure 4.4.1-1 Compressor Intermediate Case

The structural struts in the core section are a combination of 65 circular arc and 400 series airfoils -- 65 circular arc series between the leading edge and maximum thickness point and then 400 series to the trailing edge.

4.4.3 Mechanical Design

The major components of the compressor intermediate case are the case and strut subassembly, No. 3 bearing and accessory drive system. Design details of the No. 3 bearing and accessory drive system are contained in Sections 5.4 and 5.5, respectively.

Case and Strut Subassembly -- The intermediate case assembly is shown in Figure 4.4.3-1. It consists of three major cases. The inner case forms the inner core flowpath wall and supports the Nos. 1, 2 and 3 main shaft bearings, plus the accessory drive towershaft. A center case forms the outer core flowpath wall as well as the inner fan duct wall. This case carries low- and high-pressure compressor case loads, case pressure loads, fan duct loads, and engine torque loads. The outer wall of the fan duct is formed by the third case. This case supports the top mounted accessory gearbox and the outer ends of the structural struts. Outer fan duct loads and loads associated with nacelle moments are carried by this case. Both the inner and center cases are made of titanium (AMS 4928) and the outer case is constructed from an aluminum alloy (AMS 4135).

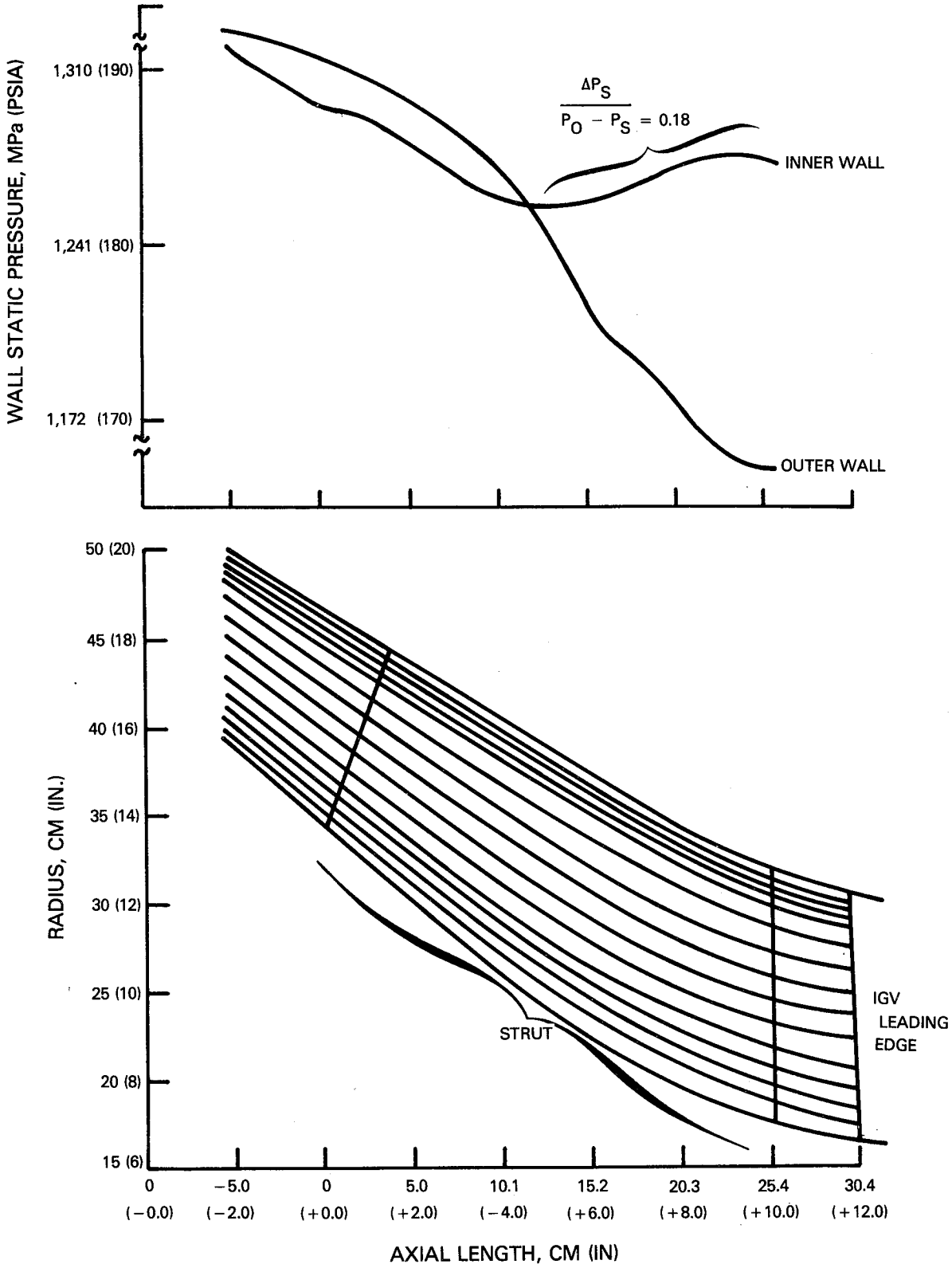

Figure 4.4.2-1 Intermediate Case Core Section Flowpath and Wall Static Pressure Distribution

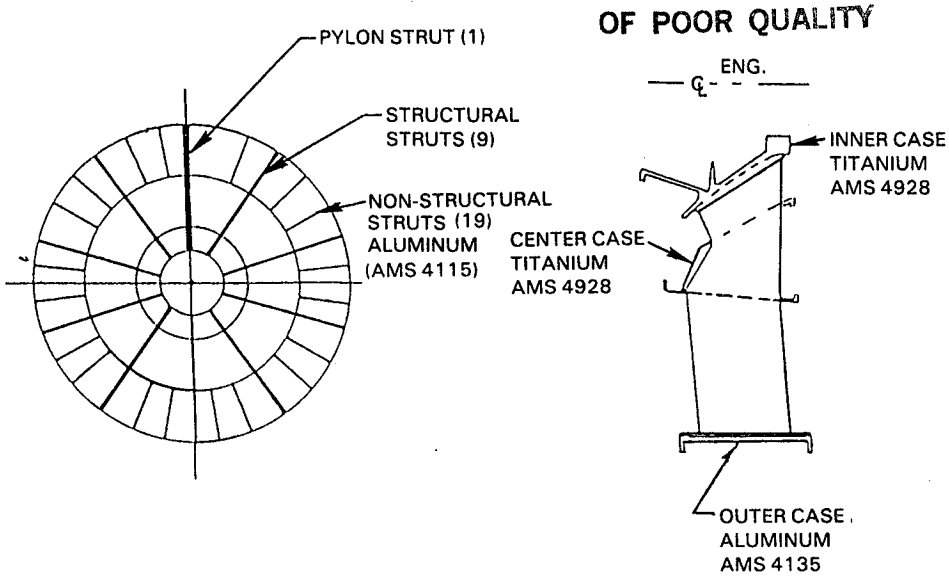

Figure 4.4.3-1 Intermediate Case Assembly

The core cases are connected to the fan cases by ten structural struts constructed from titanium (AMS 4928). The struts are hollow to reduce weight as well as provide passages for the accessory drive towershaft and lubrication system plumbing. The airfoil section in the core gaspath is uncambered, while the section in the fan duct is cambered to satisfy aerodynamic requirements. The topmost strut forms the forward portion of the pylon and, consequently, is thicker than the other struts. This strut, as shown in Figure 4.4.3-2, is sized to contain the towershaft and aerodynamically fair the leading edge into the pylon. The outer portion of this strut is hollow, while the inner portion is solid.

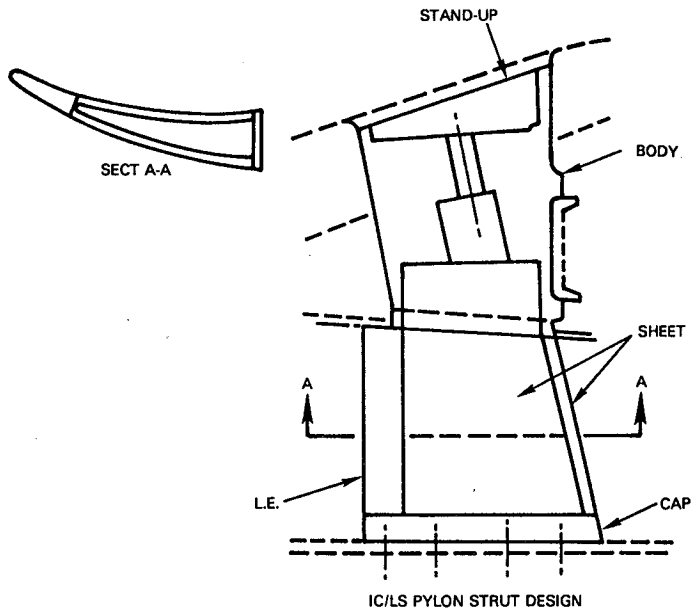

Figure 4.4.3-2 Integrated Core/Low Spool Pylon Strut Design

The 19 nonstructural exit guide vanes are mounted in the fan duct and are generally located in groups of two between the ten structural struts. However, the vane immediately adjacent to the pylon on the convex side was eliminated during pylon matching in order to reduce flow area blockage. These vanes are made from a wrought aluminum base alloy (AMS 4115).

No. 3 Bearing -- The No. 3 bearing is an under-race cooled configuration and is lubricated by oil supplied to an axial scoop. The bearing is fabricated from M50 steel alloy. A titanium alloy (AMS 4928) is used for the outer bearing support, the support structure for the static portion of the rear labyrinth seal and the damper spring.

Accessory Drive System -- Accessory power is obtained from the front of the high-pressure rotor shaft by an integral bull gear, spiral bevel pinion shaft gear and towershaft. The towershaft gears and the shafts are made of wrought steel alloys. Bearings are constructed of M50 steel alloy.

4.4.4 Design Substantiation and Supporting Analyses

The intermediate case was analyzed in terms of different types of loading effects on deflections and stresses. The following types of loads were considered in these analyses: (1) inlet and outer fan case gust, (2) inner fan duct, (3) thrust, (4) aerodynamic loads on the struts, (5) fan blade loss, (6) low- and high-pressure rotor support, (7) accessory drive towershaft support, and (8) low and high-pressure compressor case.

Cases

Gust and thrust loadings were analyzed using finite element and other conventional structural analyses. Results showed that static loads imposed during maximum thrust operation will not cause in excess of 0.01 cm (0.004 in) radial ovalization at the inner case. Further analysis indicated the No. 3 bearing support damper will not be affected by this deflection because damping occurs at low spool speeds where inner case distortion is negligible.

A fan blade loss evaluation led to thickening of the flange and wall connections at the No. 1 and 2 bearing support interface and at the high-pressure compressor front case interface to achieve acceptable stress levels.

The impact of strut gas loads was analyzed using three-dimensional NASTRAN analysis for the center casing and more conventional calculations for the struts themselves. From these analyses, tangential case deflections resulting from loads induced by the pylon strut were obtained. Results showed center casing tangential deflection between starting and maximum thrust conditions to cause 0.330 cm (0.130 in) of outer case rotation. In addition, deflection of the pylon strut itself was estimated to cause 0.179 cm (0.070 in) of outer casing rotation. Excessive towershaft spline misalignment was avoided for the integrated core/low spool by mounting the gearbox pad 0.254 cm (0.100 in) tangentially in the direction opposite to case rotation.

Twisting of the inner casing system caused by strut-induced axial moments was also analyzed, using conventional techniques. Results showed case stiffness to be such that deflections were negligible, and no local distortions were predicted.

Structural Struts

Stresses in the structural struts were determined to be low because the overall structural stiffness of the intermediate case minimizes deflections and ensures that tight engine running clearances are maintained. A maximum stress of approximately 206.8 MPa (30 ksi) is predicted at the rear of the struts as a result of the axial loads from the high-pressure compressor case.

Nonstructural Struts

Vane stresses are of no consequence because the nonstructural struts carry only their own tangential aerodynamic loads. Strut flutter stability was also assessed and found to be adequate.

4.4.5 Differences Relative to the Flight Propulsion System

The major difference in the compressor intermediate case for the flight propulsion system is the substitution of materials to provide a more flight weight structure. Table 4.4.5-I presents a comparison of case materials for the flight engine and the integrated core/low spool.

TABLE 4.4.5-I

INTERMEDIATE CASE MATERIAL COMPARISON

	Flight Propulsion System	Integrated Core/Low Spool
Inner Case	PWA 1262	AMS 4928
Nonstructural	AMS 4911	AMS 4115
Outer Case	AMS 4150	AMS 4135

4.5 HIGH-PRESSURE COMPRESSOR

4.5.1 General Description

The high-pressure compressor, complete with the intermediate case assembly, is shown in Figure 4.5.1-1. The compressor is a ten-stage configuration, designed to produce a 14:1 pressure ratio and achieve an efficiency goal of 86.5 percent. The design features a drum rotor, extensive use of titanium in the static structure and significantly fewer airfoils than the reference engine. Variable geometry vanes are used in the first four stages and active clearance control is used in the rear stages. Internal aerodynamics are improved by the use of low loss and highly-loaded airfoils. Additional contributions to lowering system losses are made by employing recessed abradable blade tip seals and reducing interstage cavity volume.

4.5.2 Aerodynamic Design

The compressor design point is an altitude of 10,668 m (35,000 ft) and flight Mach number of 0.8. The integrated core/low spool compressor design parameters at this condition are listed in Table 4.5.2-I. For the purpose of simulating engine performance, the design pressure ratio and efficiency include intermediate case losses. Also, the corrected flow is defined at the inlet to the intermediate case.

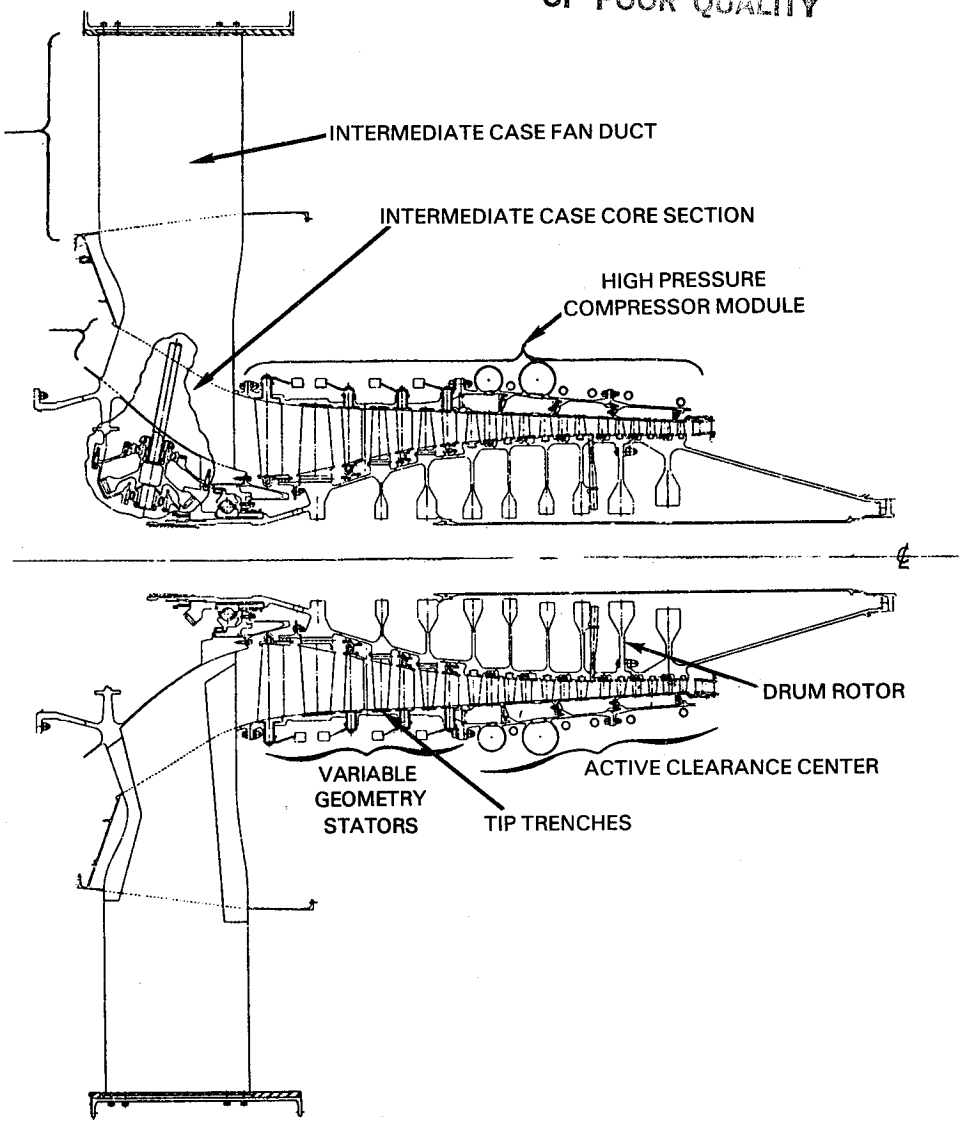

Figure 4.5.1-1 High-Pressure Compressor Cross Section

Figure 4.5.2-1 shows the flowpath of the high-pressure compressor component. The flowpath approximates a constant mean diameter with some local variation to achieve the design surge margin. At the compressor exit plane, the flowpath is canted 5-degrees outward from the centerline to aerodynamically match the diffuser and combustor section. The inlet hub/tip ratio of 0.56 represents the lowest ratio attainable within the mechanical constraints of the No. 3 bearing. The annular area distribution is set for an inlet specific flow of 17 kg/sec-m^2 (38 lb/sec-ft^2) at the first rotor leading edge with an essentially linear axial velocity decrease to a no-blockage exit Mach number requirement of 0.28.

Predicted stage loading characteristics are shown in Figures 4.5.2-2 and -3, respectively, for axial distributions of diffusion factor and static pressure. The shape potentials were derived from loading limit correlations, which indicate a higher loading potential in the rear stages than in the front stages. In both cases, the surge loadings are distributed smoothly with approximately the same shape as the predicted potential.

TABLE 4.5.2-I

HIGH PRESSURE COMPRESSOR AERODYNAMIC DESIGN PARAMETERS
(10,668 m (35,000 ft) Alt., 0.8 Mach No.)

No. of Stages	10
Pressure Ratio	14.1
Surge Margin, %	20
Inlet Corrected Airflow, kg/sec (lb/sec)	35.1 (77.5)
Inlet Corrected Tip Speed, m/sec (ft/sec)	379 (1245)
Adiabatic Efficiency, %	86.5
Inlet Hub-to-Tip Radius Ratio	0.56
Exit Hub-to-Tip Radius Ratio	0.924
Inlet Corrected Specific Airflow, kg/sec-m^2 (lb/sec-m^2)	17 (38.0)
Exit Mach No. (Without Blockage)	0.28
Average Axial Velocity-to-Wheel Speed Ratio (Cx/U)	0.559
Average Airfoil Aspect Ratio	1.52
Average Gap-to-Chord Ratio	0.89
Average Diffusion Factor	0.456
Average Endwall Loading, ($\Delta P_S/P_0-P_s$)	0.413

Including the inlet and exit guide vanes, the compressor contains a total of 1298 airfoils -- 608 blades and 690 vanes. The blades are controlled diffusion airfoils, with the exception of the first two blade rows. These blades are a multiple circular arc design to accommodate a supersonic tip Mach number on the sixth-stage rotor and a transonic Mach number at the tip of the seventh-stage rotor. Table 4.5.2-II summarizes the meanline stage average conditions.

The nonturning struts in the core section of the compressor intermediate case necessitated that the inlet guide vanes add 13 to 23 degrees of preswirling from root to tip to match the Mach number and loading requirements of the front stage blades. Consequently, this vane is a 400 series airfoil because of its large incidence range and choke margin capabilities.

Initial efficiency optimization studies resulted in a 50 percent reaction design. This reaction level results in a turning requirement of 52 degrees to remove the substantial swirl through the last vane row and permit an axial discharge. A single row of controlled diffusion exit guide vanes was selected for the design with the intent of capitalizing on the potential for short length, fewer airfoils and lower weight relative to a double row system. The exit guide vane aspect ratio was set at 0.52 and the pitch to chord ratio (tau/b) was set at 0.4 to limit the diffusion factor to an acceptable level.

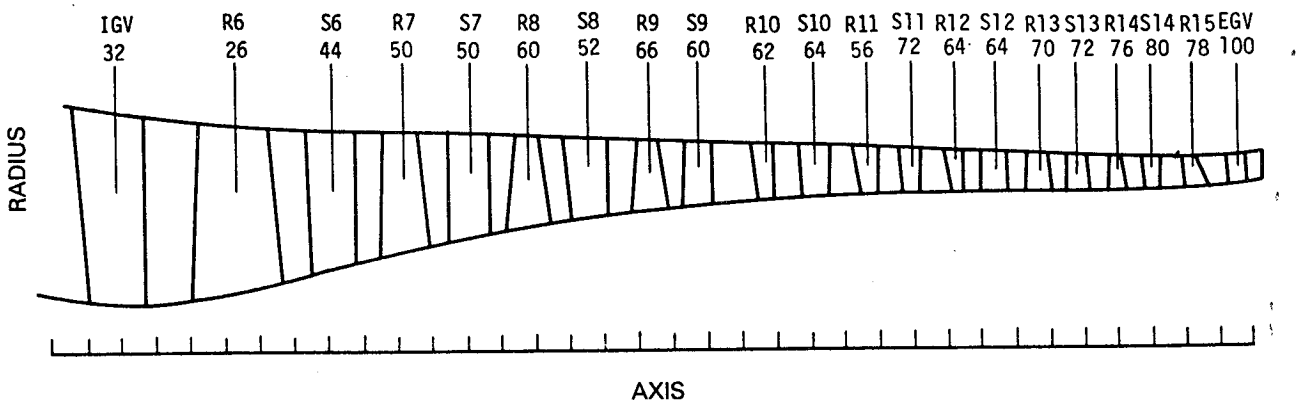

Figure 4.5.2-1 Flowpath of the High-Pressure Compressor

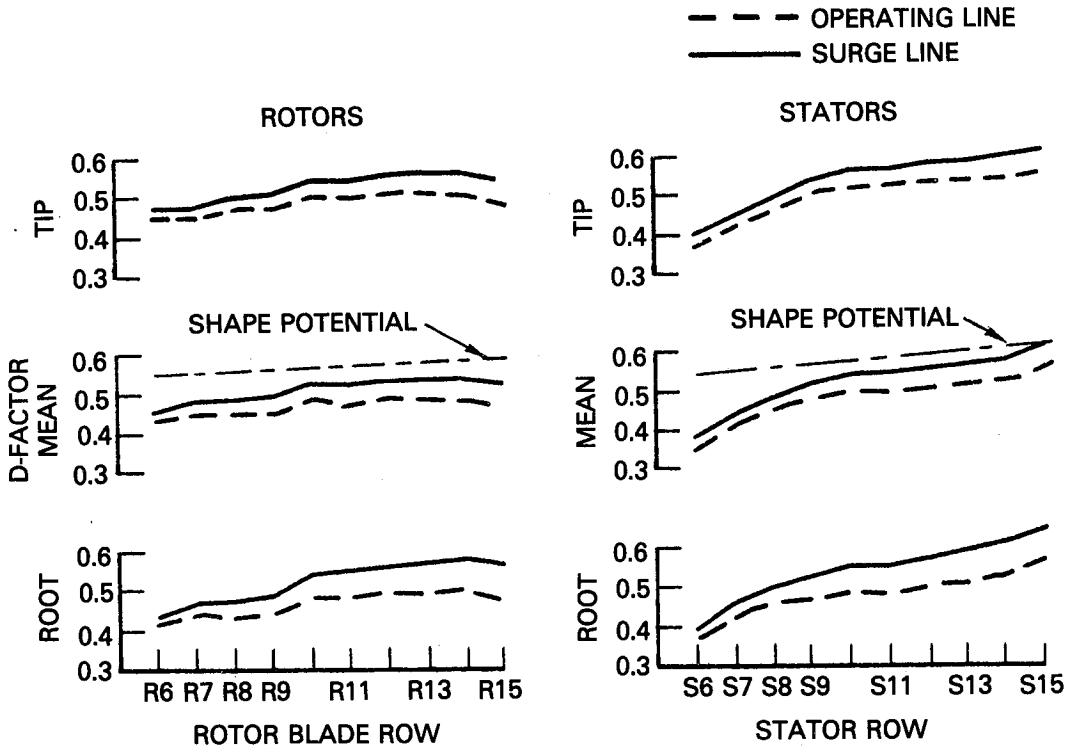

Figure 4.5.2-2 High-Pressure Compressor Diffusion Factor Distribution

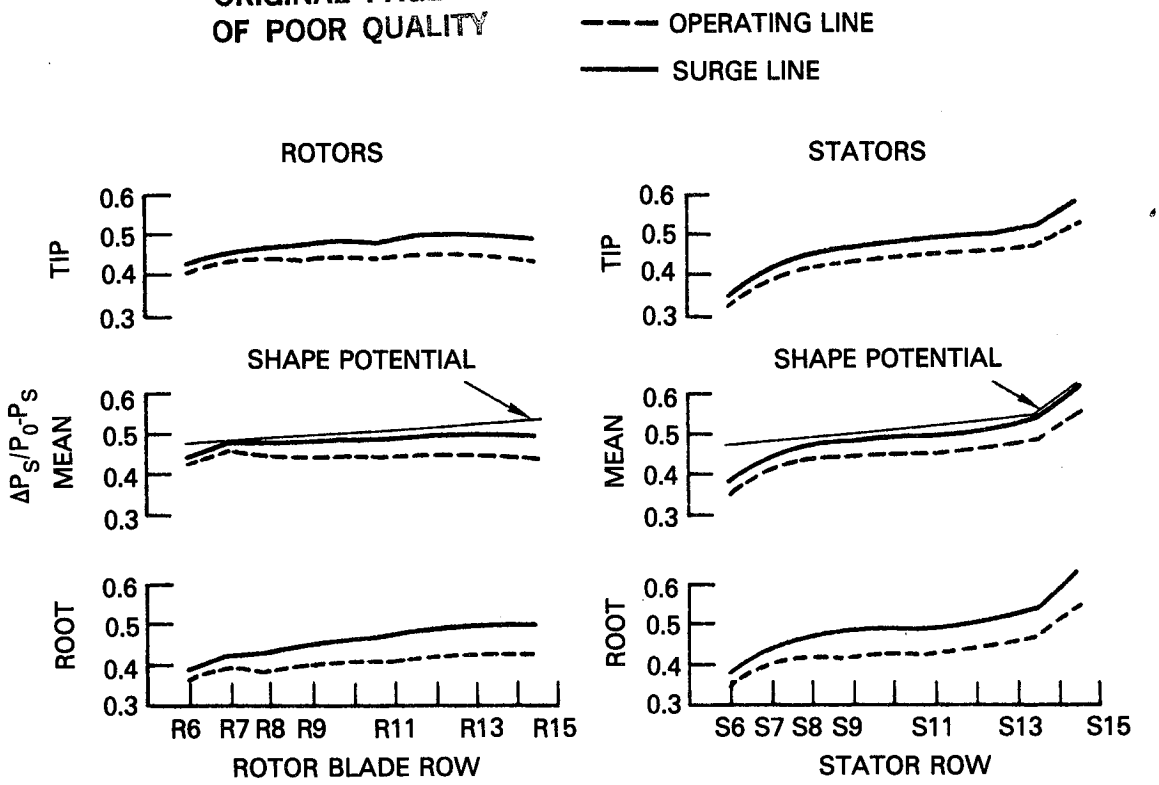

Figure 4.5.2-3 High-Pressure Compressor Static Pressure Distribution

4.5.2-II

HIGH-PRESSURE COMPRESSOR MEANLINE
STAGE AVERAGE CONDITIONS

Row	To/ T2 °C (°F)	Meridianal Velocity m/sec (ft/sec)	Swirl m/sec (ft/sec)	Cx/U	Reaction	AR	Solidity
R6	20.6 (69.1)	183.3 (601.6)	64.8 (212.6)	.613		1.52	1.42
S6		190.1 (623.8)	192.1 (630.4)	.609	.605	2.35	1.27
R7	19.6 (67.4)	199.8 (655.7)	90.6 (297.5)	.644		2.25	1.28
S7		188.5 (618.6)	209.8 (688.5)	.552	.543	2.11	1.16
R8	19.5 (67.2)	185.1 (607.3)	102.1 (335.2)	.580		2.14	1.22
S8		179.4 (588.9)	219.4 (719.9)	.525	.501	1.70	1.16
R9	19.7 (67.6)	181.5 (595.7)	101.8 (334.1)	.559		1.87	1.17
S9		176.6 (579.7)	219.8 (721.3)	.513	.501	1.74	1.04
R10	19.5 (67.1)	174.2 (571.7)	101.8 (334.2)	.533		1.70	1.00
S10		170.6 (559.9)	219.6 (720.6)	.493	.500	1.61	1.00
R11	18.3 (65.1)	168.0 (551.4)	101.4 (332.8)	.521		1.26	1.01
S11		166.5 (546.4)	218.2 (716.0)	.481	.499	1.50	1.00
R12	18.3 (65.0)	164.0 (538.1)	102.3 (335.8)	.500		1.24	1.01
S12		159.1 (522.1)	219.3 (719.6)	.466	.504	1.16	1.00
R13	15.8 (60.6)	156.7 (514.2)	102.9 (337.7)	.480		1.21	1.00
S13		150.5 (493.9)	214.3 (703.4)	.447	.500	1.16	1.03
R14	15.1 (59.3)	149.7 (491.3)	99.4 (326.4)	.461		1.18	1.01
S14		145.6 (478.0)	209.3 (686.9)	.438	.501	1.05	1.14
R15	13.3 (56.1)	145.9 (478.8)	88.8 (291.6)	.452		1.09	1.01
S15 (EV)		137.2 (450.2)	193.4 (634.8)	.424		0.52	2.50
Exit		166.4 (546.1)	0				

4.5.3 Mechanical Design

The major subassemblies of the compressor are the rotor system, front case and stator assembly, and rear case and stator assembly.

Rotor System

A cross-sectional view of the compressor rotor is shown in Figure 4.5.3-1. It consists of a titanium drum rotor from stages six through thirteen bolted to a nickel alloy (PWA 1099) tandum disk for stages fourteen and fifteen with 36 Inconel bolts (0.792 cm (0.312-in) diameter). The rotor drum is electron beam welded between each disk stage. The interstage seals are integral to the drum, with the exception of the sixth-stage knife-edge seal. In addition, the rotor features flow guides on both sides of the inner cavities in stages nine through fourteen. Details of the flow guide and interstage seal designs are also shown in Figure 4.5.3-1.

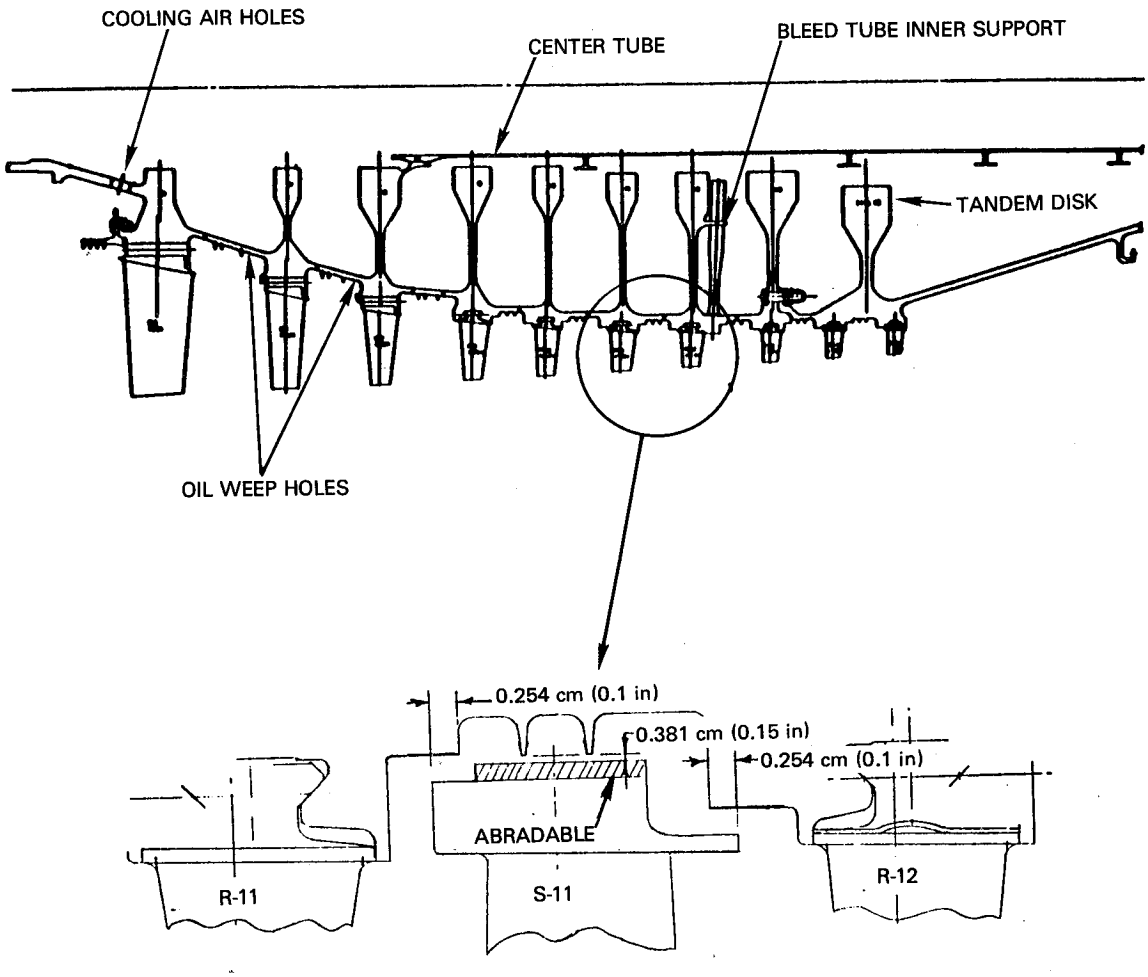

Figure 4.5.3-1 High-Pressure Compressor Rotor

Two small holes are installed in front of the seventh- and eighth-stage disks to drain any accumulated liquid. A three-piece steel center tube seals the drum from the eighth stage rearward to the high-pressure compressor/high-pressure turbine flange. Also, holes are installed in the sixth-stage hub for bore cooling air.

The compressor bleed is located behind the twelfth-stage blade. There are 22 radial bleed tubes providing a total flow area of 19.8 cm^2 (3.1 in^2). The tubes are carried on the drum rim and are supported by a flange off the bore of the twelfth-stage disk.

A summary of the compressor blade design characteristics is presented in Table 4.5.3-I. Titanium is used for the blades in the first two stages and a nickel base alloy is used in the remaining stages for fire prevention. Blade tilt is computed to give low foil edge buckling stresses at takeoff. Radial lengths are set at 0.127 cm (0.050 in) over the cold span to permit grinding in assembly to obtain accurate cold gaps.

TABLE 4.5.3-I

HIGH-PRESSURE COMPRESSOR BLADE DESIGN CHARACTERISTICS

	R6	R7	R8	R9	R10	R11	R12	R13	R14	R15
Airfoil Series	MCA	MCA	CDA	CDA	CDA	CDA	CDA	CDA	CDA	CDA
Number of Blades	26	50	60	66	62	56	64	70	76	78
Root Radius (hot) cm (in)	17.399 (6.850)	20.172 (7.942)	21.887 (8.617)	22.987 (9.050)	23.583 (9.285)	24.015 (9.455)	24.236 (9.542)	24.282 (9.560)	24.282 (9.560)	24.282 (9.560)
Tip Radius (hot) cm (in)	29.679 (11.685)	29.093 (11.454)	28.811 (11.343)	28.381 (11.174)	28.064 (11.049)	27.719 (10.913)	27.421 (10.796)	27.068 (10.657)	26.799 (10.551)	26.54 (10.450)
Root Chord, cm (in)	7.086 (2.790)	3.822 (1.505)	3.439 (1.354)	3.009 (1.1849)	2.622 (1.0323)	2.924 (1.1514)	2.569 (1.0116)	2.3111 (.90992)	2.1309 (.83895)	2.0751 (.81698)
Tip Chord, cm (in)	9.062 (3.568)	4.099 (1.614)	3.025 (1.191)	2.7241 (1.0725)	2.6271 (1.0343)	2.9255 (1.1518)	2.5664 (1.0104)	2.30883 (.90899)	2.12902 (.83820)	2.07147 (.81554)
t/b (root to tip)	.097 - .0237	.08154 - .0467	.0906 - .0454	.0974 - .0454	.1006 - .0456	.1115 - .0406	.101 - .0457	.101 - .0458	.1011 - .0461	.1007 - .0457
Chord Angle, deg (root to tip)	72.3 - 33.7	70.7 - 37.4	70.2 - 36.1	65.9 - 37.6	60.8 - 37.3	57.2 - 37.4	58.9 - 38.1	55.2 - 37.4	52.0 - 36.9	45.6 - 36.1
Tip Speed m/sec (ft/sec)	443 (1455)	434 (1426)	430 (1412)	423 (1391)	419 (1376)	413 (1356)	409 (1344)	404 (1327)	400 (1314)	396 (1301)
Broach Type	axial	axial	axial	tang.	tang.	tang.	tang.	tang.	tang.	tang.
Aspect ratio (Average)	1.733	2.332	2.000	1.786	1.697	1.258	1.235	1.206	1.181	1.089
Hub/tip (Average)	.586	.694	.761	.811	.841	.867	.884	.897	.906	.915

In stages six, seven, and eight, an axial blade attachment design is used with a 15-degree broach angle. This configuration maintains a reasonable foil overhang and meets stress ratio requirements. Sixth-stage blades are retained by a trapped tang behind the knife edge seal, while shear pin locks are employed in the seventh and eighth stages for blade retention. Tangential attachments are used in the remaining stages with turreted "in groove" locks. All tangential stages are fitted with light sheet metal ladder seals, except at the locking and loading slots.

The blades are glass bead peened to improve fatigue strength, then burnished in a cutting medium to obtain a surface quality of 20AA. Blade attachments are also shot peened and then treated for anti-galling conditioning.

Front Case and Stator Assembly

The compressor front case, shown in Figure 4.5.3-2, is an axially split design. The case is a titanium (AMS 4928) structure with bolt flanges located at the horizontal center line. Steel (AMS 5613) inserts are used under the blade tip abradable material (PWA 407 silicon rubber) to prevent a fire in the event of a severe rub or blade loss. Pressed-in bushings are used in the case to support the variable vanes. The case is designed with provisions to install blade tip clearance probes, and borescope bosses are provided at three locations.

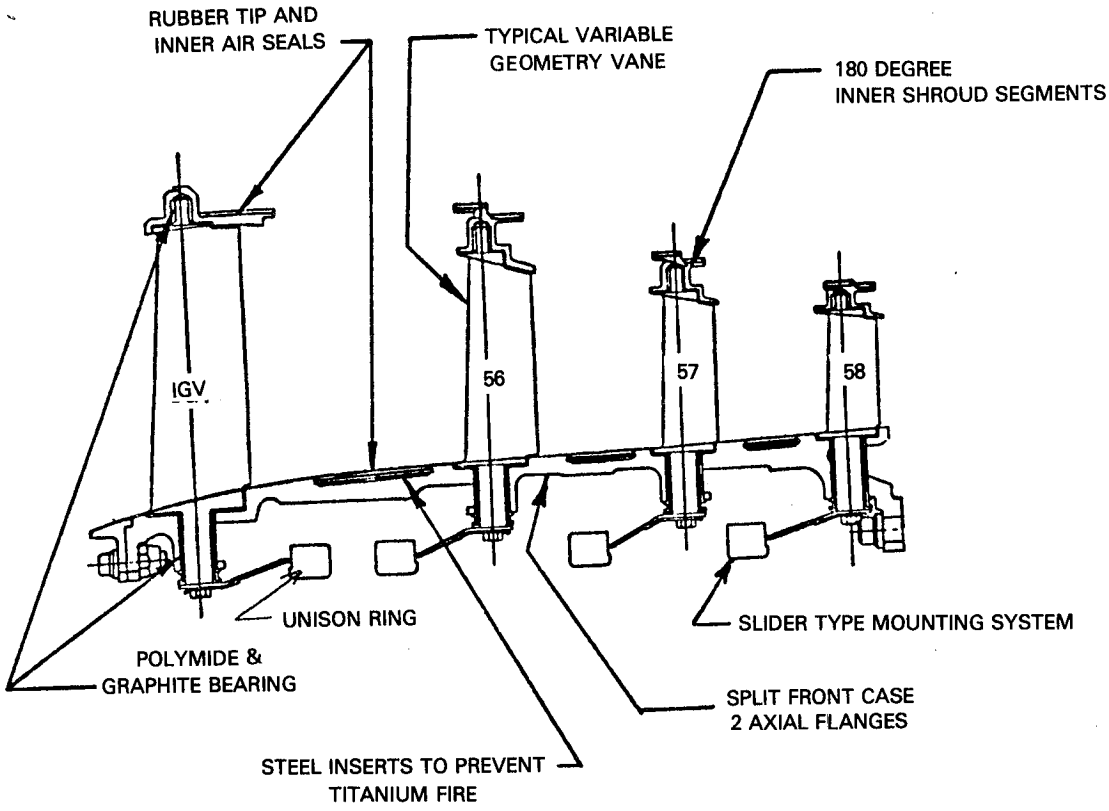

Figure 4.5.3-2 High-Pressure Compressor Front Case

The vanes are fully variable and are fabricated from AMS 5613 steel. The vane inner shroud is made of the same material and is configured as a two-piece half ring construction, pinned and bolted together. The rubstrips on the interstage seals are a silicon rubber (PWA 407) material. Design characteristics of the vanes are listed in Table 4.5.3-II.

The actuation system for the variable-geometry vanes closely resembles a production engine system. Actuation levers and aluminum unison rings with slide type mounting are used to operate the vanes. Each ring is supported in at least eight places on the case by plastic Vespel® sliders.

TABLE 4.5.3-II

HIGH-PRESSURE COMPRESSOR VANE DESIGN CHARACTERISTICS

	IGV	S6	S7	S8
Airfoil Series	400	CDA	CDA	CDA
Number of Stators	32	44	50	52
Radius, ID (hot)	16.45	18.968	21.203	22.50
cm (in)	(6.48)	(7.468)	(8.348)	(8.86)
Radius, OD(hot)	30.70	29.268	28.945	28.587
cm (in)	(12.09)	(11.523)	(11.396	(11.255)
Chord, ID	4.201	3.850	3.243	3.175
cm (in)	(1.654)	(1.516)	(1.277)	(1.250)
Chord, OD	5.458	4.922	4.097	3.982
cm (in)	(2.149)	(1.938)	(1.613)	(1.568)
t/b (Inner to	0.090	0.052	0.051	0.051
Outer Diameter)	0.090	0.090	0.090	0.0901
Chord Angle (Inner	99.1	61.0	56.6	55.0
to Outer Diameter)	104.5	51.6	47.4	45.57
Hub/tip (Avg)	0.536	0.648	0.733	0.7871
Aspect Ratio	2.61	2.09	1.89	1.53

Rear Case and Stator Assembly

Figure 4.5.3-3 shows the rear compressor case. This is a one-piece structure made from titanium to match the thermal growth characteristics of the titanium drum rotor. An extension of the Inconel 718 diffuser case provides material compatibility over the nickel alloy (PWA 1099) tandum drum rotor in stages fourteen and fifteen.

The compressor vanes in stages nine through thirteen are an iron base alloy (AMS 5616) and the vanes in the last two stages are a nickel base alloy (AMS 5662). Design characteristics of these vanes are presented in Table 4.5.3-III. Two rows of vanes are used for each shroud assembly, so only three shroud assemblies are required. A typical assembly is shown in Figure 4.5.3-4. The outer shrouds are cut into 90-degree segments and connected by hooks to the outer case. The inner shrouds are cut into three or four vane clusters to reduce stress and increase active clearance control response. Feather seals are used to seal the gap between outer diameter quarter segments and "W" seals are used to seal the case to shroud hook joints.

Manifolds for eighth-stage customer bleed air, tenth-stage start and turbine active clearance control bleed air are integral to the case design. Heat shields are incorporated in all bleed holes to minimize the possibility of titanium fires. Borescope inspection ports have been installed at every stator location, except at the eleventh stage. Also, bosses have been provided in the plane of the bore bleed tubes for rotor fixturing support during turbine assembly.

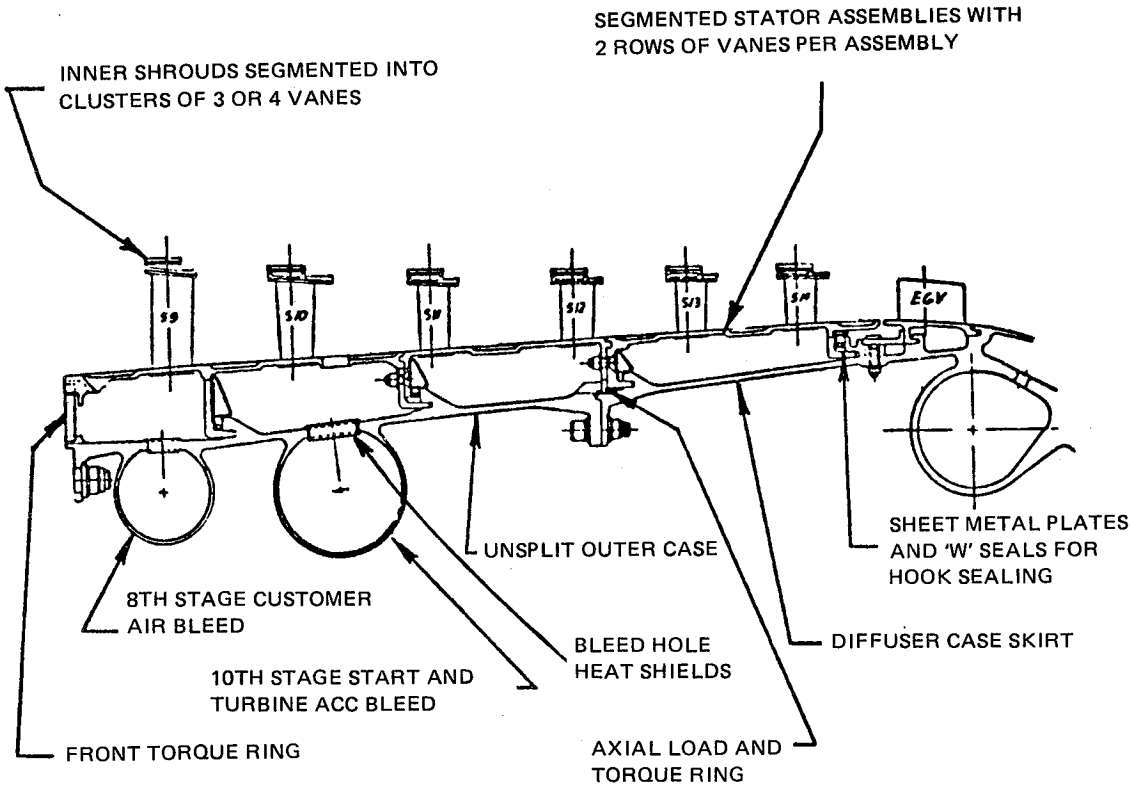

Figure 4.5.3-3 High-Pressure Compressor Rear Case

TABLE 4.5.3-III

HIGH-PRESSURE COMPRESSOR VANE DESIGN CHARACTERISTICS

	S9	S10	S11	S12	S13	S14	S15
Airfoil Series	CDA	CDA	CDA	CDA	CDA	CDA	CDA
Number of Stators	60	64	72	64	72	80	100
Radius, ID (hot), cm (in)	23.327 (9.184)	23.820 (9.378)	24.157 (9.511)	24.28 (9.56)	24.28 (9.56)	24.28 (9.56)	24.523 (9.655)
Radius, OD (hot), cm (in)	28.201 (11.103)	27.899 (10.984)	27.55 (10.85)	27.218 (10.716)	26.939 (10.606)	26.672 (10.501)	26.61 (10.483)
Chord, ID, cm (in)	2.799 (1.102)	2.540 (1.000)	2.263 (.891)	2.529 (.996)	2.291 (.902)	2.258 (.889)	3.985 (1.569)
Chord, OD, cm (in)	2.804 (1.104)	2.540 (1.000)	2.263 (.891)	2.529 (.996)	2.291 (.902)	2.258 (.889)	4.020 (1.583)
t/b (ID to OD)	.073 - .073	.070 - .071	.084 - .084	.082 - .082	.073 - .073	.071 - .071	.08 - .081
Chord Angle, deg (ID to OD)	54.5 - 44.0	52.6 - 42.6	50.6 - 42.5	47.7 - 41.6	47.1 - 41.6	49.1 - 43.8	67.0 - 71.7
Hub/tip (Avg)	.827	.854	.877	.892	.901	.910	.921
Aspect Ratio	1.74	1.61	1.50	1.16	1.16	1.06	.52

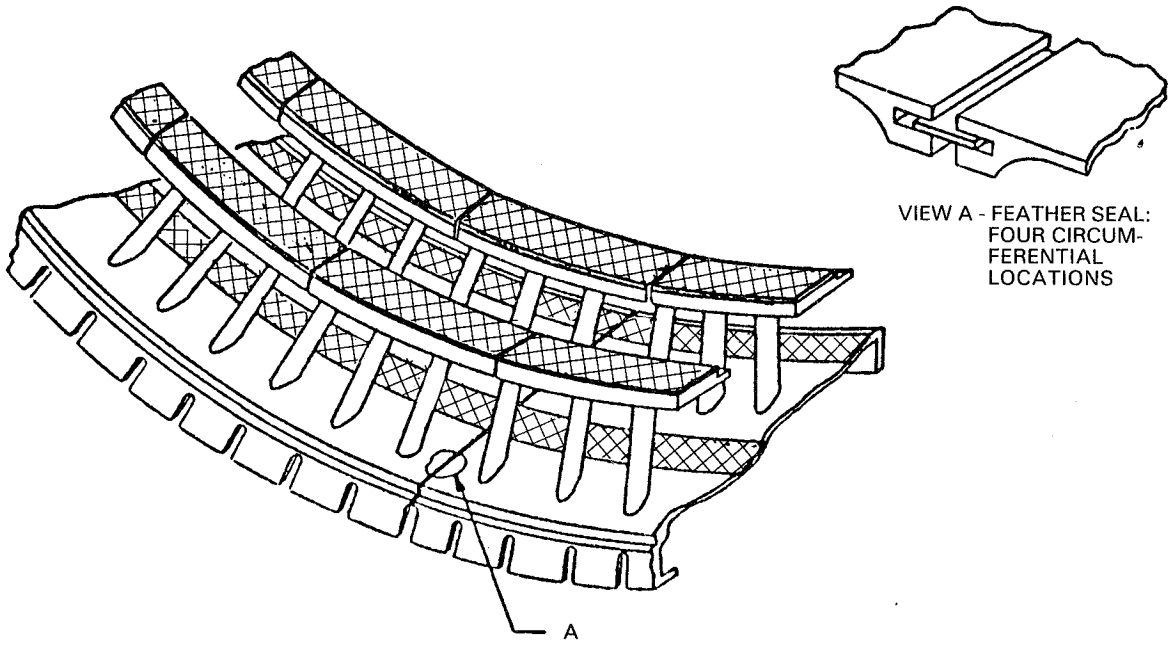

Figure 4.5.3-4 Rear Stator and Shroud Assembly

4.5.4 Design Substantiation and Supporting Analyses

4.5.4.1 Predicted Performance

Figure 4.5.4-1 shows the predicted operating map of the compressor component based on the aerodynamic definition. Initial testing of the high-pressure compressor under the full scale compressor rig test effort demonstrated an adiabatic efficiency within one percentage point of the goal, while the goals for pressure ratio and airflow were achieved. Surge margin was somewhat less than the goal, but adequate for testing the integrated core/low spool.

A stability audit was conducted at the major points in the flight envelope to establish high-pressure compressor surge margin requirements. For each of these points, the surge margin reduction resulting from surge line or operating line degradation was examined to determine the validity of the design surge margin requirement. The destabilizing factors for the high-pressure compressor include variable vane tracking errors, engine deterioration, inlet pressure or temperature distortion, control production tolerance and deterioration, and engine production tolerance. The stability audit made at takeoff is shown in Table 4.5.4-I. Results show takeoff operation to be surge-free. Similar audit results are listed in Table 4.5.4-II for the other potentially critical flight conditions. The overall audit shows that the high-pressure compressor surge margin requirement of 25 percent at the aerodynamic design point is adequate to ensure ample surge margin at all major operating conditions without the use of stability bleeds.

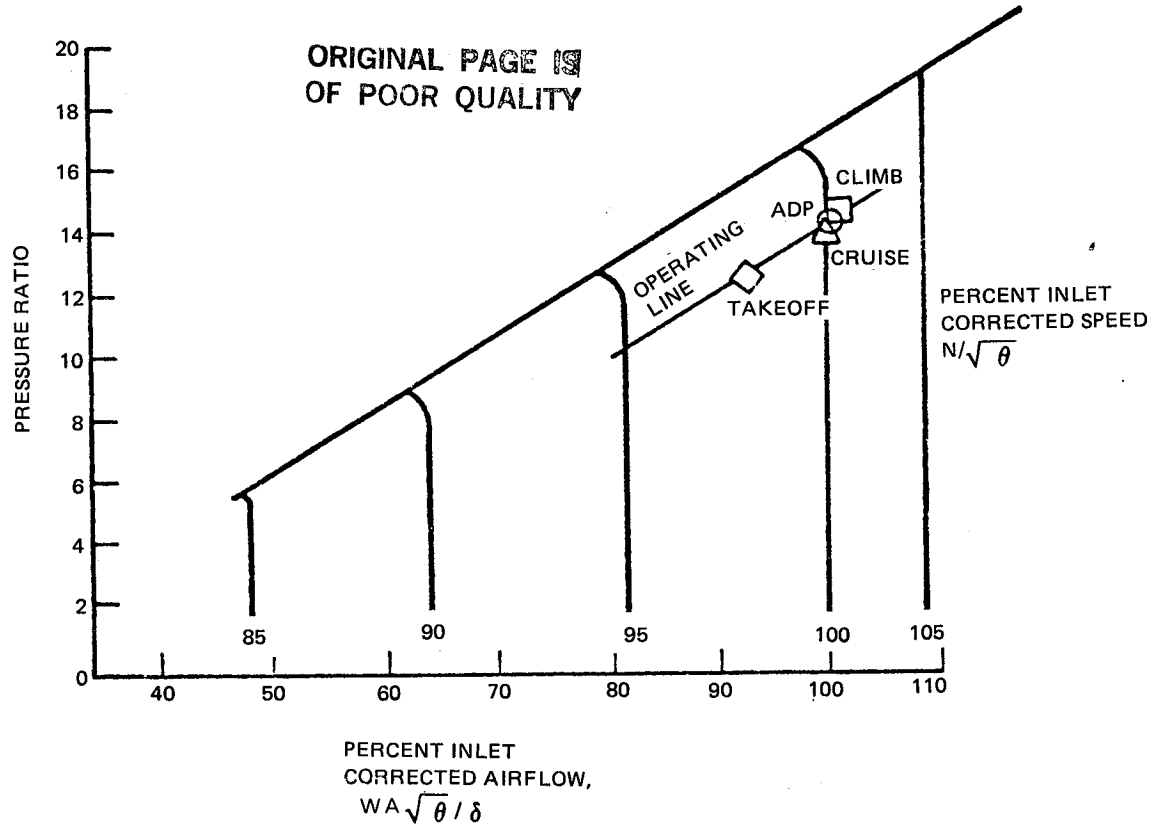

Figure 4.5.4-1 Predicted High-Pressure Compressor Operating Map

TABLE 4.5.4-I

HIGH-PRESSURE COMPRESSOR STABILITY AUDIT RESULTS AT TAKEOFF

Surge Line Degradation	Fixed Quantity (%)	Random Quantity (%)
Reynolds Number	-1.0	0
Steady State Vane Tracking Error	0	±0.9
Engine Deterioration	2.0	±1.0
Distortion	1.0	0
Engine Production Tolerance	0	±1.9
Operating Line Degradation		
Engine Power Transients	7.0	0
Control Production Tolerance	0	±1.0
Control Deterioration	0	±0.7
Engine Deterioration	0	±1.2
Engine Production Tolerance	0	±0.7
Sum of Fixed	9.0	
Sum of Random (RSS)		±3.0
Required Surge Margin	12	
Available surge Margin	21.4	

TABLE 4.5.4-II

HIGH-PRESSURE COMPRESSOR STABILITY AUDIT RESULTS AT MAJOR OPERATING POINTS

Flight Condition	% Flow	Surge Margin (%) Required	Available
Aerodynamic Design Point (1)	100	13.4	25
Idle (SLS)	37.8	18.6	23
Takeoff	95.7	12	21.4
Reverse	91.0	15.0	20.5

(1) Representative of maximum cruise and climb operation

4.5.4.2 Structural and Life Analyses

During the mechanical design, sufficient analyses were conducted on the major subassemblies in the high-pressure compression system to ensure structural integrity in the integrated core/low spool. The structural characteristics of the major components are discussed in the following sections.

Rotor System Components

Compressor disks were analyzed for plastic growth properties, low cycle fatigue life, burst margin, radial stresses, creep life, and bore fracture mechanics. Results indicated no limiting or restricting conditions. A summary of predicted rotor temperatures and stresses is presented in Figure 4.5.4-2. Table 4.5.4-III identifies the predicted stresses for the rotor tiebolt.

TABLE 4.5.4-III

TIEBOLT PREDICTED STRESS LEVELS

Stresses, MPa (ksi)	
Assembly Tensile	786 (114)
Assembly Principle Shear @ f = 0.05	503.3 (73.0)
Assembly Thread Shear (nut)	217.9 (31.6)
Separation Tensile	571.6 (82.9)
Separation Principle Shear	300.6 (43.6)
Separation Thread Shear (nut)	158.6 (23.0)
Rotor Seizure Bolt Shear	74.5 (10.8)
Low Cycle Fatigue Life, Cycles	10,000
Creep Life, cycles	10,000

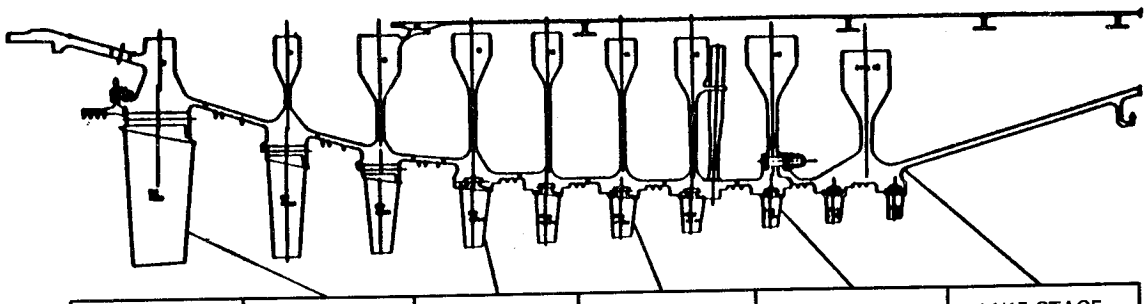

ITEM	6 STAGE	9 STAGE	11 STAGE	13 STAGE	14/15 STAGE
AVE TANG MAX STRESS MPa (ksi)	312.3 (45.3)	324.1 (47.0)	326.8 (47.4)	339.9 (49.3)	599.2 (86.9)
RIM TANG MAX STRESS MPa (ksi)	237.9 (34.5)	207.5 (30.1)	199.9 (29.0)	168.9 (24.5)	392.3 (56.9)
DISK AVE TEMP °C (°F)	111 (232)	262 (504)	336 (638)	413 (776)	465 (869)
BORE TEMP °C (°F)	95 (203)	237 (459)	297 (568)	369 (696)	382 (720)
RIM TEMP °C (°F)	118 (245)	309 (589)	416 (781)	491 (916)	555 (1032)

Figure 4.5.4-2 Rotor Temperature and Stress Summary

The rotors are tuned to avoid low order and other critical resonances between minimum cruise and redline speed. Calculations were made using a coupled bending-torsion beam analysis. Frequency margins were determined by commercial engine design practice. Particular attention was directed to the sixth and seventh stages, which were tuned to avoid a 10E (intermediate case strut order) resonance. Sufficient chord was initially included in both of these stages to avoid a 2E first mode resonance. The eighth and ninth stages were stiffened in the root area of the blade to provide margin on 3E first mode and 4E first mode resonances, respectively. The ninth stage was considered particularly critical, because of the bleed extraction immediately forward of this stage. The eleventh stage thickness to chord (tau/b) distribution was revised to provide frequency margin on an 8E first mode resonance at redline speed. This change was made to avoid a stator order of 8E in the immediate area. The remaining stages exhibited sufficient frequency margin and did not require further resonance tuning. Resonance diagrams for rotors six through nine are shown in Figures 4.5.4-3 through -6.

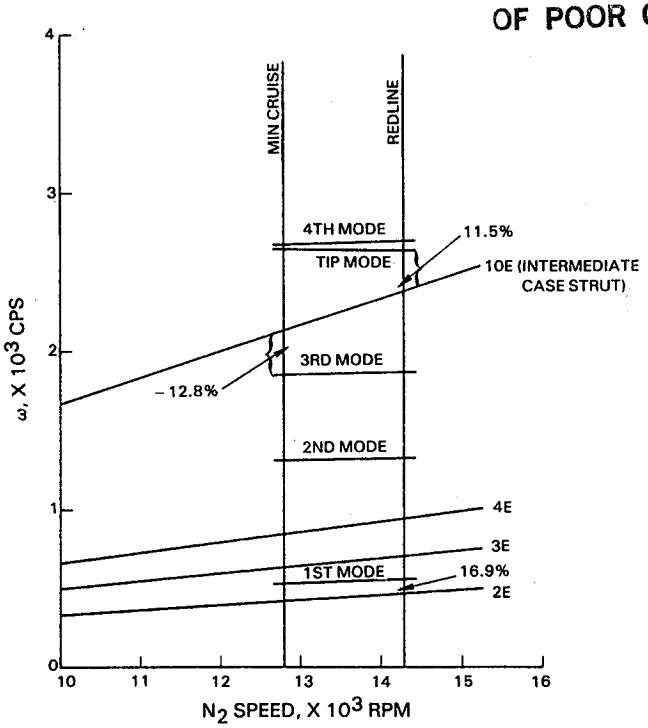

Figure 4.5.4-3 Resonance Diagram Rotor 6

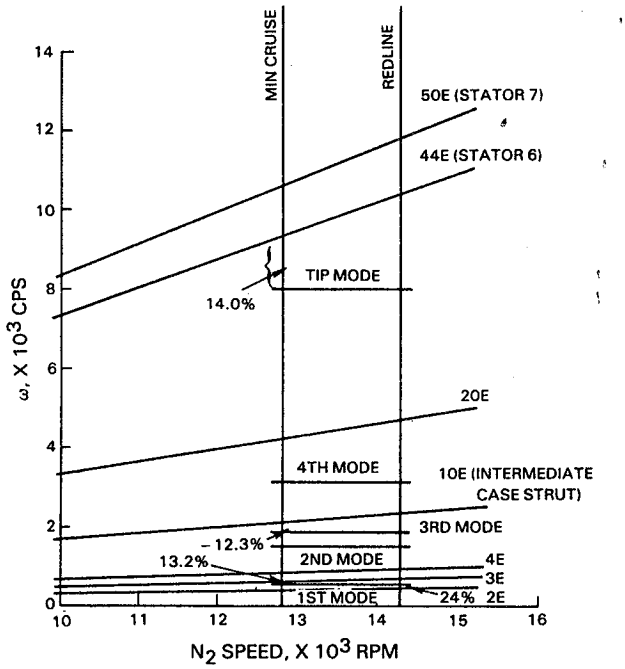

Figure 4.5.4-4 Resonance Diagram Rotor 7

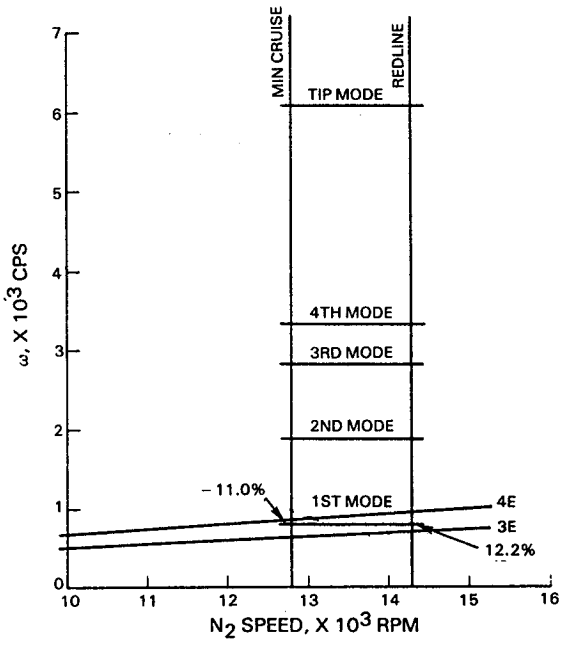

Figure 4.5.4-5 Resonance Diagram Rotor 8

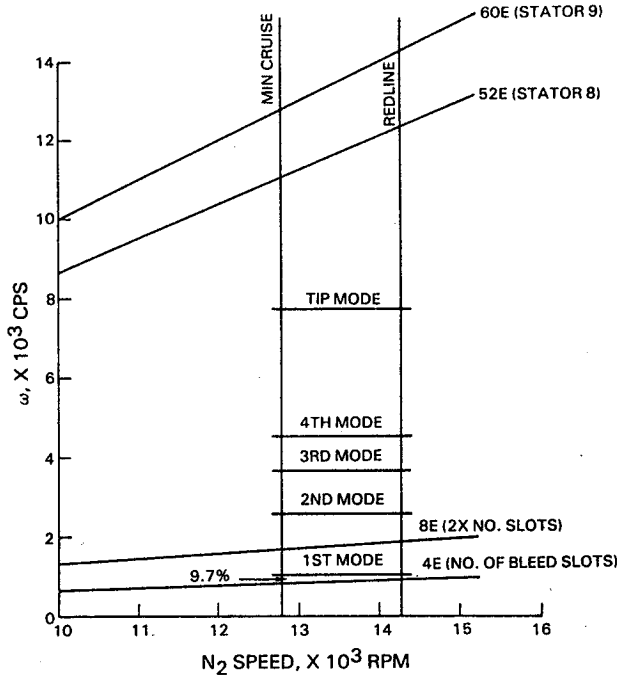

Figure 4.5.4-6 Resonance Diagram Rotor 9

All blades are within the bending and torsion flutter limits. Blade platforms have been sized to provide acceptable frequency margin on adjacent vane passing orders. Both axial and tangential stages are designed to preclude premature attachment failures under normal vibratory loading. Blade attachment and disk lug stresses were calculated for the tangentially-slotted stages using finite element analysis. Initially, the eighth stage was deemed unacceptable and was redesigned as an axial attachment to provide adequate life. All other bearing and disk lug fillet stresses were deemed acceptable. Attachment stresses, as summarized in Table 4.5.4-IV, are acceptable for integrated core/low spool operation.

TABLE 4.5.4-IV

ATTACHMENT STRESSES

Stage	Stress MPa (ksi)	Actual (N=14,270)	Actual (N= 13,936)
6	Combined	312.3 (45.3)	
	Tensile	149.6 (21.7)	142.0 (20.6)
	Shear	112.3 (16.3)	106.8 (15.5)
	Bending	162.7 (23.6)	155.1 (22.5)
	Bearing	280.6 (40.7)	
7	Combined	383.3 (55.6)	
	Tensile	99.2 (14.4)	94.4 (13.7)
	Shear	82.7 (12.0)	79.2 (11.5)
	Bending	210.9 (30.6)	201.3 (29.2)
	Bearing	284.0(41.2)	
8	Combined	439.8 (63.8)	
	Tensile	140.6 (20.4)	134.4 (19.5)
	Shear	119.2 (17.3)	113.7 (16.5)
	Bending	299.2 (43.4)	285.4 (41.4)
	Bearing	402.6 (58.4)	
9	Combined	515.0 (74.7)	
	Tensile	172.3 (25.0)	164.0 (23.8)
	Shear	178.5 (25.9)	170.3 (24.7)
	Bending	342.6 (49.7)	327.5 (47.5)
	Bearing	458.5 (66.5)	
10	Combined	410.9 (59.6)	
	Tensile	149.0 (21.6)	142.0 (20.6)
	Shear	136.5 (19.8)	130.3 (18.9)
	Bending	262.0 (38.0)	250.2 (36.3)
	Bearing	365.4 (53.0)	
11	Combined	365.4 (53.0)	
	Tensile	133.0 (19.3)	126.8 (18.4)
	Shear	121.3 (17.6)	115.8 (16.8)
	Bending	233.0 (33.8)	222.7 (32.3)
	Bearing	296.4 (43.0)	
12	Combined	290.9 (42.2)	
	Tensile	122.0 (17.7)	116.5 (16.9)
	Shear	99.2 (14.4)	95.1 (13.8)
	Bending	168.9 (24.5)	161.3 (23.4)
	Bearing	243.3 (35.3)	
13	Combined	307.5 (44.6)	
	Tensile	110.3 (16.0)	105.5 (15.3)
	Shear	117.2 (17.0)	111.7 (16.2)
	Bending	196.5 (28.5)	187.5 (27.2)
	Bearing	434.3 (63.0)	
14	Combined	284.1 (41.2)	
	Tensile	118.5 (17.2)	113.1 (16.4)
	Shear	99.9 (14.5)	95.1 (13.8)
	Bending	165.4 (24.0)	157.9 (22.9)
	Bearing	367.5 (53.3)	
15	Combined	262.0 (38.0)	
	Tensile	108.9 (15.8)	104.1 (15.1)
	Shear	91.7 (13.3)	87.5 (12.7)
	Bending	153.1 (22.2)	146.2 (21.2)
	Bearing	337.8 (49.0)	

Front Case and Stator Assembly

A summary of front case stresses, based on the interactive effects of various load sources, is presented in Figure 4.5.4-7. Analyses indicated that the dominant load governing front case design was fan blade loss moment in the case walls and flanges although containment set case wall thickness at the eighth-stage rotor trench. Case bending and ovalization were also analyzed to ensure that case deflections resulting from these sources would not unduly compromise blade tip clearance goals. Results showed deflections of only one to two mils, which represents a nominal 10 percent contribution to the minimum clearance goal. Therefore, deflections are not a dominant concern in the front case design.

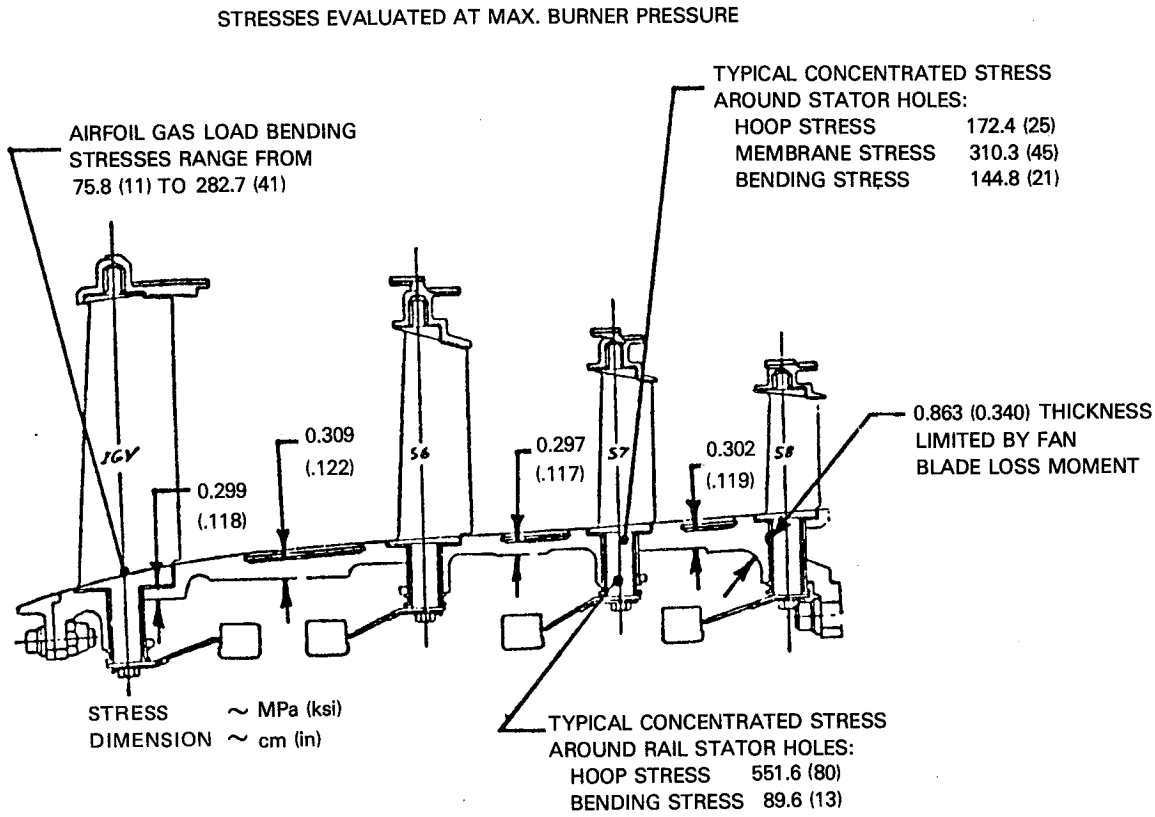

Figure 4.5.4-7 Front Case Stress Summary

Maximum anticipated vane unison ring actuation loads were calculated for distortion and other stress factors. The calculation considered the aerodynamic vane load, friction of the vane pins in their bushings, and twisting of the lever arms by the unison ring pins. The determined loads and maximum tangential unison ring defections are shown in Table 4.5.4-V.

TABLE 4.5.4-V

CALCULATED LOADS AND MAXIMUM TANGENTIAL UNISON RING DEFLECTION SUMMARY

	Unison Ring Actuation Loads, N (lb)		Maximum Tangential Unison Ring Deflectors, cm (in)
	Max N_2	Idle	
IGV	-1,659 (-373)	-182 (-41)	0.017 (0.007)
6	1,054 (237)	115 (26)	0.007 (0.003)
7	1,107 (249)	124 (28)	0.010 (0.004)
8	1,236 (278)	137 (31)	0.015 (0.006)

Rear Case and Stator Assembly

A series of sequential analyses was required for structural characterization of the rear case assembly. These included (1) thermal and shell analyses, (2) a buckling analysis to determine wall thickness requirements, (3) NASTRAN analysis of the vane shrouds to investigate asymmetric properties and determine circumferential variations in radial deflection, (4) containment analysis to establish the thicknesses required to contain a blade failure at each stage, and (5) analysis to determine fan blade loss effects on case design. Static load and blow-off load considerations were included throughout the analysis.

As a result of these analyses, case wall thickness was set by buckling under limit loads. The size of the flanges and bolts was set by the fan blade loss load. The resultant design produced a case in which all stresses are within engine allowables. A rear case stress summary at maximum engine combustor pressure rating is shown in Figure 4.5.4-8.

Case bending and ovalization were investigated to ensure that case deflections would not severely compromise blade tip clearance goals. Results showed only a nominal 0.0025 cm (0.001 in) deflection, as in the front case analysis, which represents only a nominal 10 percent contribution to the minimum clearance goal.

All stators, including the inlet and exit guide vanes, have been designed to provide bending and torsional flutter stability.

4.5.5 Differences Relative to the Flight Propulsion System

The high-pressure compressor for the flight engine retains the same aerodynamics as the design for the integrated/core low spool. The major differences are material changes for the weight and durability requirements of a flight engine, although several small mechanical differences are noteworthy.

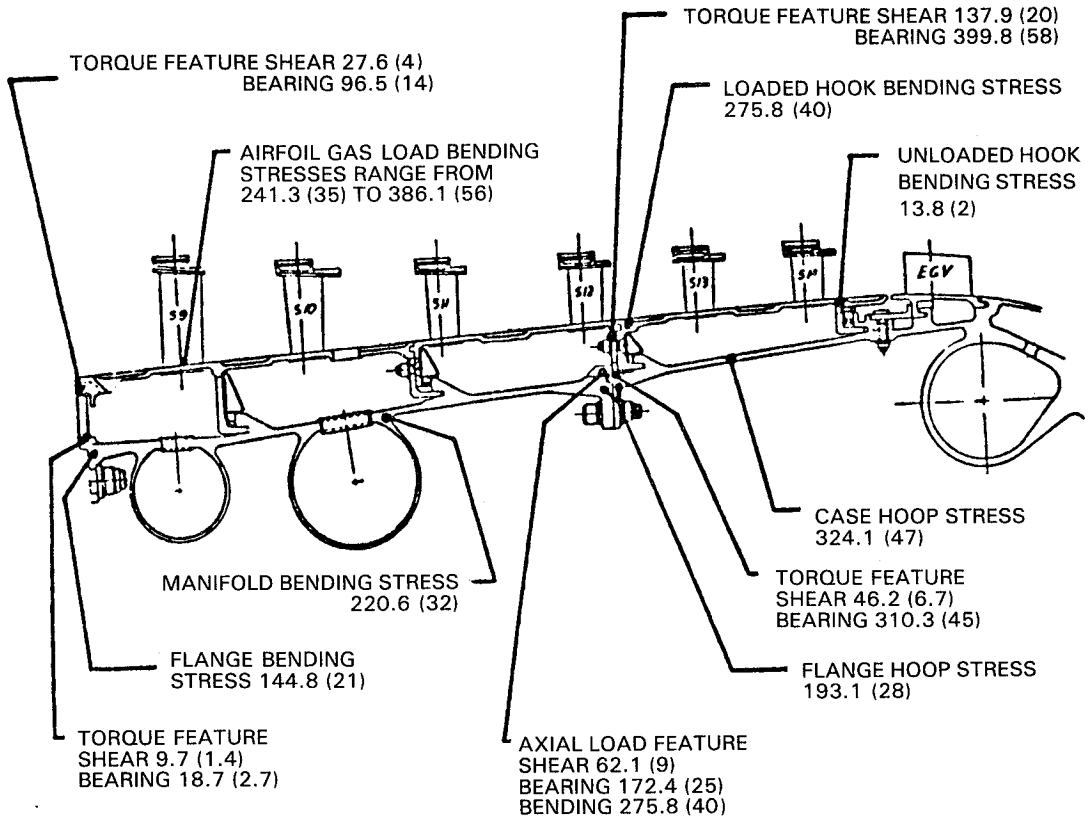

Figure 4.5.4-8 High-Pressure Compressor Rear Case Stress Summary -- Loads at Maximum Burner Pressure, MPa (Ksi)

A comparison of the materials for the flight propulsion system and integrated core/low spool is presented in Table 4.5.5-I. The significant materials substitutions are the use of PWA 1225, a beta forged titanium alloy, for the twelfth and thirteenth-stage rotors and MERL 80, an improved form of PWA 1099, for the tandem fourteen/fifteen-stage disk. In addition, the integral rotor knife edge seals have a silicon carbide coating to improve durability.

In the flight engine, the flow guides are removed in stages nine through fifteen. As a result, the compressor axial length would be shortened by approximately 1.8 cm (0.7 in). Other revisions include a lightweight thin center tube with "I" section stiffeners, added thickness or increased fillet radii in the blade root slots to reduce local stresses and the use of seals to eliminate the need for drainage holes.

TABLE 4.5.5-I

MATERIAL COMPARISON

	Flight Propulsion System	Integrated Core/Low Spool	Rationale for Difference
Blades 6, 7	PWA 1202	AMS 4928	Schedule
Disks 12, 13	PWA 1225	PWA 1226	Availability and Cost
Disks 14, 15	MERL 80	PWA 1099	Flight Propulsion System Material not Available
IG Vane	AMS 4132	AMS 5613	Aluminum Difficult to Instrument
Vanes 9-12	AMS 5508	AMS 5616	Cost Saving and Schedule
Vanes 13, 14	AMS 5596	AMS 5662	Cost Saving and Schedule
Exit Guide Vane	PWA 649	AMS 5663	Cost Saving and Schedule
IGV ID Shroud	AMS 4132	AMS 5613	Compatibility with Vane

4.6 COMBUSTOR

4.6.1 General Description

The combustor design for the integrated core/low spool is shown in Figure 4.6.1-1 and the design goals are presented in Table 4.6.1-I. The combustor is an annular, two-zone configuration that combines advances in aerodynamics and structure-mechanics to provide a compact system capable of low emissions and high performance. The combustion concept is based on the technology from the NASA-sponsored Experimental Clean Combustor Program. Some of the key features are a short curved-wall prediffuser section, segmented liners with a counter-parallel FINWALL® cooling technique, and compact carburetor tube main zone fuel injectors. Details of the combustor design are contained in Reference 3.

TABLE 4.6.1-I
COMBUSTOR COMPONENT DESIGN GOALS

Exhaust Emissions* (max)	
Unburned Hydrocarbons	0.4
Carbon Monoxide	3.0
Oxides of Nitrogen	3.0
Smoke Number	20
Aerothermal Performance	
Pattern Factor (max)	0.37
Pressure Loss ($\%P_{T3}$)	5.50
Exit Radial Temperature Profile, (max) °C (°F)	121 (250) peak to average

*Environmental Protection Agency Parameter (pound pollutant/1000 pound=thrust thrust hour/cycle)

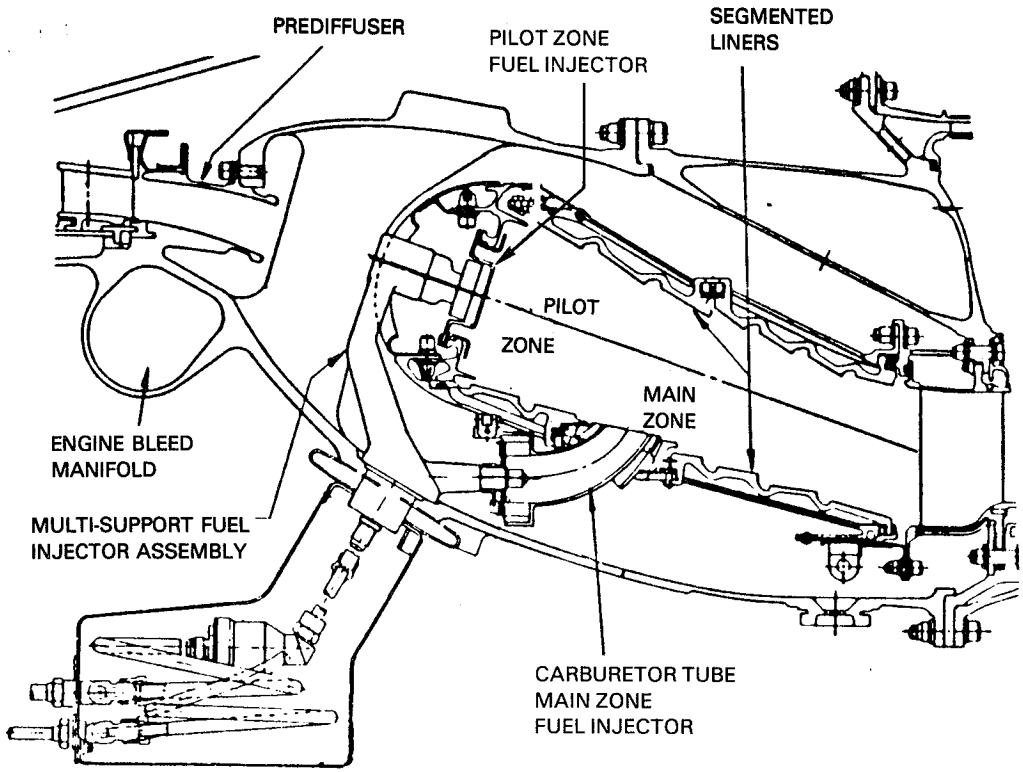

Figure 4.6.1-1 Cross-Sectional View of Combustor Component for the Integrated Core/Low Spool

4.6.2 Aerodynamic Design

The diffuser consists of the prediffuser, dump section and combustor case inner and outer annuli. As shown in Figure 4.6.2-1, the prediffuser has a strutless, curved-wall flowpath to maintain stable, separation-free flow at all operating conditions as well as provide diffusion and turning in a relatively short length. The structural struts, which are characteristically located in the prediffuser flowpath, are located in the lower Mach number dump region in order to reduce the aerodynamic losses attributable to the struts. Because of the radial offset between the compressor exit and turbine inlet, a curved-wall geometry more closely aligns the compressor flow with the combustor centerline to reduce the pressure loss with flow turning around the combustor front end. The prediffuser has an area ratio of 1.5 and a length to inlet height ratio of 3.5. Other design characteristics are summarized in Table 4.6.2-I.

TABLE 4.6.2-I

SUMMARY OF PREDIFFUSER AERODYNAMIC GEOMETRY

Length, cm (in)	7.1 (2.8)
Airflow Turning Angle (with CEGV), deg	14.0
Inlet Mach Number	0.28
Exit Mach Number	0.18
Total Pressure Loss, %	0.8

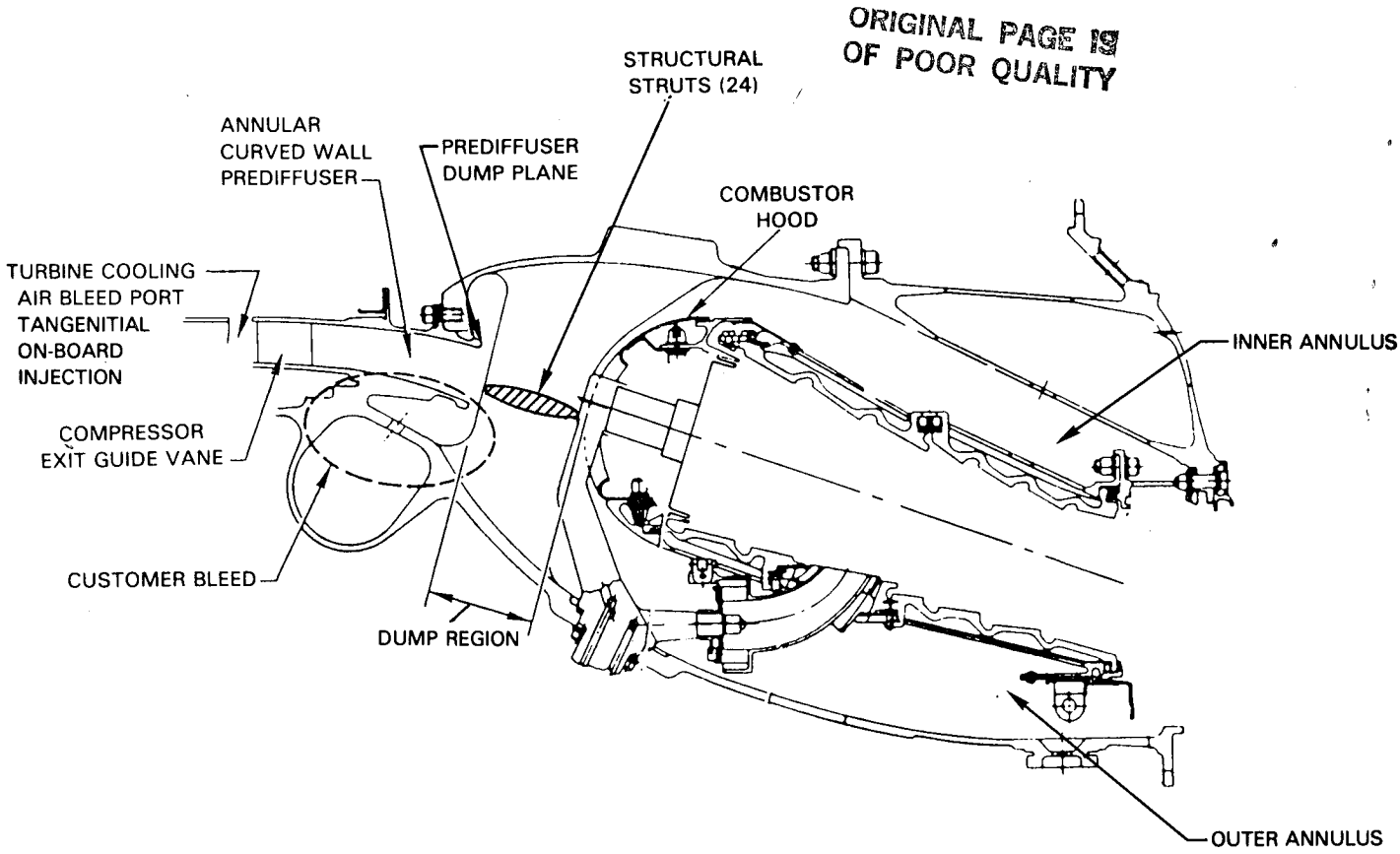

Figure 4.6.2-1 Combustor Flowpath Definition

The prediffuser contains bleed ports for both customer air and turbine tangential on-board injection (TOBI) cooling air. Air for customer usage amounts to 9.3 percent of the total high-pressure compressor exit flow at idle and is extracted downstream of the compressor exit. The tangential on-board injection bleed extracts 3.5 percent of the compressor exit flow from a port forward of the exit guide vane.

The dump region at the prediffuser exit is defined by the diffuser case height and contour. This region is sized to distribute the prediffuser exit flow without immediate flow attachment to the case walls. The 24 struts in the dump region provide the structural connection between the diffuser inner and outer case walls and are aerodynamically shaped to minimize pressure loss.

The inner and outer diffuser annuli are designed to minimize pressure loss and provide a positive static pressure differential across the liners at all locations to prevent aspiration. Both annuli are sized to ensure a normal air velocity of less than or equal to 45 m/sec (150 ft/sec) over the full length of the annuli at the design airflow.

The combustor has two separate combustion zones -- a pilot and a main zone -- for emissions control. The pilot zone is designed to minimize idle emissions and provide adequate stability and relight. This zone is a direct fuel injection swirl-stabilized design with fuel introduced through 24 single pipe aerated injectors. Figure 4.6.2-2 shows a cross-sectional view of the single pipe aerated injector. This type of injector relies on shearing of low velocity fuel by the surrounding high velocity airstreams to achieve good fuel atomization. The internal and external airstreams are corotationally swirled to distribute the fuel and provide the recirculatory flow required for combustion stability.

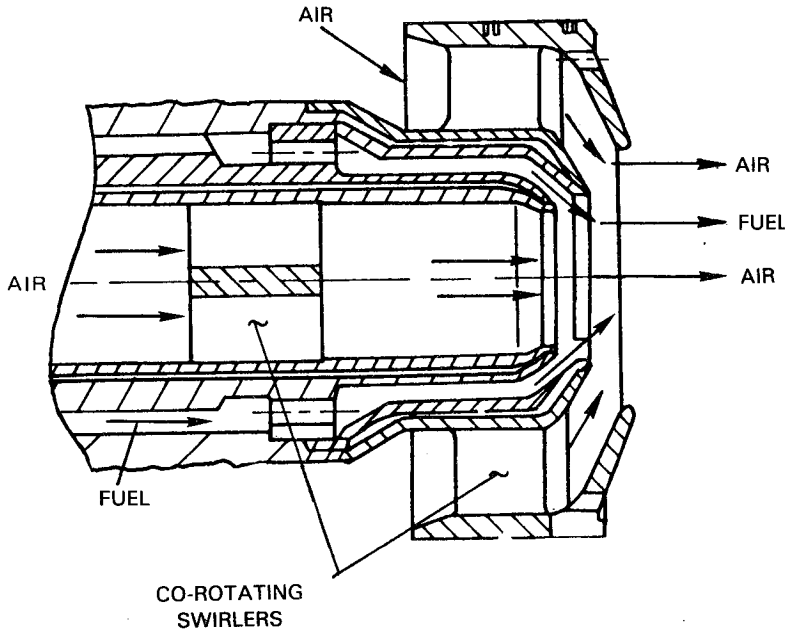

Figure 4.6.2-2 Pilot Zone Fuel Injector

In the main zone, lean combustion occurs to minimize the formation of oxides of nitrogen and smoke. This zone is designed for a low heat release rate, low velocity and high residence time, all of which are conducive to low emissions, good relight and stability. A major design feature is the compact carburetor tube injection system. The carburetor tube, as shown in Figure 4.6.2-3, premixes fuel and air prior to ignition for better atomization. Fuel is supplied to each of the 48 carburetor tubes by a simplex pressure atomizer. A fraction of the fuel is vaporized in the tube, while the remaining fuel is centrifuged to the walls of the tube by air introduced through a radial inflow swirler.

The fuel film formed at the exit plane of the tube is sheared into droplets by the swirling core and secondary airflow jets. The core radial inflow swirler consists of ten curved vanes with an overall width of approximately 1 cm (0.7 in). The secondary airstream swirler contains nine 20-degree axial vanes.

C-2

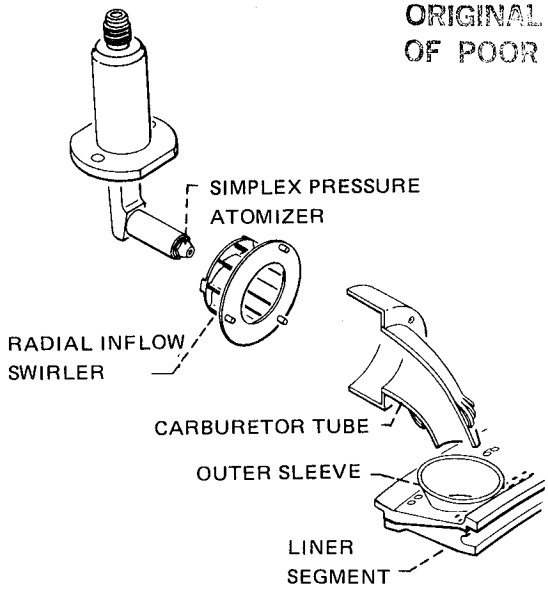

Figure 4.6.2-3 Main Zone Carburetor Tube Injector

The two combustion zones are enclosed by segmented liners. The requirement for this type of construction, as opposed to a more conventional louvered design, was dictated by the flight propulsion system life goal of 8000 hours, the high combustor operating pressure at sea level static takeoff and a liner cooling airflow limit of 35 percent of the total combustor airflow. A typical liner segment is shown in Figure 4.6.2-4. The annular combustor contains 120 liner segments. Axial feather seals are on the sides of the segments to control leakage. Cooling is accomplished with the counter-parallel FINWALL® technique. This technique, as shown in Figure 4.6.2-4, consists of a series of axial cooling holes across the segment. Cooling air enters the liner through slots on the liner cold wall. It is then split to flow both counter and parallel to the hot gas flow. At sea level takeoff conditions, the coolant temperature is 565°C (1050°F) and the pressure is 3.1 MPa (448 psia).

The relative percentages of both pilot and main zone airflow are shown in Figure 4.6.2-5. Most of the main zone combustion air is supplied through the carburetor tube core and secondary passages. The remaining airflow enters the combustor through dilution holes in the liners and cooling air slots.

4.6.3 Mechanical Design

The combustor component consists of three major subassemblies. These include the diffuser section, combustion section and fuel injectors. The mechanical design of these subassemblies is summarized in the following sections.

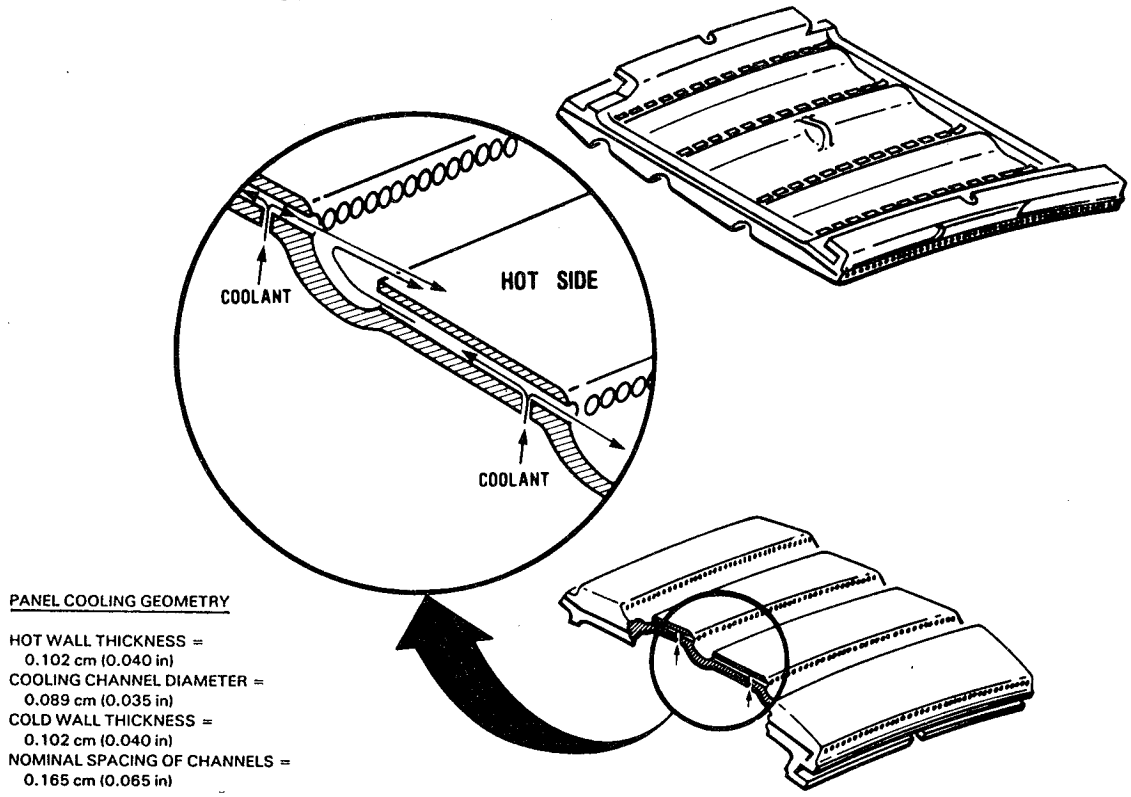

Figure 4.6.2-4 Typical Liner Segment

Diffuser Section

The diffuser case, as shown in Figure 4.6.3-1, consists of the inner and outer cases, bleed manifold and 24 internal structural struts. These components are fabricated from Inconel 718 material. Connected to the inner flange of the case is the tangential on-board injection support case. Also, the inner wall of the prediffuser is bolted to the front of the case. The bleed manifold and ports are located on the outer flange. Fuel injector support assembly bosses, combustor support pin bosses, and ignitor bosses are located in the cast portion of the outer diffuser case. A forged rear skirt, which includes a fuel drain port, is welded to the outer case casting and bolted at the rear to the high-pressure turbine case.

At the prediffuser inlet, the compressor exit guide vanes are mounted on an inner and outer platform with a turbine-style vane foot attachment. The vanes are machined from Inconel 718 material and welded in clusters of five to satisfy requirements for damping, high-pressure compressor stage interaction, leakage, and assembly.

Combustion Section

The combustor comprises the front-end subassembly and segmented liners. The front-end subassembly is illustrated in Figure 4.6.3-2. The hood is supported by the bulkhead, which acts as the major structural member connecting the inner and outer liner support frames, hood, and injector guides to the engine outer case. Heatshields protect the bulkhead support structure from pilot zone thermal radiation. All major hardware is fabricated from Hastelloy X material.

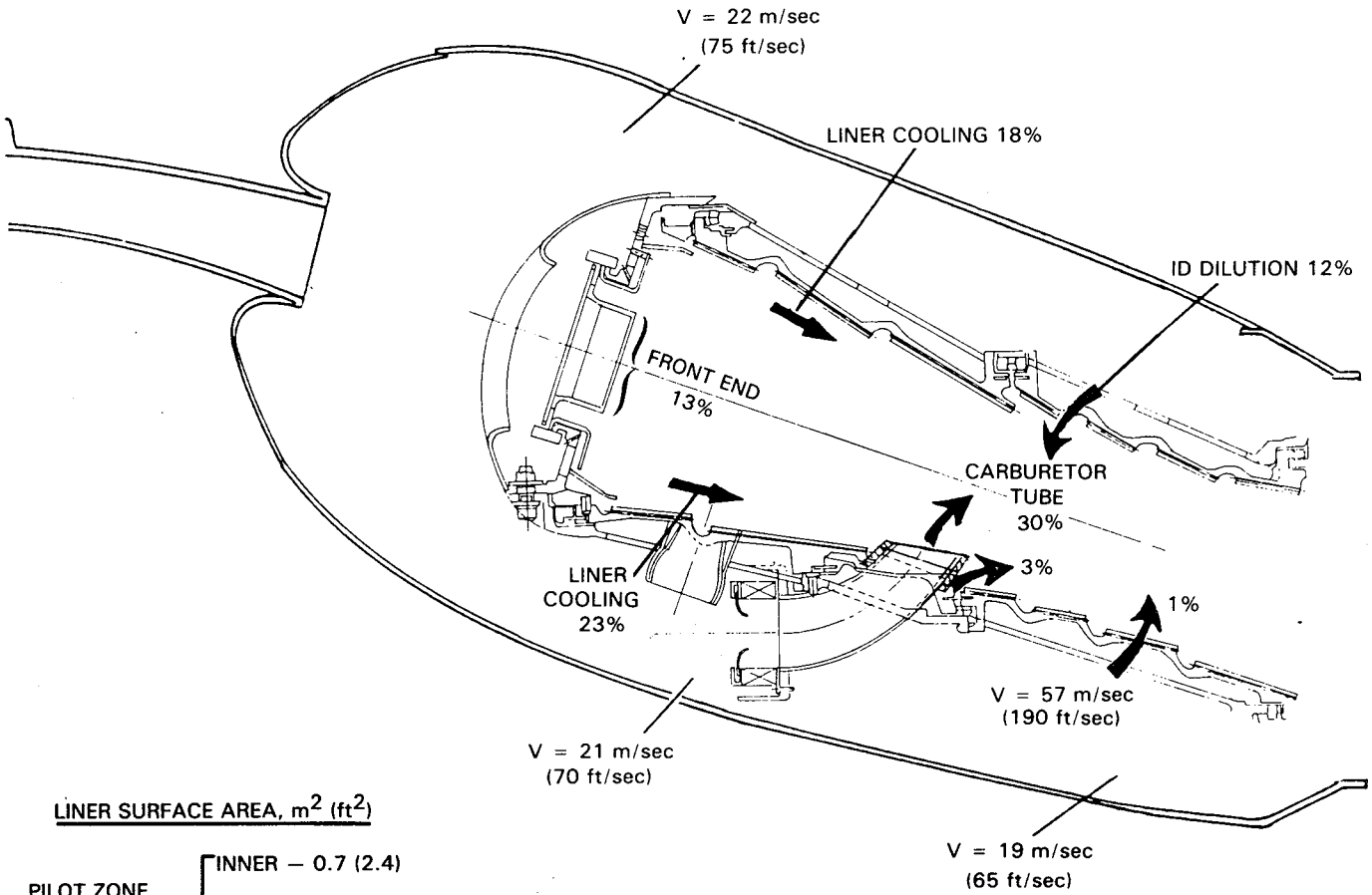

Figure 4.6.2-5 Combustor Airflow Distribution (Based on Sector Combustor Rig Testing)

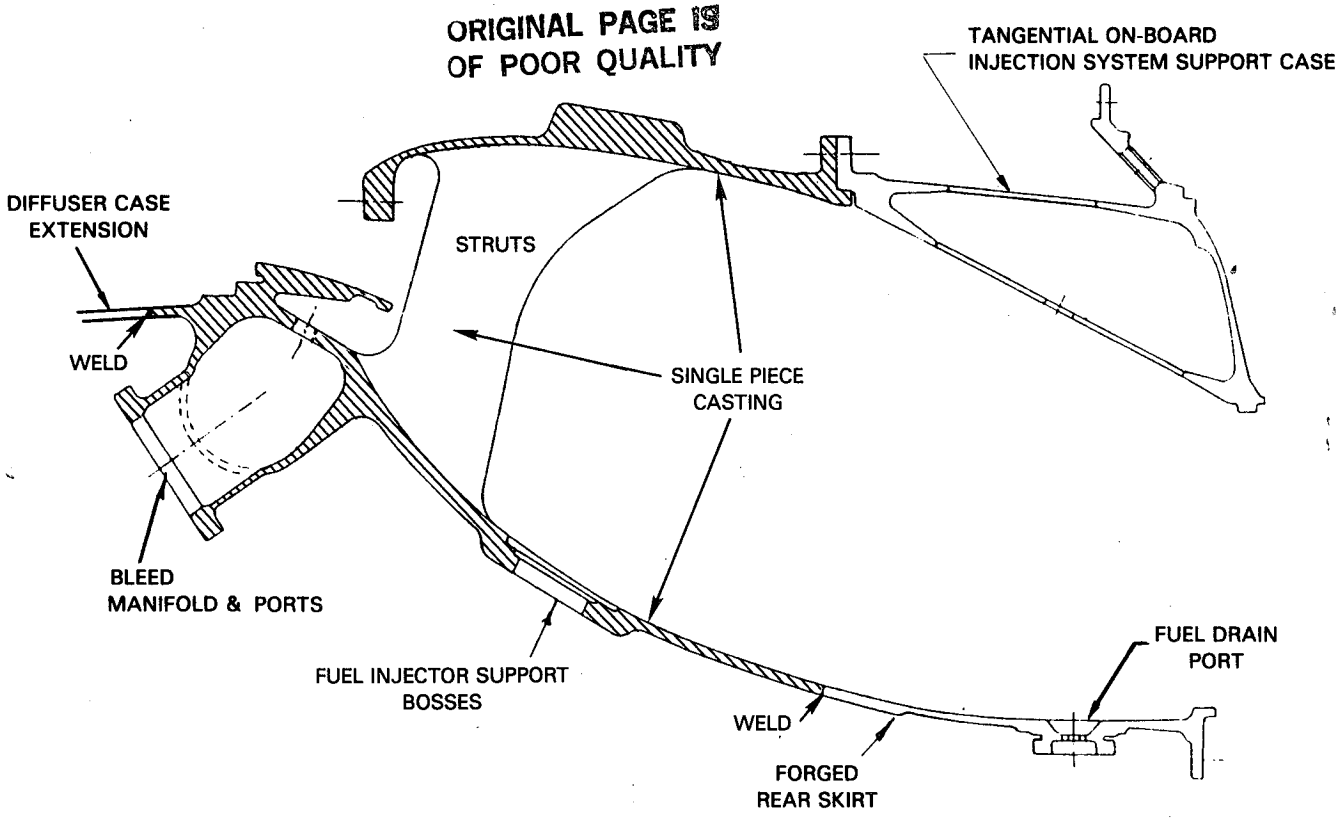

Figure 4.6.3-1 Diffuser Case Mechanical Design

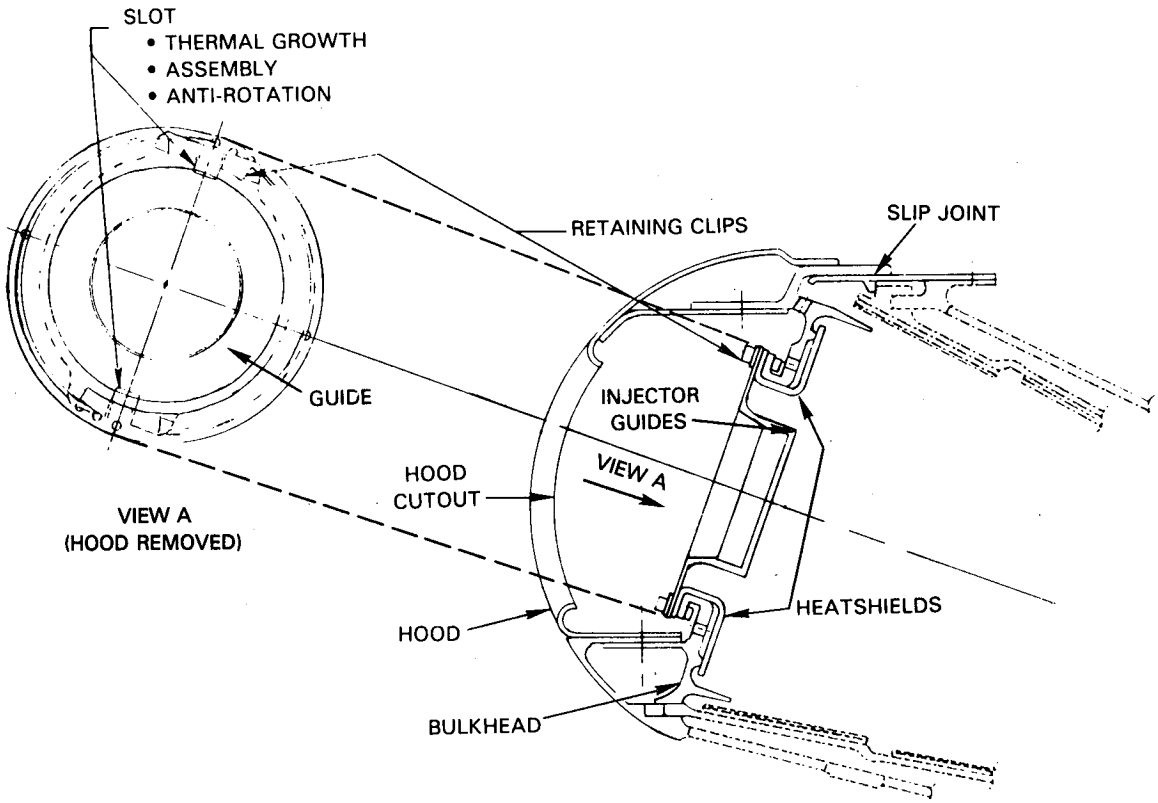

Figure 4.6.3-2 Design and Major Components of Front-End Subassembly

The liner segments are fabricated from B-1900 + Hf, an investment cast nickel base alloy with good strength properties in the 760 to 1037°C (1400 to 1900°F) temperature range. The material allows operation at a maximum metal temperature of 1010°C (1850°F). The counter-parallel FINWALL® holes are electrochemically machined into the liner. Cooling air feed slots, which intersect the FINWALL® holes and supply cooling air from the cold side of the liners, are electro-discharge machined. The liner segments, as illustrated in Figure 4.6.3-3, are supported by inner and outer structural frames machined from Hastelloy X material. Conventionally machined hooks on the back of each segment engage with the circumferential rails on the structural frame to position the segments.

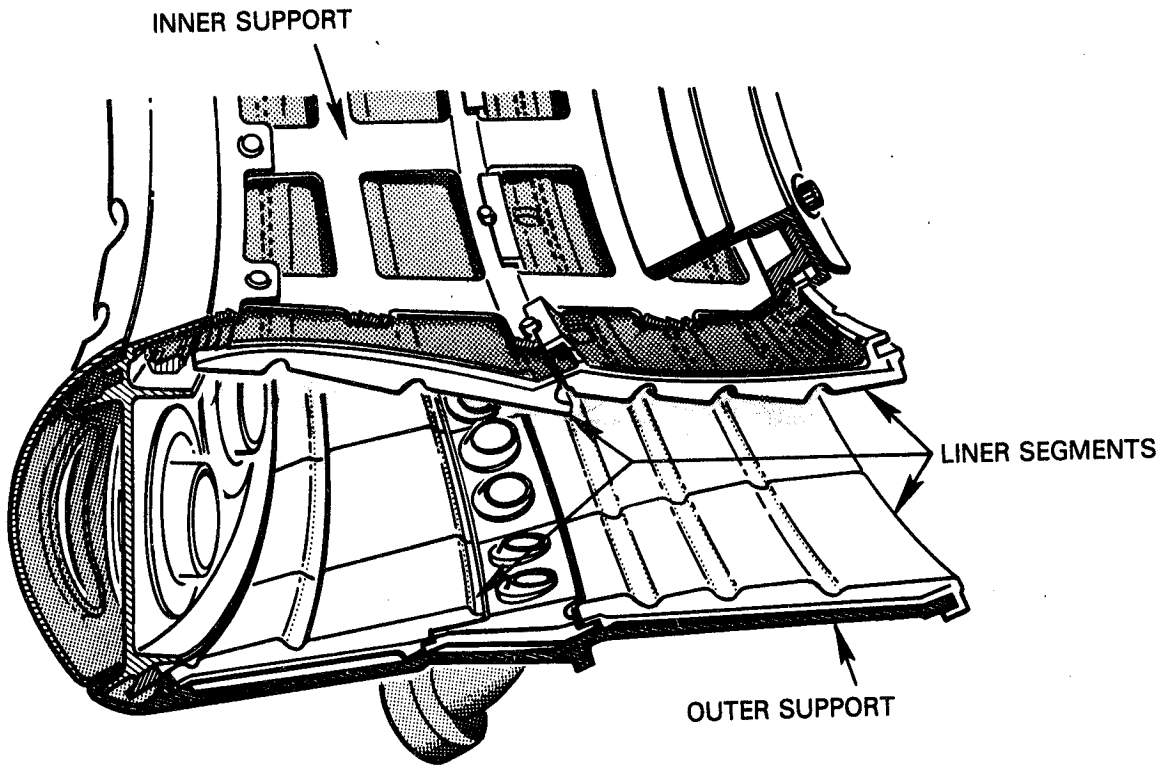

Figure 4.6.3-3 View of Segmented Liners and Support Frame

Fuel Injectors

The fuel injectors in the pilot and main zones are supported by the assembly shown in Figure 4.6.3-4. This assembly is cast from AISI 347 stainless steel and contains two main zone pressure atomized injectors and a pilot zone aerated injector. Separate manifolds are used to supply fuel to the pilot and main zones. Each of the 24 fuel injector assemblies is inserted through the case from the inside of the engine and secured to the case with four bolts. To minimize the possibility of fuel coking as the fuel passes through the fuel injector, all exposed surfaces are protected by sheet metal heatshields.

The ignitor plugs penetrate the pilot zone outer liner wall. The two plugs required for the Energy Efficient Engine combustor are identical and are a modification of a conventional design.

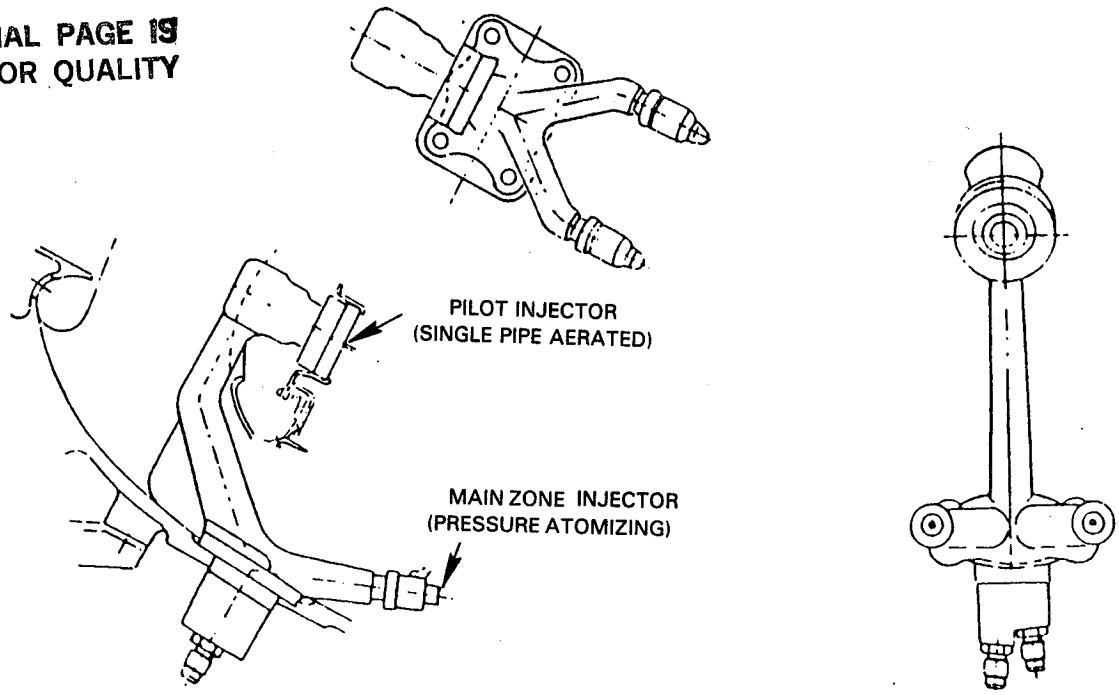

Figure 4.6.3-4 Fuel Injector Support Assembly

4.6.4 Design Substantiation and Supporting Analyses

4.6.4.1 Predicted Performance

The design of the combustor component was verified during the Sector Combustor Rig Technology Program (Ref. 4). The results of experimental testing demonstrated that with the exception of oxides of nitrogen all environmental and performance goals can be achieved. In addition, testing at the high pressure and temperature levels anticipated for the Energy Efficient Engine verified the structural integrity of the advanced segmented liner with counter-parallel FINWALL® cooling. Table 4.6.4-I presents a synopsis of the demonstrated combustor performance.

4.6.4.2 Structural/Life Analyses

The combustor component design meets the structural and life requirements for both the integrated core/low spool and the flight propulsion system. From a structures standpoint, the diffuser case and segmented liner are of particular interest because of the uniqueness of the designs as well as structural requirements.

A stress and temperature summary of the diffuser case, as calculated for a sea level takeoff hot day condition, is presented in Figure 4.6.4-1. The case meets the structural requirements imposed by thermal loads, an axial blow-off load of 572,038 N (128,600 lb) and minimum deflection at the high-pressure compressor discharge seal. Furthermore, it meets the flight propulsion system life goal of 15,000 cycles when cast from hot isostatically pressed material. However, to minimize cost and meet the fabrication schedule, the case casting for the integrated core/low spool will not be hot isostatically pressed.

TABLE 4.6.4-I

SUMMARY OF TEST RESULTS

	Goal	Louvered (2) Liner		Segmented (3) Liner	
Exhaust Emissions (max)					
Hydrocarbons(1)	0.4	0.18*	0.26**	0.26*	0.38**
Carbon Monoxide(1)	3.0	1.54*	2.07**	1.71*	2.30**
Oxides of Nitrogen(1)	3.0	3.80*	4.65**	3.85*	4.70**
Smoke, SAE Number	20		1		4
Pattern Factor	0.37 (Max)		0.15		0.26
Section Pressure Loss, (%P_{T3})	5.5		5.37		5.22
exit Radial Profile, °C (°F)	121 (250) (peak to avg)		21 (70)		65 (150)

(*) As measured
(**) Includes margins for development and variability
(1) Environmental Protection Agency Parameter (pound pollutant/1000 pounds-thrust hour/cycle)
(2) Tested up to 1.6 MPa (230 psia)
(3) Tested up to 3.1 MPa (445 psia)

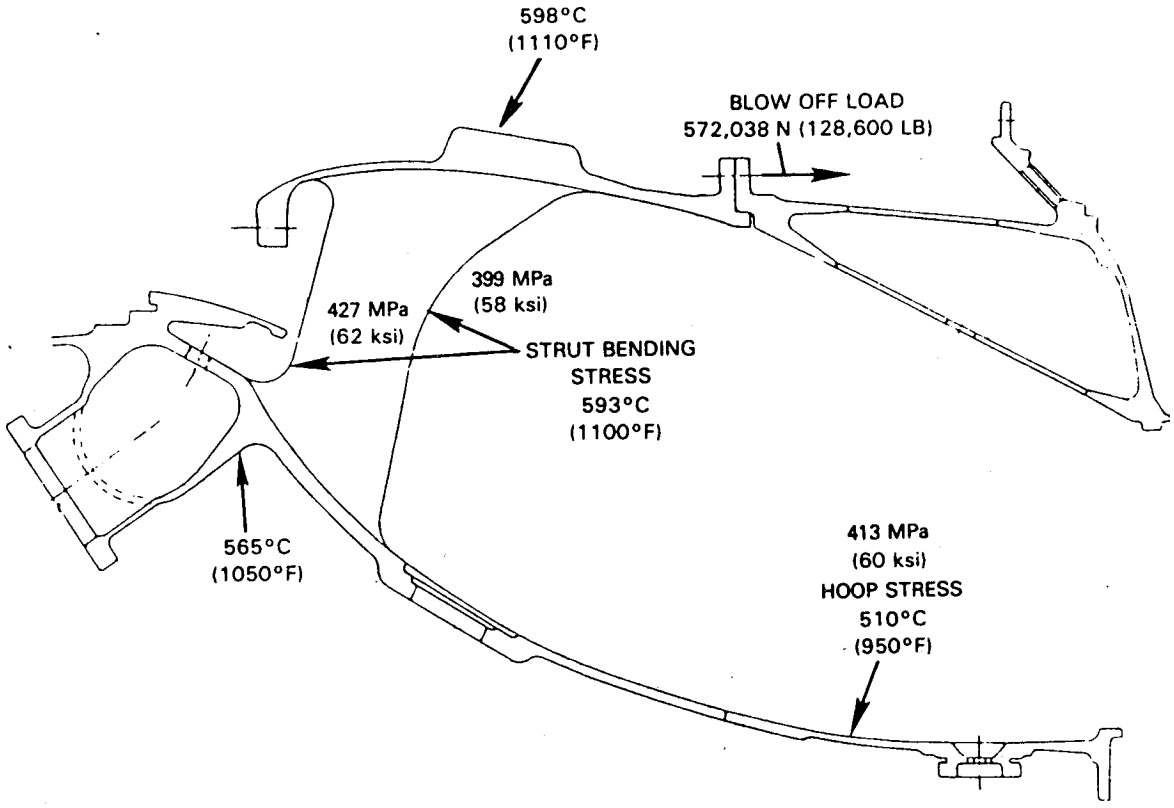

Figure 4.6.4-1 Diffuser Case Stress and Temperature Summary at Sea Level Takeoff Condition on an 28°C (84°F) Day

Various analyses were performed to provide a thermal and structural characterization of the segmented liner design. A thermal analysis was made based on deteriorated engine sea level takeoff hot day conditions to determine the liner temperature distribution. The results in Figure 4.6.4-2 show the cooling passage size and spacing required to achieve the indicated liner temperature distribution.

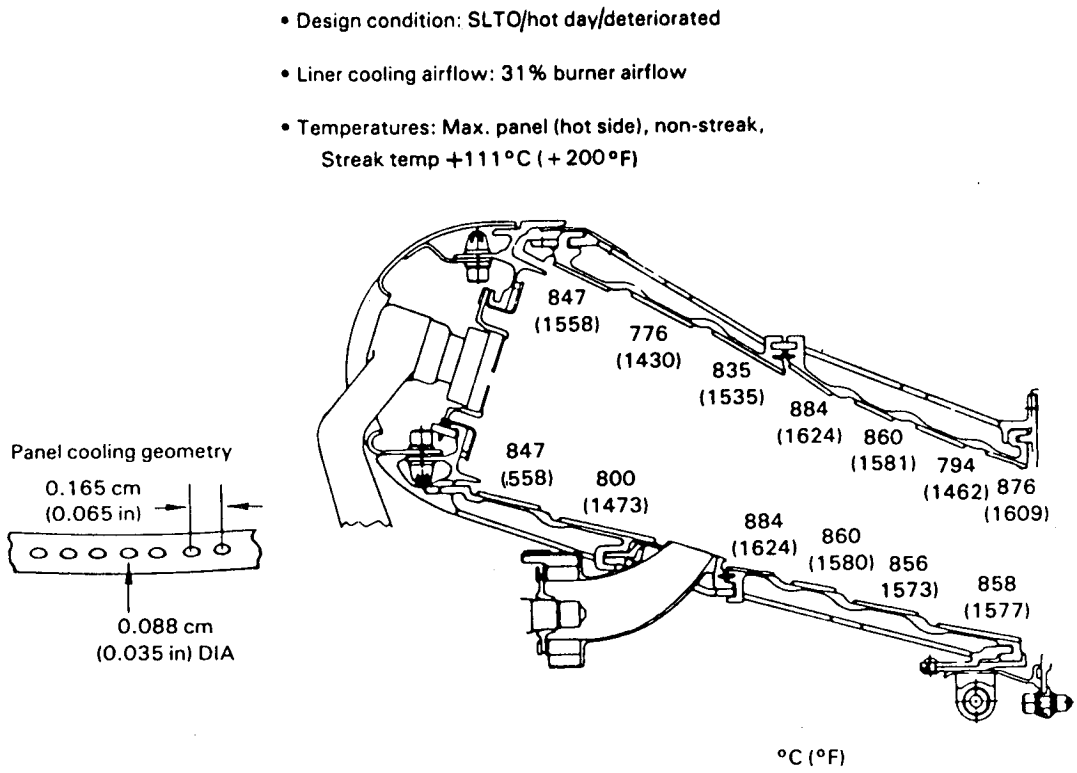

Figure 4.6.4-2 Optimized Segment Panel Cooling Geometry for Liners

A detailed structural analysis was conducted using an analytical model of the segment geometry. A finite element computer program with nonlinear analysis capability was used to study dimensional instability from accumulating creep and plasticity during cycling. In addition, an elastic analysis was used to set attachment clearances and calculate cyclic life. Two conditions were analyzed to determine maximum stresses. These were sea level takeoff and the maximum temperature gradient during acceleration. Results showed a maximum stress of 462 MPa (67.7 ksi) when the maximum temperature difference occurred at the hook section during acceleration. The maximum stress was consistently located at the ends of the segment over the attachment rails.

4.6.5 Differences Relative to the Flight Propulsion System

The combustor component for the integrated core/low spool is aerodynamically and mechanically identical to the design for the flight propulsion system. The only differences are in the method of manufacturing certain parts.

The diffuser case for the flight propulsion system is cast and hot isostatically pressed to meet the flight propulsion system life goal of 15,000 cycles. In contrast, the isostatic pressing operation is omitted for the integrated core/low spool case, since the high fatigue life is not necessary. Also, the compressor exit guide vanes in the flight propulsion system will be cast, compared to being machined for the integrated core/low spool.

4.7 High-Pressure Turbine

4.7.1 General Description

The high-pressure turbine is a single-stage configuration designed to operate at a high velocity ratio and low through flow velocity to wheel speed (Cx/U) for high efficiency. The turbine design for the integrated core/low spool is shown in Figure 4.7.1-1 and a listing of the various technology features is presented in Table 4.7.1-I. Details of the turbine component design are contained in Reference 5.

The design of the high-pressure turbine is based largely on advancements in the areas of aerodynamics, materials/cooling management and structures. Both the vanes and blades use single crystal alloys for improved durability. Leakage is effectively reduced by the use of full ring, boltless sideplates as well as the extensive use of feather seals and "W" seals. Also, an active clearance control system maintains close blade tip operating clearances throughout the operating range.

TABLE 4.7.1-I

HIGH-PRESSURE TURBINE ADVANCED TECHNOLOGY CONCEPTS

REDUCED COST CONCEPTS:
- Single-Stage Turbine

INCREASED AERODYNAMIC EFFICIENCY CONCEPTS:
- High AN^2/High Rim Speed
- Contoured Vane End Walls
- Low Loss Airfoils
- Active Clearance Control
- High Airfoil Loadings
- Improved Airfoil Cooling Effectiveness

REDUCED COOLANT FLOW CONCEPTS:
- Reduced Number of Airfoils
- Single Crystal Airfoil Material
- Thermal Barrier Platform Coatings
- Efficient Coolant Supply System
- Low Windage

REDUCED LEAKAGE CONCEPTS:
- Reduced Leakage Length
- Improved Gap Sealing
- Improved Rim Sealing
- "W" Seals

4.7.2 Aerodynamic Design

The general parameters governing the aerodynamic design of the integrated core/low spool turbine are listed in Table 4.7.2-I for the aerodynamic design point (Mach number 0.8 at an altitude of 16,668 m (35,000 ft)). The resulting flowpath is presented in Figure 4.7.2-1, showing the elevation and axial length. In the single stage, there is a total of 24 vanes and 54 blades. The number of vanes minimizes blockage and optimizes the positioning of the vanes with the combustor fuel injector nozzles.

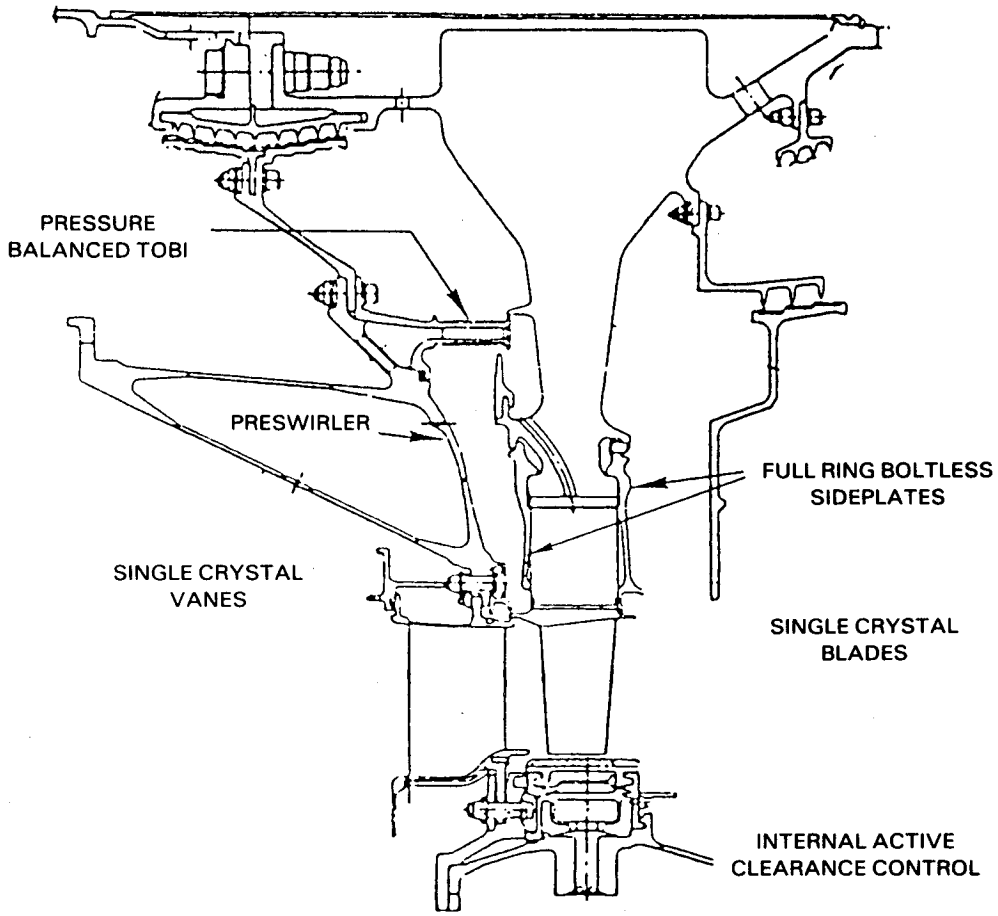

Figure 4.7.1-1 Energy Efficient Engine High-Pressure Turbine Component

TABLE 4.7.2-I

HIGH-PRESSURE TURBINE AERODYNAMIC DESIGN PARAMETERS

PT_{IN}, MPa (psia)	1.3 (192.1)
RIT, °C (°F)	1269 (2316)
Rotor Speed, (rpm)	13232
ΔH, (Btu/sec)	13384.
FP_{in}, $(W \sqrt{T_T}/P_T)$	16.984
W_c/A, $(\%W_{ae})$	14.56
PR	4.0
Reaction, %	43.0
Velocity Ratio	0.556
NASA Work Factor, $(\Delta h/u^2)$	1.62
Cx/U	0.351
AN^2 $(in^2\ rpm^2)$	4.06×10^{10}
U_{RIM}, m/sec (ft/sec)	481 (1580)
Clearance, cm (in)	0.0469 (0.0185)
Efficiency, % (Design)	87.9

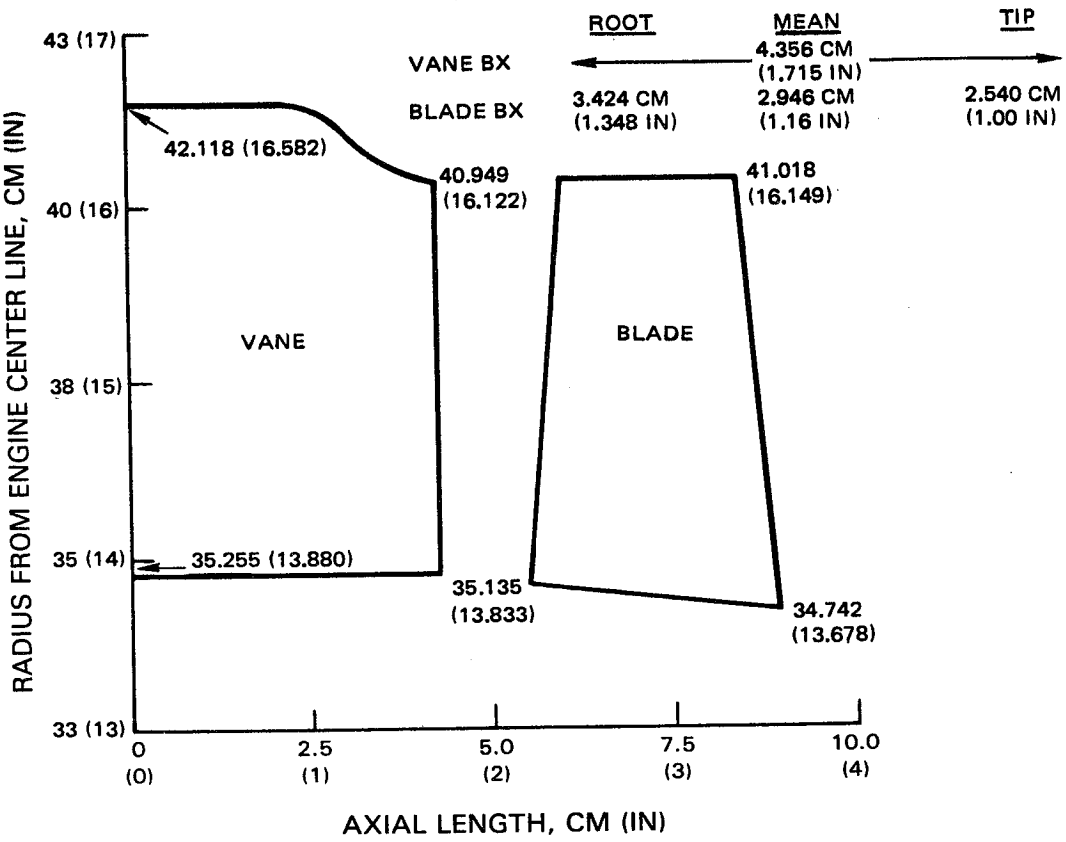

Figure 4.7.2-1 High-Pressure Turbine Flowpath Definition

Because of the small number of vanes, the airfoils are substantially larger than those in current gas-turbine engines. The vane is characterized by aerodynamic sections having a blunt leading edge and a long chord with the maximum airfoil thickness near the leading edge. The inner shroud is cylindrical, while the outer is contoured in an "S" shape. The large aerodynamic section thickness reduces the losses associated with the introduction of cooling flow and the "S" wall design reduces endwall losses. Also, the airfoil sections are designed so that the flow accelerates past the throat area with low, smooth backend diffusion. The uncovered turning and exit wedge angle have been optimized to minimize pressure loss.

The blades are highly tapered with a conical inner wall. Airfoil sections are designed to the same pressure distribution criteria as the vane. Uncovered turning and exit angle have been optimized to reduce blade profile as well as trailing edge and shock losses. The stage reaction level is 43 percent. Airfoil velocity triangle data are contained in Table 4.7.2-II

The turbine secondary flow system has several features to enhance cooling effectiveness and control leakage. These include:

- Tangential on-board injection (TOBI) system for positive blade coolant flow supply
- Front rim cavity mini tangential on-board injection (TOBI) system
- Boltless and full ring rotor sideplates
- A multi knife-edge, stepped high-pressure compressor discharge seal.

TABLE 4.7.2-II

GAS TRIANGLES*

	Root	Mean	Tip
VANE			
α IN, deg	90	90	90
α OUT, deg	11.6	10.3	9.1
Mn IN	0.09	0.08	0.07
Mn OUT	1.0	0.92	0.85
θ GAS, deg	78.4	79.7	80.4
BLADE			
β IN, deg	33.5	42.7	63.6
β OUT, deg	15.9	16.9	17.7
Mn IN	0.36	0.25	0.14
Mn OUT	1.22	1.24	1.28
θ GAS, deg	130.6	120.4	98.7
α OUT, deg	38.0	43.8	48.4
Mn OUT	0.54	0.52	0.52

*Based on flat inlet temperature and flat loss profiles.

The benefits derived from these features, in conjunction with improved sealing concepts, result in the use of only 14.56 percent of the core engine inlet flow for cooling the disk, blades, vanes, and case. A further discussion of the secondary flow system is presented in Section 5.7.

4.7.3 Mechanical Design

The mechanical definition of the high-pressure turbine component evolved from the aerodynamic design effort and the results from several supporting technology programs. The resultant configuration, shown previously in Figure 4.7.1-1, consists of three main assemblies: the rotor, vane and inner case, and blade tip outer airseal.

Rotor Assembly

The turbine rotor is illustrated in Figure 4.7.3-1. Besides the disk and blades, it contains the compressor discharge seal, No. 4 bearing buffer air seal and thrust balance seal. The rotor design is different from most previous Pratt & Whitney Aircraft designs in that it is straddle mounted, or simply supported, rather than cantilevered off the rear high-pressure spool bearing. This eliminates having the bearing compartment forward of the disk and adds rigidity to improve performance retention and critical speed response.

Disk -- The disk design is shown in Figure 4.7.3-2 and is characterized by the thick bore region dictated by the high rim speed requirement. The selected material is PWA 1099, a high strength nickel base alloy. It has adequate mechanical properties to meet the life criterion for the integrated core/low spool and is currently available.

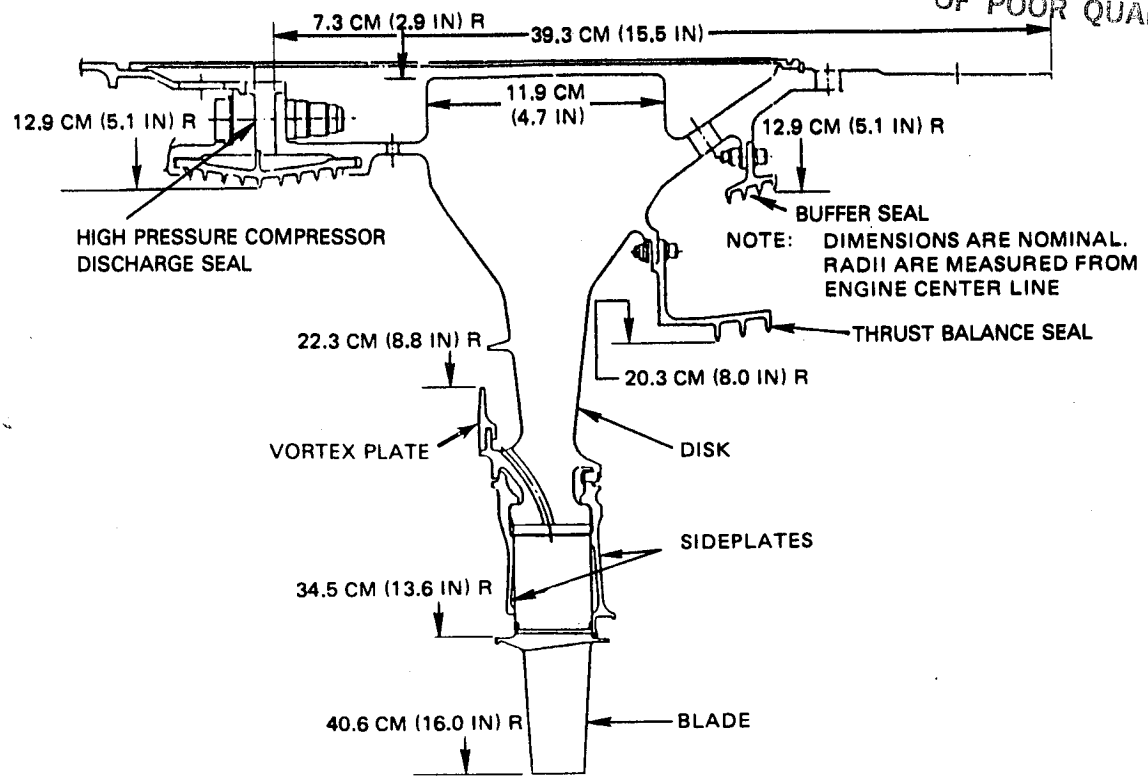

Figure 4.7.3-1 Mechanical Design of the High-Pressure Turbine Rotor Assembly

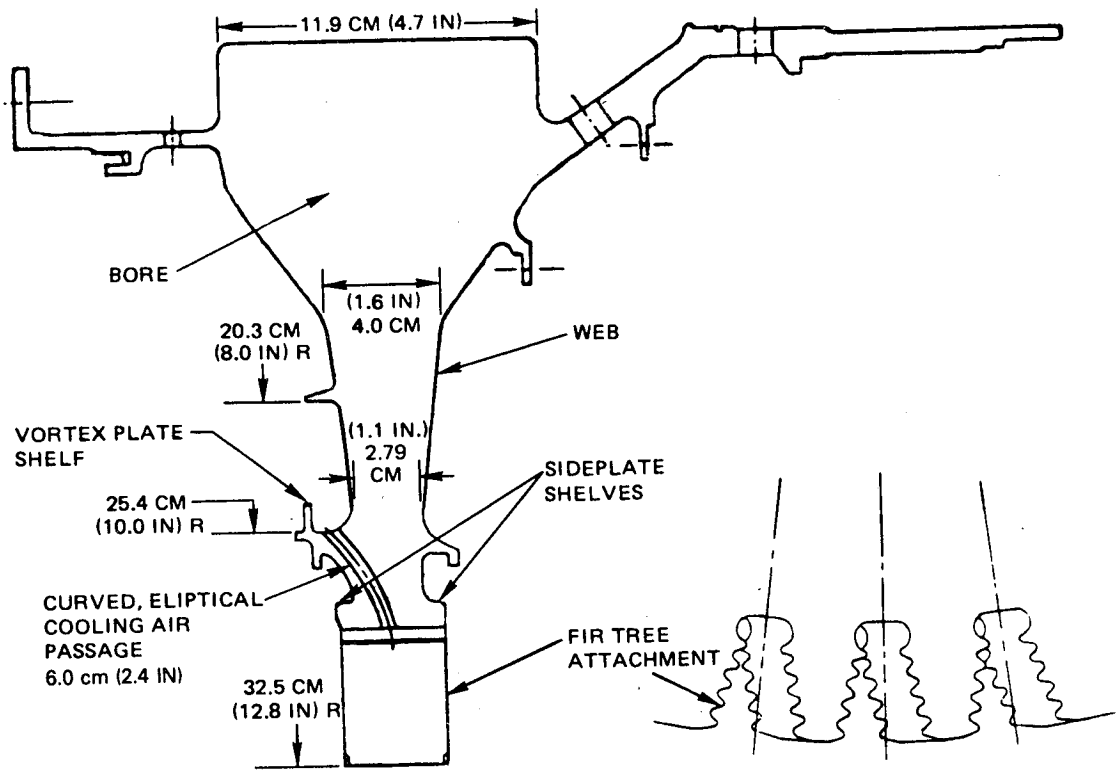

Figure 4.7.3-2 High-Pressure Turbine Disk Design Features

The rim has a firtree attachment to hold the blades, shelves to support the front and rear sideplates, and a flange to support the vortex plate. The curved elliptical cooling air holes supply coolant from the tangential on-board injection nozzle to the blade root. These passages are designed to minimize the width of the rim, control rim breakout stress concentrations, and provide the required coolant flow to the blade root.

A vortex plate is used to contain blade cooling air and provide a passage for free-vortex pressure rise to augment the pressure of the flow exiting the tangential on-board injection nozzle. Pumping action through the curved elliptical hole also increases the pressure before the flow enters the blade root cavity. The vortex plate is attached to the disk by bayonet connectors (engaged lugs and slots), thus providing a boltless scheme to eliminate the need for windage covers.

The boltless, full ring sideplates perform the dual function of blade retention and sealing in the rim areas. Furthermore, this type of design eliminates broach angle/bolt incompatibility, reduces rim cavity size and eliminates flow restrictions caused by the proximity of the bolt to the rim cooling air source. As shown in Figure 4.7.3-1, the sideplates are trapped by bayonet connectors. Leakage is controlled by damper seals along the blade platform and by a "W" seal trapped by the blade and rear sideplate.

Blades -- The blade is a one-piece casting of PWA 1480, which is a nickel base single crystal alloy. An overlay coating (PWA 270 -- NiCoCrAlY) is used for protection against oxidation and erosion.

The blade is designed with a decrease in radial taper from root tip, a slight amount of tilt and a minimum wall thickness. The attachment is a five-tooth firtree geometry. Taper is used to control the radial distribution of mass so centrifugal forces can be maintained at an acceptable level. The amount of tilt is aimed at balancing stresses from centrifugal and gas bending loads. Wall thicknesses and cooling passage ribs are tailored to provide the desired distribution of radial mass. Figure 4.7.3-3 shows the defined wall and rib thicknesses at the blade root, mean and tip sections.

The blade thermal design is based on the average exit temperature profile produced by the vanes as well as maintaining a metal temperature below 982°C (1800°F). The blade is cooled with 2.75 percent of the core engine inlet air flow. A schematic of the cooling design is shown in Figure 4.7.3-4. The internal surface is cooled by convection, while external surfaces are film cooled from the leading edge showerhead holes and tip pressure side holes. There are no film cooling holes on either the pressure or suction surfaces of the airfoil.

Cooling air enters the blade through three root passages. The front passage supplies approximately 25 percent of the flow to cool the leading edge and tip. The middle passage utilizes approximately two-thirds of the cooling flow. Flow circulates through the internal cavity, making two spanwise excursions, and enters the trailing edge where it passes through an array of pedestals before being discharged into the gas path. The third passage directs a small percentage of air to cool part of the root area and supplement trailing edge cooling.

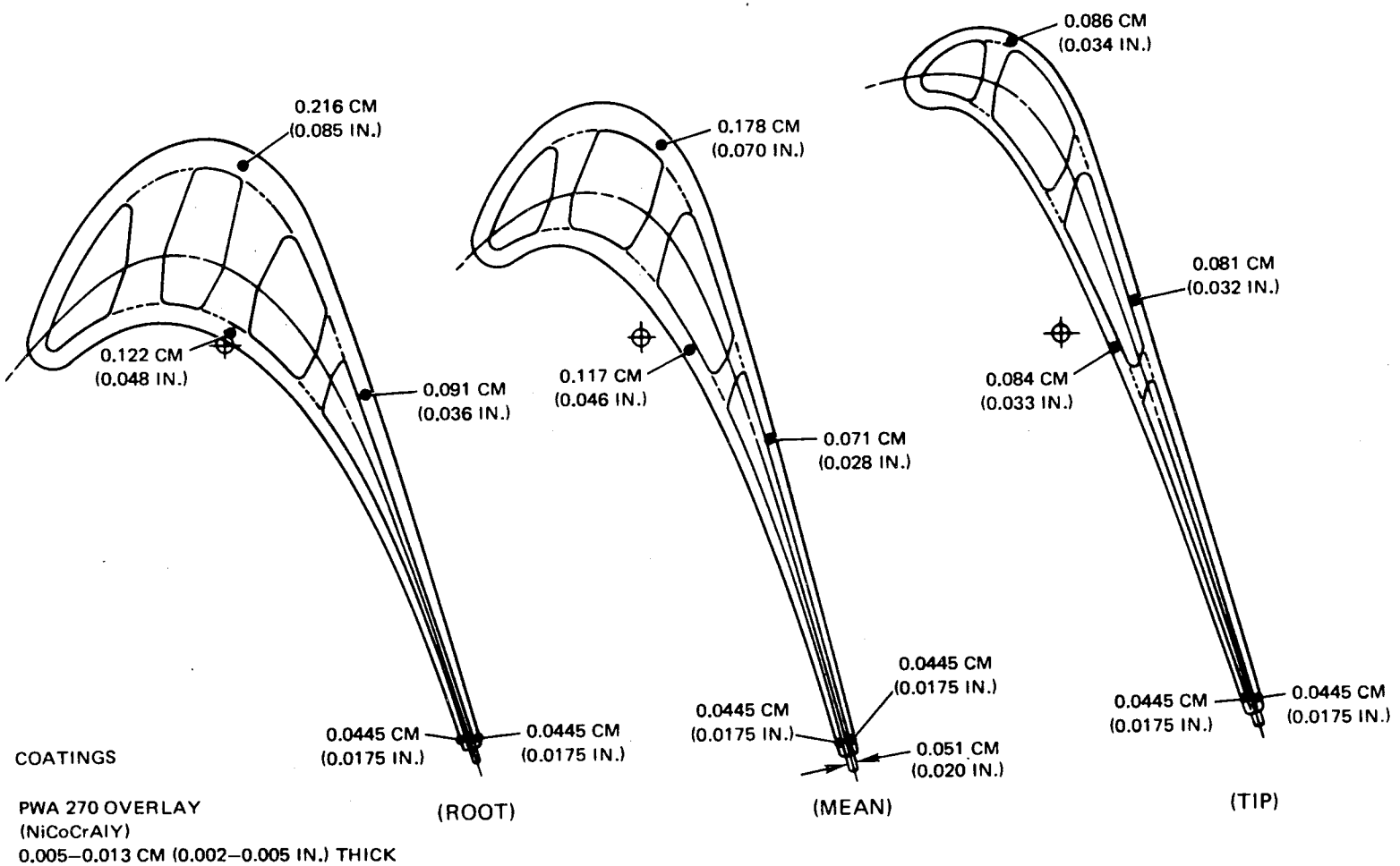

Figure 4.7.3-3 Uncoated Blade Wall Thickness and Internal Rib Design

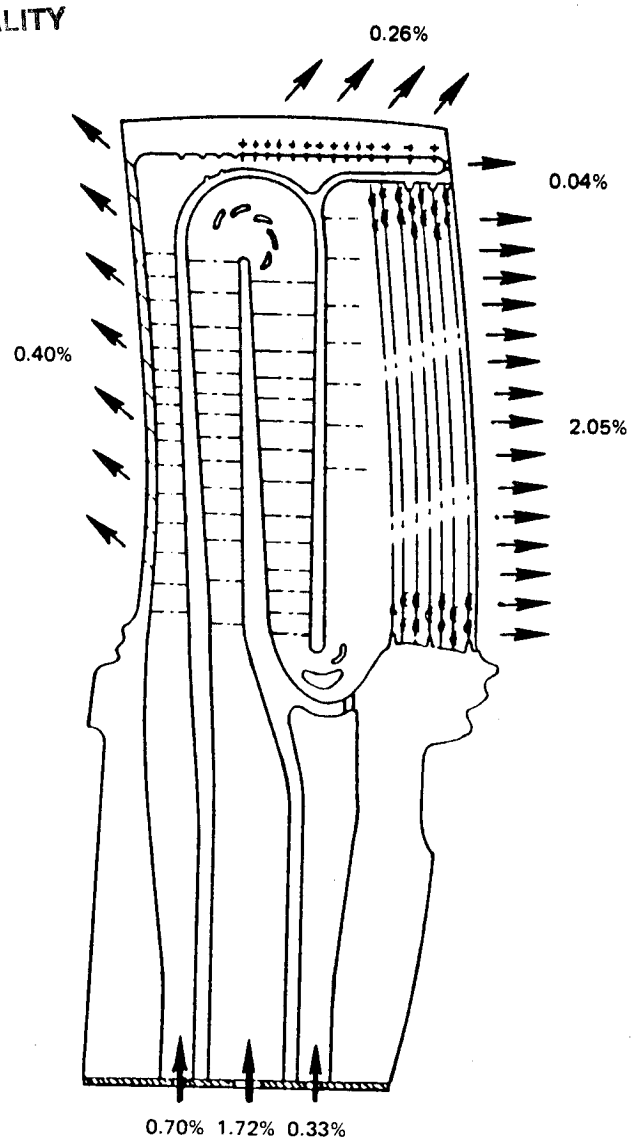

Figure 4.7.3-4 Turbine Blade Cooling System

Seals -- The turbine rotor has three knife-edge air seals: the high-pressure compressor discharge seal, No. 4 bearing buffer seal and thrust balance seal located on the rear side of the rotor. To avoid adding a bore to support the thrust balance seal, it is designed within its self-sustaining radius and thrust balance is obtained by varying the pressure within the piston area cavity. Design details, including the materials selection of these seals are shown in Figure 4.7.3-5. As a precaution against vibratory excitation, the seals are designed with dampers.

The compressor discharge seal uses a high expansion Tinidur material for the rotating member to maintain clearances between 0.027 and 0.035 cm (0.011 and 0.014 in). Clearances are set to ensure no rubs during maneuvers and to minimize the amount of rub during startup operation.

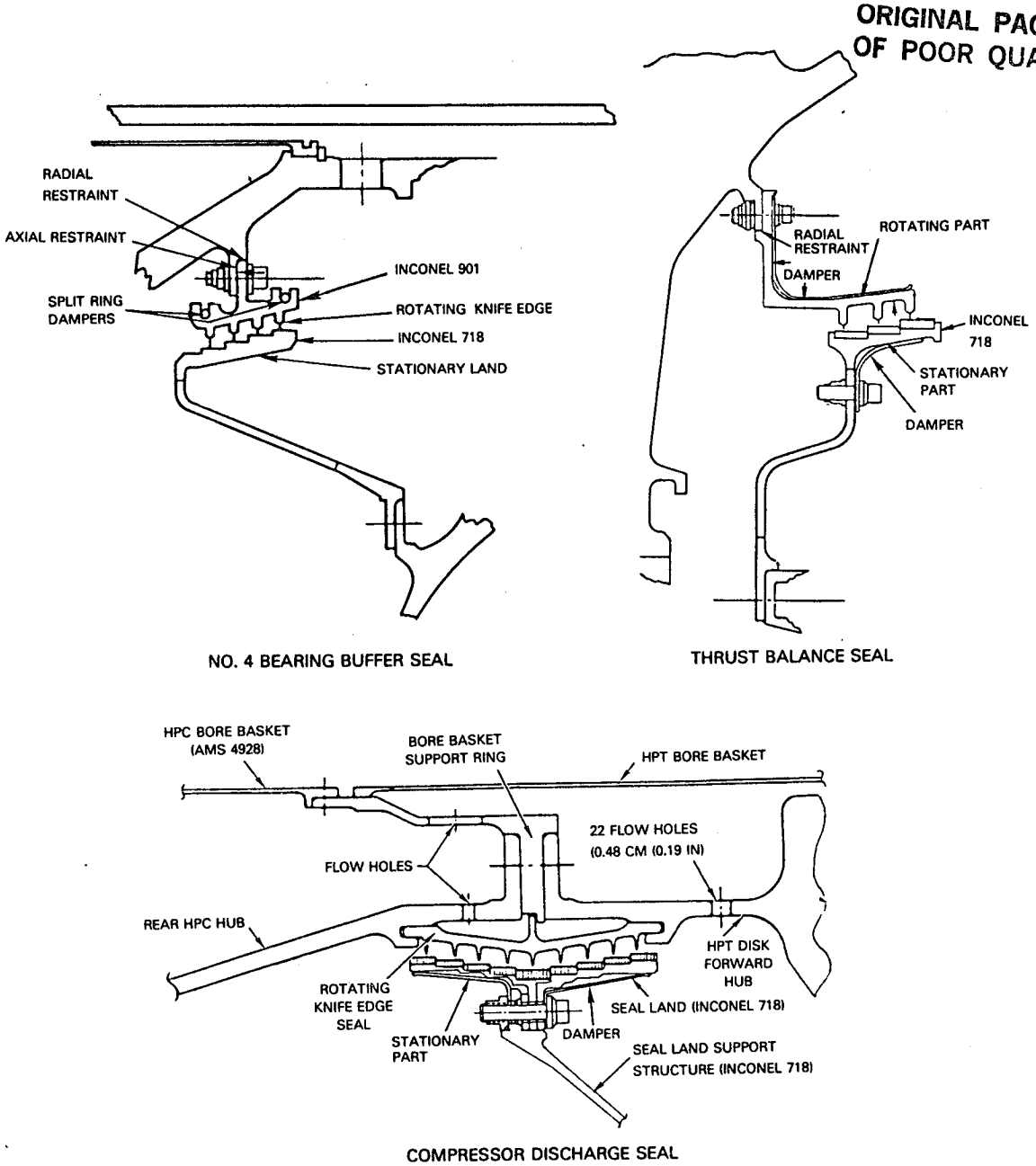

Figure 4.7.3-5 Design Details of High-Pressure Turbine Knife-Edge Seals

Vane and Inner Case Assembly

The vane and inner case assembly is illustrated in Figure 4.7.3-6. The primary components are the vanes, the vane support structure, the tangential on-board injection (TOBI) system, and the compressor discharge seal support. With the exception of the vanes, these components are designed using forgings and Inconel 718 welded construction.

Vanes -- The turbine vane assembly, shown in Figure 4.7.3-7, comprises 24 vanes supported at the outer surface by two bolts through the outer flange. These bolts absorb radial loads and provide circumferential restraint. To minimize leakage caused by vane twisting, both the inner and outer surfaces are clamped along chordal cuts. By having a chordal cut, axial tilting of the vane from differential axial growth between the inner case and outer combustor case is accommodated without binding or opening up a leak path.

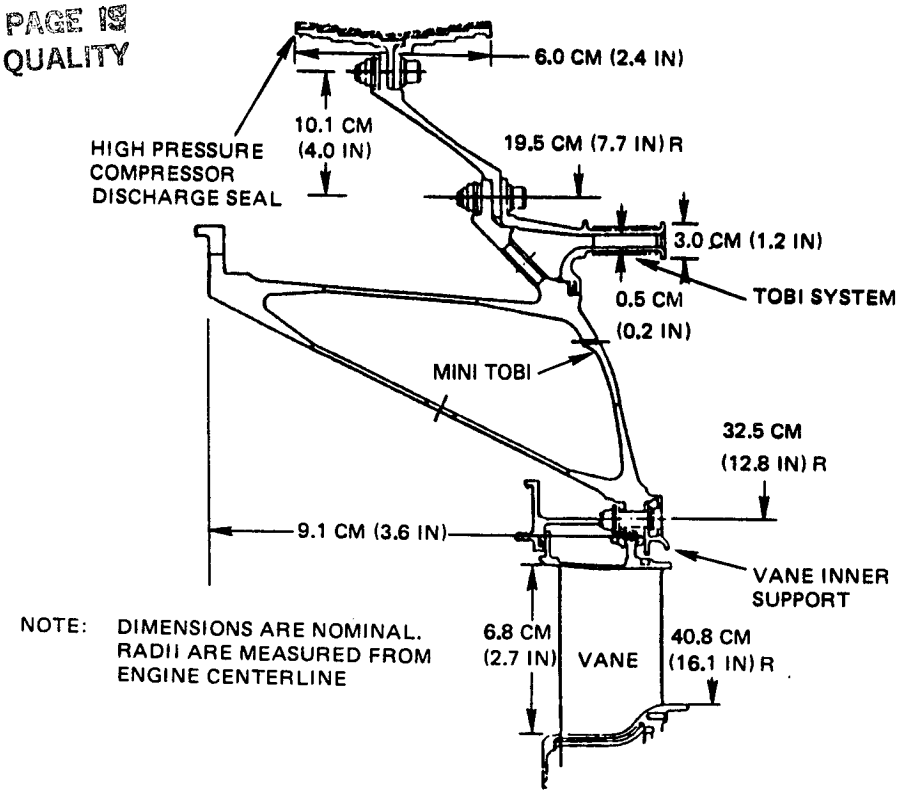

Figure 4.7.3-6 Turbine Vane and Inner Case Assembly

Like the blades, the vanes are fabricated from PWA 1480 single crystal material and the external surface is coated with PWA 270. In addition, the platforms are coated with PWA 264, a ceramic thermal barrier coating.

Excluding inner and outer platforms, the vane requires only 6.41 percent of core engine inlet flow for cooling. This is a small percentage of flow, considering the large size of the airfoil. When compared to current commercial engines operating at similar turbine stator inlet temperatures, this represents a 1.2 percent reduction in the cooling requirement.

A schematic of the vane cooling system is presented in Figure 4.7.3-8. Internal surfaces are convectively cooled by impingement tubes made of Inconel 625 sheet metal stock and external surfaces are film cooled. Cooling air enters the vane at both tip and root locations and is distributed within the three internal cavities. After the front cavity is cooled, the coolant is discharged through leading edge showerhead holes and a set of holes downstream of the leading edge on the suction wall to film cool the external surface. The showerhead hole angles are tailored to provide maximum heat transfer effectiveness in the thick leading edge area. Because of the vane contour, the stagnation point appears on the pressure surface. This surface is film cooled by two sets of two rows of 0.058-cm (0.023-in) diameter holes to offset this heat load. The suction surface downstream of the leading edge has three rows of 0.050-cm (0.020-in) diameter holes. The middle and rear vane cavities have impingement tubes from which numerous cooling air jets are impinged against the inside surface. The air is subsequently discharged through axially-angled holes to film cool the airfoil pressure surface. Air in the rear cavity is passed through the trailing edge pedestal array and discharged at the trailing edge.

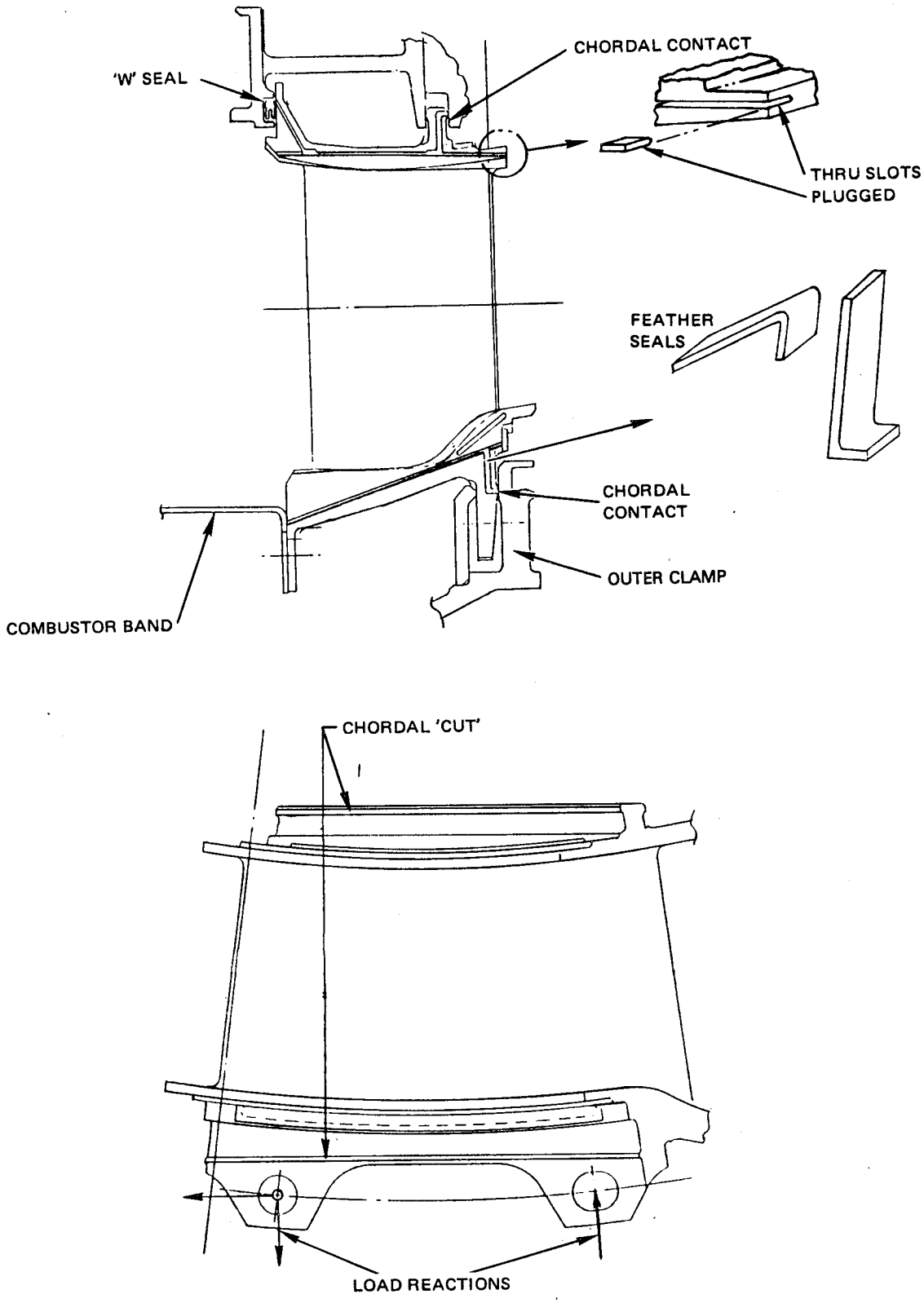

Figure 4.7.3-7 Turbine Vane Assembly

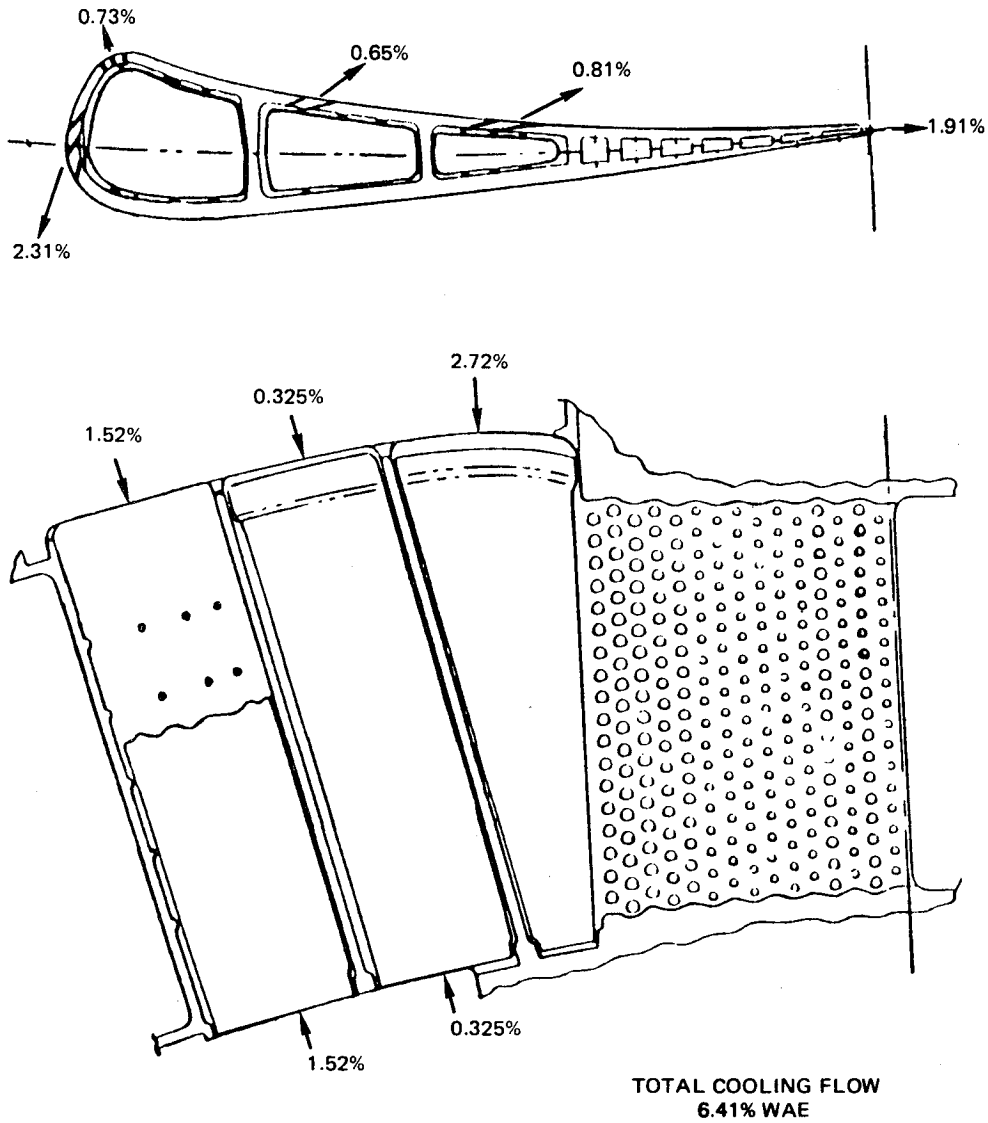

Figure 4.7.3-8 Turbine Vane Cooling Design

The platform cooling scheme is based on Pratt & Whitney Aircraft experience and utilizes a combination of impingement cooling under the platform and convection cooling on the platform gaspath surface provided by air emanating from drilled holes. Cooling flow percentages are 0.49 and 0.32 percent for the outer and inner platforms, respectively.

Inner Case -- The inner vane case, shown previously in Figure 4.7.3-6, supports both the inner portion of the vane and the compressor discharge seal land. The vane is connected to the support through bolts that tie both the vane and inner combustor liner together into the support. The support member for the compressor discharge seal and primary tangential on-board injection nozzle is bolted to the inner case structure.

The primary tangential on-board injection nozzle supplies cooling air to the disk rim area and blade root. It is fabricated from Hastelloy X material and has 36 vanes brazed into slots in both the inner and outer walls. The primary purpose of the secondary (or mini) tangential on-board injection nozzle is to induce swirl into the coolant flow at the front side of the turbine disk, thereby reducing windage heat up of the coolant flow in the disk front rim cavity front sideplate.

Blade Tip Seal Outer Airseal

The turbine blade tip seal is part of the internal active clearance control system. The seal design is shown in Figure 4.7.3-9, which identifies the major components. These include the front and rear outer airseal support rails, outer air seal shoe and impingement ring. The seal assembly is supported by the high-pressure turbine outer case, which incorporates the manifold for the active clearance control system. The outer case is attached to the outer vane support. For these components, Waspaloy® and Inconel 718 materials are extensively used to ensure the necessary dynamic resistance to satisfy blade containment criteria.

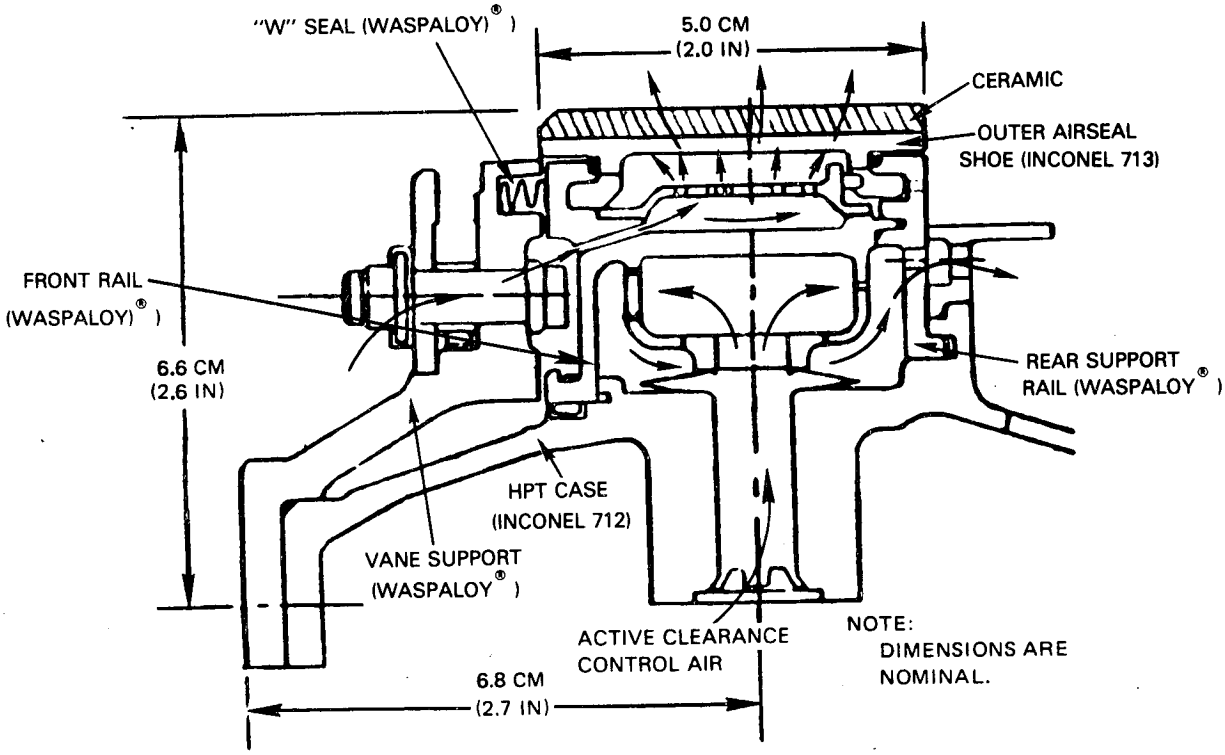

Figure 4.7.3-9 Turbine Blade Tip Seal Assembly

Figure 4.7.3-10 shows the detailed design of a seal shoe segment. The shoe is a cast Inconel 713 material and coated with a thin layer of yttrium-stabilized zirconia, an abradable ceramic. Slots are installed to reduce the spring rate and prevent overstressing the ceramic as it cools following a transient. To minimize cooling air leakage, "W" seals are used on the front and rear hooks of the shoe and feather seals are used at the circumferential ship lap joint between shoes. This type of joint protects the feather seals from pressure pulses caused by the passing blades.

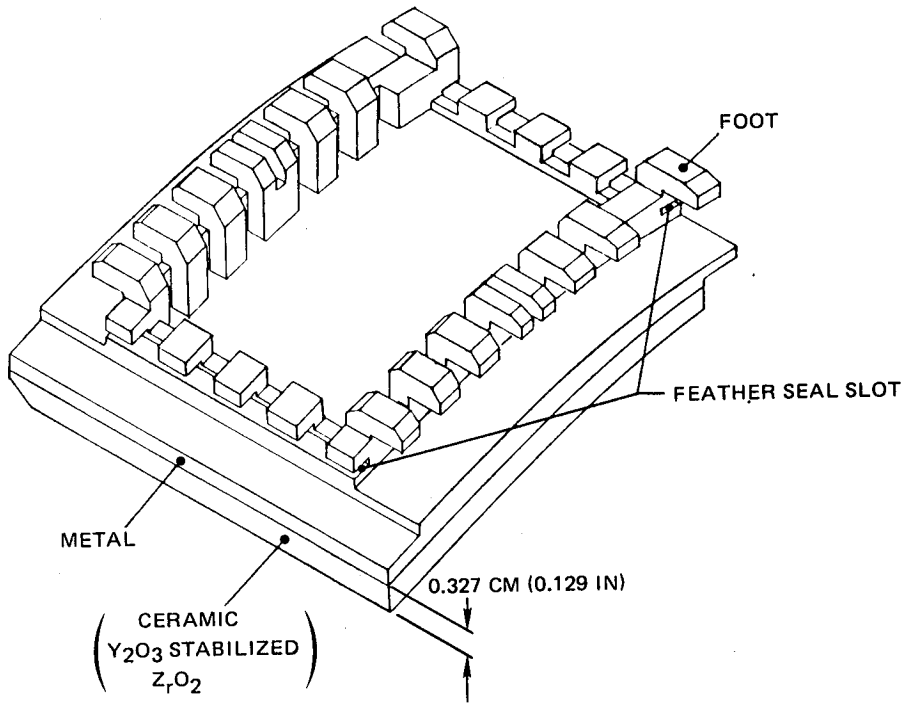

Figure 4.7.3-10 Details of the Outer Airseal Shoe Design

The active clearance control system maintains close blade tip clearances at all operating conditions by impinging controlled temperature air on the outer air seal support rails. Air for active clearance control is acquired from different bleed stations in the high-pressure compressor, depending on the specific operating condition. The cooler temperature air lowers the turbine case metal temperature and corresponding thermal expansion, thereby controlling the radial movement of the seal shoes towards the blade tip. The goal blade tip clearances are 0.068 cm (0.027 in) at takeoff and 0.047 cm (0.0186 in) at cruise (the aerodynamic design point). A more detailed discussion of the high-pressure turbine active clearance control system is presented in Section 5.6.

4.7.4 Design Substantiation and Supporting Analyses

4.7.4.1 Predicted Performance

The turbine for the integrated core/low spool has a goal efficiency of 87.9 percent. Design substantiation as well as demonstration of efficiency and other performance goals is based largely on the results acquired from the High-Pressure Turbine Uncooled and Warm Rig Tests. The Uncooled Rig Test Program (Ref. 6) verified the aerodynamic design. The recently completed Warm Rig Performance Test demonstrated a system efficiency of 88.5 percent at the design condition. This exceeds the performance predicted for both the integrated core/low spool and the flight propulsion system.

4.7.4.2 Structural Analyses/Life Analyses

Structural analyses of all major components were performed as part of the design process. A durability assessment was restricted to the turbine airfoils and focused primarily on demonstrating the life goals for the flight propulsion system. Salient results from the different analyses are summarized in the following sections.

Disk

Table 4.7.4-I summarizes disk life and stress characteristics. Burst margin is adequate and disk web thickness is controlled to avoid possible low order (2E through 4E) first coupled mode resonances. However, the average tangential stress for the rim, blade attachment and sideplates is slightly higher than desired and will require additional refinement to meet the 1000 cycle goal.

TABLE 4.7.4-I

DISK LIFE AND STRESS SUMMARY

	Integrated Core/ Low Spool
Bore Life (x 10^{-3} cycles)	8.5
Rim Life (x 10^{-3} cycles)	80
Average Tangential Stress MPa (ksi)	759.4 (110.1)

A finite element analysis was undertaken to identify the low cycle fatigue life of the disk rim, sideplates and vortex plate. Results showed that low cycle fatigue lives exceed the 12,000 cycle requirement for the flight propulsion system. Analysis also indicated that limiting stress rupture points occur on the front sideplate outer diameter, where the temperature is estimated at 732°C (1350°F), and on the front sideplate snap diameter fillet, where the temperature is 593°C (1100°F) but the stress is higher than that at the outer diameter. Stress rupture lives at both areas are greater than 1000 cycles at hot day sea level takeoff conditions. Stresses at all other locations on the sideplate and vortex plate are lower, and therefore have stress rupture lives greater than 1000 cycles.

The adequacy of the secondary flow system in maintaining acceptable disk metal temperatures was verified by a thermal analysis of a detailed element breakup model. The model and corresponding temperatures for the disk and parts of the static structure are shown in Figure 4.7.4-1. The temperatures shown are for a hot day takeoff condition.

A buckling analysis of the front sideplate was also conducted to assess the possible effects of thermal gradients encountered during the flight cycle. This analysis indicated that no buckling occurs at any point in the flight cycle.

Airfoils

Blades -- Structural evaluation of the single crystal blade was performed using the NASTRAN analytical technique. The model utilized plane stress elements for the airfoil skin and ribs, while the blade neck is simulated with beam elements. The model also included the stiffness properties of the single crystal atomic orientation. This enabled optimizing the crystallographic orientation to ensure sufficient margin from critical vibratory excitations.

The analysis was based initially on a configuration with 14 structural struts in the turbine intermediate case. Also, the single crystal axes orientation was arbitrarily aligned with the engine axis system (primary axis in the radial direction, secondary in the axial direction), recognizing that the secondary axis <010> and <100> could be re-oriented spacially, if required.

Results of this analysis indicated unacceptable frequency margins in the engine operating range. However, reducing the number of structural struts to 11 and re-orienting the secondary crystallographic axis provided sufficient frequency margin in the critical vibratory modes. As shown by the resonance diagram in Figure 4.7.4-2, acceptable margin is achieved with the revised configuration.

The reduced velocity flutter parameter for the blades is 2.1, which is well below the established design limit for shroudless turbine blades. Blade damper load was set at 4448 N (1000 lb) to control both buffet and resonant stresses.

Table 4.7.4-II summarizes the results of a blade attachment analysis for the nominal stresses of shear, bending, bearing, and tension. These results are based on the most stress-limiting tooth in the firtree geometry. Shear and bearing stresses exceed the limit by 8 and 11 percent, respectively. The remaining values are substantially below the limit, except for tension, which is only marginally higher than the acceptable limit. However, rig testing of single crystal root attachment specimens has been successfully conducted both at and above these stress levels with no evidence of material distress. On the basis of this testing, the attachment design is considered structurally adequate and the predictions are believed to be conservative.

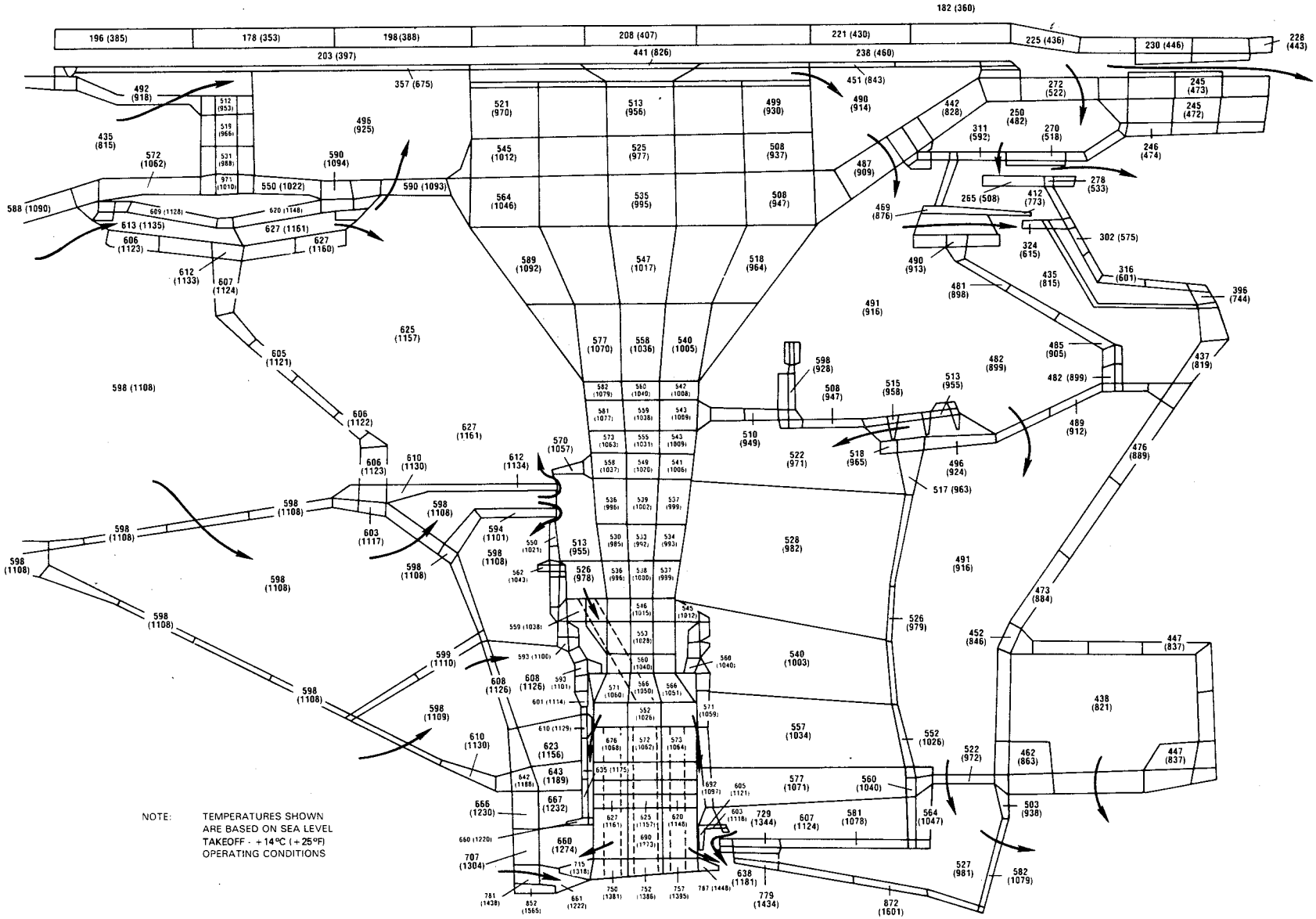

ORIGINAL PAGE IS
OF POOR QUALITY

Figure 4.7.4-1 Detailed Turbine Model Used for Thermal Analysis

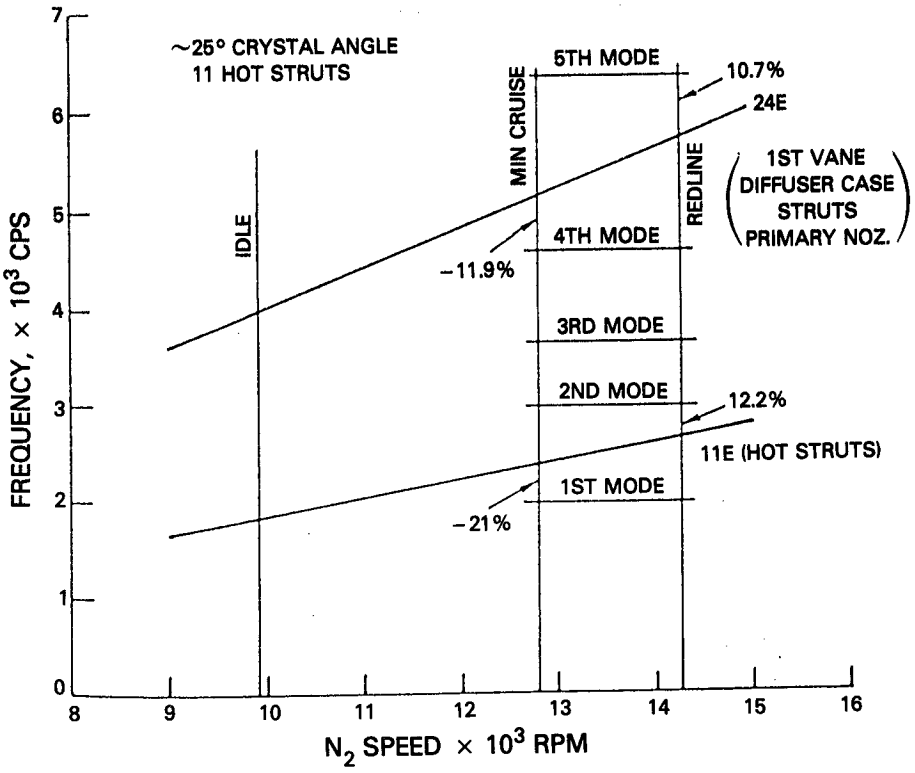

Figure 4.7.4-2 Predicted Frequency with Modified Configuration

TABLE 4.7.4-II

BLADE ATTACHMENT STRESS SUMMARY

Stress Mode	Location	% Above (Or Below) Design System
Shear	Blade	+11*
	Disk	-21
Bending	Blade	-48
	Disk	-63
Bearing	Blade	+ 8*
	Disk	-17
Tension	Blade	+ 2
	Disk	+ 1

*Rig testing has been conducted at these levels without material distress.

A series of durability analyses was conducted to verify the thermal design of the blade. Results confirmed the capability of the cooling system design to maintain acceptable metal temperatures. The isotherm plot of the blade mid-span section in Figure 4.7.4-3 shows the average metal temperature is 954°C (1750°F). The highest temperature is slightly above 1093°C (2000°F) and occurs on the suction wall surface near the first rib. A profile of pressure and suction surface temperatures is shown in Figure 4.7.4-4.

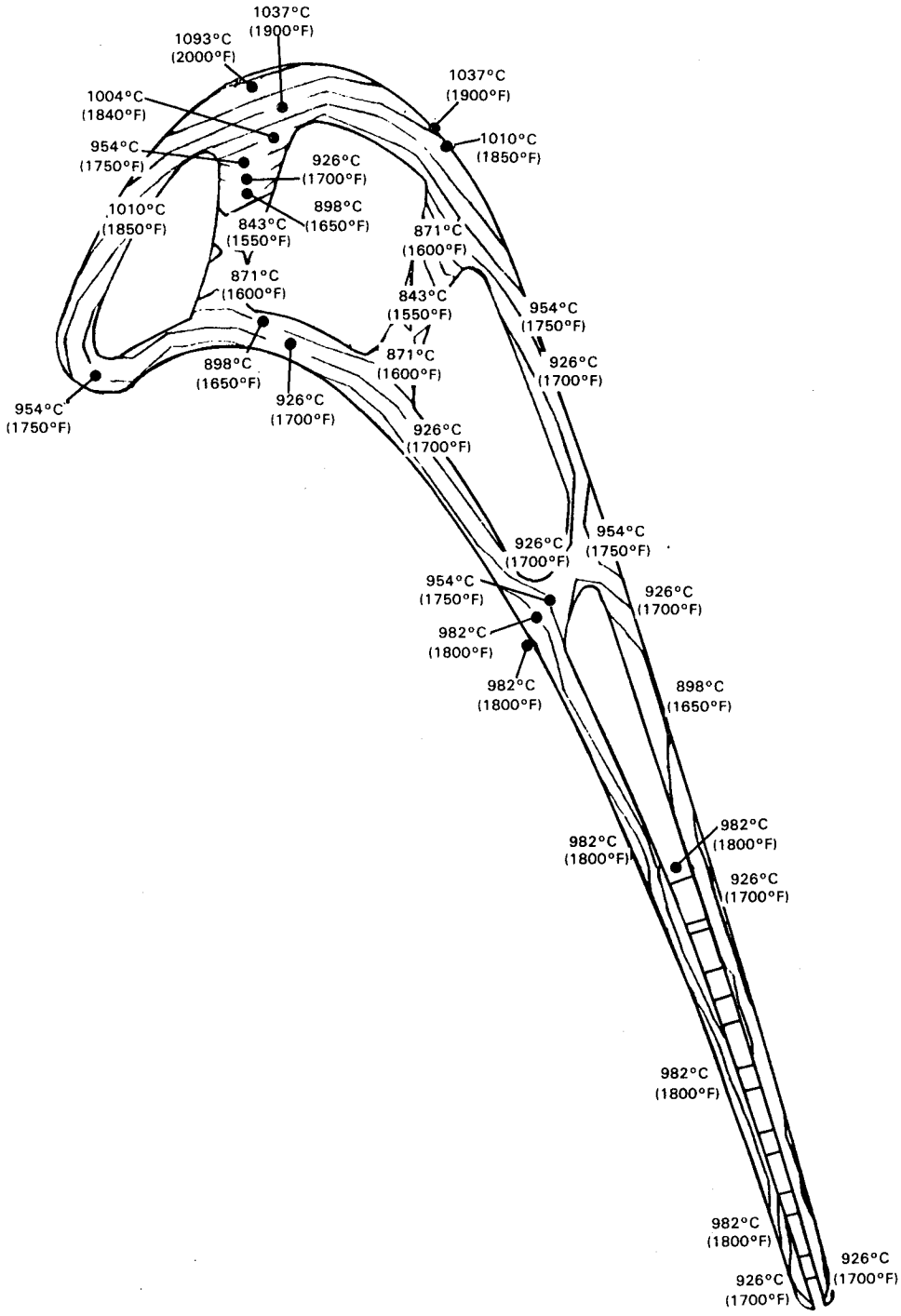

Figure 4.7.4-3 Blade Thermal Analysis Results (Midspan Location)

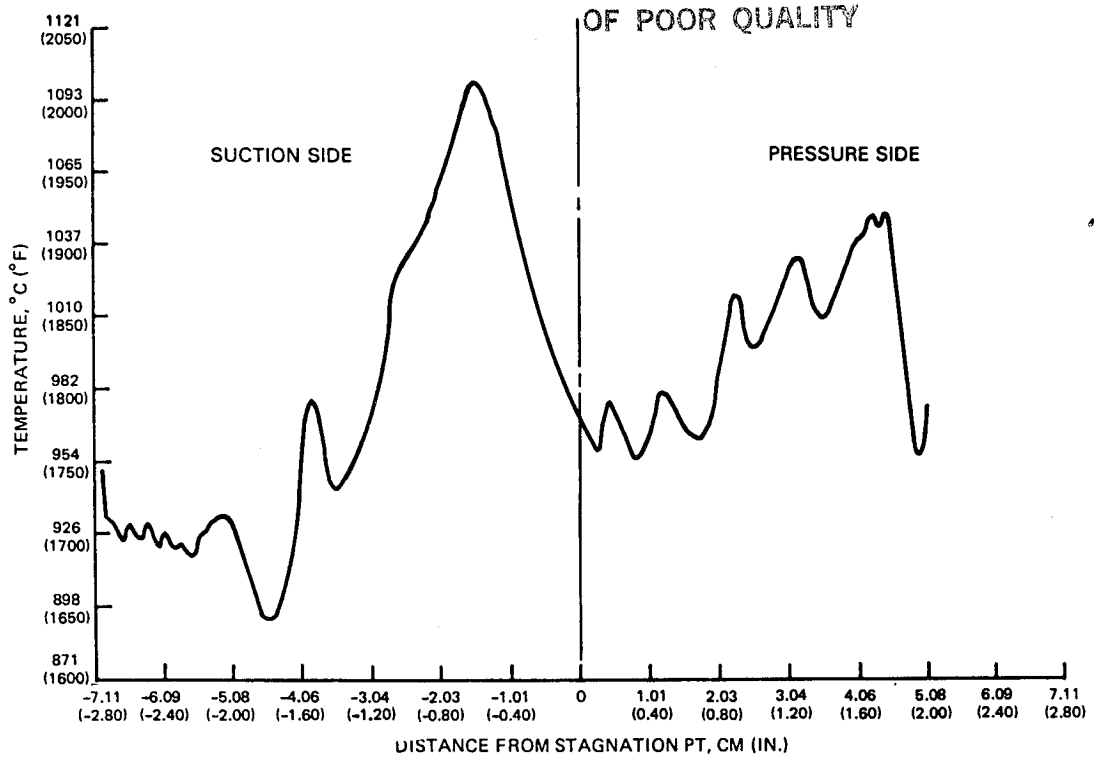

Figure 4.7.4-4 Blade Surface Temperature Profile

An analysis of transient strains occurring in the flight cycle showed that predicted lives meet the durability goals. Results indicated that the first rib is subjected to the highest strain (0.55 percent range). A synopsis of strain ranges is presented in Figure 4.7.4-5.

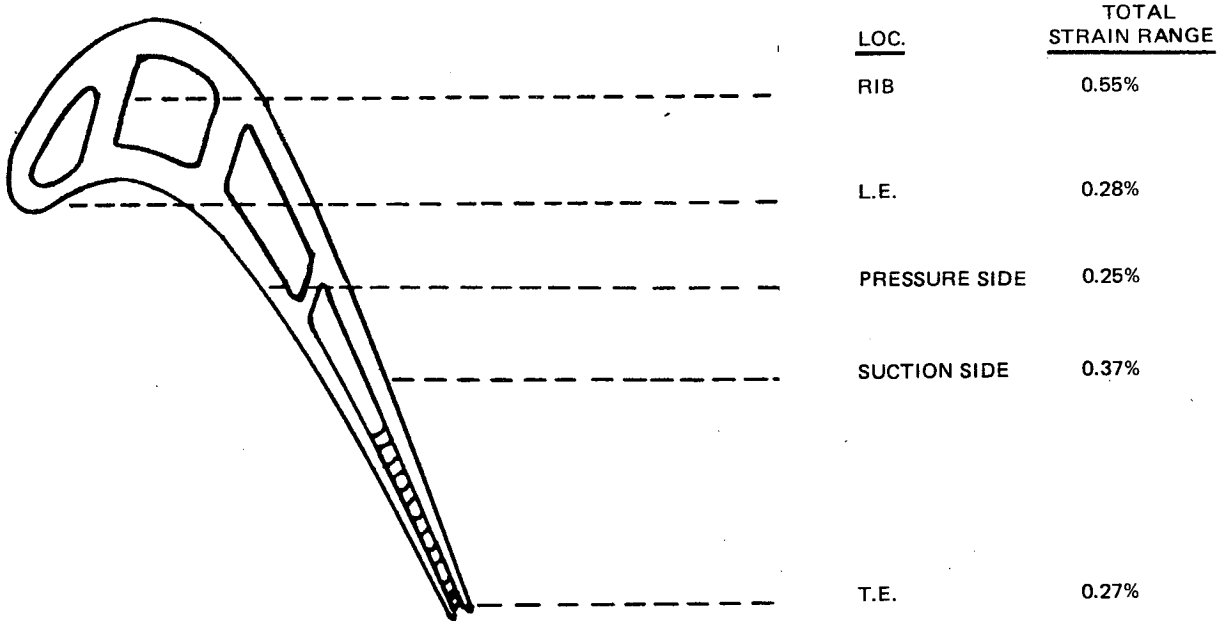

Figure 4.7.4-5 Predicted Strain

Life predictions for oxidation and cracking are summarized in Table 4.7.4-III. Durability goals for both the integrated core/low spool and flight propulsion system are surpassed by an appreciable margin, as shown by these results.

TABLE 4.7.4-III

BLADE LIFE PREDICTIONS

	Required	Calculated
FLIGHT PROPULSION SYSTEM		
Oxidation	6,000 Hours	16,000 Hours
Cracking*	10,000 Hours (2200 Flight Missions)	16,000 Hours (3500 Flight Missions)
INTEGRATED CORE/LOW SPOOL		
Oxidation	50 Hours (Hot Time)	400 Hours (Hot Time)
Creep	50 Hours (Hot Time)	80 Hours (Hot Time)

*Cracking as a result of interacting creep and low cycle fatigue

Vanes -- Results of a thermal analysis, based on the predicted combustor exit profile, are presented in Figure 4.7.4-6. This isotherm plot shows the highest metal temperature (1226°C (2239°F)) occurring on the suction wall adjacent to the third cavity. Figures 4.7.4-7 and -8 show profiles of film temperatures on the vane pressure and suction surfaces, respectively. Of particular importance in Figure 4.7.4-8 is the fact that the leading edge film holes provide effective film protection for the entire suction surface with 2.31 percent of the total engine flow. Based on these distributions, Figure 4.7.4-9 shows the resulting profile of vane surface temperatures.

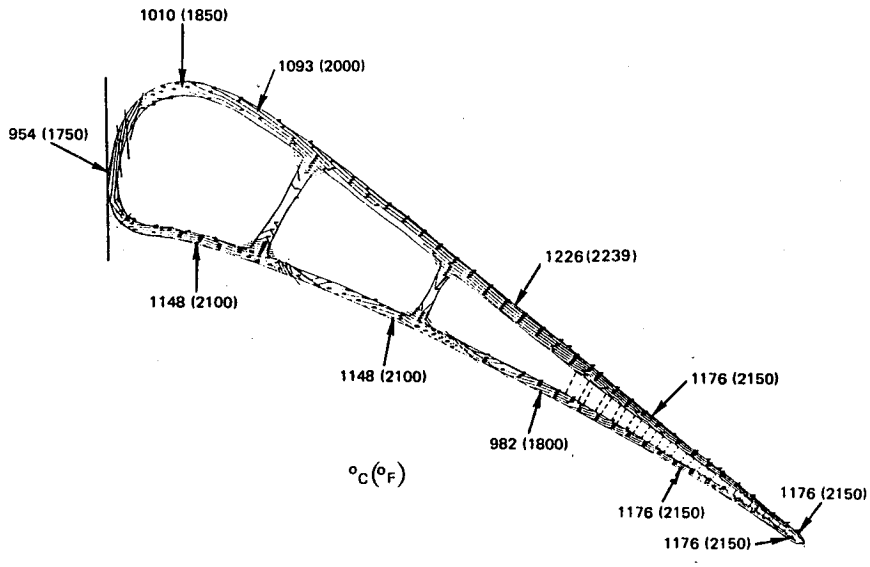

Figure 4.7.4-6 Vane Thermal Analysis Results

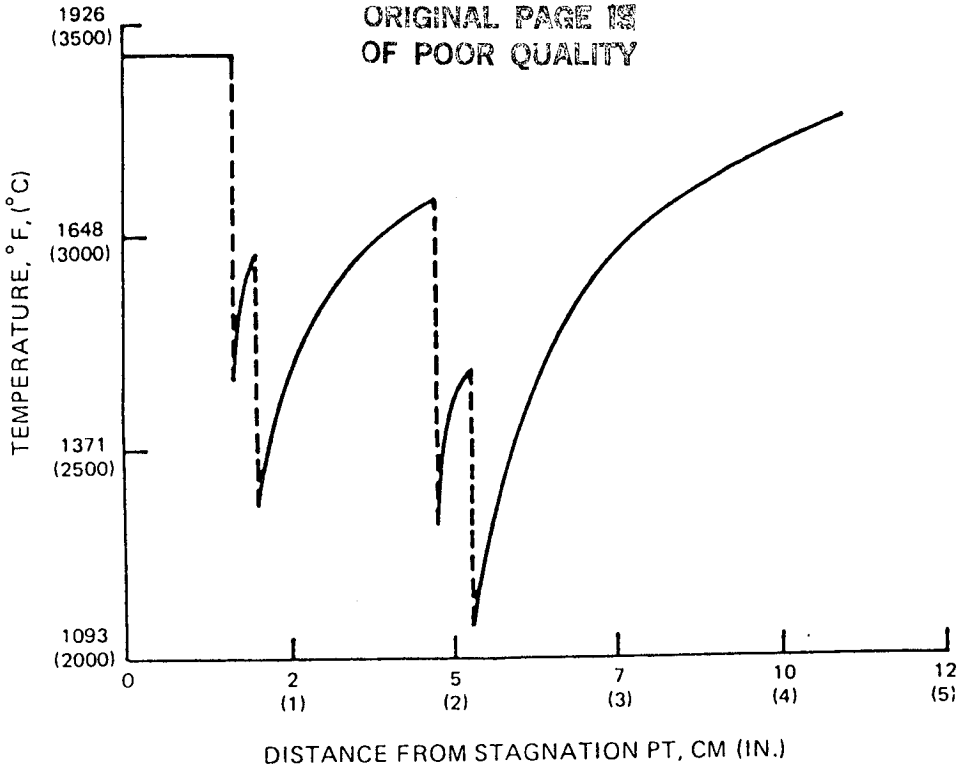

Figure 4.7.4-7 Pressure Wall Film Temperatures

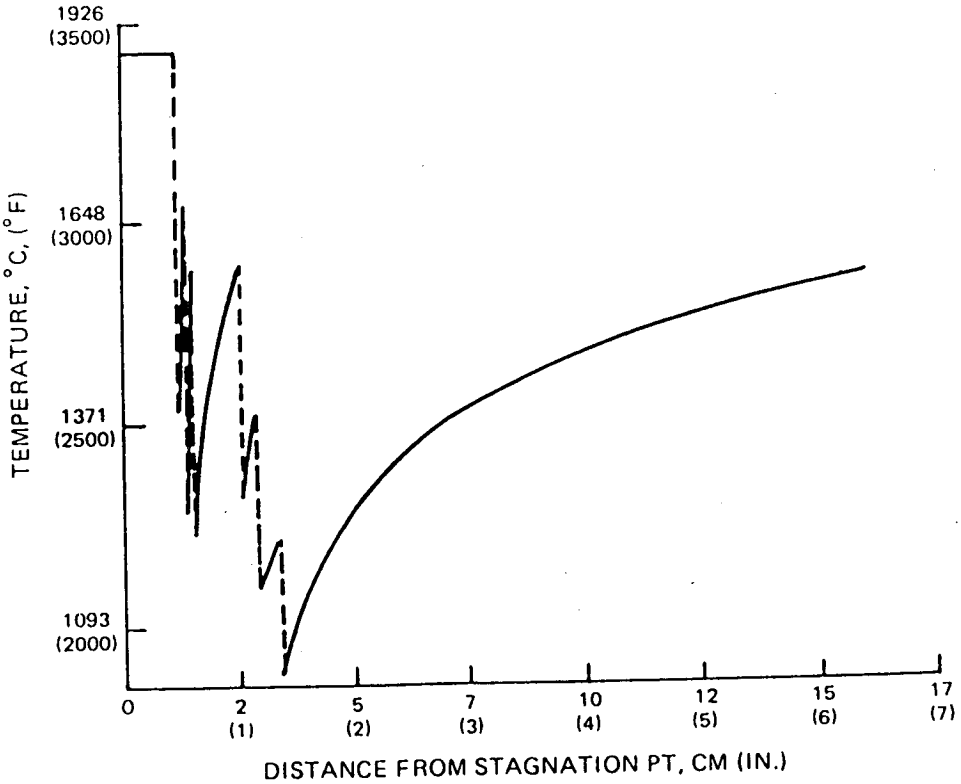

Figure 4.7.4-8 Suction Wall Film Temperatures

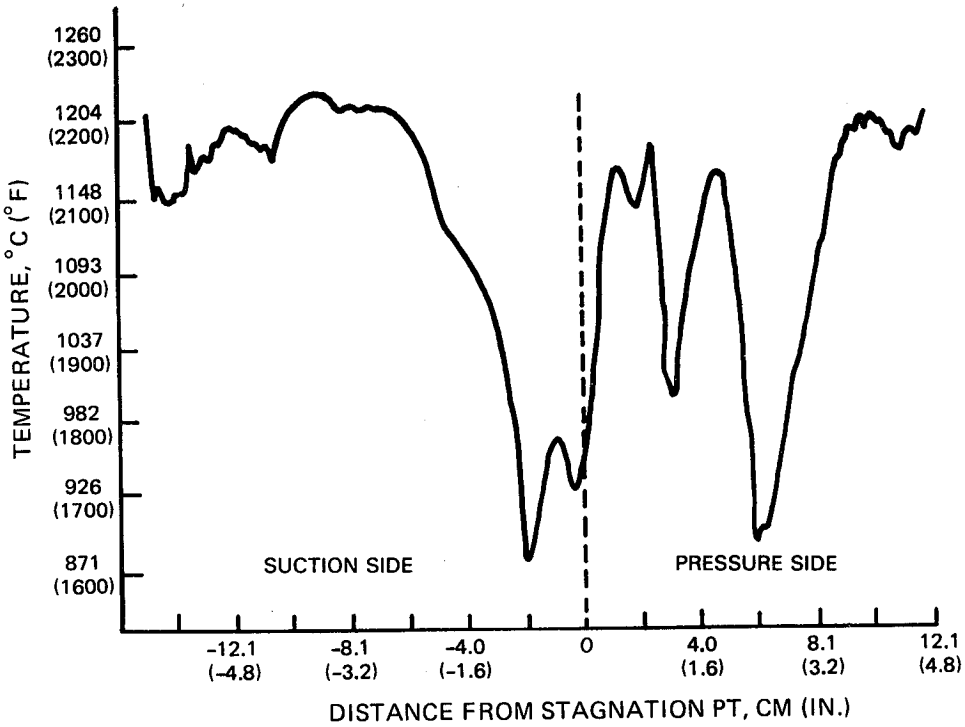

Figure 4.7.4-9 Vane Surface Temperature Profile

The calculated vane life for the flight propulsion system and the integrated core/low spool is presented in Table 4.7.4-IV. Oxidation life and cracking life exceed the goal values by 1000 hours or 300 cycles.

TABLE 4.7.4-IV

VANE LIFE

	Required	Calculated
FLIGHT PROPULSION SYSTEM		
Oxidation	6000 Hours*	7000 Hours*
Cracking	10000 Hours (2200 Flight Missions)	11000 Hours (2500 Flight Missions)
INTEGRATED CORE/LOW SPOOL		
Oxidation	50 Hours (Hot Time)	100 Hours (Hot Time)

*10,000 hours achieved with one recoating

Estimates of strain during transient operation were made to assess vane cyclic life. Results showed that the vane leading edge experiences the greatest total strain range (0.7 percent). The predicted strain ranges for the vane are identified in Figure 4.7.4-10.

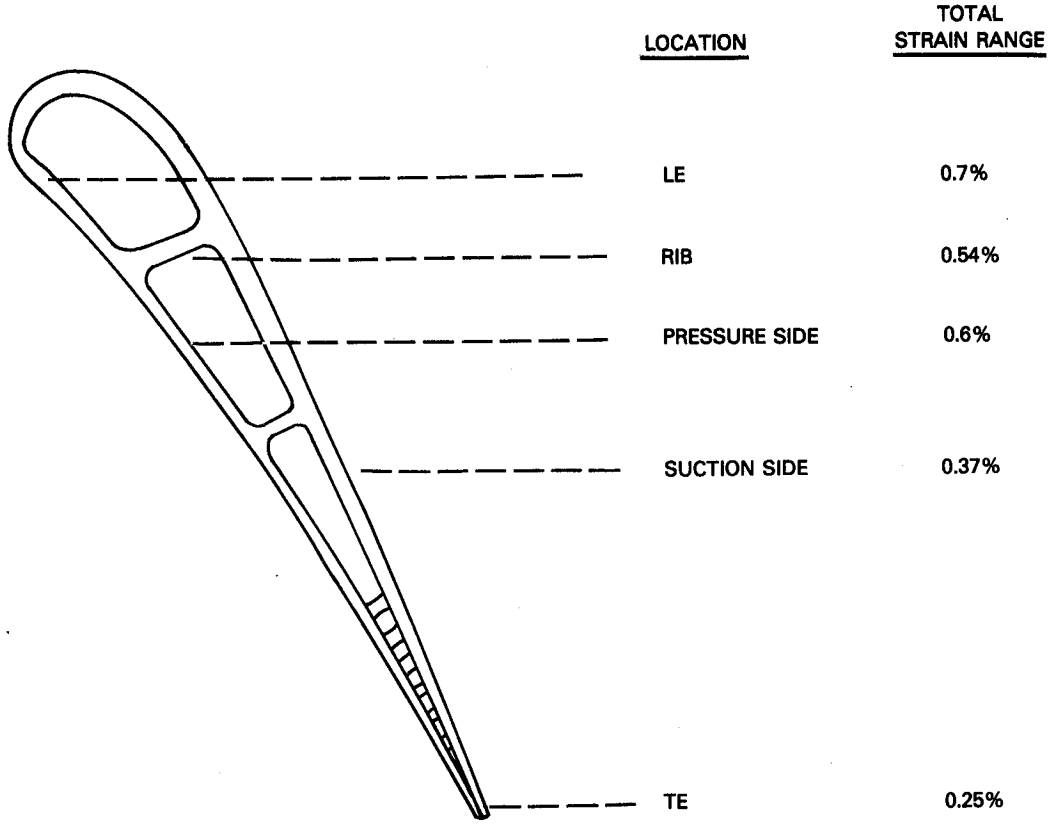

Figure 4.7.4-10 Predicted Strain

Vane Inner Case

The inner case design was analyzed to ensure suitable load-carrying ability for the first vane blow-off loads, while at the same time minimizing deflections. The total blow-off load of the first vanes, acting in an aft direction on the inner and outer attachment points, is 222,410 N (50,000 lb) at sea level takeoff. Half of this amount is absorbed by the inner case.

A detailed shell analysis was conducted for a hot day sea level takeoff condition, and the calculated stresses are shown in Figure 4.7.4-11. These levels are low relative to the high strength of Inconel 718 material. Using the same analytical model, the impact of axial and radial deflections was evaluated. Results indicated that the calculated radial clearances are not considered critical except at the compressor discharge seal, where maintenance of seal clearance tolerances is more important. The critical axial deflection is at the vane inner support. At this location, excessive axial motion could create undesirable leakage paths at the vane and blade platform interface.

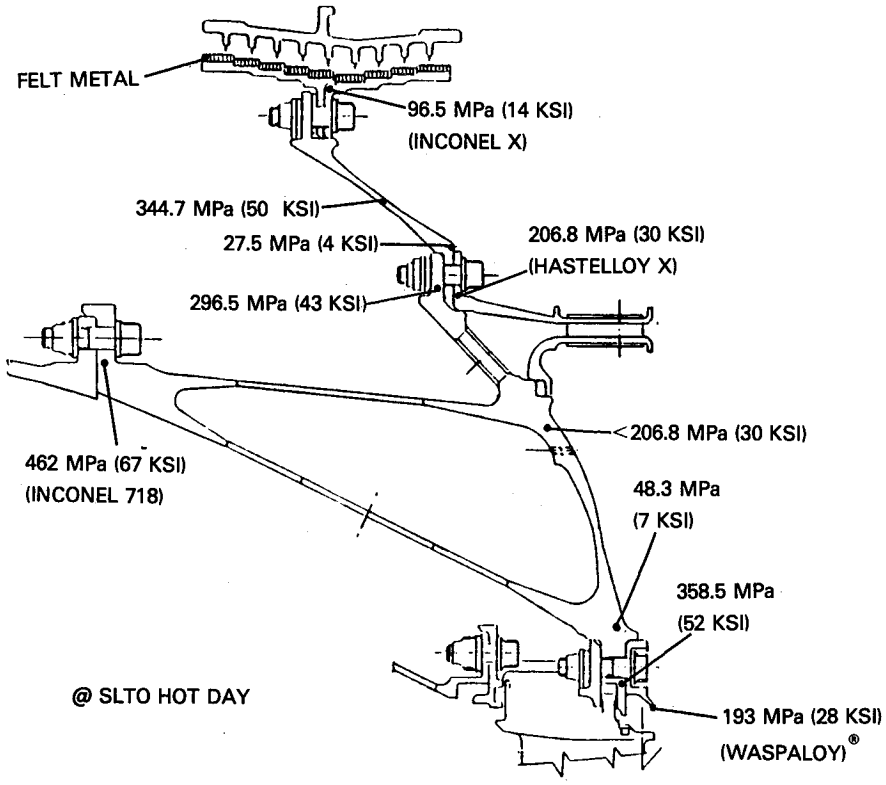

Figure 4.7.4-11 Inner Vane Case Stress Summary

Blade Tip Seal

Structural analysis of the tip seal assembly was performed with an analytical model that considered pressure loadings, vane and shoe support reactions, and thermal gradients based on a hot day sea level takeoff condition. Figure 4.7.4-12 shows the calculated metal temperatures and typical stresses are shown in Figure 4.7.4-13. These values are well below allowables at the assumed steady-state condition.

Knife-Edge Seals

Both stationary and rotating members of the thrust balance seal, No. 4 bearing buffer seal and compressor discharge seal were analyzed for resonance margin, coincidence margin and flutter stability.

A frequency response analysis of the rear thrust balance seal assembly showed that margins for resonance and coincidence met or exceeded requirements for commercial applications. Predicted resonance margins are 46 percent for the stationary seal land and 20 percent for the rotating knife edge. The estimated coincidence margin is 69 percent. Also, the maximum stability energy was calculated to be less than 0.0005 cm-kg/cm (0.001 in-lb/in), predicting flutter free operation.

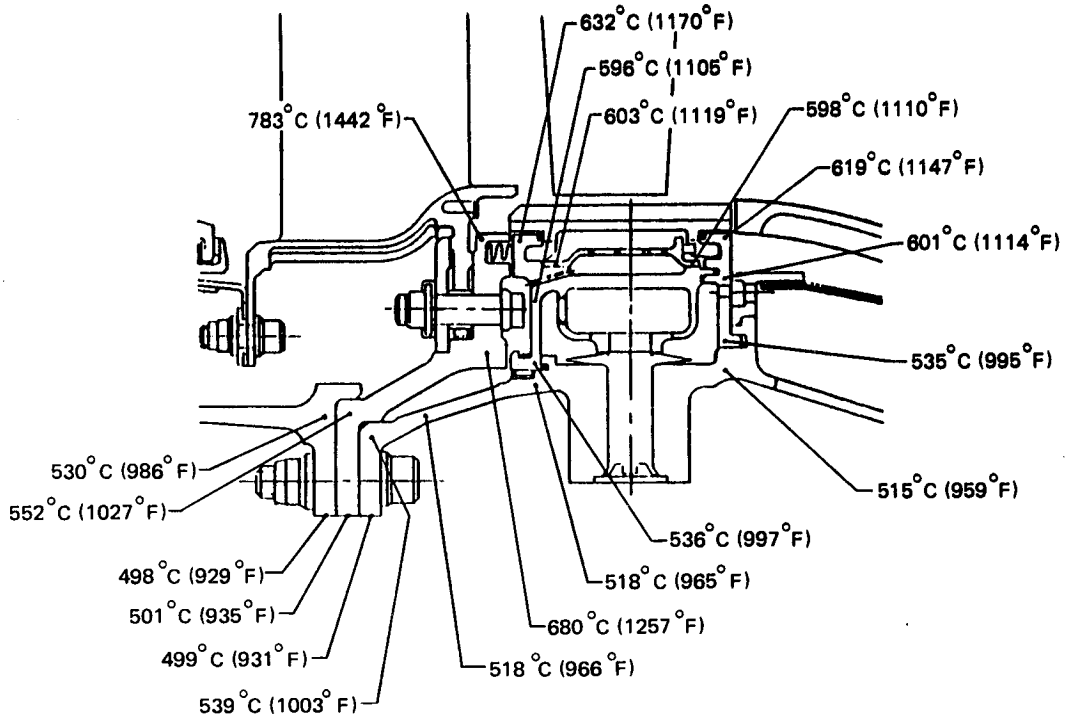

Figure 4.7.4-12 Temperature Map

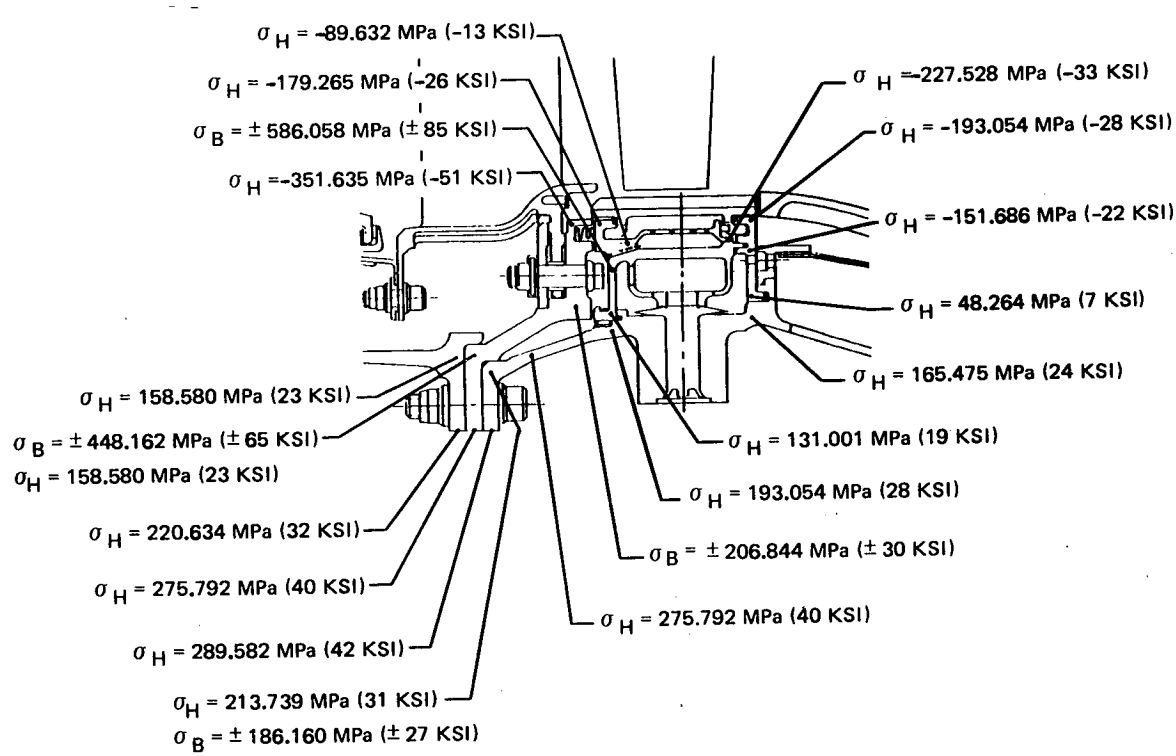

Figure 4.7.4-13 Stress Map

Resonance margins for the bearing buffer seal are 37 percent for the seal land and greater than 100 percent for the knife edge. These levels surpass commercial requirements. The coincidence margin is 48 percent. Like the thrust balance seal, the buffer seal has a calculated maximum stability energy less than 0.0005 cm-kg/cm (0.001 in-lb/in) and is predicted to be free from flutter.

An analysis of the compressor discharge seal frequency response indicated more than adequate margin throughout the operating range. Resonance margins are 35 percent for the seal land and greater than 100 percent for the knife edge. The coincidence margin for the seal assembly is greater than 100 percent.

4.7.5 Differences Relative to the Flight Propulsion System

The aerodynamics of the high-pressure turbine in the integrated core/low spool are basically the same as the component for the flight propulsion system. There are, however, some subtle differences in the mechanical design.

The materials and coatings used in the flight engine are advanced derivatives of those selected for the integrated core/low spool. Both the blades and vanes are designed using a second-generation single crystal alloy (SC 2000). This material offers an additional 27.7°C (50°F) advantage in temperature capability over the first-generation single crystal alloy, PWA 1480. Also, an advanced overlay coating (PWA 286) is used for improved resistance to oxidation and erosion. Vane platforms are coated with an advanced thermal barrier coating (TBC 100) for added temperature capability. In contrast to the integrated core/low spool, the internal cavities of the airfoils are coated with an aluminide coating (PWA 275) for resistance to oxidation. In addition, MERL 80 is the material selected for the disk.

In the inner vane case subassembly, the various components are designed using forgings and Inconel 718 welded construction. Cast materials would be used in the flight engine.

The blade tip seal for the flight engine features an abrasive blade tip material and an advanced ceramic outer air seal material. This type of system offers improved sealing capability as well as decreases the amount of performance deterioration that would normally result in the event of a blade tip rub. With the exception of the ceramic seal material, the outer airseal configuration, including the internal active clearance control system design, is the same as that defined for the integrated core/low spool. The blade tip, however, is designed with a tip squealer and abrasive tip cap. The tip squealer is designed for compatibility with the cap configuration by incorporating a 0.127 cm (0.050 in) nominal wall thickness that provides adequate surface area for the application of an abrasive grit. A 0.4 percent gain in performance is predicted by using only the squealer with a 0.088 cm (0.035 in) wall thickness. Increasing the wall thickness to 0.127 cm (0.050 in) decreases this improvement by 0.1 percent, although the use of an abrasive tip cap more than offsets this slight penalty.

4.8 TURBINE INTERMEDIATE CASE

4.8.1 General Description

The turbine intermediate case provides the gaspath transition between the high- and low-pressure turbines. In addition, it provides structural support for the rear bearing compartment and the rear engine mounts.

A cross-sectional view of the intermediate case design is shown in Figure 4.8.1-1. The case contains eleven structural struts to support the rear bearing compartment. To minimize blockage and pressure loss, the struts are encased by aerodynamically-shaped fairings. Insulated plumbing tubes for bearing compartment oil supply and scavenge are routed through the hollow fairings in the cavity just forward of the strut leading edge. Details of the design are published in Reference 7.

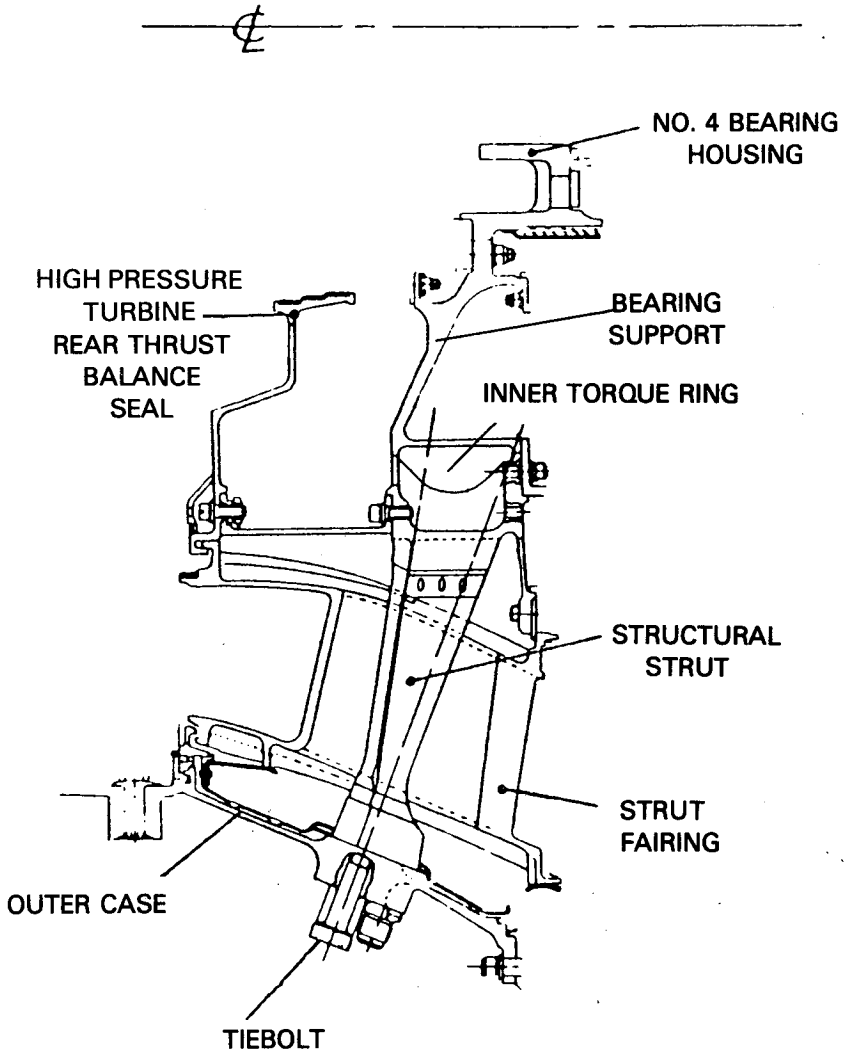

Figure 4.8.1-1 Turbine Intermediate Case Design

4.8.2 Aerodynamic Design

The flowpath for the turbine intermediate case is shown in Figure 4.8.2-1. The flowpath is relatively short with an axial length of 19.8 cm (7.8 in). Key parameters include an effective area ratio of 1.42, an annulus area ratio of 1.57 and a length to height ratio of 3.0. This design is aggressive, requiring a high level of diffusion as indicated in Figure 4.8.2-2. Although the pressure coefficients at the outer wall are near the levels for the onset of flow separation, experimental testing during a supporting technology program (Ref. 8) verified separation free performance.

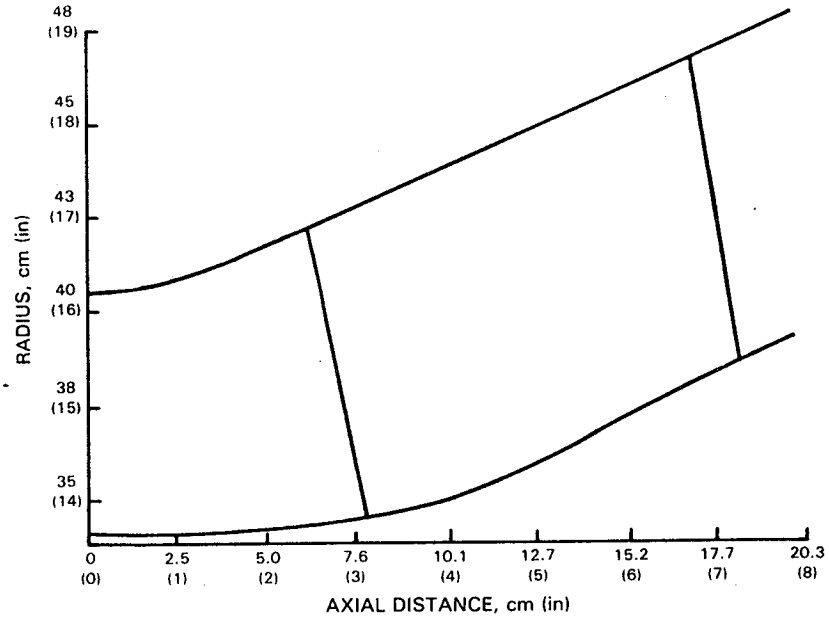

Figure 4.8.2-1 Turbine Intermediate Case Flowpath

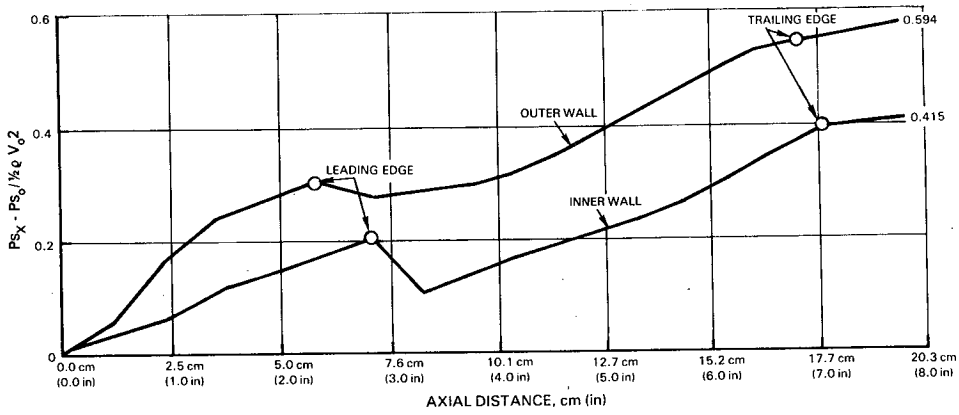

Figure 4.8.2-2 Analytically Defined Wall Pressure Distribution Profiles Showing a High Loading on the Outer Wall Design

The case is designed with a total of eleven strut fairings. The fairing is a standard 400 series airfoil, designed to turn the flow 5 degrees axially to satisfy low-pressure turbine inlet aerodynamics. The fairing is canted approximately 11 degrees, with the root section shifted axially rearward. This canted posture is dictated by structural requirements. To accommodate the structural strut and bearing compartment service lines, the airfoil thickness is 2.54 cm (1.0 in). A summary of the fairing aerodynamic design is presented in Table 4.8.2-I, and the stacking arrangement of the airfoil is shown in Figure 4.8.2-3.

TABLE 4.8.2-I

STRUT FAIRING AERODYNAMIC DESIGN SUMMARY
(AIRFOIL PLANAR SECTIONS)

Spanwise Section	1	2	3	4
Radius*, cm (in)	35.00 (13.78)	39.19 (15.43)	42.74 (16.83)	47.44 (18.68)
Axial Chord, cm (in)	10.9 (4.32)	11.2 (4.43)	11.5 (4.53)	11.7 (4.64)
Actual Chord, cm (in)	20.4 (8.03)	17.3 (6.81)	15.6 (6.14)	14.9 (5.88)
Maximum Thickness, cm (in)	2.54 (1.0)	2.54 (1.0)	2.54 (1.0)	2.54 (1.0)
Gap/Chord Ratio	0.98	1.29	1.59	1.82
Inlet Metal Angle, deg	150.2	144.5	138.7	131.6
Inlet Air Angle, deg	148.5	142.5	141.8	148.1
Inlet Mach No.	0.51	0.50	0.48	0.43
Exit Metal Angle, deg	33.4	44.1	51.0	54.9
Exit Air Angle, deg	31.9	35.3	38.4	42.4
Exit Mach No.	0.37	0.40	0.40	0.31

*At Stacking Point

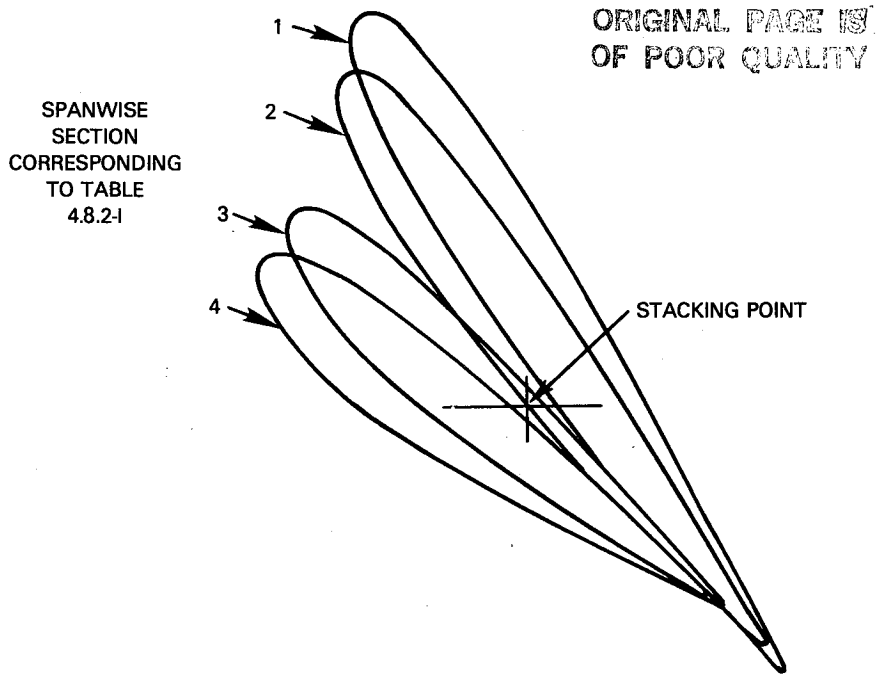

Figure 4.8.2-3 Strut Fairing Stacking Arrangement

4.8.3 Mechanical Design

The major components of the intermediate case assembly are the strut, fairing, inner torque ring, outer case, and rear engine mount structure.

The structural struts are forged from Inconel 718 material. Details of the design are shown in Figure 4.8.3-1. Each strut contains three circular internal cooling air passages. For added protection against thermal radiation and possible local conductive heating from contact with the fairing, the external surface is flame sprayed with an aluminum oxide insulation coating. Each strut is electron beam welded to the inner torque ring and retained at the outer case with a single, high-strength tiebolt. Externally removable dowels are also installed on each side of the tiebolt to absorb twisting moments from blowoff and thermal loads as well as to prevent potential shear loads on the tiebolt at the strut-to-outer case joint surface. The struts are designed to carry a rearward thrust balance load of approximately 111,205 N (25,000 lb), while maintaining an acceptable bending stress level.

The fairings are cast in eleven circumferential segments from MAR-M-509 cobalt alloy. These segments are sealed at the inner and outer platforms by feather seals fabricated from Haynes 188 cobalt alloy. Oil supply and scavenge lines for the rear bearing compartment are routed through the cavity formed between the structural strut and fairing. These lines are fully insulated for protection from the high temperature environment.

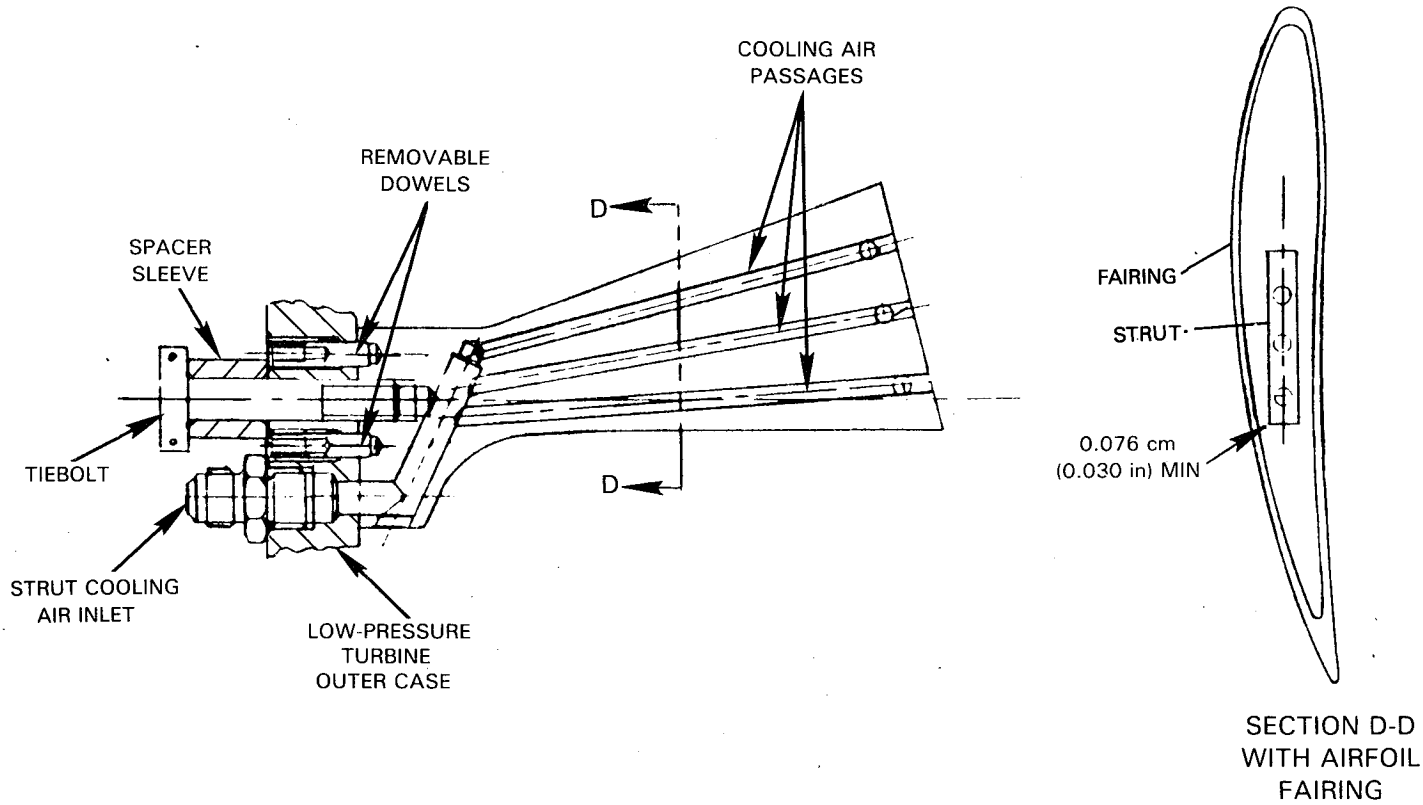

Figure 4.8.3-1 Structural Strut Design Details

The outer case is a continuous ring machined from an Inconel 718 forging. The case has a Hastelloy S material heatshield to channel hot discharge air from the high-pressure turbine blade tip seal along the case inner wall. This flow raises the case temperature to prevent a thermal mismatch of the strut with the outer case and inner torque ring during engine acceleration. Although the heatshield operates at a higher temperature than the outer case, its' lower coefficient of expansion maintains closely matched rates of thermal growth.

As shown in Figure 4.8.3-2, the rear mount arrangement consists of three double lugs located between struts on the upper half of the outer case. The lugs are electron beam welded to the outer case and designed only for test stand load conditions. Single lugs for ground handling are welded to the outer case, one in each bottom quadrant at the aft end of the case strut ring, leaving the forward area free for instrumentation bosses.

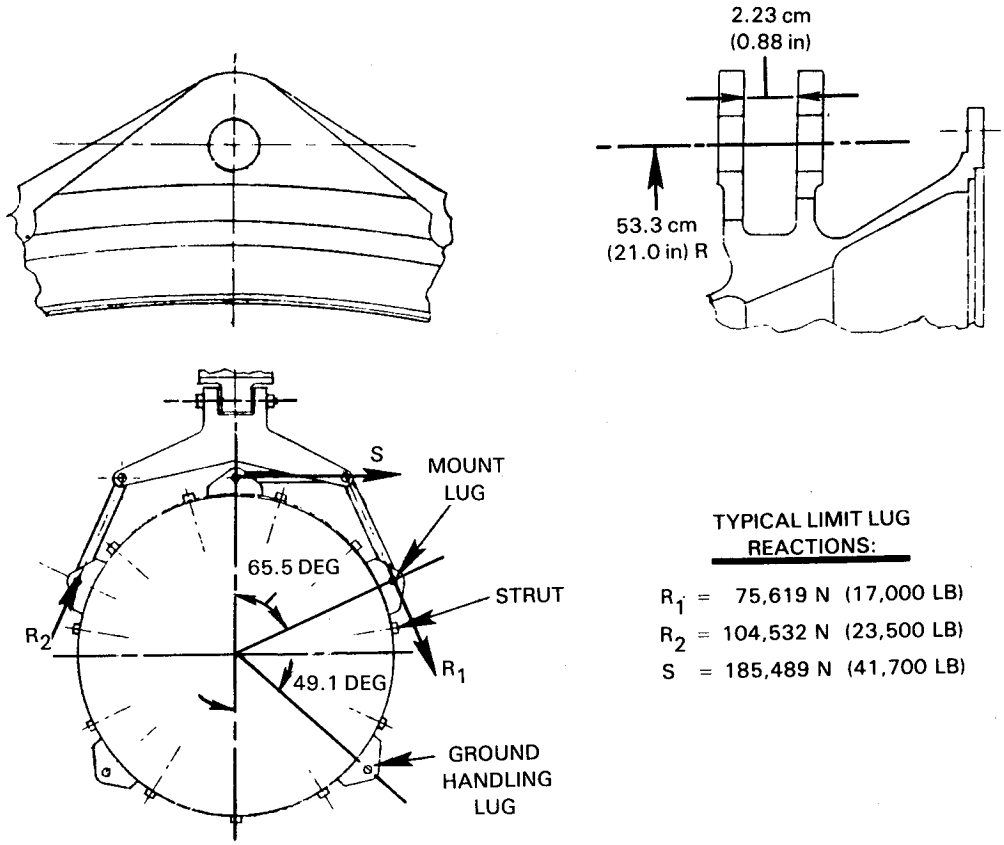

Figure 4.8.3-2 Engine Rear Mount Arrangement

4.8.4 Design Substantiation and Supporting Analyses

4.8.4.1 Predicted Performance

The predicted total duct pressure loss is 1.5 percent $\Delta P_T/P_T$. Experimental model tests, which were performed as part of a related supporting technology program (Ref 8), demonstrated a pressure loss of 1.59 percent $\Delta P_T/P_T$ at design point conditions. This is very close to the predicted level.

4.8.4.2 Structural/Life Analyses

A three-dimensional analysis was undertaken to determine load paths, loading and deflections in the various intermediate case components. A full 360-degree NASTRAN model, comprising of 900 plate and bar elements, was used to define nonaxisymmetric loads and a NASTRAN model of a segment was used to analyze axisymetric loads such as thermal loading. Thermal and pressure loads were simulated for acceleration, steady-state takeoff and deceleration conditions. Results showed that acceleration thermals produced the largest thermal loads. As part of this study, rear bearing support spring rates were analyzed and shown to satisfy critical speed requirements.

The amount of strut deflection under circumferential and axial loads was also established. Analysis showed that circumferential deflection of the strut is almost entirely from a thermal gradient between the strut and the inner and outer cases. Approximately 40 percent of the axial deflection results from a thermal gradient between the strut and the inner and outer cases, and 60 percent from the large axial pressure load. Results from a deflection analysis established that a minimum clearance of 0.076 cm (0.030 in) is required between the strut and fairing at a section near the outer diameter. This represents the worst possible dimensional tolerance stack-up and occurs during a snap acceleration. For an added margin of safety, the struts are coated with a 0.025 cm (0.01 in) thick ceramic to prevent any metal-to-metal contact between the fairing and strut.

Loads in the structural strut, as determined from the NASTRAN analysis, were used to define stresses in the strut. The stresses, together with appropriate stress concentration factors, are summarized in Figure 4.8.4-1. The calculated life was found to be greater than the design requirement of 1000 cycles or 50 hours at maximum temperature to 0.1 percent creep. Also presented in Figure 4.8.4-1 are the stress levels for the tiebolt. The preload indicated was set at a level to prevent separation of the strut from the outer case during "worst case" loads that occur during acceleration. Furthermore, low-pressure and high-pressure turbine blade loss analyses indicated that the strut and tiebolts could successfully resist imbalance loads caused by loss of either a high-pressure turbine blade or a fifth stage low-pressure turbine blade.

A durability analysis of the strut fairing was conducted with a simplified NASTRAN model, where the fairing airfoil and platforms were assumed to be plate elements. Figure 4.8.4-2 summarizes the calculated maximum steady stresses and indicates the highest stress occurs at the leading edge inner fillet. The material used for the strut fairing is expected to undergo local creep deformation from these stresses at the hot spot temperatures. However, this will not be a limiting factor, and predicted hot time life for coating oxidation is 90 hours.

4.8.5 Differences Relative to the Flight Propulsion System

The intermediate case for the flight propulsion system has several distinct design differences. The most pronounced are in the aerodynamic definition. Figure 4.8.5-1 presents a comparison of the case flowpath for the flight propulsion system scaled to the duct in the integrated core/low spool. As indicated, the major geometric differences are in the outer wall curvature, radial height and strut fairing definition. These changes are necessary for compatibility with low-pressure turbine inlet aerodynamics in the flight propulsion system.

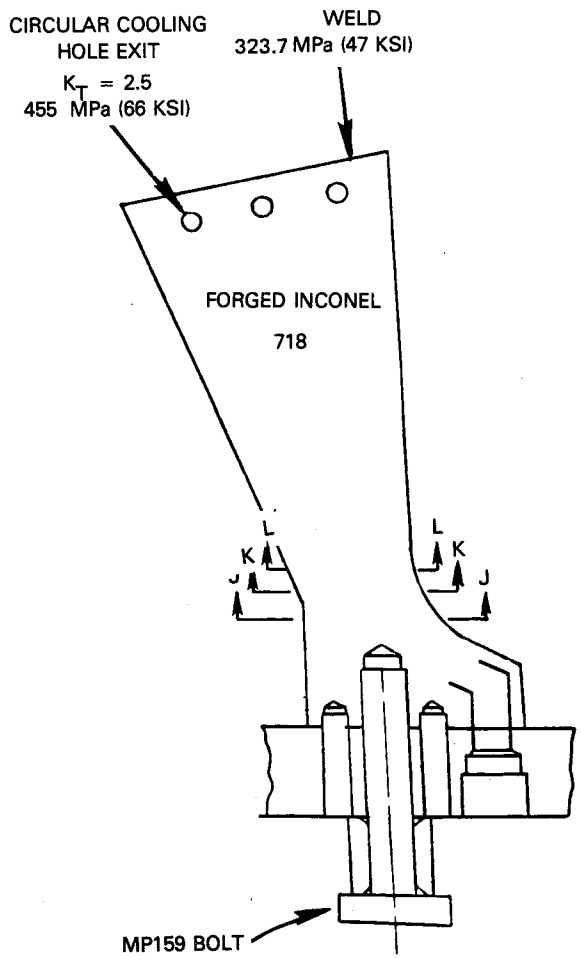

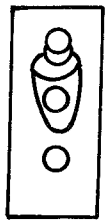

SECT J-J
K_T = 1.9
310 MPa (45 KSI)

SECT K-K
K_T = 1
565 MPa (82 KSI)

SECT L-L
K_T = 1
799 MPa (116 KSI)

TIEBOLT STRESS

COLD ASSEMBLY

MAX DIRECT TENSILE	1241 MPa (180 KSI)
MAX SHEAR	827 MPa (120 KSI)
MAX PRINCIPAL	1434 MPa (208 KSI)
YIELD STRENGTH	1654 MPa (240 KSI)
ULTIMATE STRENGTH	1896 MPa (275 KSI)

STEADY STATE

MAX DIRECT TENSILE	1006 MPa (146 KSI)
MAX SHEAR	579 MPa (84 KSI)
MAX PRINCIPAL	1082 MPa (157 KSI)
YIELD STRENGTH	1378 MPa (200 KSI)
ULTIMATE STRENGTH	1551 MPa (225 KSI)

ASSEMBLY PRELOAD

57,824 N
(13,000 LBS)

Figure 4.8.4-1 Structural Strut Stress and Life Summary

LOCATION	CALCULATED STRESS (ELASTIC)		COMMENTS
	PRESSURE LOADS, MPa (ksi)	HOT SPOT, MPa (ksi)	
1. AIRFOIL	36.5 (5.3)	8.9 (1.3)	– LOCAL DEFORMATION AT HOT SPOTS
2. ID FILLET	157.2 (22.8)	36.5 (5.3)	
3. ID FILLET	49.6 (7.2)	14.4 (2.1)	– MAX CREEP <1.3%
4. OD FILLET	112.3 (16.3)	12.4 (1.8)	– LOCAL DEFORMATION AT HOT SPOTS
5. ID PLATFORM	44.1 (6.4)	17.2 (2.5)	– MAX. CREEP <1.0%

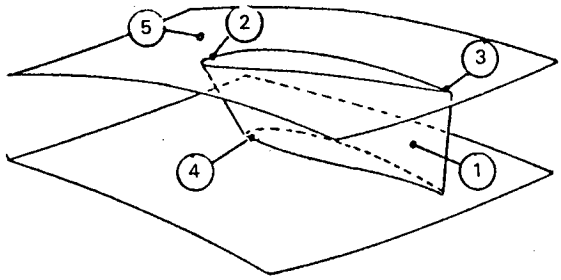

Figure 4.8.4-2 Strut Fairing Durability Assessment

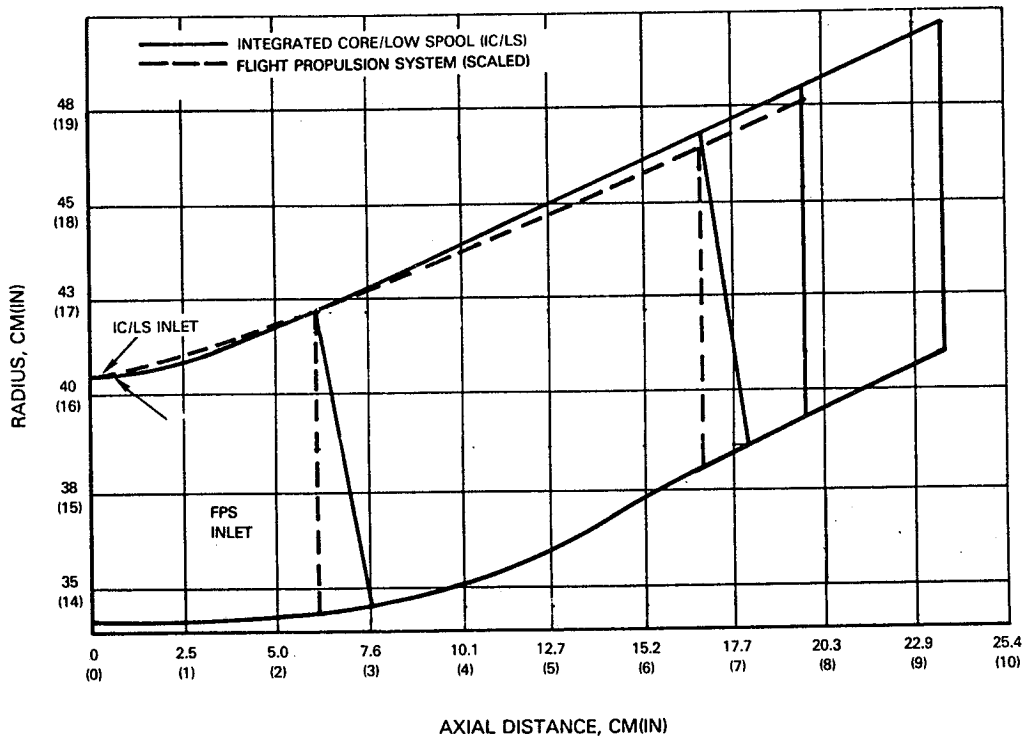

Figure 4.8.5-1 Comparison of Flowpath Definitions for the Integrated Core/Low Spool and Flight Propulsion System

A summary of the geometry differences is presented in Table 4.8.5-I. The exit annulus area is reduced by 5 percent, resulting in an annulus area ratio of 1.50 and an effective area ratio of 1.26. These variations do not affect the length-to-height ratio, which is 3.0 for each configuration. The strut fairing is a nonworking airfoil. The fairing is a standard 65 circular arc series airfoil and a total of 11 is required for the case design. Overall, this definition is more conservative from an aerodynamic standpoint than the design for the integrated core/low spool.

TABLE 4.8.5-I

INTERMEDIATE CASE GEOMETRY COMPARISON

DUCT	Flight Propulsion System	Integrated Core/ Low Spool
Length, cm (in)	21.0 (8.2) (7.7 scaled)	19.8 (7.8)
Length/height ratio	3.0	3.0
Ann. Area Ratio	1.50	1.57
Eff. Area Ratio	1.26	1.42
Duct Exit Gas Angle (deg)		
Hub	30	35
Midspan	36	39
Tip	33	40
Duct Exit Mach No.		
Hub	0.50	0.40
Midspan	0.44	0.39
Tip	0.41	0.30
STRUT	NONWORKING	WORKING
No. of Foils	11	11
Type	65 C/A	400 Series
Effective Turning, deg	0	5

In terms of mechanical design, only slight differences exist between the two configurations. These differences, as summarized below, are mainly to meet structural and durability requirements for a commercial engine.

The material selected for the tiebolt is Inconel 718 because of its higher strength properties. For the same reason, SC 2000 material, which is an advanced single crystal alloy, is used for the fairing. However, Inconel 718 is still the chosen material for the structural strut.

The outer case is a lightweight design, featuring a polygonal cross section at the strut connection plane. Also, the three cooling passages in the strut are elliptical rather than circular for a lower stress concentration factor and, consequently, longer life. Finally, the engine mount lugs are integrally forged with adequate strength to sustain flight-induced loads.

4.9 LOW-PRESSURE TURBINE

4.9.1 General Description

The low-pressure spool compression system is powered by a highly-loaded, four-stage turbine. Figure 4.9.1-1 shows the mechanical arrangement of the turbine component, including the exit guide vane assembly. Some of the technology features are low loss airfoil designs, counterrotation relative to the high-pressure spool, and a low ratio of throughflow velocity to wheel speed (C_x/U). Additional performance gains are achieved by minimizing endwall losses through incorporation of flow guides on airfoil platforms, improved interstage sealing and active clearance control. Turbine airfoils are fabricated from high strength/high temperature materials to eliminate cooling. Details pertaining to the design of the low-pressure turbine are contained in Reference 7.

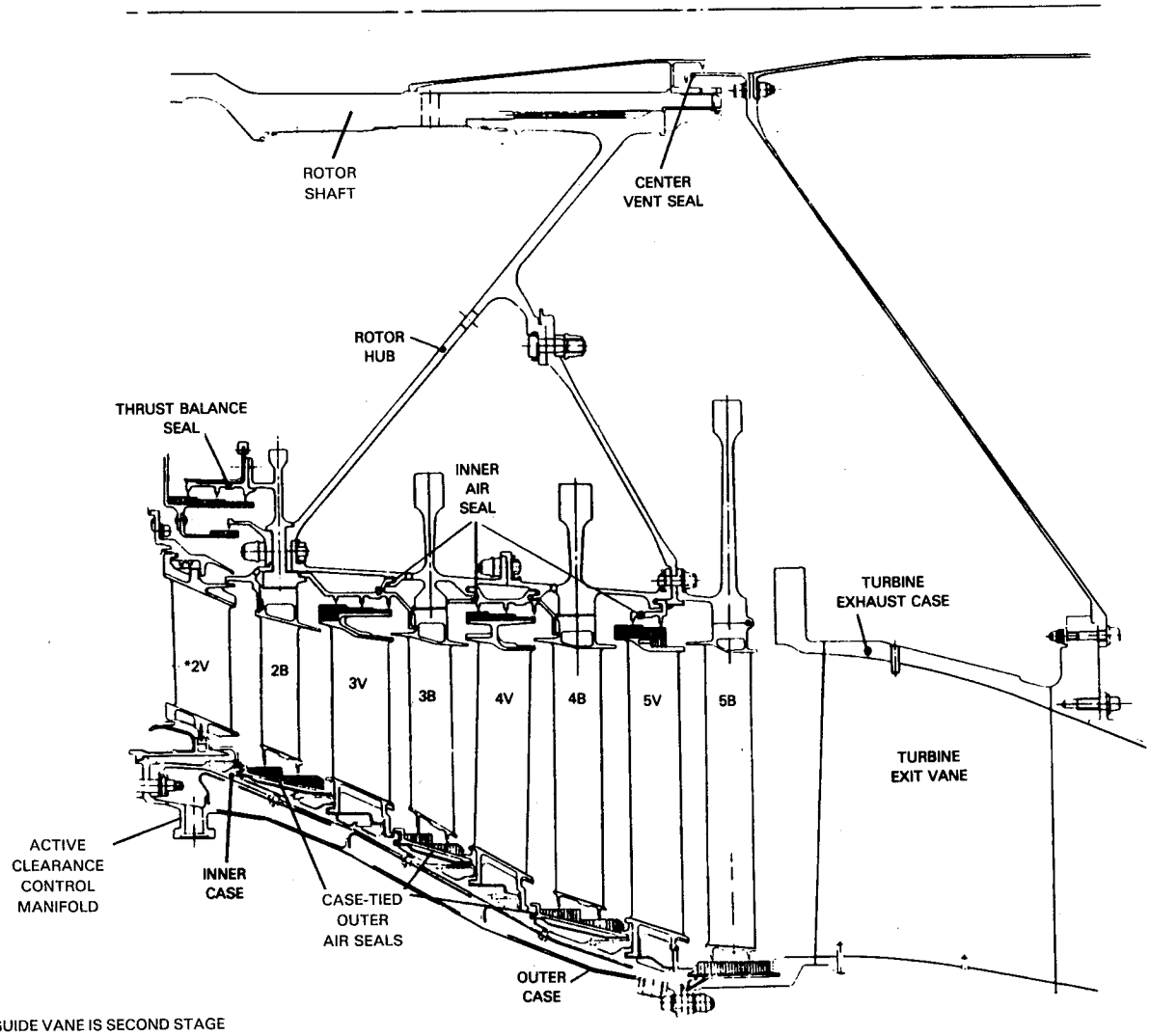

Figure 4.9.1-1 Cross-Sectional View of Low-Pressure Turbine Component with Exit Guide Vane Assembly

4.9.2 Aerodynamic Design

The general parameters governing the aerodynamic design of the integrated core/low spool low-pressure turbine are presented in Table 4.9.2-I, and the resulting flowpath is shown in Figure 4.9.2-1. The four stages contain 756 airfoils. Axial spacing between rotating and stationary stages is sufficient for the use of flow guides to minimize recirculation losses. There is a total of 30 turbine exit guide vanes.

TABLE 4.9.2-I

LOW-PRESSURE TURBINE AERODYNAMIC DESIGN PARAMETERS
(At Aerodynamic Design Point)

Stages	4
Rotation	Counter
Speed (rpm)	3902
Inlet Total Pressure, Pa (psia)	319,229 (46.3)
Inlet Total Temperature, K (°R)	1161 (2090)
Inlet Corrected Flow, W $\sqrt{T}$/Pt	69.342
Exit Corrected Flow, W $\sqrt{T}$/Pt	323.17
Pressure Ratio	5.51
ΔH, (Btu/sec)	12760.0
Mean Velocity Ratio	0.468
Work Factor, ($\Delta h/u^2$)	2.28
Average Flow Coefficient, Cx/u	0.76
Work Split, %	23/24/26/27
Mean Reaction	.45/.45/.45/.46
Goal Clearances, cm(in)	0.051 (0.020)
Estimated Overall Efficiency, %	90.4
Goal Overall Efficiency, %	91.5

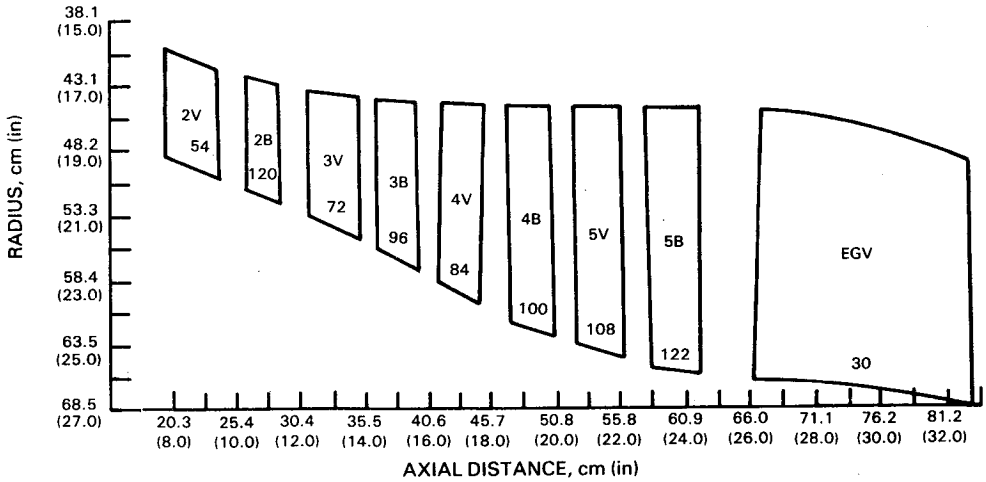

Figure 4.9.2-1 Low-Pressure Turbine Flowpath

Aerodynamically, the turbine design is characterized by a high expansion ratio (5.5) compared to the number of stages, a low mean velocity ratio (0.468) and a low ratio of throughflow velocity to wheel speed (C_x/U) (0.76). Also, it is counterrotating in relation to the high-pressure turbine. This results in a low camber inlet guide vane for improved performance with airfoils in the remaining stages having a high level of turning.

The airfoils are designed as individual sections based on a controlled vortex philosophy. In this manner, vane trailing edge root sections are opened and the trailing edge tip sections are closed relative to a free vortex design. This maintains the meanline aerodynamics, while reducing the turning at the blade root and increasing the blade root reactions. The change in root section aerodynamics reduces endwall losses. The airfoils also incorporate aft-loaded pressure distributions designed with elliptical leading edges to further enhance performance. The advantage of an aft-loaded airfoil design was verified during the related Subsonic Cascade Test Program (Ref. 9). A summary of velocity triangle data is presented in Table 4.9.2-II.

The exit guide vane is a controlled diffusion airfoil, designed to ensure an attached boundary layer and attain the desired gas exit angle. Endwall contours are defined for compatibility with the internal exhaust mixer, and the vane is contoured to present the mixer with a low Mach number, zero swirl flow field. A design summary is presented in Table 4.9.2-III.

The secondary flow system in the low-pressure turbine is designed to control leakage and to cool the components with a minimum of cooling flow. The main features of this system are identified in Table 4.9.2-IV. A total of 2.48 percent of the core engine airflow is used for cooling and active clearance control. Further discussion of the secondary flow system is presented in Section 5.7.

4.9.3 Mechanical Design

The mechanical configuration of the low-pressure turbine component consists of several major subassemblies. These include the rotor system, vanes and outer case structure, and turbine exhaust case.

Rotor System

The rotor assembly is illustrated in Figure 4.9.3-1. Its primary elements are the winged disks with nonintegral hubs, blades, inner cavity knife edge seals, and shaft.

Disk Assembly -- The disk and hub assembly is an A-frame construction to provide adequate stiffness to control deflections. As shown in Figure 4.9.3-1, the second-and fifth-stage disks are bolted to the legs of the frame, while the third-and fourth-stage winged disks are bolted to the second and fifth stages to form the base of the A-frame. The interstage seals between stages two-three and three-four are multifunctional. They provide gaspath sealing between stages, shield the disk flanges from hot gaspath air and furnish a passage for cooling air to the disk rim and airfoil attachments. The hub material is Incoloy 901. For thermal compatibility, both the inner seals and the disks are fabricated of PWA 1099, a modified Inconel 100.

TABLE 4.9.2-II

GAS TRIANGLE SUMMARY
(Aerodynamic Design Point)

	Inlet Angle (deg)	Exit Angle (deg)	Inlet Mach No.	Exit Mach No.	Turning (deg)	Gas Convergence	V_{exit}/V_{inlet}
IGV							
R	144.3	26.6	0.396	0.666	9.1	1.43	1.65
M	141.3	24.2	0.394	0.658	14.5	1.47	1.64
T	139.4	21.7	0.306	0.534	19.0	1.53	1.73
B2 R	43.9	23.0	0.433	0.614	113.2	1.27	1.40
1/4R	41.4	24.2	0.422	0.638	114.4	1.34	1.48
M	40.7	25.9	0.394	0.620	113.3	1.42	1.58
1/4T	42.9	27.6	0.335	0.580	109.5	1.51	1.70
T	50.2	28.7	0.256	0.543	101.2	1.78	2.09
V3 R	36.0	30.3	0.350	0.601	113.6	1.44	1.69
1/4R	41.7	24.2	0.373	0.648	114.0	1.48	1.70
M	47.6	22.8	0.350	0.656	109.6	1.61	1.85
1/4T	54.4	22.2	0.307	0.631	103.3	1.80	2.00
T	59.3	21.9	0.266	0.590	98.8	1.90	2.17
B3 R	53.5	23.5	0.380	0.645	102.9	1.42	1.67
1/4R	42.4	23.2	0.383	0.679	114.5	1.47	1.73
M	41.7	22.7	0.365	0.665	115.7	1.56	1.78
1/4T	44.7	22.1	0.324	0.629	113.3	1.72	1.90
T	49.9	21.7	0.278	0.599	108.5	1.83	2.12
V4 R	37.5	28.9	0.368	0.647	113.6	1.41	1.72
1/4R	40.1	22.4	0.391	0.700	117.5	1.48	1.79
M	42.9	21.2	0.357	0.689	115.9	1.62	1.88
1/4T	47.5	20.3	0.309	0.644	112.2	1.75	2.03
T	52.4	19.6	0.279	0.598	108.0	1.88	2.10
B4 R	49.2	22.1	0.397	0.692	108.7	1.40	1.70
1/4R	38.9	22.1	0.401	0.738	118.9	1.49	1.79
M	40.9	22.2	0.359	0.689	116.9	1.64	1.87
1/4T	46.7	22.4	0.286	0.649	110.9	2.03	2.21
T	55.5	22.5	0.228	0.643	101.9	2.28	2.76
V5 R	37.2	32.4	0.409	0.685	110.5	1.36	1.63
1/4R	39.4	27.3	0.426	0.728	113.3	1.42	1.66
M	45.6	22.6	0.348	0.736	111.8	1.70	2.05
1/4T	53.9	22.6	0.297	0.704	103.5	1.89	2.29
T	57.8	22.6	0.289	0.648	99.7	1.87	2.19
B5 R	55.3	37.3	0.450	0.784	87.5	1.35	1.69
1/4R	48.9	28.8	0.439	0.818	102.3	1.43	1.79
M	44.7	25.5	0.385	0.791	108.9	1.60	1.98
1/4T	52.0	27.0	0.325	0.770	101.0	1.86	2.28
T	62.7	29.5	0.263	0.741	87.8	2.0	2.72
EGV R	55.7	90.0	0.515	0.396	34.3		
1/4R	47.9	90.0	0.507	0.373	42.1		
M	50.1	90.0	0.441	0.350	39.9		
1/4T	58.1	90.0	0.405	0.366	31.9		
T	67.9	90.0	0.415	0.390	22.1		

TABLE 4.9.2-III

EXIT GUIDE VANE AERODYNAMIC CHARACTERISTICS
(Planar Sections)
Integrated Core/Low Spool - Aerodynamic Design Point

(10,668 m (35,000 ft) 0.8 Mn)

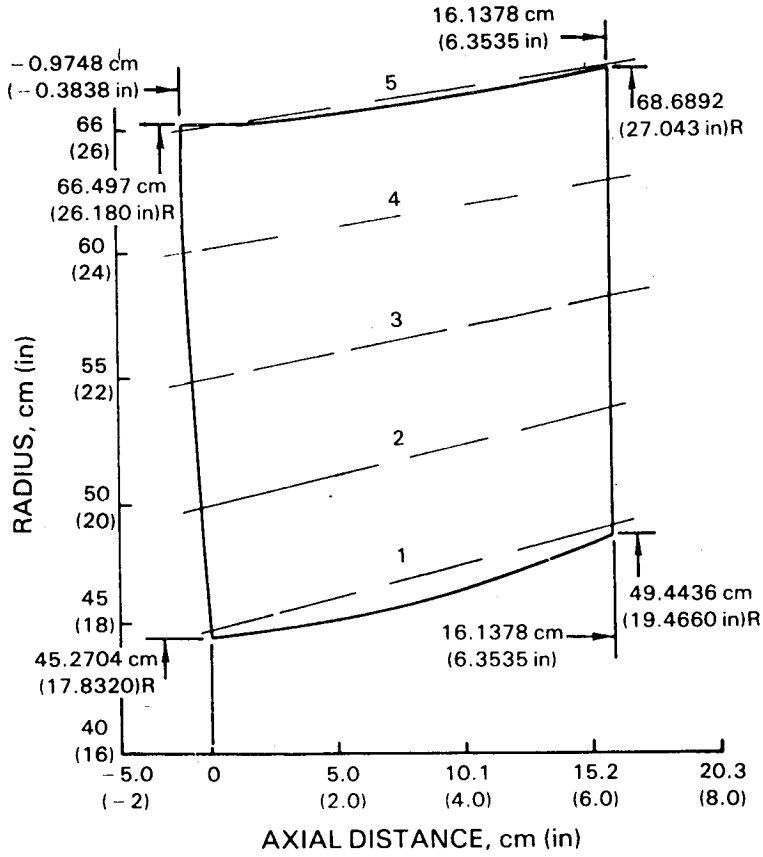

	1	2	3	4	5
Radius LE, cm (in)	45.270 (17.823)	50.505 (19.884)	55.740 (21.945)	60.972 (24.005)	66.207 (26.066)
Radius TE, cm(in)	49.443 (19.466)	54.254 (21.360)	59.067 (23.255)	63.878 (25.149)	68.689 (27.043)
Inlet Gas Angle, deg	55.67	47.6	49.5	54.4	66.8
Exit Gas Angle, deg	90.0	90.0	90.0	90.0	90.0
Inlet M_N	0.516	0.503	0.452	0.410	0.412
Exit M_N	0.395	0.372	0.350	0.366	0.386
Incidence, deg	-5.5	-4.5	-4.5	-4.0	-3.5
Deviation, deg	0	3.3	5.9	6.9	5.8
Gap/chord	0.598	0.644	0.701	0.762	0.826
Diffusion Factor*	0.33	0.455	0.465	0.390	0.250
RE_{Bact} @ inlet	2.86×10^5	3.0×10^5	2.88×10^5	2.65×10^5	2.51×10^5
Chord, cm (in)	17.310 (6.815)	17.650 (6.949)	17.642 (6.946)	17.559 (6.913)	17.421 (6.859)

*"D" Factor = $1 - \frac{C2}{C1} + \frac{Cu}{2C1} \cdot \tau / b_{act}$

TABLE 4.9.2-IV

LOW-PRESSURE TURBINE SECONDARY FLOW SYSTEM DESIGN FEATURES

Rotor Cooling System

Pressure-balanced system independent of rim seal clearances.
A-frame rotor construction with uniform cooling flow to disk rims.
Individually metered cooling air to disk rims.
Rim shields to thermally isolate disk-blade attachments from rim cavities.
Flow guides to minimize hot gas ingestion and recirculation.

Case Cooling System

Cooling and active clearance control system combined to minimize total flow requirements.
Thermal isolation of structural case from gaspath.
Circumferential staggering of vane and air seal segment to minimize leakage.
Active clearance control shield-to-case flow passage tailored to each stage for optimum thermal response.
Temperature modulation of active clearance control air to provide minimum blade tip clearance.

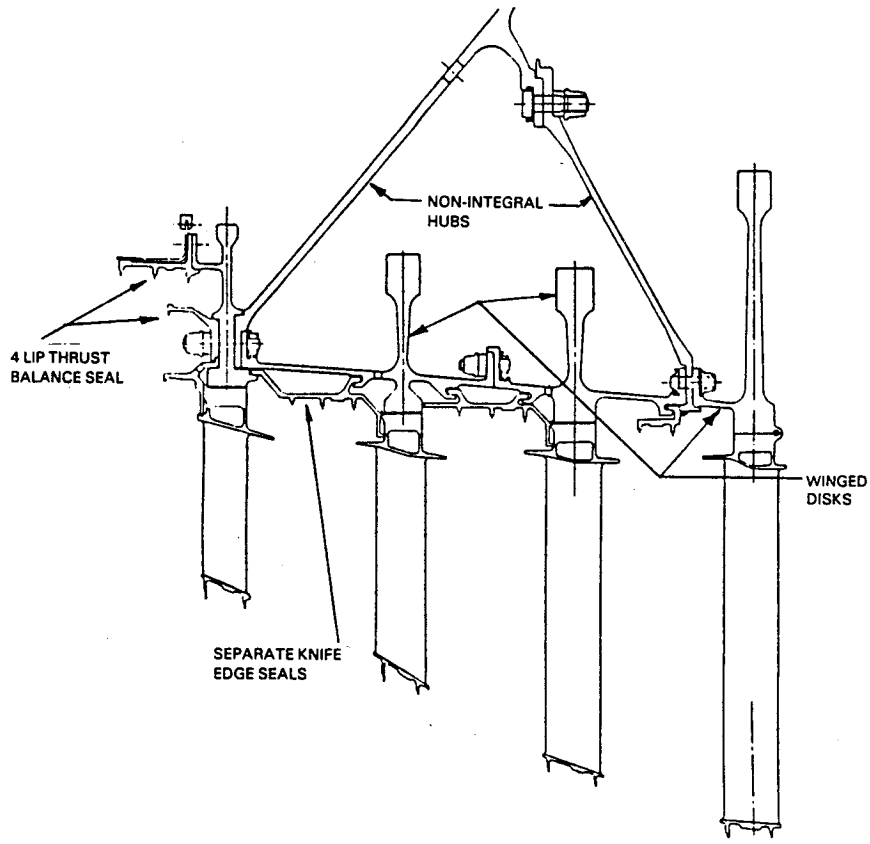

Figure 4.9.3-1 Low-Pressure Turbine Disk and Hub Assembly

The rotor is mounted on the rear of the shaft and cantilevered off of the No. 5 bearing. A center vent seal is located at the aft end of the shaft. The shaft material is AMS 6304.

Turbine Blades -- The main criterion governing the mechanical design of the blades was the elimination of the requirement for cooling. Besides the gain in performance, it also eliminates the need for a complex internal cooling system and allows fabricating the airfoils from solid castings.

In the four stages there is a total of 438 blades. Figure 4.9.3-2 summarizes the design characteristics. Also shown are details of the blade attachment, which is a two-tooth broach geometry. A conventional blade retention tang is used in the second, third and fourth stages, while the fifth stage has a shear lock arrangement. Blade platforms in the fourth and fifth stages incorporate flow guides. Platform weight is minimized by providing cast, conical, constant thickness surfaces at the flowpath and cast pockets at the underside. To balance out gas bending moments at the blade root, all blades incorporate a slight amount of built-in tilt. Tip shrouds are included on the blades to enhance performance and control vibration.

The second-stage blade is cast of MAR-M-247 material and coated with a conventional diffused aluminide overlay coating (PWA 73). Blades in the remaining stages are cast of Inconel 713 material. Because of the gas temperature and capability of this material, no coating is required.

Vane and Case Assembly

Vanes -- There are 318 vanes and, like the blades, these airfoil are designed with high strength/high temperature materials to eliminate the requirement for cooling. The general design characteristics are shown in Figure 4.9.3-3. All vanes are stacked on a radial line passing through the center of gravity at the root section and have a slight amount of tangential tilt to balance out root bending stresses. The leading edges are elliptical and the inner platforms in stages three, four and five have flow guides for compatibility with the adjacent blades.

Vanes in the third, fourth and fifth stages are cantilevered from the case and attached with conventional vane feet and case hooks. However, the method of support for the second-stage vane is somewhat different. The second vane outer support is a simple hook arrangement that permits the vane to move radially, but restrains axial motion. The inner support has a double hook arrangement, in conjunction with an anti-rotation pin to provide the required axial, radial, and torque restraint.

For greater strength and lower leakage, semi-machined vanes are Transient Liquid Phase (TLP®) bonded together into clusters. The cluster size in the second stage is limited to two vanes, with each cluster incorporating one anti-rotation pin. Vanes in the remaining stages are bonded in clusters of three, with each vane in the cluster having one anti-rotation pin.

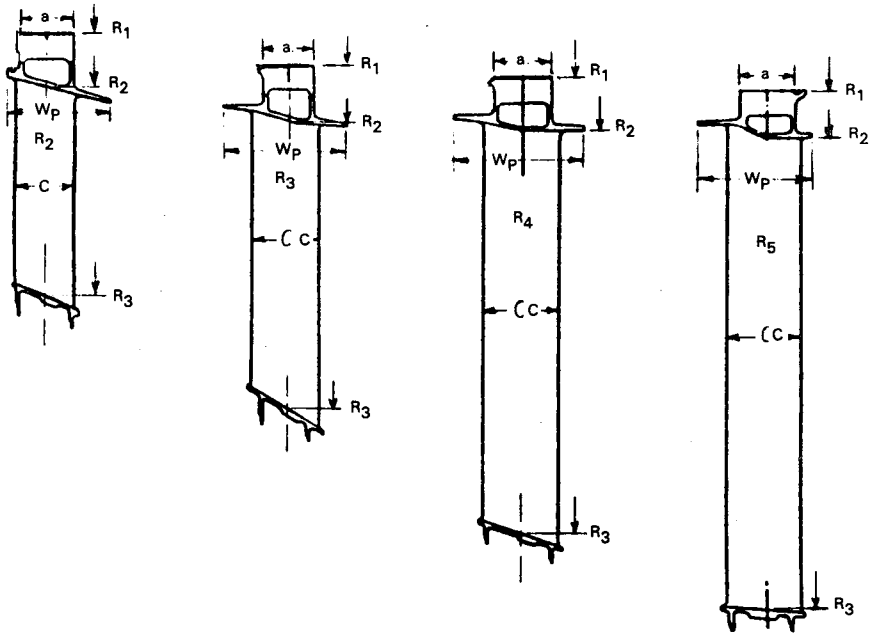

	STAGE			
	2nd	3rd	4th	5th
BLADE DETAILS				
ATTACHMENT AXIAL LENGTH, (a), cm (in)	2.41 (0.95)	2.28 (0.90)	2.54 (1.00)	2.41 (0.95)
AVERAGE AIRFOIL CHORD, (C), cm (in)	2.66 (1.05)	3.07 (1.21)	3.37 (1.33)	3.42 (1.35)
R_1, cm (in)	40.1 (15.8)	41.6 (16.4)	42.1 (16.6)	42.6 (16.8)
R_2, cm (in)	42.4 (16.7)	44.1 (17.4)	44.4 (17.5)	44.7 (17.6)
R_3, cm (in)	51.5 (20.3)	56.6 (22.3)	61.9 (24.4)	65.2 (25.7)
PLATFORM AXIAL WIDTH, W_P INCLUDING FLOW GUIDE, cm (in)	4.77 (1.88)	5.61 (2.21)	5.91 (2.33)	5.46 (2.15)
ATTACHMENT DETAILS				
BROACH ANGLE	11°	7°30′	15°	0
PLATFORM GAP ANGLE, α_G	14°45′	25°	15°	27°15′
PLATFORM GAP, L_{PG} cm (in)	0.030 (0.012)	0.030 (0.012)	0.025 (0.010)	0.030 (0.012)
TAPER ANGLE, α_T	22°	22°	22°	22°
RESTAGGER CAPACITY	±4°30′	±3°	±3°	±3°
L_1 cm (in)	0.78 (0.31)	0.78 (0.31)	0.78 (0.31)	0.78 (0.31)
L_2, cm (in)	0.81 (0.32)	0.81 (0.32)	0.81 (0.32)	0.81 (0.32)

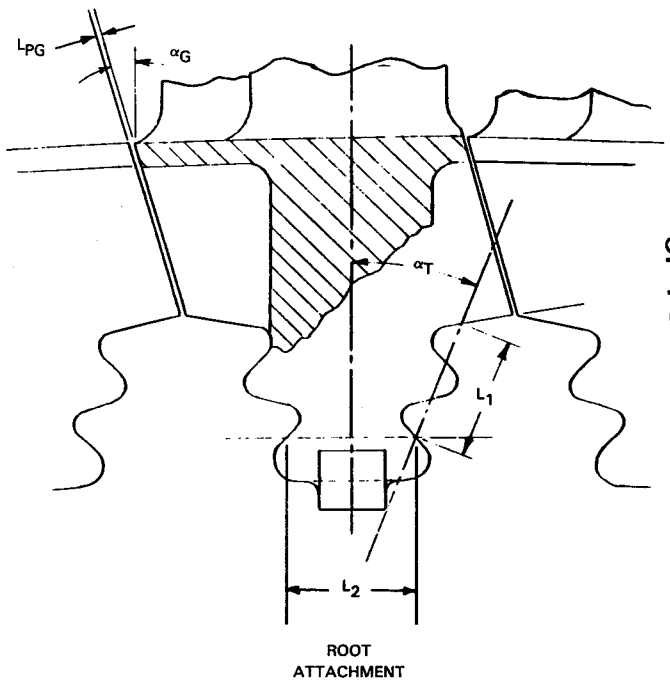

Figure 4.9.3-2 Turbine Blade Summary

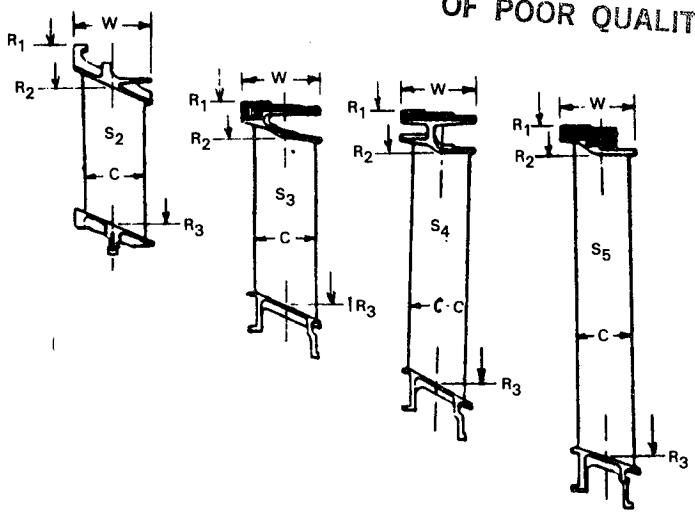

	STAGE			
	2nd	3rd	4th	5th
NO. OF VANES	54	72	84	108
WIDTH (W), cm (in)	4.97 (1.96)	5.18 (2.04)	4.87 (1.92)	5.02 (1.98)
AVERAGE AIRFOIL CHORD, (C), cm (in)	3.96 (1.56)	4.08 (1.61)	3.73 (1.47)	3.68 (1.45)
R_1, cm (in)	37.5 (14.8)	41.4 (16.3)	41.9 (16.5)	42.9 (16.9)
R_2, cm (in)	40.3 (15.9)	43.6 (17.2)	44.4 (17.5)	44.7 (17.6)
R_3, cm (in)	49.0 (19.3)	54.1 (21.3)	59.4 (23.4)	64.0 (25.2)

Figure 4.9.3-3 Low-Pressure Turbine Vane General Characteristics

The second vane is cast from a single crystal nickel base alloy (PWA 1480) and coated with a diffused aluminide overlay coating. The third vane is cast from a nickel base alloy (PWA 1455) and also coated with an overlay coating. Vanes in the remaining stages are fabricated from Inconel 713 material and are not coated. The inner airseals in these stages have a 0.158 cm (0.0625 in) cell honeycomb made from 0.005-cm (0.002-in) thick Hastelloy X foil.

Vane Cases -- The turbine case is a double wall structure designed to ensure blade containment and provide active clearance control. The outer case is constructed from an iron base alloy (A 286), primarily for thermal expansion considerations, while the inner case material is Inconel 718 because of its inherent strength at elevated conditions. The case-tied outer airseals are fabricated from forged rings by electron beam cutting. The abradable honeycomb rubstrip, which is Hastelloy X material, has a cell size of 0.157 cm (0.062 in) and a foil thickness of 0.005 cm (0.002 in). The heatshields are also fabricated from Hastelloy X in segments of eight per stage.

Clearances for both the outer and inner airseals are tailored to the operating conditions by the active clearance control system. Air for clearance control, either tenth- or fifteenth-stage high-pressure compressor bleed air, enters the low-pressure turbine case through a manifold and is directed aft between segmented baffles and the inner case. These baffles are attached to the inner case with rivets and spacers to provide a controlled dimension at each stage and optimum case response. A portion of the flow is metered through holes in the inner turbine case wall to internal manifolds adjacent to the vane feet. This cooling air flows around the vane feet area and reduces heat transfer from the vanes and outer airseals into the case. Further discussion of the active clearance control system, including a definition of seal clearances, is presented in Section 5.6.

Turbine Exhaust Case

The turbine exhaust case is an integral ring-strut-ring, welded structure with the 30 struts doubling as airfoils for the exit guide vanes. The mechanical design is shown in Figure 4.9.3-4. The vanes are solid castings of Greek Ascoloy material. The inner and outer rings and flanges are forged from the same material and welded together into a single assembly.

The inner ring supports the exhaust plug. A flange at the rear of the outer ring provides support for the exhaust mixer and serves as the engine-to-fan duct interface for cowl load sharing. The front outer support flange transfers axial loads from the exhaust case forward to the turbine case and provides containment for the fifth-stage blade.

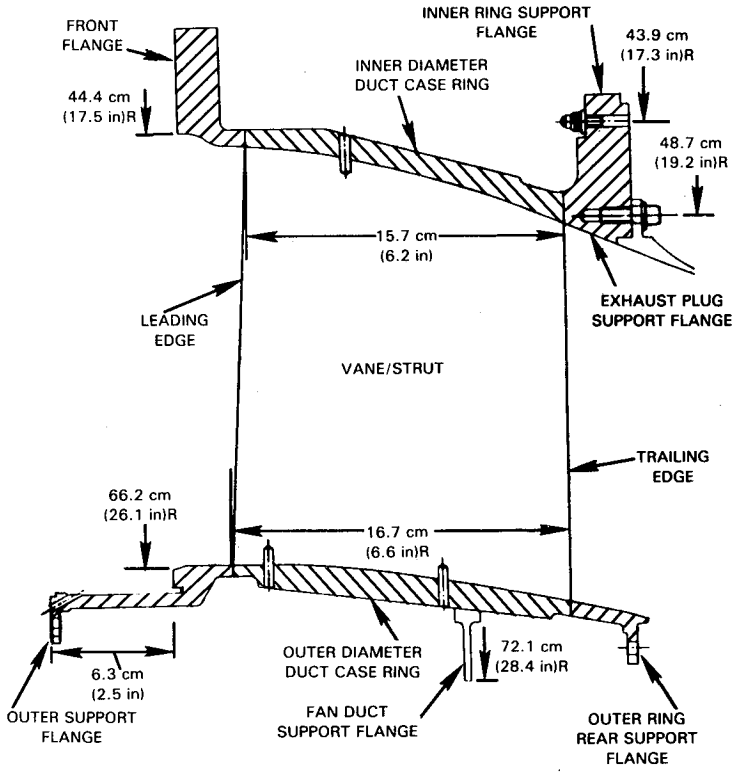

Figure 4.9.3-4 Mechanical Definition of the Exit Guide Vane

4.9.4 Design Substantiation and Supporting Analyses

4.9.4.1 Predicted Performance

The component efficiency goal, as defined for both the flight propulsion system and the integrated core/low spool, is 91.5 percent. For the integrated core/low spool, the estimated turbine efficiency is 90.4 percent. This value includes performance deficits for the nonflight quality of experimental hardware, in addition to the attendant higher leakage rates and larger operating clearances of a demonstrator vehicle. Life requirements are consistent with the integrated core/low spool goal of at least 50 hours of hot time operation or 1000 cycles.

4.9.4.2 Structural/Life Analyses

Disk and Hub

Results of structural analyses for the disk and hub assembly are presented in Figure 4.9.4-1. Metal temperatures are based on sea level takeoff hot day conditions, and the resultant stresses are based on this temperature distribution as well as an assumed acceleration to takeoff power. Disk burst margins, creep life and average tangential rim stresses are summarized in Table 4.9.4-I. All stresses and lives meet integrated core/low spool requirements.

TABLE 4.9.4-I

DISK STRUCTURAL SUMMARY

	Rotor 2	Rotor 3	Rotor 4	Rotor 5
Burst Margin	1.66	1.43	1.36	1.48
Creep Life, hrs.	10^4	10^4	10^4	10^4
Avg. Tangential Stress, MPa (ksi)	434.3 (63)	584.6 (84.8)	652.2 (94.6)	549.5 (79.7)

Interstage seal vibration characteristics were also analyzed. Resonance margins are 85 percent for the second-third stage seal, 74 percent for the third-fourth stage seal and over 100 percent for the fourth-fifth stage seal. In addition, all seals are free of coincidence problems.

A summary of the front and rear shaft temperatures and stresses is shown in Figure 4.9.4-2 for sea level takeoff hot day conditions. All stresses are within acceptable limits. Low cycle fatigue lives in all locations exceed 20,000 cycles, with the exception of the front spline, which has a predicted life of 1300 cycles. However, this is no constraint for the integrated core/low spool. In the flight propulsion system, the deficiency would be resolved by increasing the pitch diameter and increasing the fillet radius. Both the intershaft and center vent seals have adequate burst margin with no indications of either resonance or coincidence problems.

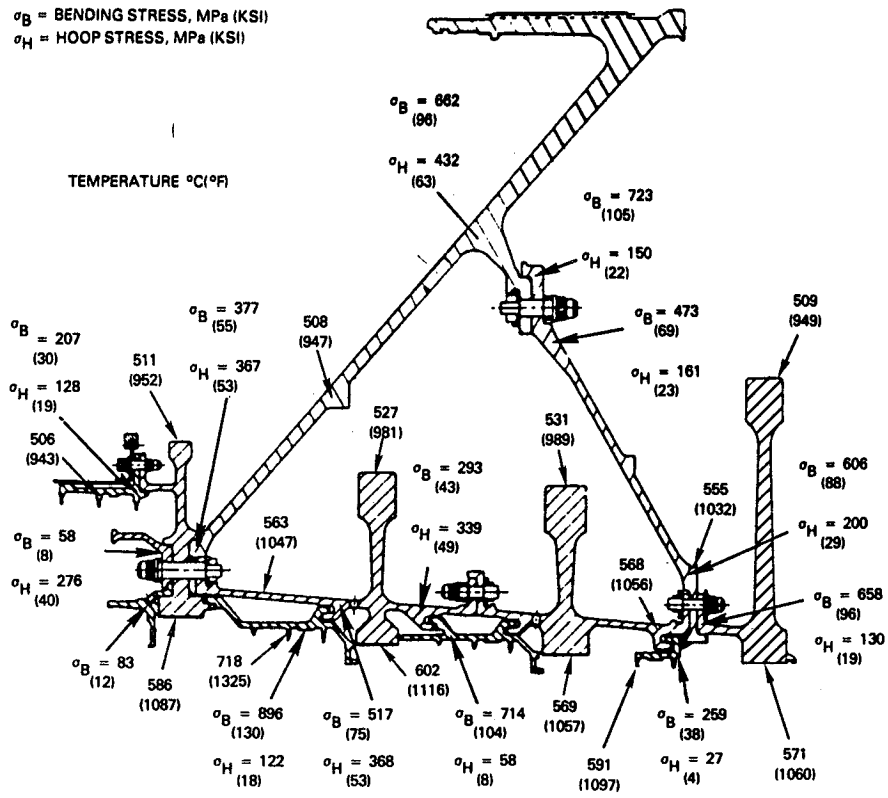

Figure 4.9.4-1 Summary of Turbine Disk Stress and Temperatures

Airfoils

The turbine blade designs were analysed for stage vibration and flutter characteristics. In assessing critical engine order resonances, the second-stage rotor response to 11E and 22E orders was a concern because of the close proximity of the 11 intermediate case strut fairings. Results showed a frequency margin of 9.8 percent at the maximum rotor speed for the 11E first mode and a margin of -10.7 percent at the minimum cruise speed for 22E first mode. All critical second mode resonances occur well outside of the operating range. Resonance margins for blades in the remaining stages are also acceptable. In addition, the results of a flutter analysis indicated that all four stages operate well above the unstable limit.

Blade attachment stresses were calculated with consideration given to axial gas loads, airfoil and shroud residual moments, blade centrifugal pulls, and platform offset moments. Results showed adequate stress margin for all stages. Similarly, tip shroud stresses were calculated for bearing and curling. Results again showed adequate stress margins for all stages.

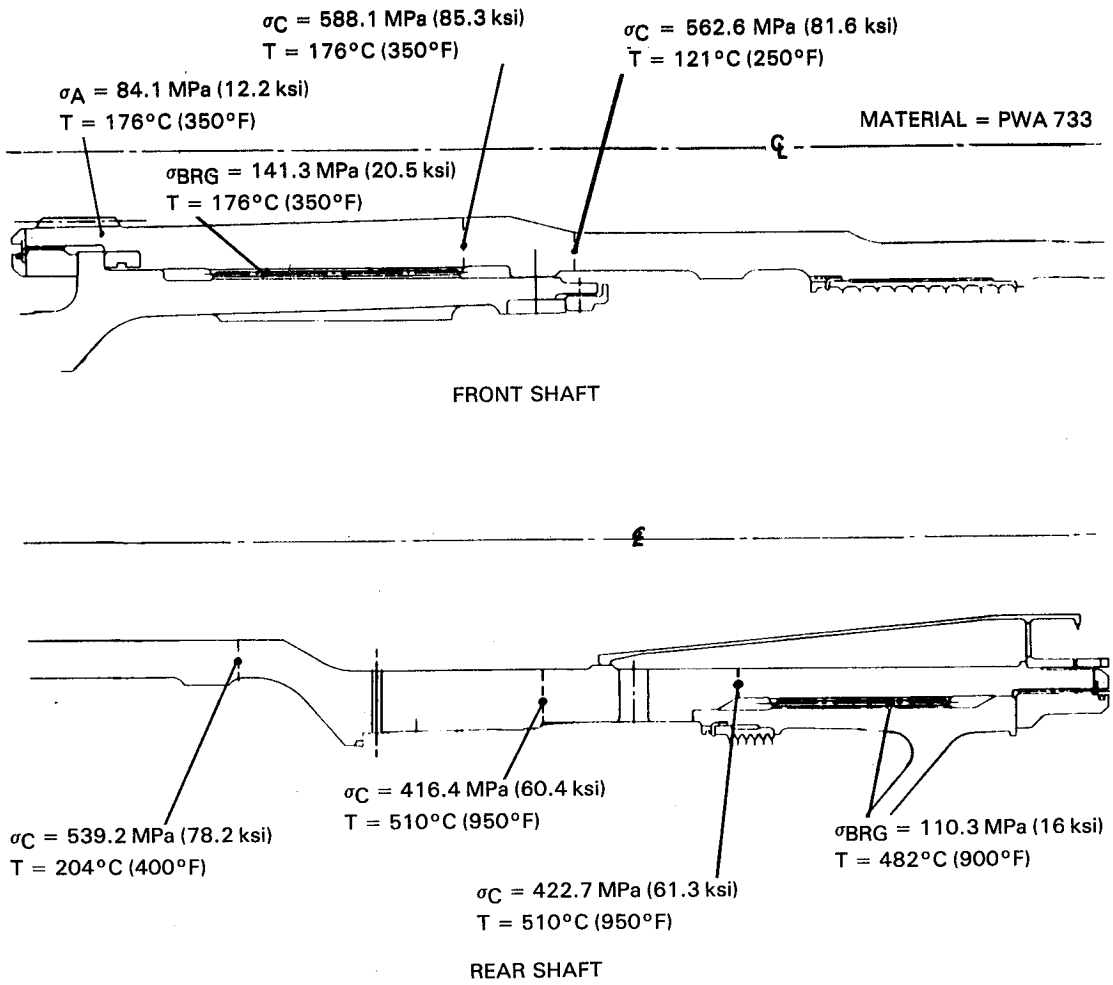

Figure 4.9.4-2 Front and Rear Shaft Stress and Temperature Summary

Vane stress levels were determined by assuming sea level takeoff operating conditions, hot streak temperatures and limits commensurate with the integrated core/low spool design goals. Calculated stress levels were all within defined limits, with the highest being a combined stress of 226.1 MPa (32.8 ksi) at the second-stage vane inner hook and a bending stress of 226.8 (32.9 ksi) at the third-stage antirotation pins.

Since the second and third stages operate in a high temperature environment, a transient thermal strain analysis was conducted to determine airfoil thermal fatigue life. The maximum strain ranges (i.e., strain cycle amplitudes) for these two blades are equal to or less than 0.24 percent. The strain ranges for the vanes, however, are higher because of the effects of clustering. The maximum range for the second-stage vane is 0.42 percent and 0.49 percent for the third-stage vane. The calculated airfoil lives for all stages exceed the goal of 50 hours. Also, blade creep strength margins are adequate. Oxidation of the airfoils is the only potential concern for the integrated core/low spool, since it will not accumulate enough running time to initiate cracks.

Cases

The calculated temperature and stress levels for the low-pressure turbine case are shown in Figure 4.9.4-3. These values are acceptable and, on the basis of these distributions, the case life exceeds 20,000 cycles.

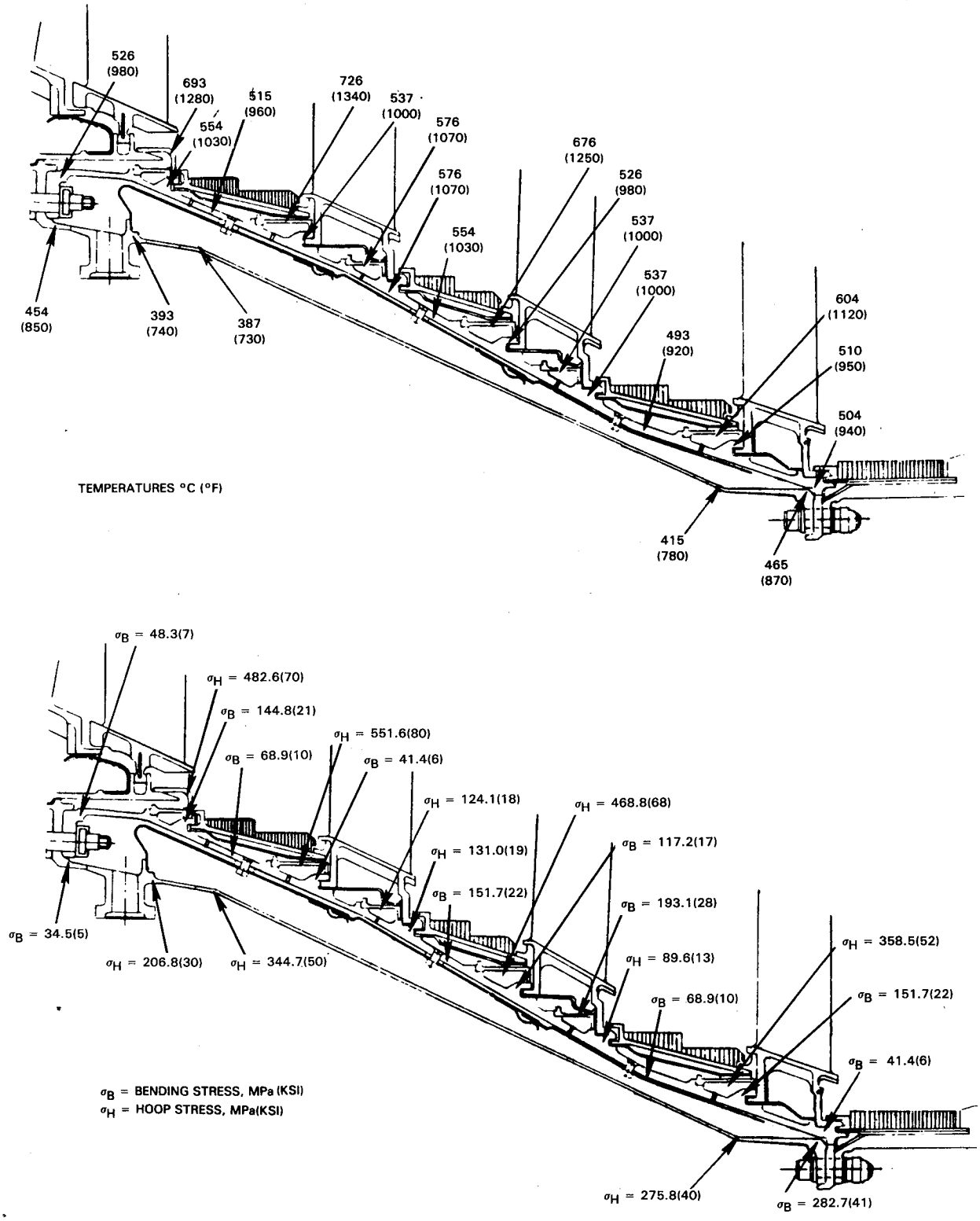

Figure 4.9.4-3 Turbine Case Stress and Temperature Summary

The structural feasibility of the turbine exhaust case is predicated on the experience with similar structures that are fabricated of lower strength materials and operate in more severe thermal environments. The maximum metal temperatures expected for the integrated core/low spool turbine exhaust case assembly are 526°C (980°F) for the inner case ring, 648°C (1200°F) for the vanes and 604°C (1120°F) for the outer case ring.

4.9.5 Differences Relative to the Flight Propulsion System

The adaptation of the turbine flowpath for the integrated core/low spool to the flight propulsion system requires a 5 percent reduction in the inlet annulus area to accommodate the lower inlet corrected flow rate of the flight propulsion system low-pressure turbine. The revised flowpath is shown in Figure 4.9.5-1. As indicated, certain modifications are required to the airfoils, resulting in a higher elevation and slightly shorter axial length.

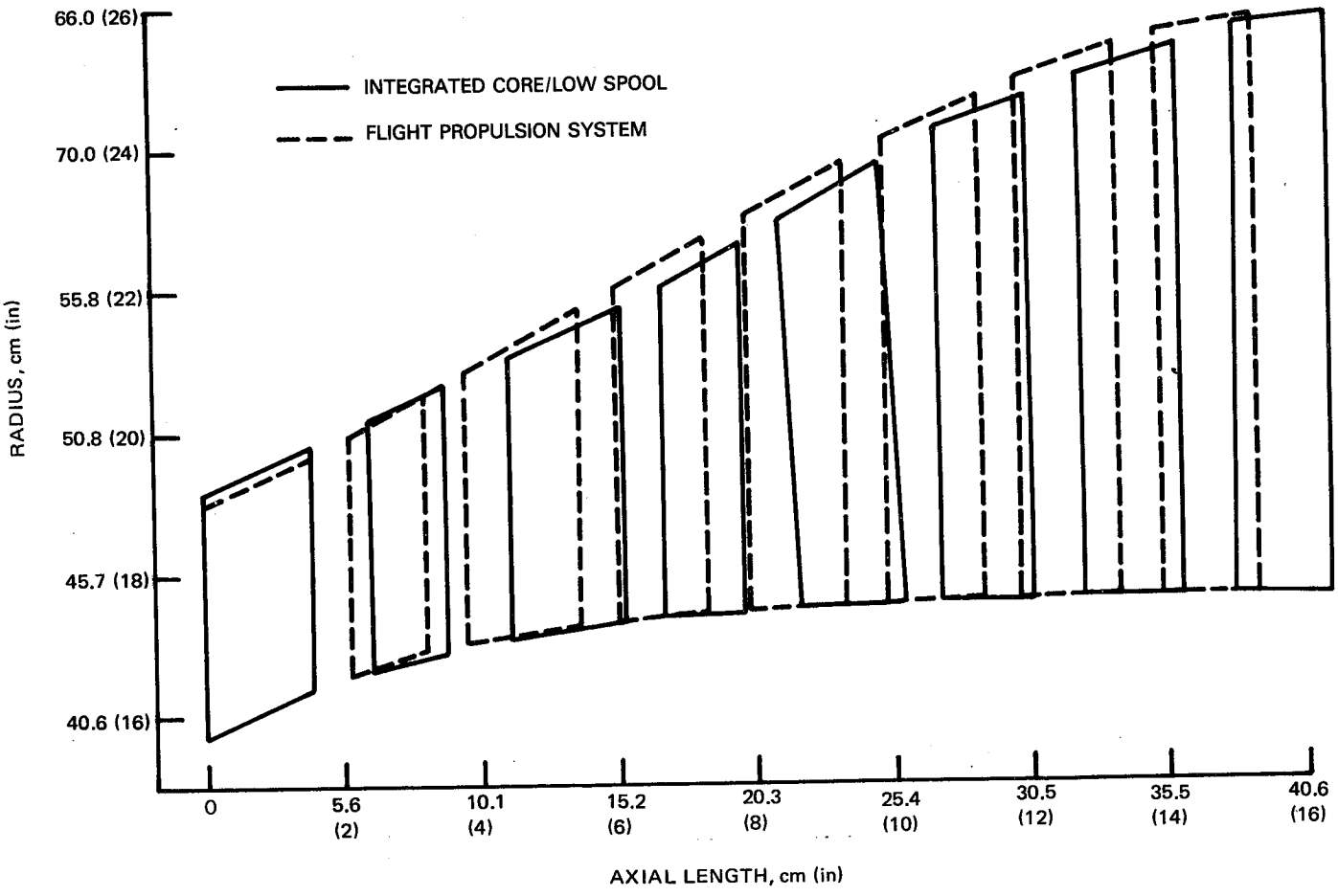

Figure 4.9.5-1 Comparison of the Turbine Flowpath for the Intergrated Core/Low Spool and Flight Propulsion System

The turbine mechanical configuration is essentially the same as for the integrated core/low spool. The major difference is substitution of materials to achieve commercial durability requirements. Table 4.9.5-I provides a synopsis of the major component materials differences between the integrated core/low spool and flight propulsion systems.

TABLE 4.9.5-I

TURBINE MATERIALS COMPARISON

	Integrated Core/Low Spool		Flight Propulsion System	
	Material	Coating	Material	Coating
First Stage Vane	PWA 1480	PWA 73	SC2000	PWA 286
First Stage Blade	PWA 1447	PWA 73	PWA 1447	PWA 270
Second Stage Vane	PWA 1455	PWA 73	PWA 1447	PWA 73
Second Stage Blade	PWA 655	---	PWA 655	PWA 73
Fifth Stage Blade	PWA 655	---	Adv Ti-Al	---
Exit Guide Vane	Greek ASCOLOY	---	Ti-Al	---
Rotor Shaft	PWA 733	---	AMS 6304	---

Besides the material difference, the exit guide vane assembly has several configurational changes. The vanes are hollow, in contrast to the solid castings in the integrated core/low spool, and the inner and outer cases are designed for cowl load sharing capability.

For active clearance control, the flight propulsion system uses a combination of eighth-and fifteenth-stage high-pressure compressor bleed air. This results in a 0.19 percent increase in efficiency and 0.28 percent thrust specific fuel consumption advantage. Tenth-stage bleed air is used for the integrated core/low spool to avoid design expense and additional hardware costs involved with external bleed plumbing to the eighth stage.

The use of eighth-stage air increases case closure capability over tenth-stage air and negates the requirement for cooling holes in the second-stage vane support hook area and third-stage vane front support hook area. Instead, these areas are filled with insulation.

4.10 EXHAUST NOZZLE AND MIXER

4.10.1 General Description

The exhaust system in the integrated core/low spool contains an internal mixer and a central plug housed within a converging exhaust nozzle. The mixer is an 18 lobe configuration, designed for a mixing efficiency of 85 percent.

4.10.2 Aerodynamic Design

The aerodynamic definition of the mixer and nozzle section is based on the results of parametric testing during the Mixer Model Test Program (Ref. 10). Figure 4.10.2-1 shows the flowpath of the resultant exhaust system arrangement that evolved from the experimental testing in this supporting technology program. The flowpath shows the relative positioning of the mixer, plug and convergent nozzle.

The mixer is an 18 lobe design with a lobe penetration of 75 percent and a mixing length-to-diameter ratio of 0.60. The lobes are scalloped and fairings, called hoods, are attached to their upstream portion. Aerodynamically, these fairings improve the characteristics of the flow entering the mixer area.

Performance parameters for the mixer/exhaust system design are presented in Table 4.10.2-I at the key engine operating conditions.

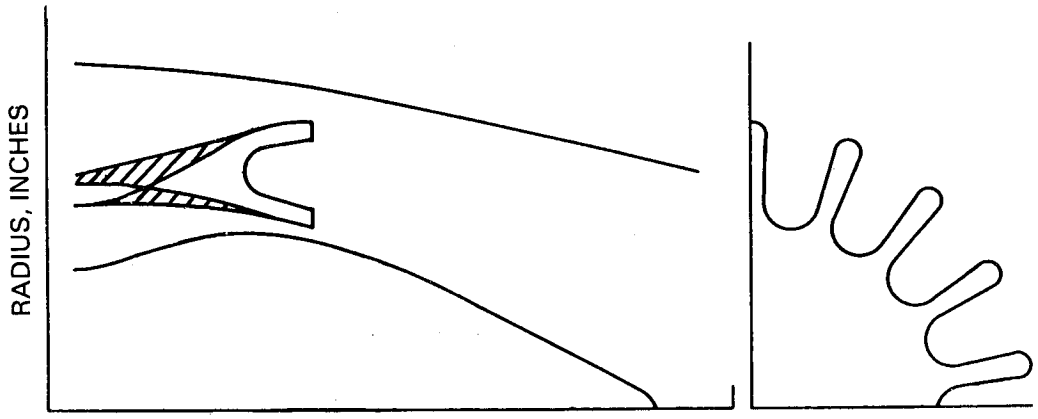

Figure 4.10.2-1 Flowpath of Integrated Core/Low Spool Exhaust System with Internal Mixer Installed

TABLE 4.10.2-I

PREDICTED MIXER PERFORMANCE AT KEY ENGINE OPERATING CONDITIONS

	Engine Operating Condition		
	Aero. Des. Point	Maximum Cruise	Takeoff
Mixer Pressure Loss, %			
(Core Section)	0.80	0.92	0.71
(Duct Section)	0.62	0.63	0.53
Mixer Efficiency, %	85.0	85.0	85.0
Tailpipe Pressure Loss %	0.35	0.39	0.30

4.10.3 Mechanical Design

The mechanical design of the mixer and related components is shown in Figure 4.10.3-1. The lobe convolutions are formed by inner and outer shells. The outer shell consists of 36 stampings of Inconel 625 sheet metal 0.160 cm (0.063-in) thick, which are welded together to form the fan stream flowpath. The 18 lobe weldment is joined by rivets and screwed to the structrual rings and ribs to form the primary structure for the mixer.

The triangular region bounded by the structural rings, rib and hood is effectively a hollow box beam. The beams, from which the lobes are cantilevered, are supported by two structural rings. The rear ring provides a single plane attachment for the entire assembly to the rear flange of the turbine exhaust case. With this arrangement, the mixer is a self-supporting structure.

The inner shell of the lobe is formed from two stampings of 0.109-cm (0.043-in) thick Inconel 625 sheet metal. As indicated in Figure 4.10.3-2, the inner shell sections are nested within the outer shell and are joined together by blind rivets along the axial overlap joint. This arrangement allows thermal freedom between the inner shell sections, which are exposed to the hot engine exhaust gases, and the outer shell, which is exposed to the relatively cold fan stream. The forward edge of the inner shell is riveted to a sheet metal ring that provides stability and damping action for the inner shell through the use of finger contacts with the rear support ring.

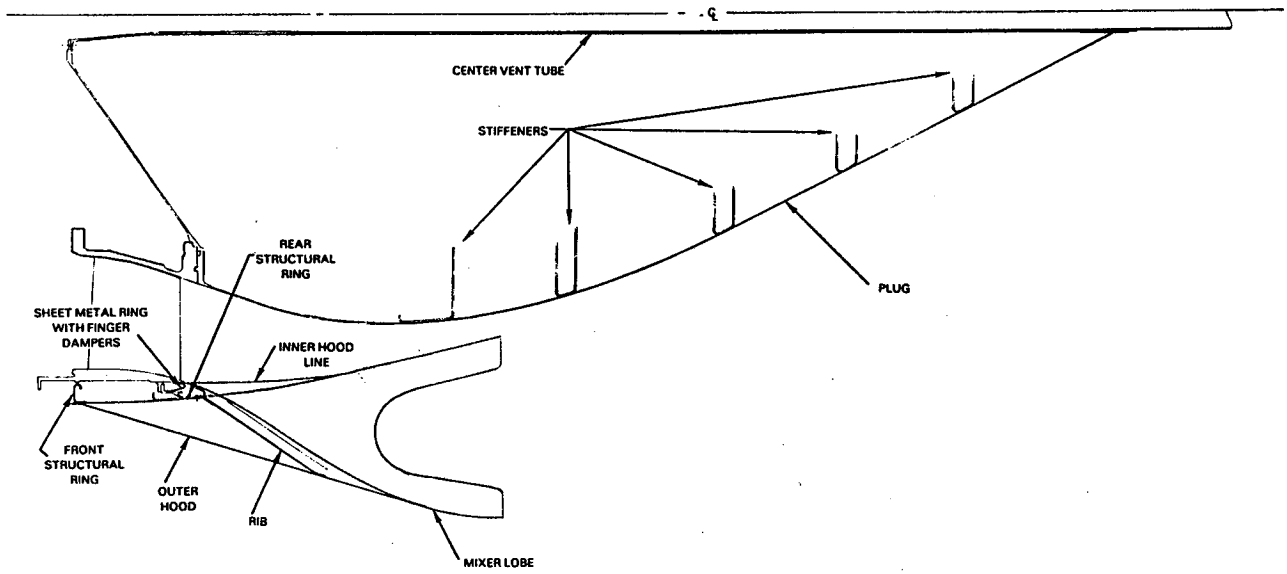

Figure 4.10.3-1 Integrated Core/Low Spool Exhaust Mixer and Plug Mechanical Design

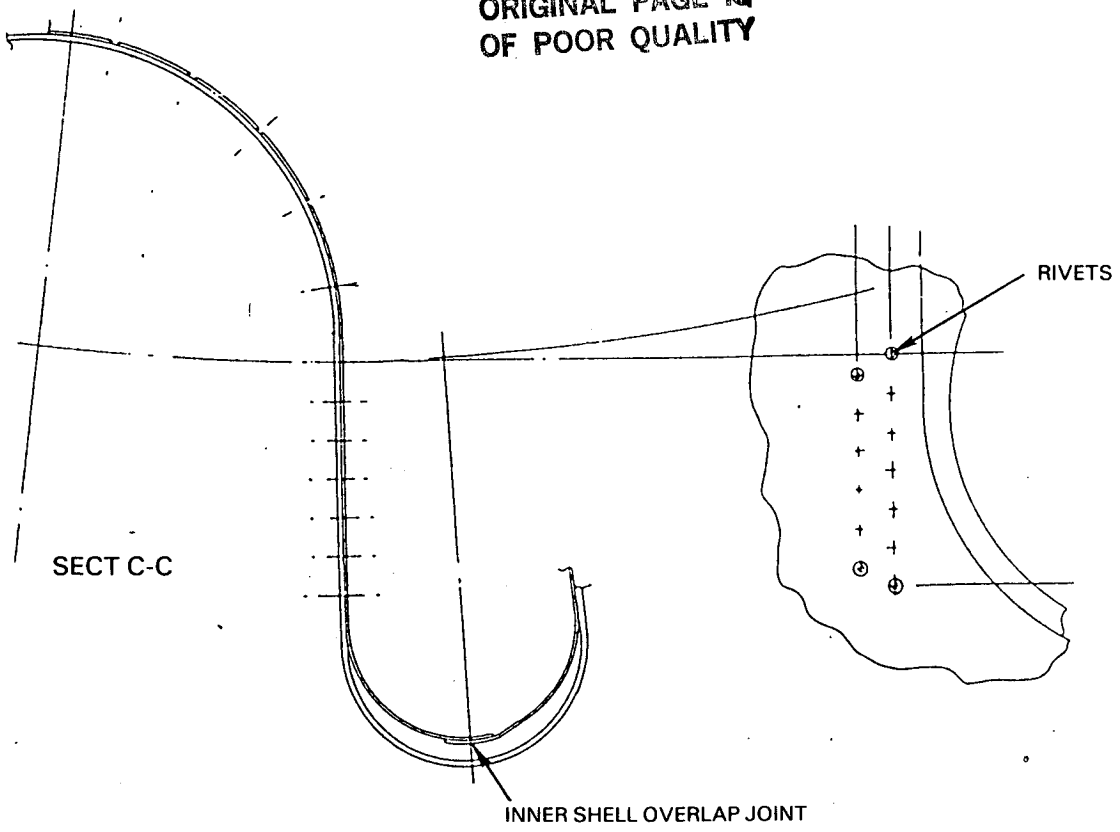

Figure 4.10.3-2 Mixer Inner and Outer Shell Joining Technique

The exhaust plug is fabricated from 0.127 cm (0.050 in) thick AMS 5510 material. The plug is designed with five structural rings to provide resistance to buckling. The ring in the plane of the mixer lobe is wider than the others to serve as an attachment point to install a damper in the event a vibratory mode is encountered during engine testing. Assembly is accomplished by sliding the plug over the engine center vent tube and bolting it to the turbine exhaust case and inner rear flange.

4.10.4 Differences Relative to the Flight Propulsion System

With minor exceptions, the exhaust nozzle and mixer for the integrated core/low spool is the same as the design for the flight propulsion system. In order to reduce cost, the integrated core/low spool exhaust mixer is fabricated from steel instead of titanium, and acoustic treatment is used on the plug. Without acoustic treatment, the integrated core/low spool plug is simplified structurally by making it a one-piece structure with five buckling resistance ring stiffeners. While the flight nozzle has a convergent/divergent nozzle for improved performance, the integrated core/low spool nozzle will be convergent to provide flexibility in achieving the desired engine match by trimming the nozzle.

SECTION 5.0
INTEGRATED CORE/LOW SPOOL SYSTEMS

5.1 INTRODUCTION

The design of the integrated core/low spool included a definition of all engine systems such as the fuel, lubrication and active clearance control systems. The design and operating characteristics of these systems is discussed in this section.

A full-size wood model of the integrated core/low spool was constructed to facilitate the design and integration of the different external accessories and plumbing. The use of this model ensured no overlapping of hardware envelopes and provided an early identification of potential interference problems. For expediency and cost considerations, available hardware is used in the design of the engine systems. Figures 5.1-1 through 5.1-4 show the engine model with most of the external hardware installed.

5.2 ENGINE DUCTS

5.2.1 General Description

To meet the requirements of the integrated core/low spool test program, engine ducts were designed for two test configurations. For the first test, which is organized to assess component and integrated system performance, the engine is configured as a nonmixed flow system because the use of a bifurcated duct is required to accommodate the large quantity of test instrumentation. The objective of the second test is to evaluate aero-acoustic performance. Therefore, the engine is configured as a mixed flow system that represents as closely as possible the flight propulsion system. Its nacelle simulates a flight engine design, and is complete with acoustic treatment. Engine ducting for both configurations is designed according to Pratt & Whitney Aircraft experimental hardware standards.

5.2.2 Nonmixed Flow Configuration (Build 1)

The ducting for the first build of the integrated core/low spool is shown in Figure 5.2.2-1. The bellmouth/inlet unit is a single-piece structure constructed from Fiberglas®. It is attached to the forward fan case, which is an aluminum structural ring that contains provisions for the inlet instrumentation. Neither the bellmouth/inlet case nor the fan case instrumentation ring contain acoustic treatment for Build 1. Internal duct contours in this region reflect the flight propulsion system nacelle aerodynamic design, which is described in Ref. 12.

To accommodate the large quantity of performance instrumentation planned for the first test, a bifurcated duct with a conical nozzle configuration is used to split the fan stream flow into two equal segments. This flow split facilitates access to the core section and decreases the losses that normally result from crossing the fan stream with instrumentation. A rear view of the bifurcated duct is presented in Figure 5.2.2-2. For the integrated core/low spool, an existing JT9D bifurcated duct set will be modified and adapted to the engine.

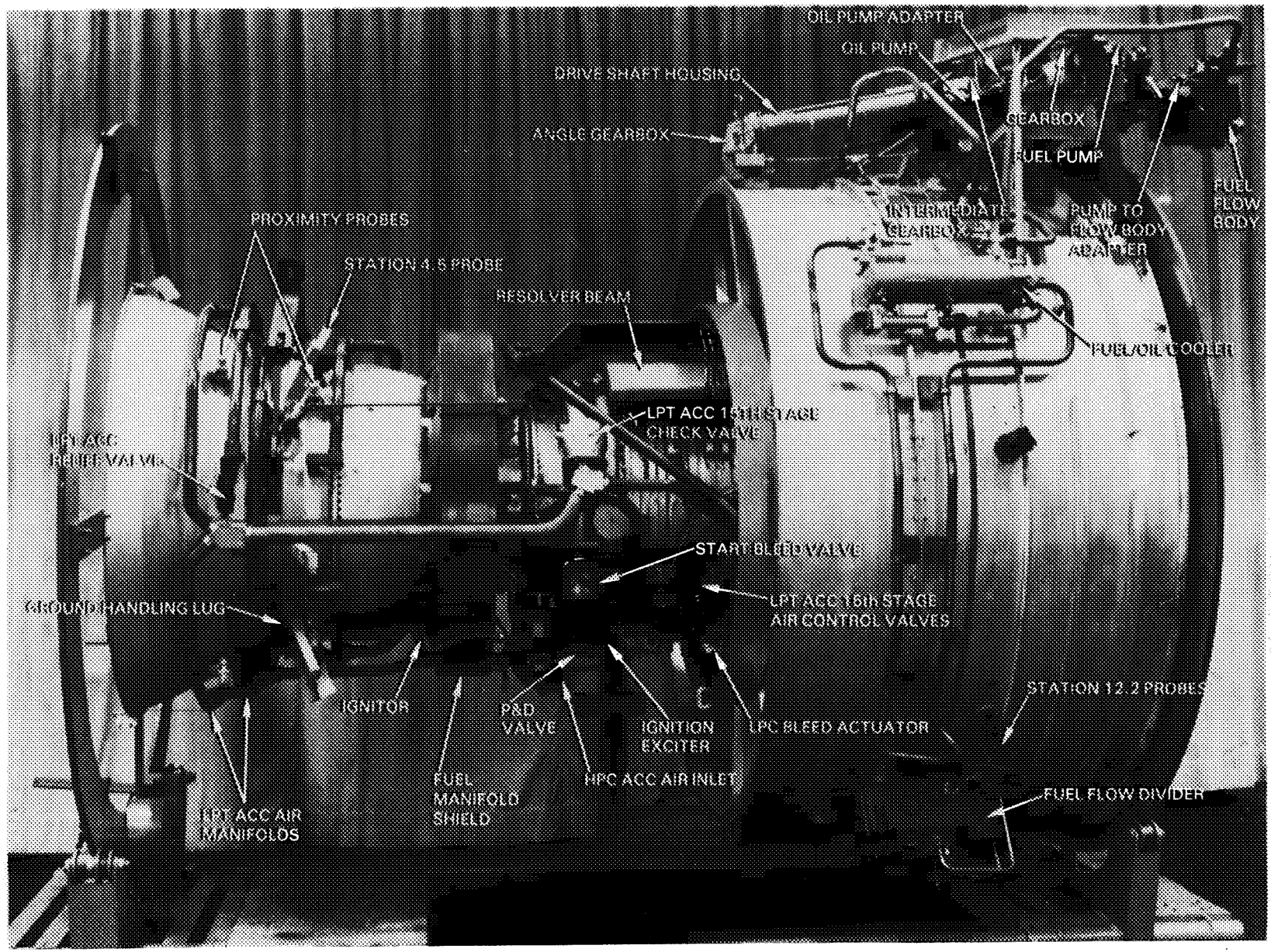

Figure 5.1-1 Integrated Core/Low Spool Model Showing Mounting of External Engine Accessory Hardware and Associated Plumbing

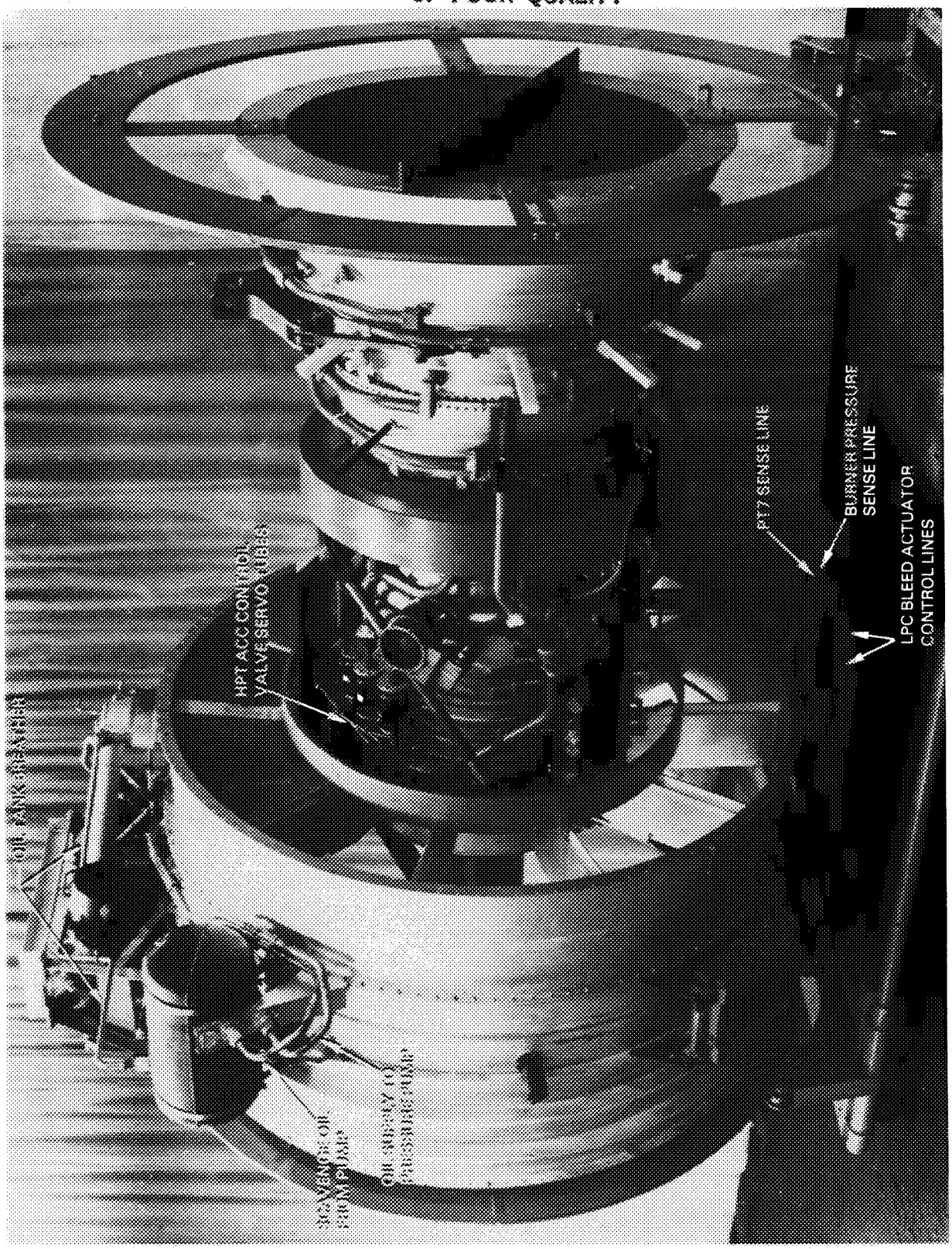

Figure 5.1-2 Integrated Core/Low Spool Model Showing Mounting of External Engine Accessory Hardware and Associated Plumbing

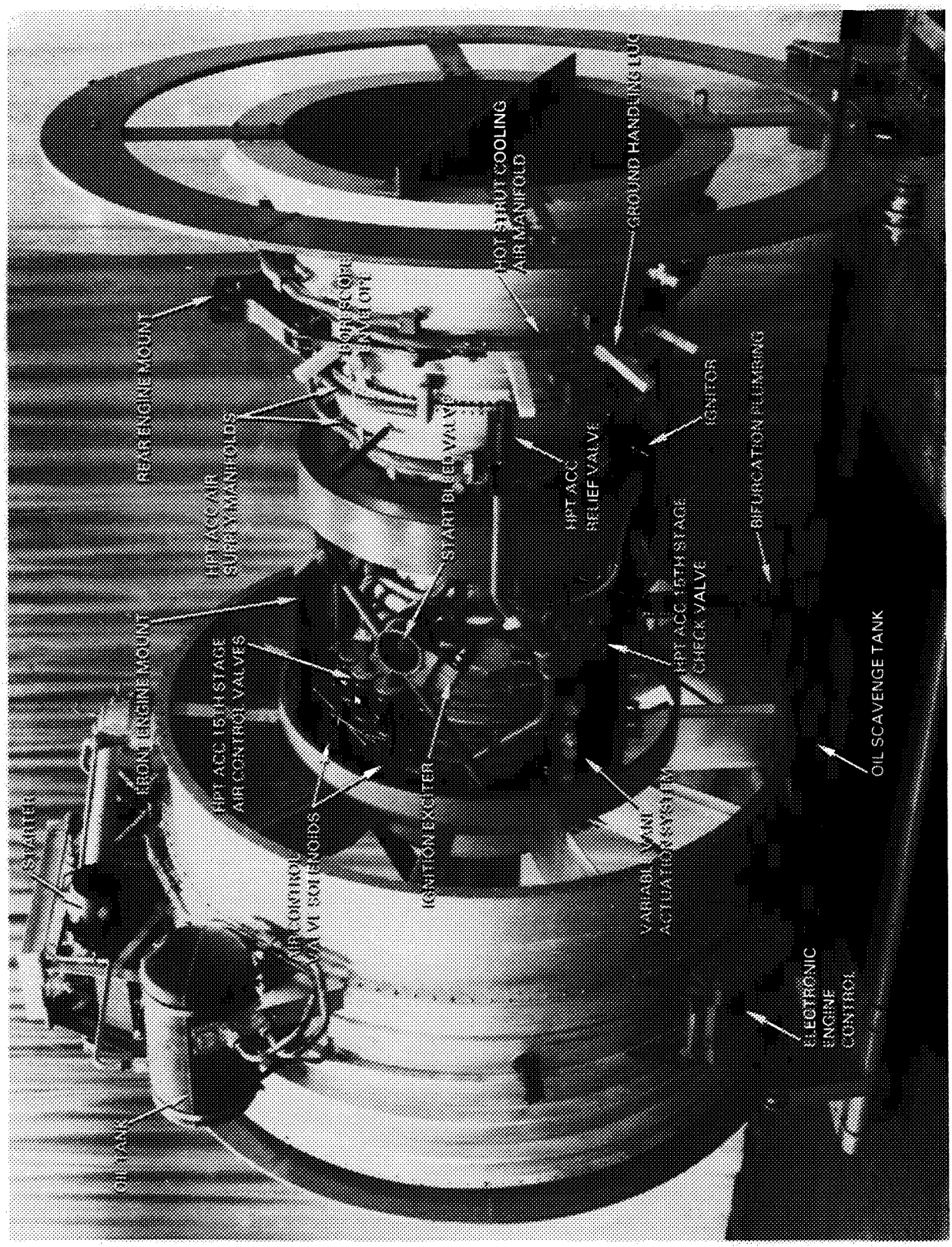

Figure 5.1-3 Integrated Core/Low Spool Model Showing Mounting of External Engine Accessory Hardware and Associated Plumbing

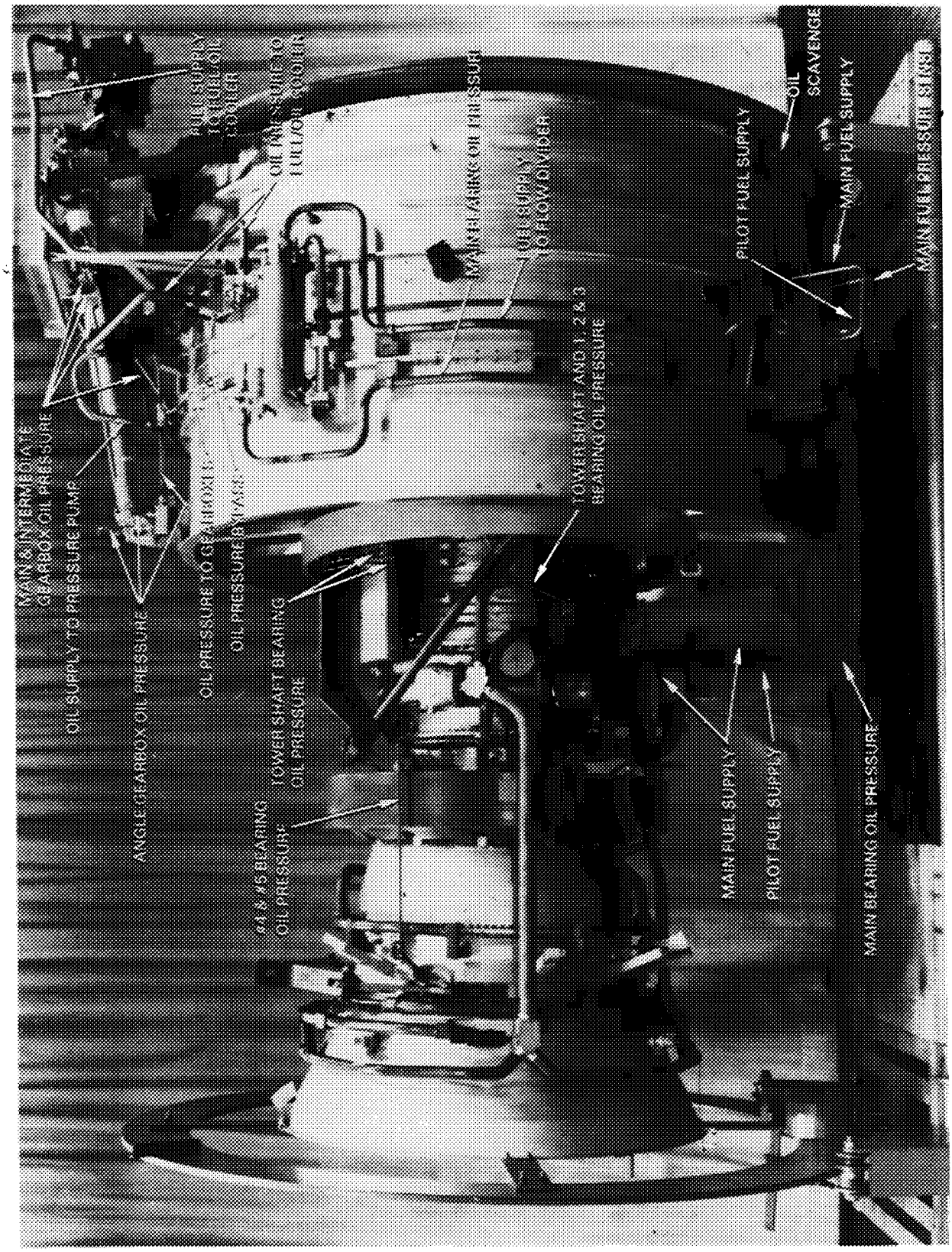

Figure 5.1-4 Integrated Core/Low Spool Model Showing Mounting of External Engine Accessory Hardware and Associated Plumbing

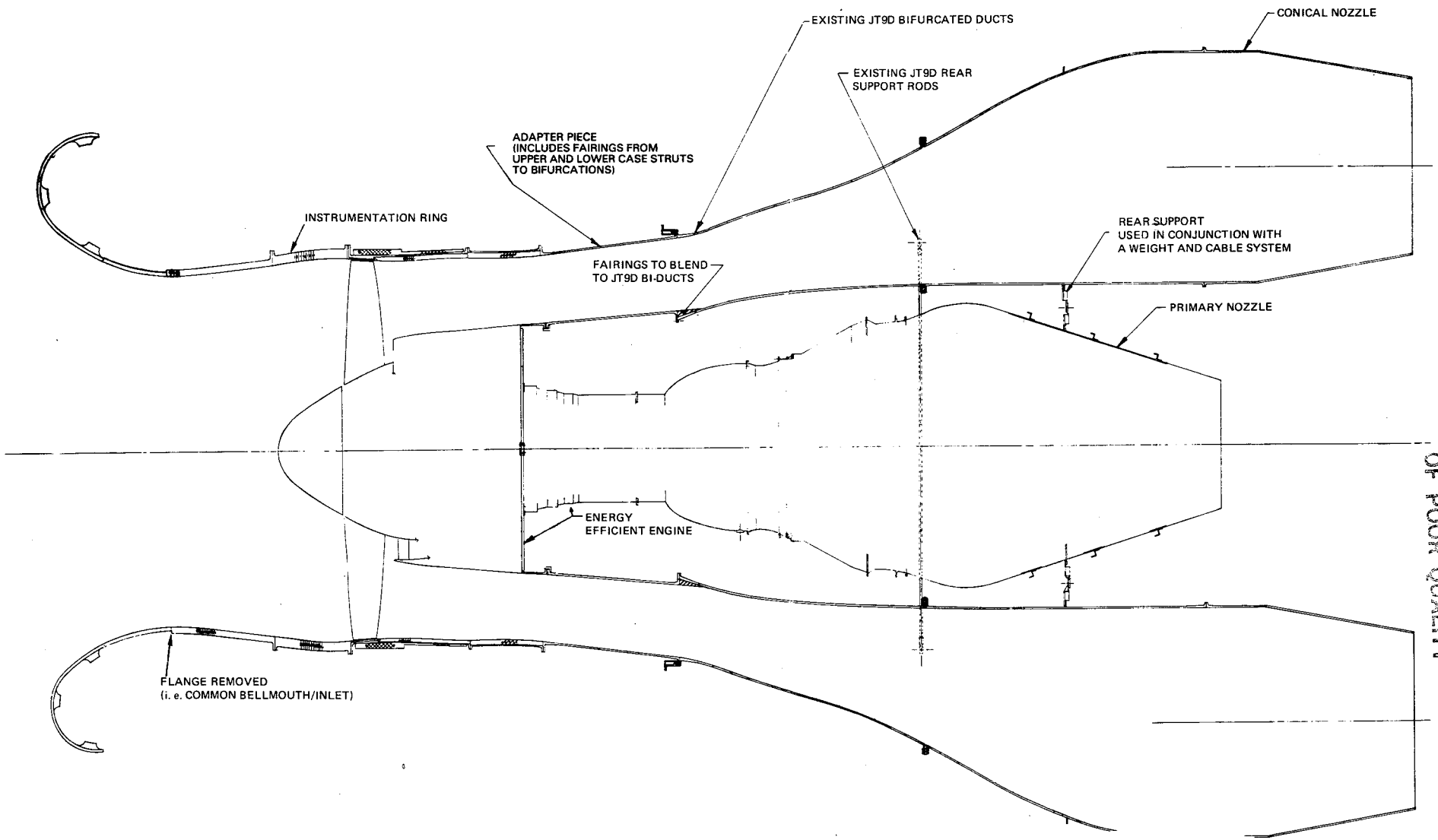

Figure 5.2.2-1 Integrated Core/Low Spool Build 1 Configuration Featuring Modified JT9D Bifurcated Duct

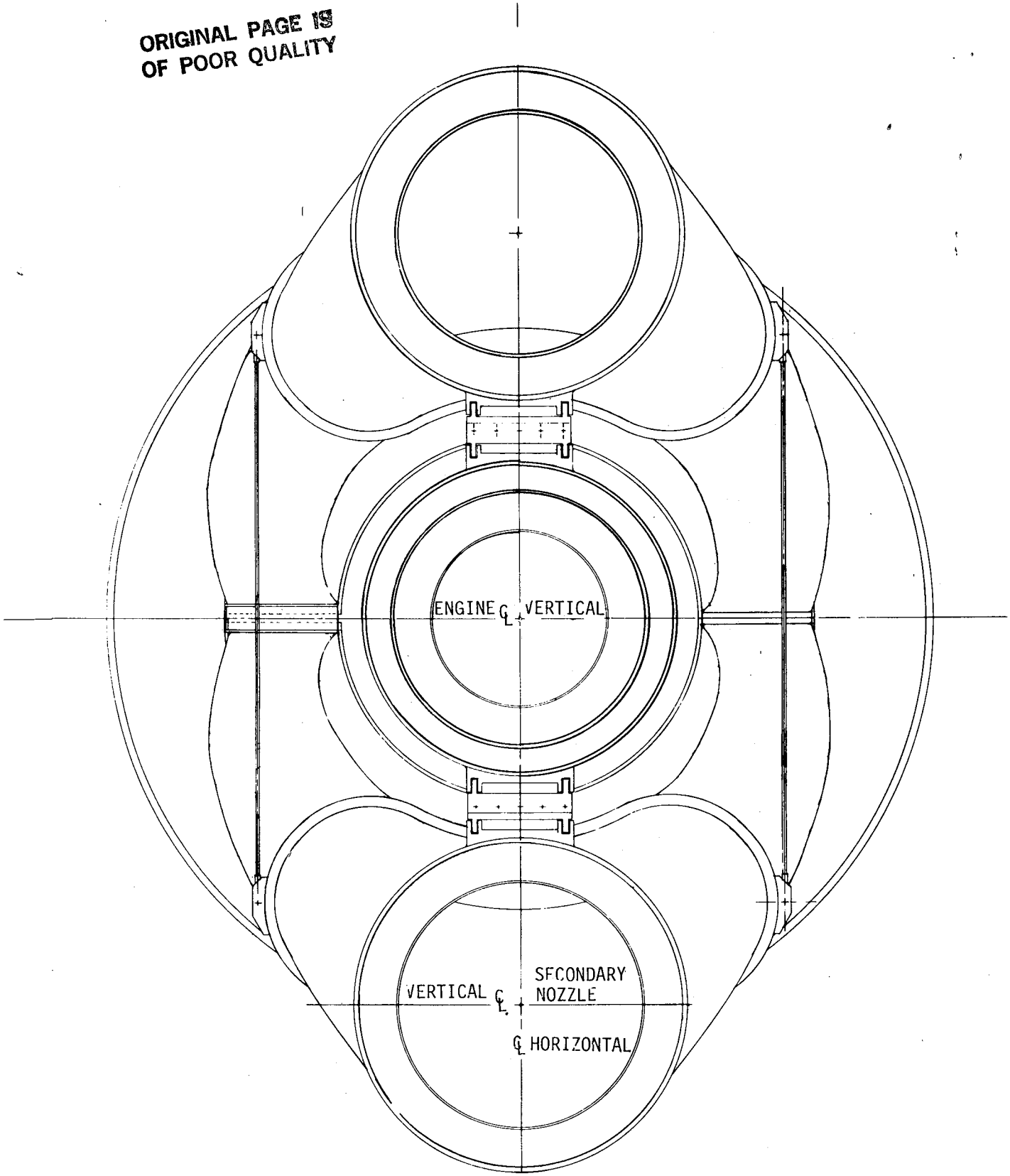

Figure 5.2.2-2 Rear View of Bifurcated Duct Configuration

An adapter, consisting of two coannular duct halves, is used to blend the flow lines of the compressor intermediate case to the bifurcated ducts. As indicated in Figure 5.2.2-1, upper and lower fairings are required between the intermediate case struts and the bifurcation walls of the duct halves. The adapter wall employs three equally-spaced groups of stiffening flanges to ensure adequate support. The number of bolts retaining the bifurcated duct adapter to the intermediate case is sufficient to withstand shear and blow-off loads. However, the bending moment of the duct system will be prevented from acting on the intermediate case flanges by the use of either a constant support hanger or a counterweight system.

In the tailpipe section, the inner wall of the bifurcated duct is attached to the primary nozzle by a Marmon clamp. The fan stream nozzles have a trim capability of +5 to -20 percent of the nominal exit area. The primary nozzle is a welded sheet metal structure that is cantilevered off the turbine exhaust case.

5.2.3 Mixed Flow Configuration (Build 2)

Figure 5.2.3-1 presents a cross-sectional view of the nacelle design for the second engine build. The design matches the internal flow lines of the nacelle for the flight propulsion system. The inlet section consists of a single-piece, fiberglas bellmouth/inlet case with an aluminum instrumentation ring. Both cases contain acoustic treatment. Attached to the intermediate case is a coannular "D" duct. As shown in Figure 5.2.3-2, the case is axially split to provide accessibility to the engine and external accessories. The "D" duct has acoustic treatment on both coannular sections. In the mixed flow configuration, both the tailpipe and nozzle plug have acoustic treatment, as indicated in Figure 5.2.3-1.

5.2.4 Differences Relative to the Flight Propulsion System

The nacelle for the flight propulsion system is designed for high performance, low weight, engine accessibility, and noise reduction. The nacelle design is shown in Figure 5.2.4-1. With the exception of the inlet leading edge section, the internal contours are essentially the same as the experimental-type structure for the integrated core/low spool.

However, there is a significant difference in the materials. The inlet section of the nacelle incorporates a wrapped layer of Kevlar® for containment. To reduce weight, the outer surface of the inlet, cowl doors and "D" ducts is composed of aluminum honeycomb wrapped with graphite/Kevlar®.

The inner wall of the "D" duct is an aluminum brazed titanium honeycomb. Titanium is required to provide load carring capability and to serve as a firewall around the gearbox compartment. This same material is used for the tailpipe.

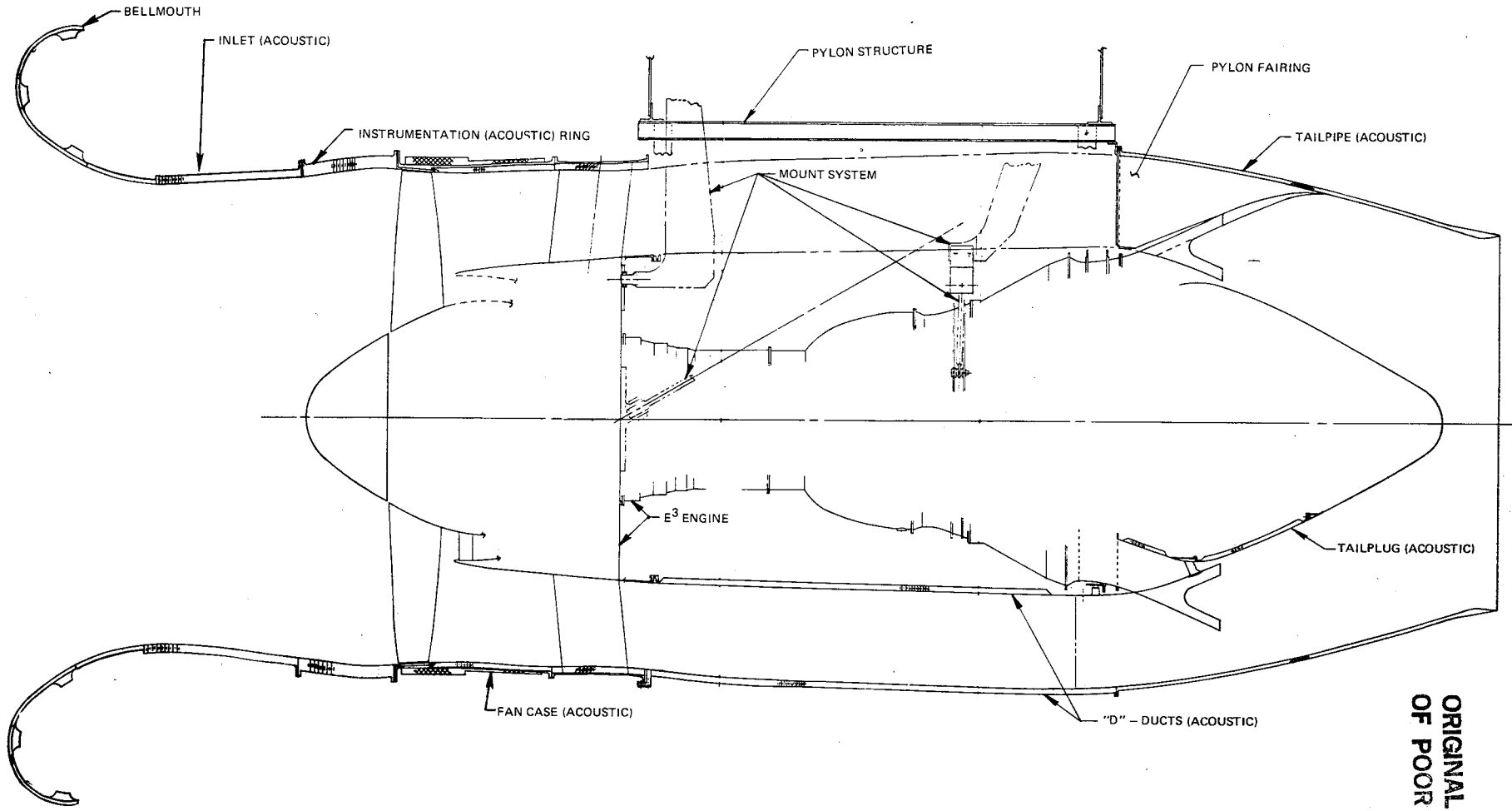

Figure 5.2.3-1 Integrated Core/Low Spool Configuration with Full Nacelle

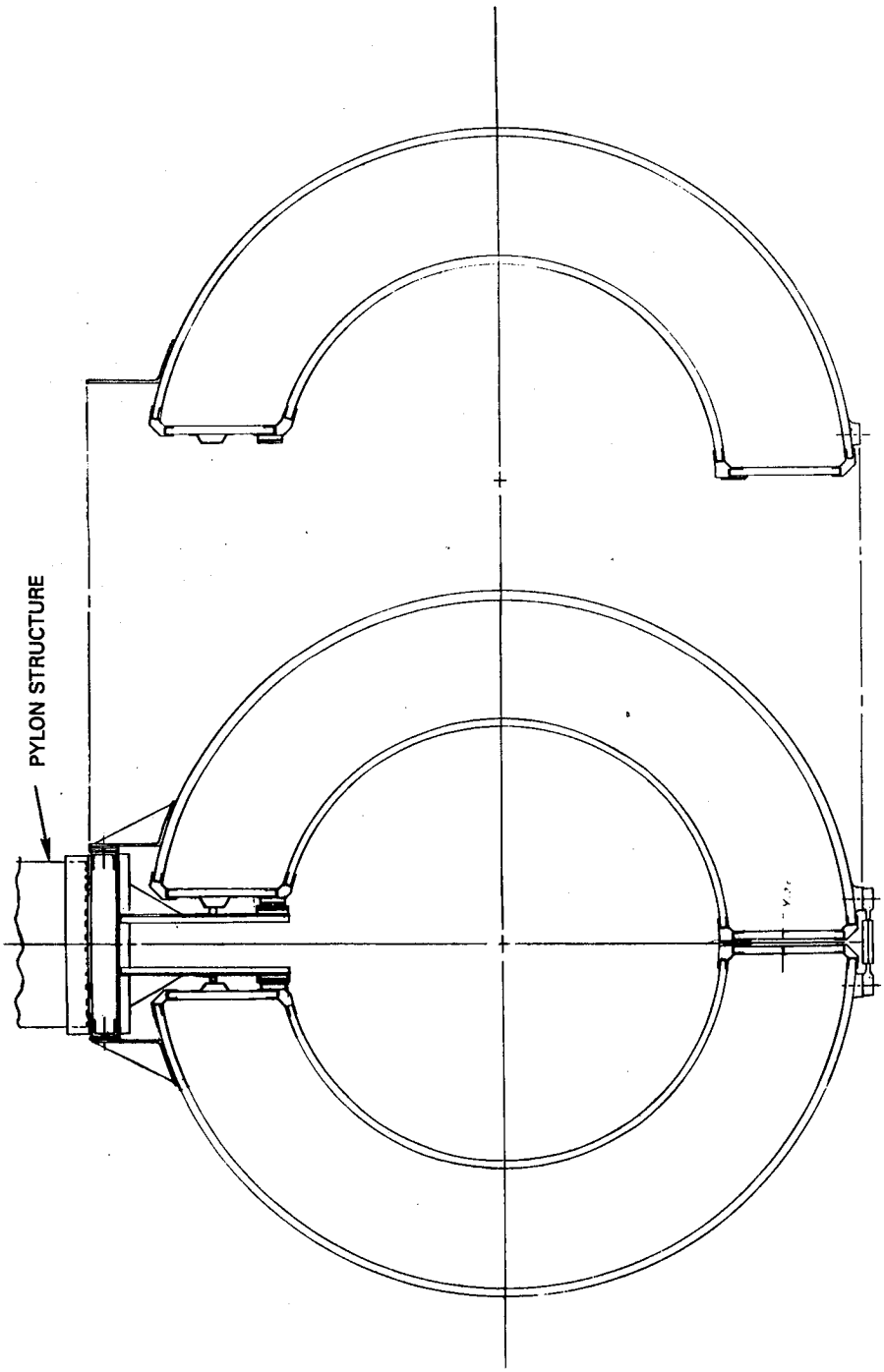

Figure 5.2.3-2 "D" Duct Configuration

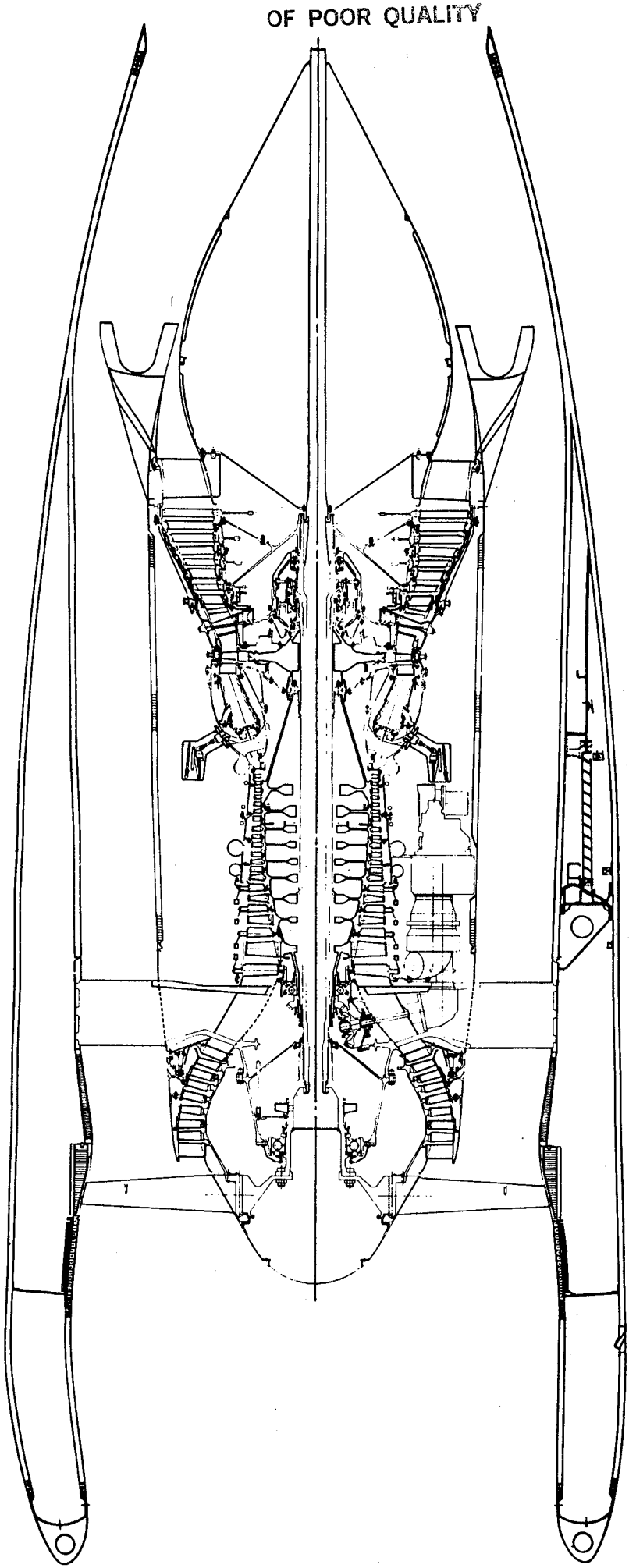

Figure 5.2.4-1 Nacelle Configuration for the Flight Propulsion System

5.3 FUEL SYSTEM

5.3.1 General Description

The principal elements of the fuel system are the fuel pump, fuel control and fuel management system. The external locations of the various fuel system components are identified in Figures 5.1-2 through 5.1-4.

The main feature of the fuel system is a dual channel full-authority electronic control. The electronic control in the integrated core/low spool is a modification of an existing design. As indicated in Figure 5.1-3, the control unit is mounted on the bottom of the fan case. Communication between channels is maintained by a "cross talk" link. An existing fuel pump supplies fuel to the metering portion of the fuel system called a flow body, which receives electrical commands from the control. A schematic diagram of the control system is shown in Figure 5.3.1-1.

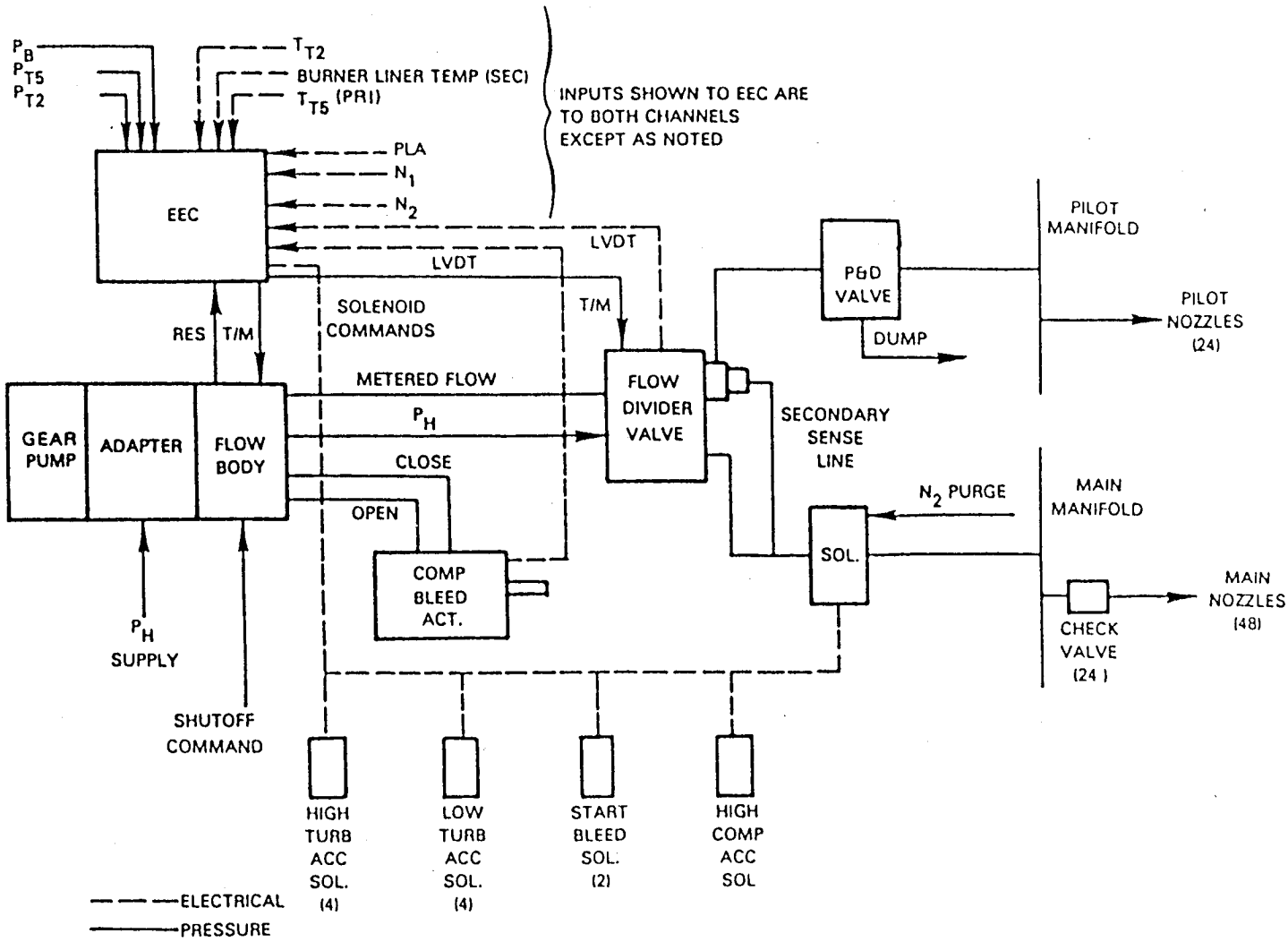

Figure 5.3.1-1 Integrated Core/Low Spool Control System Schematic

The flow body contains the torque motor, metering valve and associated pressure regulating devices. Hydraulic pressure from an outside source is supplied to the flow body for torque motor servo pressure. Commands from the control also establish the primary and secondary fuel flow splits to the combustor in the flow divider or split valve. During shutdown, fuel to the pilot zone in the combustor is dumped by a pressurizing and dump valve. A solenoid performs the same function for the main zone. The main zone fuel, downstream of the manifold, passes through 24 check valves -- one for each pair of nozzles. These valves are designed to permit the entire main fuel manifold to fill before the fuel starts to flow out of the nozzles. Figure 5.3.1-2 shows a typical section of the fuel manifold and shroud assembly. The fuel supply connections are standard cone-type fittings brazed to the casting and incorporate internal "last chance" fuel filters.

The preliminary control logic for the integrated core/low spool has been designed and verified. The total fuel flow logic is shown in block diagram form in Figure 5.3.1-3. Total fuel flow is scheduled as a function of rate limited power lever angle or as a function of engine pressure ratio versus power lever angle. A number of topping loops are incorporated in the control for structural protection of the engine during the planned test program.

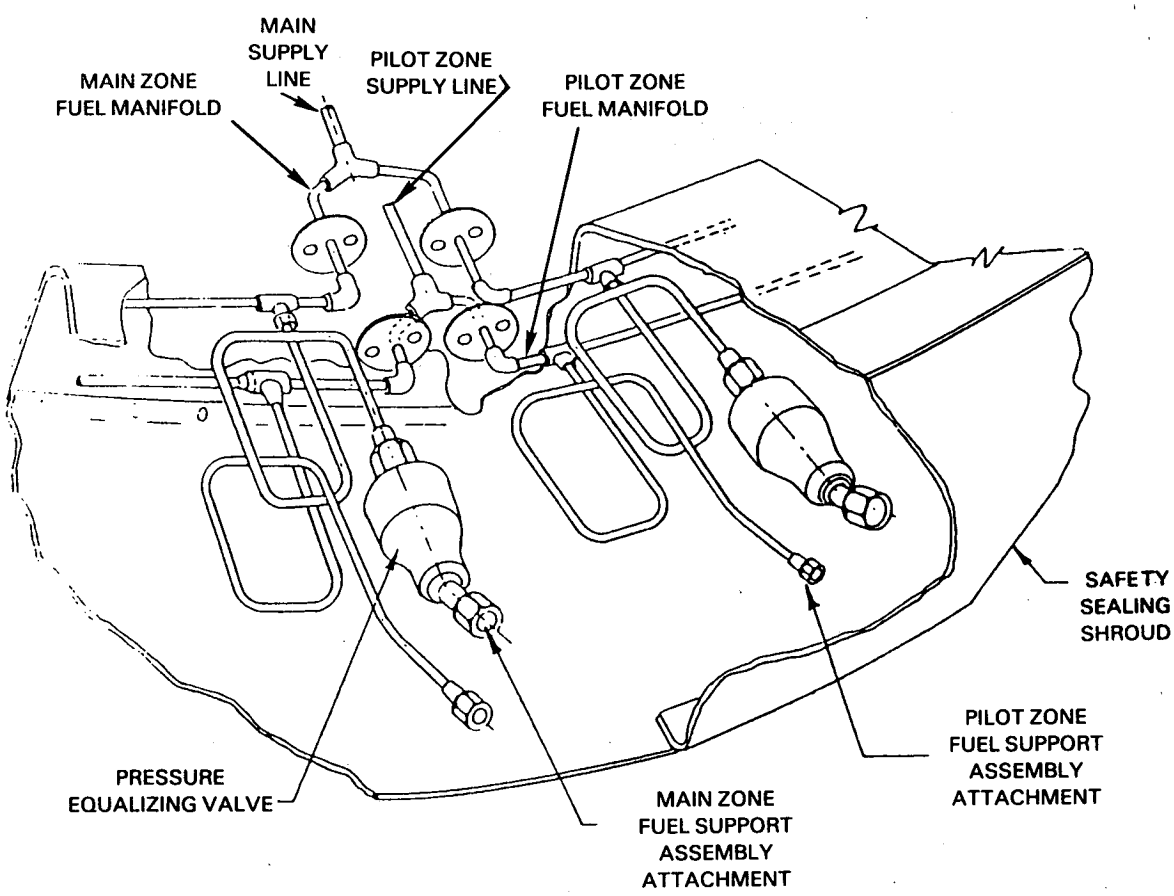

Figure 5.3.1-2 Fuel Manifold and Shroud System

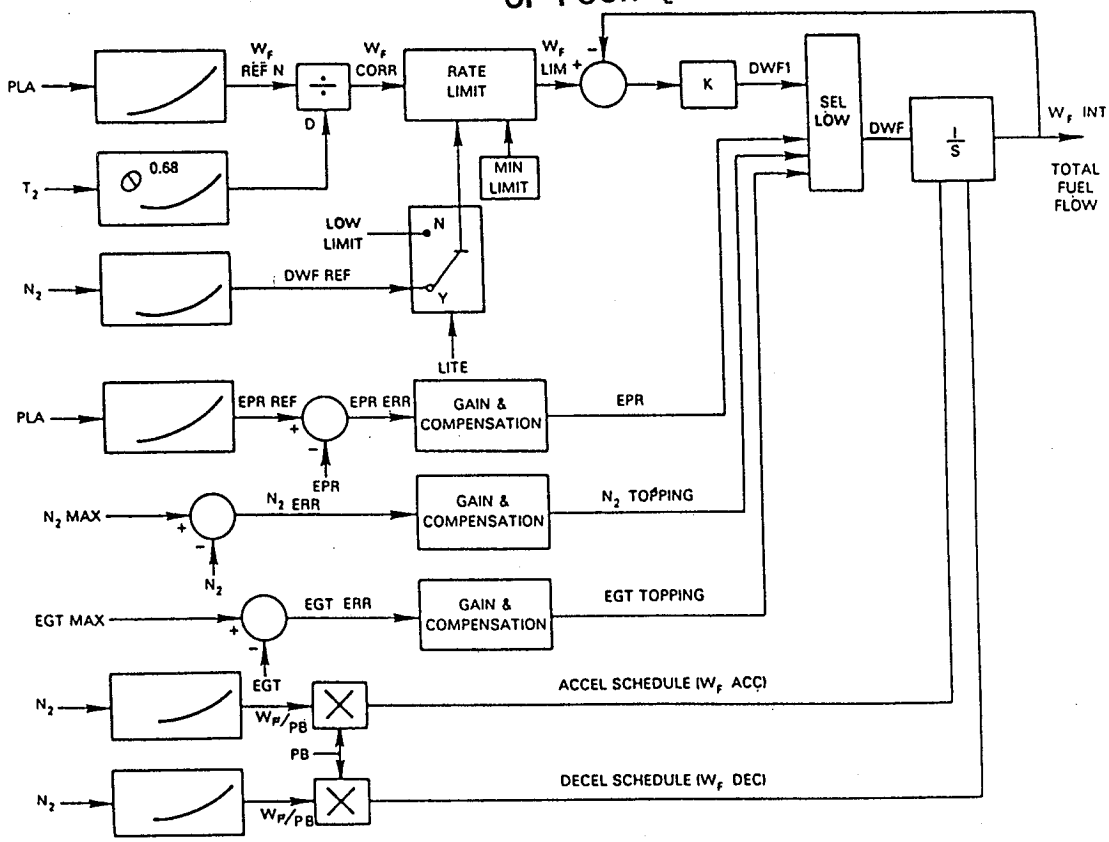

Figure 5.3.1-3 Integrated Core/Low Spool Total Fuel Flow Logic

5.3.2 Differences Relative to the Flight Propulsion System

The electronic fuel control in the flight propulsion system has not been updated since its initial definition. Details of the design and capability of the system are contained in Reference 11.

In brief, the control for the flight engine is an advanced version of a digital full-authority electronic control. The design is based on technical advancements envisioned for the late 1980 to early 1990 time frame. As conceptually defined, the system will be capable of integrated control of a dual fuel management system for the two-stage combustor, variable compressor vanes, two position start bleeds as well as the inter-compressor surge bleeds, and separate air valves for active clearance control. The primary control mode is isochronous governing of low-pressure rotor speed with governing of high-pressure rotor speed at idle. Control logic includes selective redundancy of critical components to provide the optimum balance among the parameters of mean time before failure, cost, weight, reliability, and maintainability.

5.4 BEARING AND LUBRICATION SYSTEMS

5.4.1 General Description

In the integrated core/low spool, there is a total of five mainshaft bearings located in two bearing compartments. The low-pressure spool is supported by three bearings and the straddle-mounted high-pressure spool is supported by two bearings. All bearings and bearing compartment components are existing designs and meet the structural requirements for the integrated core/low spool. A self-regulating lubrication system provides positive oil supply to the bearing compartments for lubrication and cooling.

5.4.2 Mainshaft Bearings and Seals

The front bearing compartment, as illustrated in Figure 5.4.2-1, contains the Nos. 1, 2 and 3 bearings. The front of the bearing compartment is sealed from the buffer air environment by an internally-pressurized carbon face, spring-guided seal. The rear of the compartment is sealed by a multi knife-edge labyrinth seal.

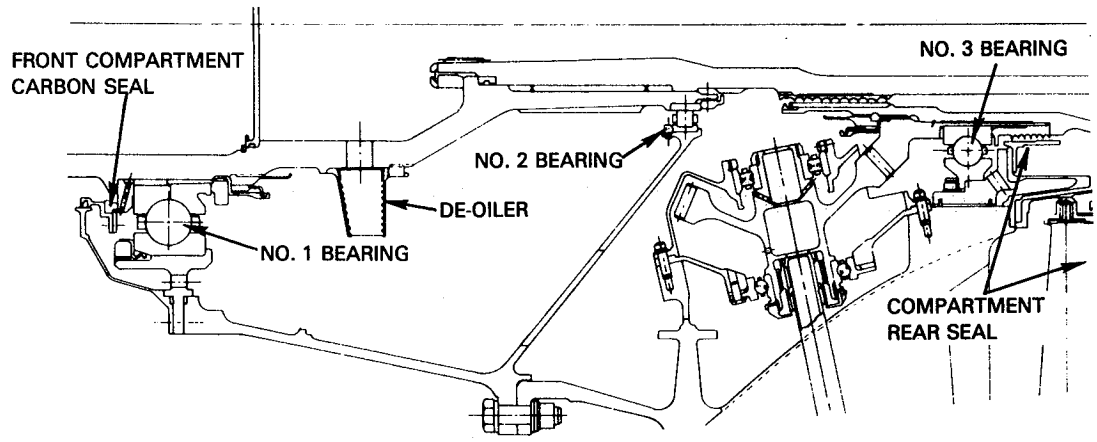

Figure 5.4.2-1 Front Bearing Compartment

A design summary of the bearings in the front compartment is presented in Table 5.4.1-I. The No. 1 bearing is an unflanged ball type with a split inner race. Oil to the bearing and front compartment seal is supplied through a single oil jet to an axial scoop.

The No. 2 bearing is an unflanged roller bearing with a double shouldered outer race. Oil is supplied to this bearing by an oil jet in the intermediate case towershaft/No. 3 bearing oil system.

The No. 3 ball bearing is under race cooled by oil supplied to an axial scoop. Consideration of rotor dynamic vibration modes resulted in the incorporation of a spring and oil-film damper.

TABLE 5.4.1-I

FRONT BEARING COMPARTMENT BEARING CHARACTERISTICS

	No. 1	No. 2	No. 3
Type	Unflanged Ball Split Inner Race	Unflanged Roller Double Shouldered Outer Race Outer Land Riding	Oil-Damped Ball
Size			
Inner Diameter	210	130	165
Outer Diameter	350	150	255
Material			
Rolling Element	PWA 793	PWA 723	---
Rings	PWA 793	PWA 723	---
Cage	AMS 4616	AMS 6414	---
Rolling Element Size cm (in)	3 (1.5625)	1 (0.5512) dia x 1 (0.5512)	2.54 (1.0)
DN Value Max	0.819×10^6	0.507×10^6	2.3×10^6
Cooling Scheme	Axial Scoop Under Race	Jet	Axial Scoop Under Race

The rear bearing compartment, shown in Figure 5.4.2-2, contains the Nos. 4 and 5 bearings. The No. 4 bearing is an oil-damped roller bearing. It is also spring centered, preloaded and under-race cooled. The viscous oil damper and soft centering spring are incorporated to satisfy high-pressure rotor dynamic response criteria. Preloading minimizes roller skidding and the under-race cooling provides positive cooling to manage thermal expansion during all operating conditions. Dimensionally, the bearing inner diameter is 165 mm, the outer diameter is 222 mm, and the roller diameter is 16 mm. This bearing operates at a DN level of 2.3×10^6. A design summary of the Nos. 4 and 5 bearings is contained in Table 5.4.1-II.

The No. 5 roller bearing has the same physical dimensions as the No. 4 bearing, but it operates at a much lower speed than the No. 4 bearing (0.64×10^6 DN). This bearing has a zero preload and a viscous oil film damper is used on the outer ring to control low-pressure rotor vibratory response.

The seal arrangement in the rear bearing compartment consists of a No. 4 front carbon seal, an intershaft seal with back to back carbon seals and a No. 5 rear carbon seal. These seals are dry-face, short carbon with cooled rotating seal plates.

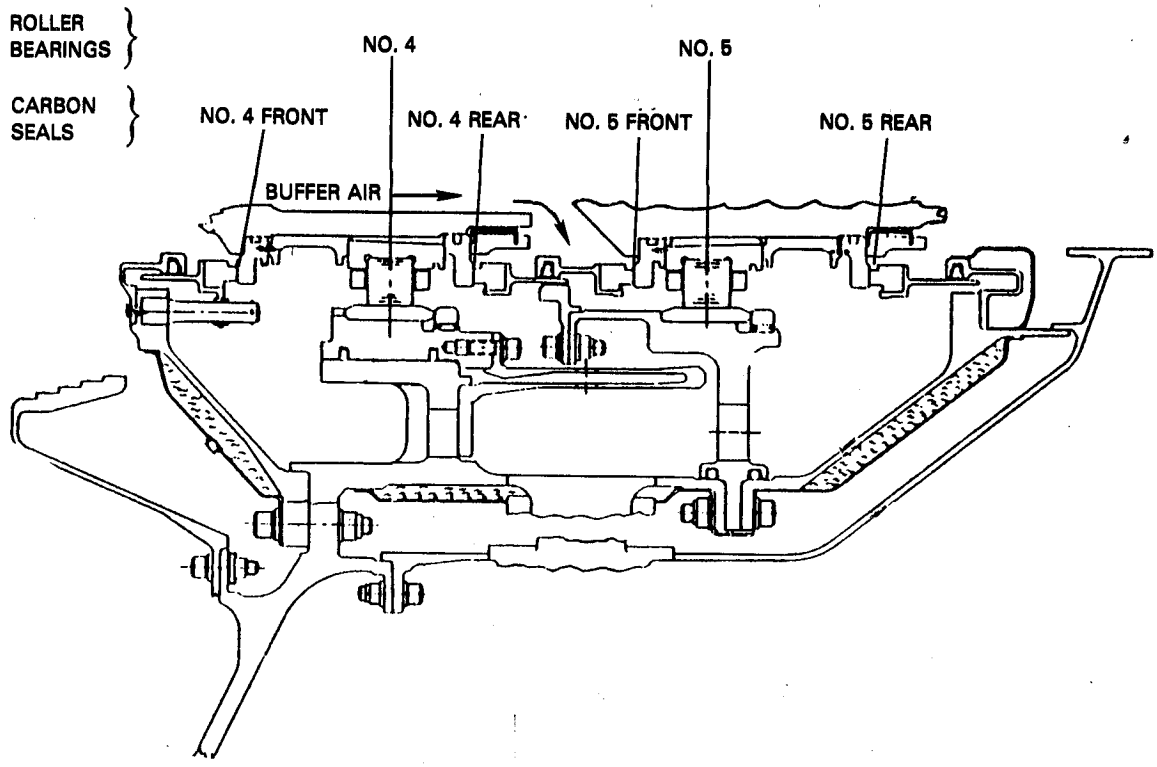

Figure 5.4.2-2 Nos. 4 and 5 Bearing Compartment Bearing and Seal Arrangement

TABLE 5.4.1-II

REAR BEARING COMPARTMENT BEARING CHARACTERISTICS

	No. 4	No. 5
Type	Oil-Damped Roller, Spring-Centered, Pre-Loaded	Oil-Damped Roller, No Pre-Load
Size		
Inner Diameter mm	165	165
Outer Diameter mm	222	222
Material		
Rolling Element	PWA 725	PWA 725
Rings	PWA 725	PWA 725
Cage	AMS 6414	AMS 6414
Rolling Element Size cm (in)	1.6 (0.63)	1.6 (0.63)
DN Value Max	2.3×10^6	0.64×10^6
Cooling Scheme	Radial Scoop, Under Race	Radial Scoop, Under Race

5.4.3 Lubrication System

A schematic diagram of the lubrication system for the integrated core/low spool is shown in Figure 5.4.3-1. The system is self regulating and circulates a total oil flow of 65 kg/min (144 lb/min) at sea level takeoff conditions. The feature of self regulation simplifies plumbing, reduces the size and number of scavenge pumps, and eliminates the need for a pressure regulating valve. The rear bearing compartment contains a blowdown system with oil and air scavenged together through the turbine intermediate case strut to the front bearing compartment. A single mainshaft de-oiler (see Figure 5.4.2-1) is located in the front bearing compartment in close proximity to the No.1 bearing. The de-oiler separates oil from breather air for all main engine bearing compartments and discharges the air through the center tube at the back of the engine.

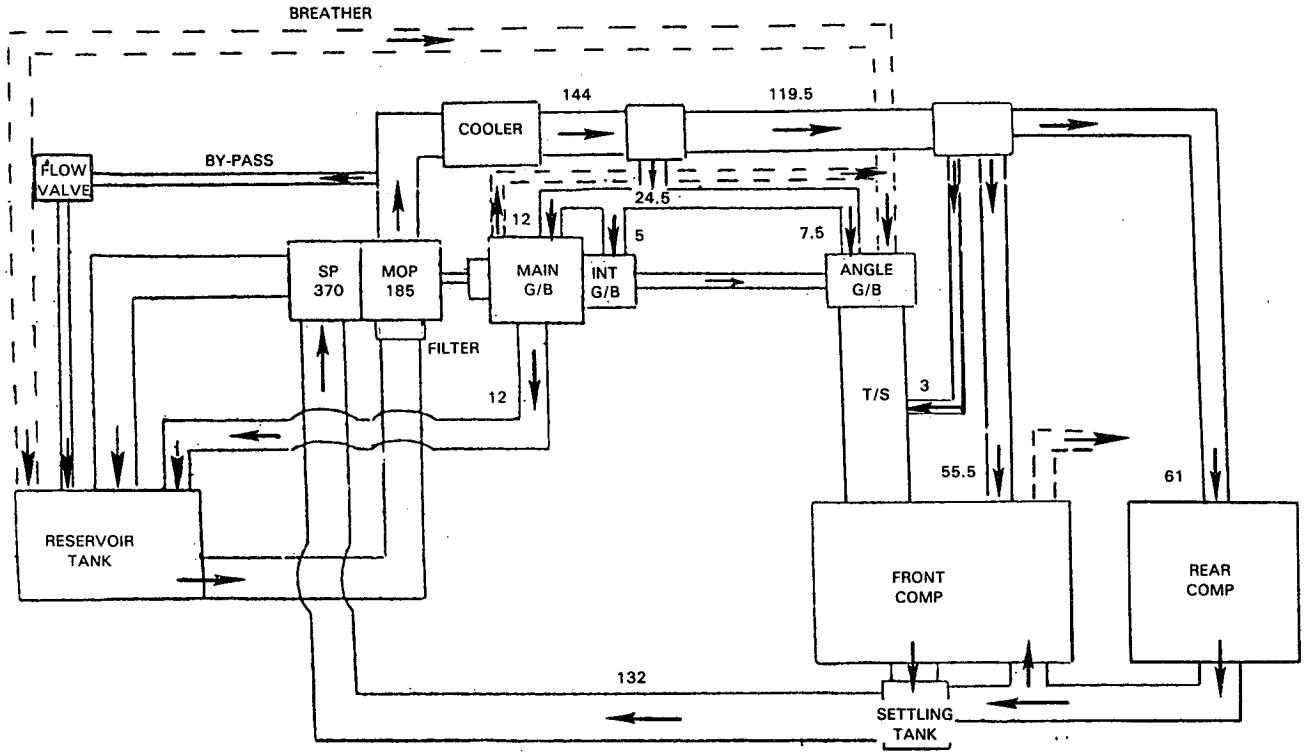

Figure 5.4.3-1 Energy Efficient Engine Integrated Core/Low Spool Lubrication System Schematic (Non-Regulated)

5.4.4 Vibratory Response Analysis

Critical speed analyses were conducted to identify high strain energy modes in the operating range. The stiff high-pressure rotor with soft effective front spring mount (No. 3 bearing) eliminates any high critical speed response in the operating range. As indicated in Figure 5.4.4-1, the most serious critical speed mode is a free-free mode with a 100 percent strain energy that occurs well above the maximum speed. A pitch mode with 4.2 percent strain energy and a bounce mode occur at operating speeds below idle. Another possible critical mode is during engine startup, when the stationary rotor becomes bowed as a result of thermals from residual heat in a nonoperating engine. This mode also occurs below idle, and acceptable bowed rotor start characteristics are achieved with the viscous film dampers on the bearing outer races.

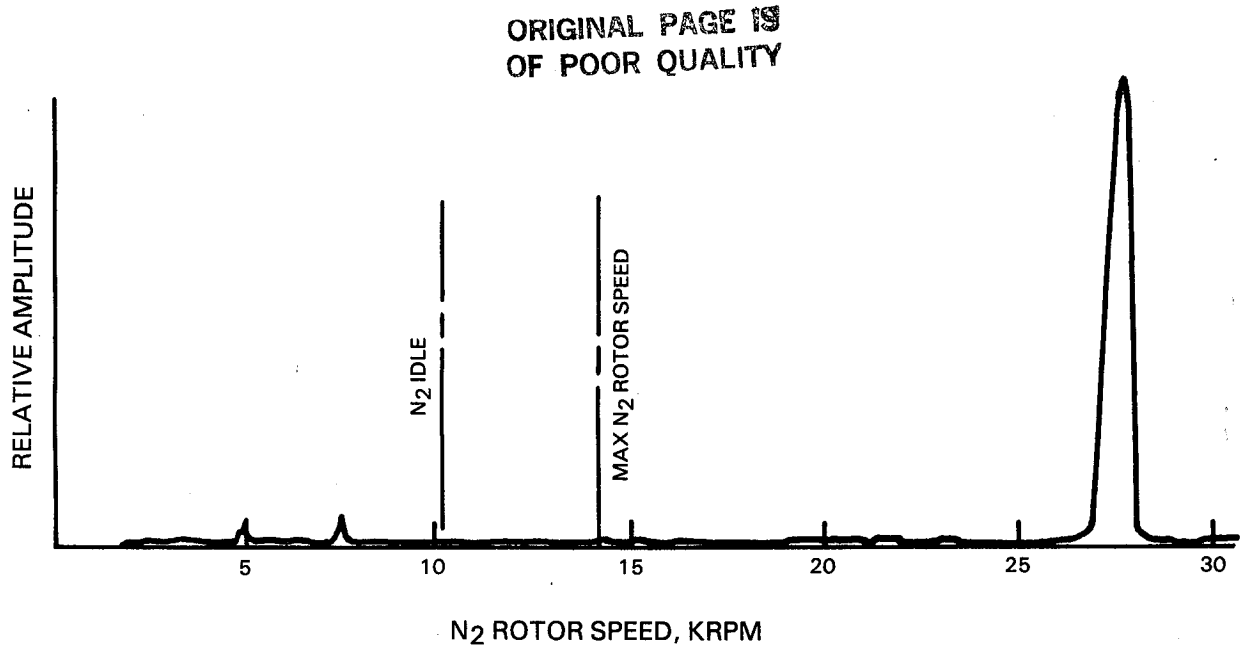

Figure 5.4.4-1 High-Pressure Rotor Critical Speed

The results of a critical speed analysis for the low-pressure rotor are presented in Figure 5.4.4-2. As shown, no high strain energy modes are anticipated in the operating speed range. The fan and low-pressure turbine modes have a low strain energy and occur below the minimum cruise speed. The high strain energy shaft bending mode occurs above the maximum rotor speed with acceptable margin.

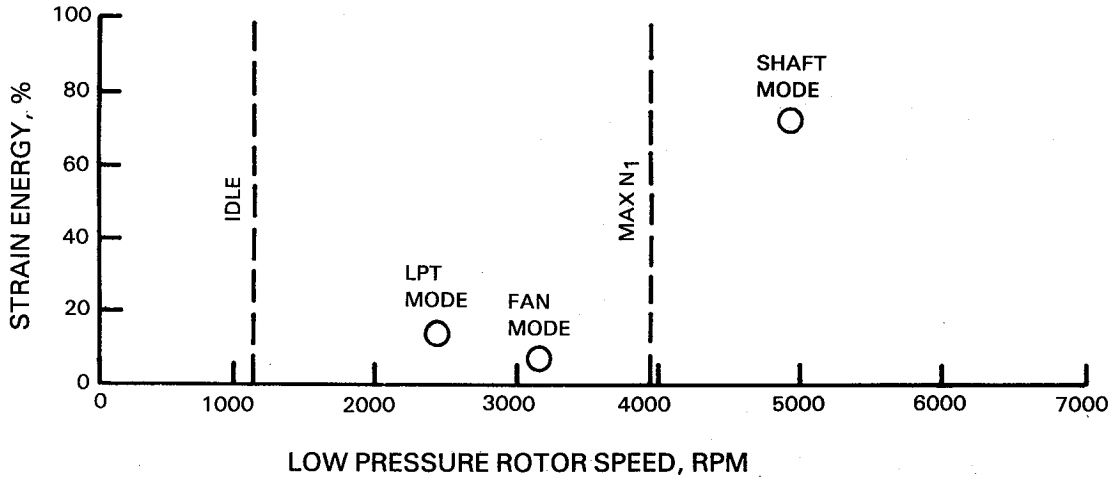

Figure 5.4.4-2 Low-Pressure Rotor Critical Speed Response

5.4.5 Differences Relative to the Flight Propulsion System

The flight propulsion system has the same rotor frame structure as the integrated core/low spool. A comparison of the mainshaft bearing sizes for the flight engine to the existing bearings used in the integrated core/low spool is presented in Table 5.4.5-I. With the exception of the No.1 bearing, where a significantly larger diameter is required in the flight propulsion system to meet commerical service life requirements, the sizes are quite similar. Table 5.4.5-II summarizes the types of bearing compartment and intershaft seals for both configurations. The seals for the integrated core/low spool closely duplicate those for the flight engine. They are derived from existing service-proven designs for minimum risk and lower cost. This is possible because the test operating environment of the integrated core/low spool is less severe than that of the flight propulsion system. Seals for the flight propulsion system will utilize a higher quality carbon for improved durability.

TABLE 5.4.5-I

MAINSHAFT BEARING SIZES

Bearing	Inner Diameter (mm)		Outer Diameter (mm)	
	Flight Propulsion System	Integrated Core/Low Spool	Flight Propulsion System	Integrated Core/Low Spool
1	269	210	385	350
2	130	130	190	180
3	160	165	250	255
4	160	165	250	222
5	160	165	230	222

TABLE 5.4.5-II

BEARING COMPARTMENT MAIN SHAFT SEAL COMPARISON

Seal Location	Flight Propulsion System	Integrated Core/Low Spool
No. 1 (Front)	Carbon	Carbon (Existing)
No. 3	6 KEL*	6 KEL* (Existing)
No. 4	Carbon	Carbon (Derived from Existing)
No. 5 (Rear)	Carbon	Carbon (Derived from Existing)
Front Intershaft	10 KEL*	10 KEL*
Rear Intershaft	2 Carbons	2 Carbons

*Knife Edge Labyrinth

5.5 GEARBOX AND ACCESSORY DRIVE SYSTEMS

5.5.1 General Description

The integrated core/low spool engine accessories and accessory gearbox are mounted on top of the outer fan case and are driven by a shaft geared to the high-pressure rotor. The gearbox configuration and mounting system are shown in Figure 5.5.1-1.

The accessory drive system components are shown in Figure 5.5.1-2 and include the towershaft, angle gearbox, and accessory gearbox. The mechanical design of these components is based on modifications to existing designs. An existing accessory gearbox is driven via the towershaft through an existing angle gearbox, a line shaft, and an adapter mounted on the accessory gearbox.

Accessory power is obtained from the front of the high-pressure rotor shaft by an integral bull gear, spiral bevel pinion shaft gear and towershaft. The towershaft consists of inner, mid and outer shaft portions. Bevel gear shaft support is provided by a roller bearing at the inboard portion and a ball bearing at the outer portion. An internal spline drives the inner shaft, which, in turn, is internally splined to the center shaft. The center shaft is positioned by two ball bearings that are preloaded by a spring. This assembly is mounted in the center case.

The towershaft gears and the shafts are made of wrought steel alloys. Bearings are constructed of M50 steel alloy. An external spline on the outer end of the center shaft drives the outer shaft. The outer shaft is positioned at the outer end by a roller bearing and shaft gear mounted in the external right angle gearbox.

Figure 5.5.1-3 presents a schematic of the lubrication system. The towershaft drive gear operates in an oil mist environment within the gear housing and is directly lubricated by an oil jet aimed between the teeth at the mesh. The No. 1 bearing is lubricated by a jet aimed at the inner diameter of the inner end of the lower shaft. Lubrication for the Nos. 2, 3 and 4 bearings is accomplished by external jets directed between the cage and the outer race. The No. 5 bearing is lubricated externally from the accessory gearbox. Splines are lubricated by an oil jet aimed up the inner portion of the towershaft.

5.5.2 Differences Relative to the Flight Propulsion System

The accessories for the flight propulsion system are core-mounted at the bottom of the engine and are described in Reference 11. Additional design studies will be necessary to determine the specific accessory drive system requirements for the flight engine application.

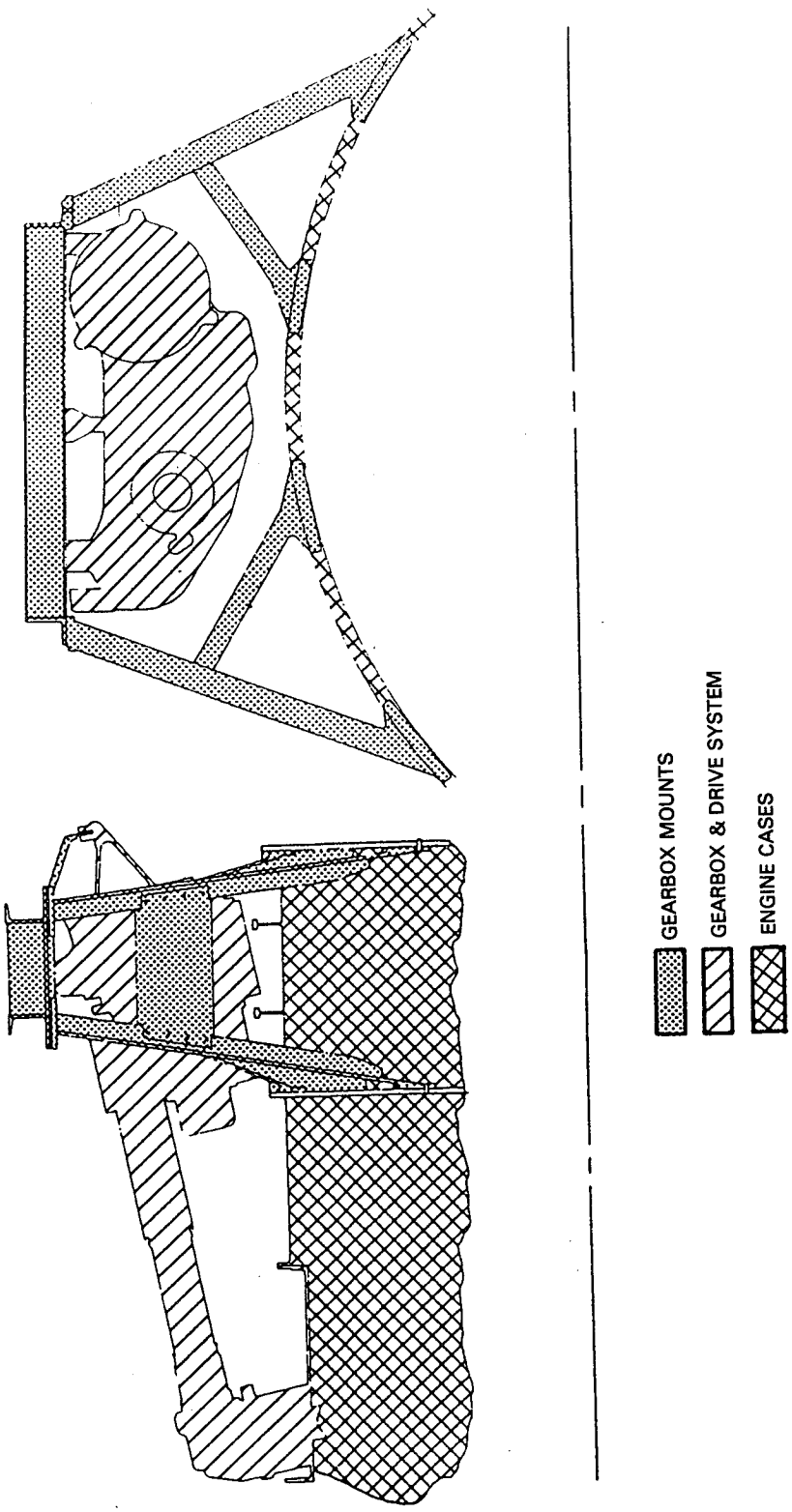

Figure 5.5.1-1 Integrated Core/Low Spool Gearbox Configuration and Mounting System

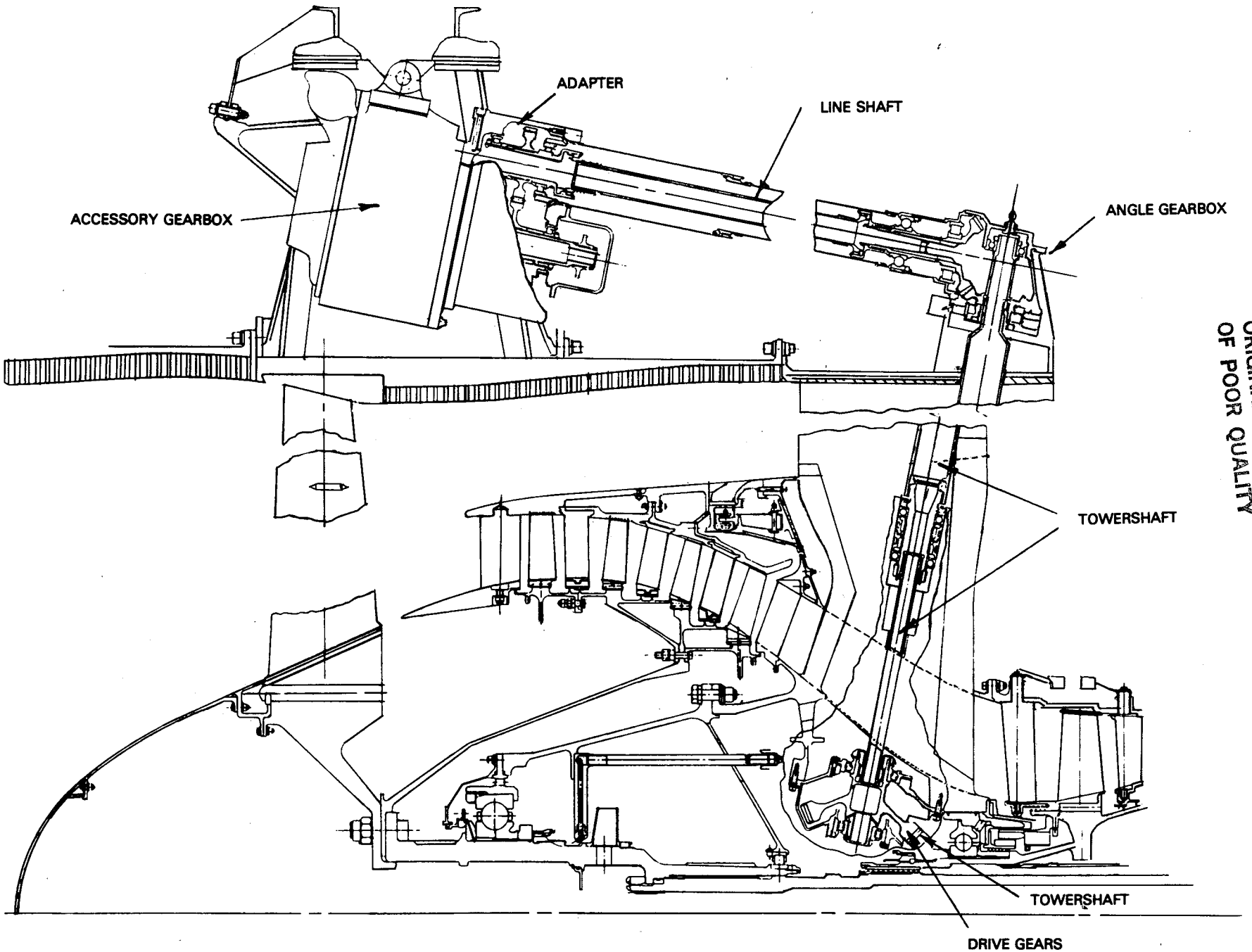

Figure 5.5.1-2 Integrated Core/Low Spool Accessory Gearbox and Drive System

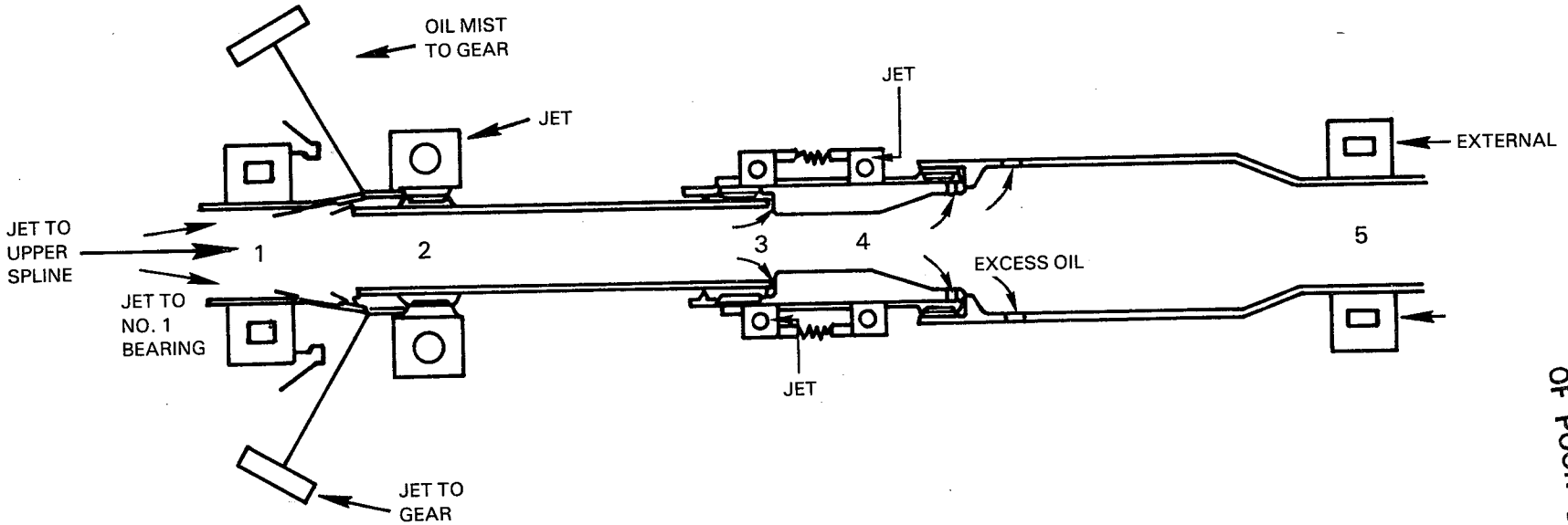

Figure 5.5.1-3 Accessory Drive System and Lubrication System Schematic

5.6 ACTIVE CLEARANCE CONTROL SYSTEM

5.6.1 General Description

Clearances between blade tips and outer air seals vary with operating conditions as a result of changes in temperature and speed. With active clearance control, tight clearances can be maintained by controlling the relative growth between the rotor and external case which supports the seals. This is accomplished by changing the thermal expansion rate of the case with controlled temperature air.

In both the integrated core/low spool and flight propulsion system, active clearance control is used in the high-pressure compressor, high-pressure turbine and low-pressure turbine. A plumbing diagram of the integrated core/low spool system is shown schematically in Figure 5.6.1-1. Also, the various components that comprise the system are identified in Figures 5.1-1 through 5.1-3. The method of operation and predicted operating clearances are summarized in the following sections.

5.6.2 Clearance Control

High-Pressure Compressor

Active clearance control is used in stages nine through fifteen of the high-pressure compressor. It is an external control system designed to achieve optimum clearances by case/rotor matching. For this application, an external as opposed to an internal system was selected because it eliminates a double wall case construction, has fewer leaks, can be tailored to varied stage-to-stage clearance requirements, and its characteristics are analytically more predictable.

The system consists of five 1.58-cm (0.625-in) diameter impingement tubes. For the initial test of the integrated core/low spool, which incorporates the bifurcated duct, facility air is used for active clearance control. However, fan discharge air is used for the second test.

Table 5.6.2-I lists the calculated blade tip clearance at the aerodynamic design point both with and without active clearance control.

High-Pressure Turbine

The blade tip sealing system in the high-pressure turbine requires an internal active clearance control design. High-pressure compressor bleed air, which totals 0.25 percent of the total core engine airflow, is introduced through eight bosses in the turbine case to regulate the radial movement of the blade tip seal shoe. At idle, fifteenth-stage bleed air heats up the rail of the outer air seal (refer to Figure 4.7.3-9), thereby moving the seal away from the blade tip in preparation for takeoff power. A mixture of tenth- and fifteenth-stage bleed air is used at takeoff and climb conditions to maintain desired clearances. At cruise, tenth-stage air closes the blade tip gap to the design clearance. The system for controlling the mixture of tenth- and fifteenth-stage bleed air for the integrated core/low spool turbine active clearance control is shown schematically in Figure 5.6.1-1.

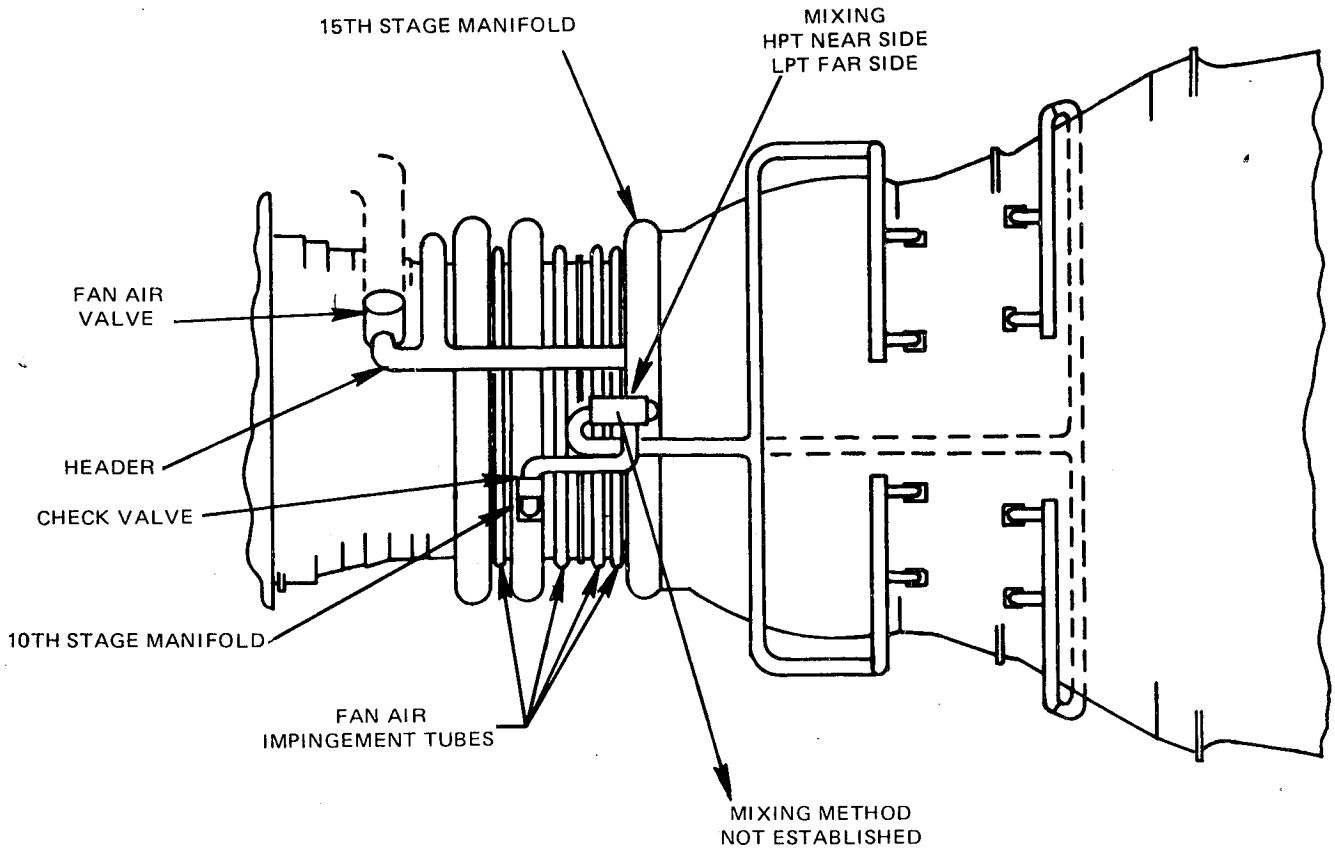

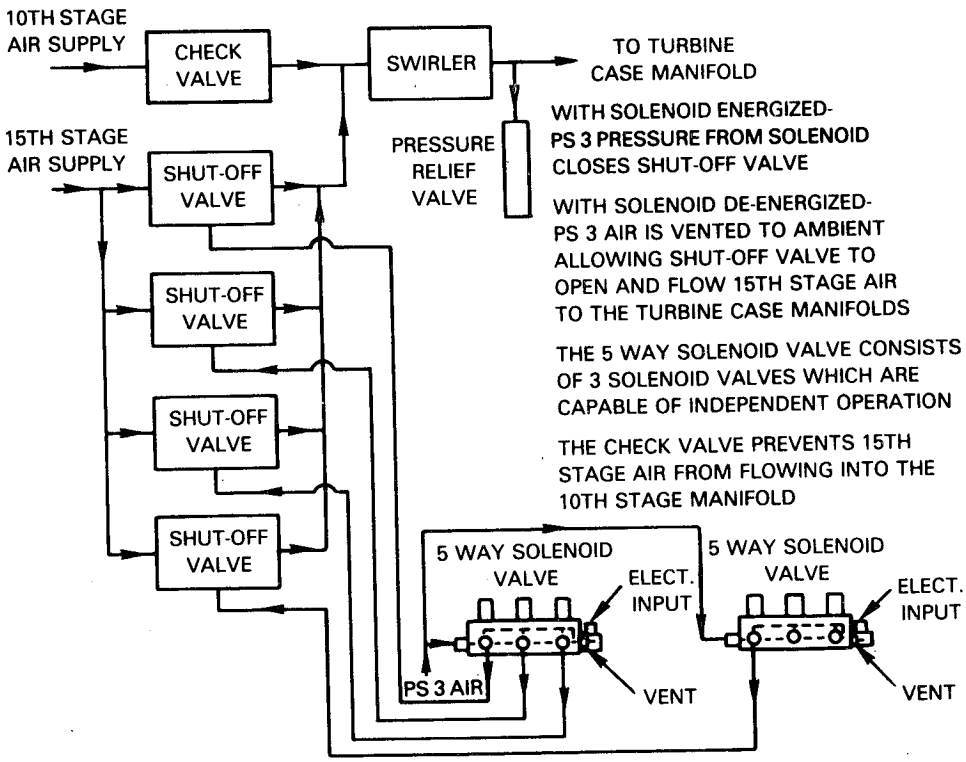

Figure 5.6.1-1 Integrated Core/Low Spool Active Clearance Control System

TABLE 5.6.2-I

HIGH-PRESSURE COMPRESSOR ROTOR TIP GAPS
(Aerodynamic Design Point)

Rotor	Component Cold gap, cm (in)	Component Without ACC, cm (in)	Component With ACC, cm (in)
6	0.078 (0.031)	0.035 (0.014)	0.035 (0.014)
7	0.086 (0.034)	0.040 (0.016)	0.040 (0.016)
8	0.109 (0.043)	0.050 (0.020)	0.050 (0.020)
9	0.078 (0.031)	0.033 (0.013)	0.033 (0.013)
10	0.083 (0.033)	0.027 (0.011)	0.027 (0.011)
11	0.091 (0.036)	0.027 (0.011)	0.027 (0.011)
12	0.096 (0.038)	0.038 (0.015)	0.025 (0.010)
13	0.099 (0.039)	0.048 (0.019)	0.025 (0.010)
14	0.119 (0.047)	0.045 (0.018)	0.025 (0.010)
15	0.088 (0.035)	0.035 (0.014)	0.022 (0.009)
Avg	0.093 (0.037)	0.038 (0.015)	0.030 (0.012)

The rotor and seal response throughout the flight cycle is shown in Figure 5.6.2-1. The critical design point is the pinch point, which occurs approximately six seconds into a snap acceleration. A clearance of 0.034 cm (0.0134 in) is maintained throughout acceleration, resulting in clearances being greater than required during the start to idle segment and at the aerodynamic design point. Although the clearances are larger, they are still significantly smaller than the design goal.

The philosophy used in determining turbine blade tip clearances is that no rubs occur in normal service when considering the following factors: thermal and centrifugal gradients; tolerances, eccentricities and rotor whirl; and maneuver and cowl loads. The final blade tip clearances are listed in Table 5.6.2-II. As indicated, the predicted clearance at the aerodynamic design point is tighter, thus resulting in an improvement in turbine efficiency.

TABLE 5.6.2-II

HIGH-PRESSURE TURBINE BLADE TIP CLEARANCE RESULTS

	Clearance, cm (in)	
	Goal	Status
Cold		0.1740 (0.0685)
Idle		0.1245 (0.0490)
Sea Level Takeoff	0.0685 (0.0270)	0.0340 (0.0134)
Aerodynamic Design Point	0.0472 (0.0186)	0.0320 (0.0126)

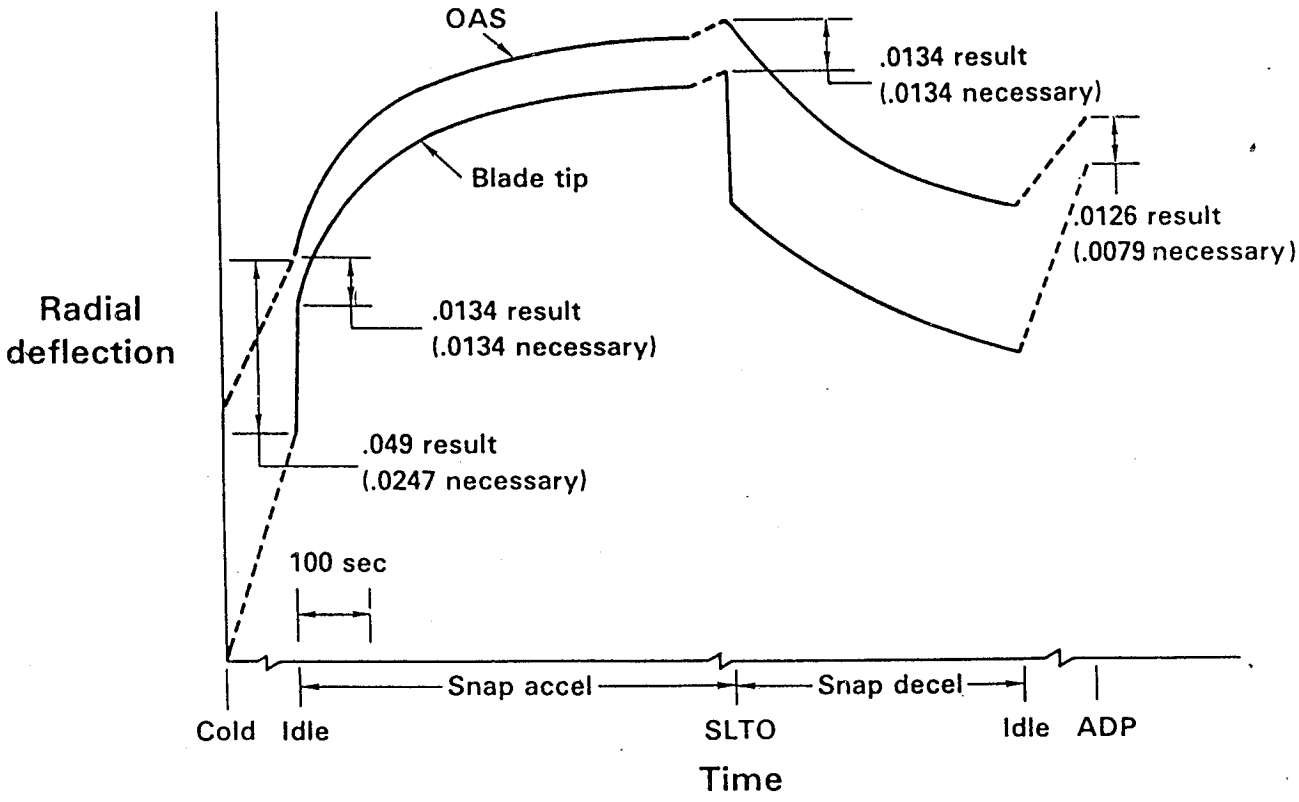

Figure 5.6.2-1 High-Pressure Turbine Blade Tip Clearances

Low-Pressure Turbine

Like the high-pressure turbine, an internal active clearance control system is used in the low-pressure turbine. Similarly, blade tip gaps are regulated with tenth- and fifteenth-stage compressor bleed air amounting to 1.0 percent of the core engine airflow. The system is inoperative at both idle and deceleration. At cruise, only tenth-stage air is used. A mixture of tenth- and fifteenth-stage air is used for sea level takeoff and acceleration.

In establishing the blade tip gapping, a no-rub philosophy was retained and the goal clearance of 0.050 cm (0.020 in) was defined at the aerodynamic design point. A series of analyses was conducted to determine the relative growth between the case and rotor as a result of centrifugal forces, thermals and pressures. Results showed the pinch point occurring at idle to takeoff power during a snap acceleration. Clearance deviations associated with maneuver loads, rotor whirl, ovalization, tolerances, and eccentricities were assumed to occur at the pinch point to ensure a no-rub condition. Combining the effects of these deviations with clearances determined from the rotor and case growth analyses resulted in gaps substantially larger than the goal. Although thermal matching with the active clearance control system produced excellent clearances at the aerodynamic design point and sea level takeoff, these benefits were negated by large maneuver deflections.

To achieve clearances closer to the aerodynamic design point, a requirement was added that the blade tip knife edges be machined at assembly to a tolerance of ± 0.005 cm (±0.002 in) on the diameter. Tolerances that cause deviation from the nominal would be allowed to rub in at the pinch point and, in effect, custom machine the blade tips and seals to a line-on-line setting. The resulting blade tip and interstage seal clearances are listed in Tables 5.6.2-III and -IV, respectively.

TABLE 5.6.2-III

ENERGY EFFICIENT ENGINE LOW-PRESSURE TURBINE
BLADE TIP CLEARANCE SUMMARY
(Clearances are in cm (in))

TENTH-STAGE ACTIVE CLEARANCE CONTROL SYSTEM AIR

Gap Component	Rotor 2	Rotor 3	Rotor 4	Rotor 5
Concentricity (1/2 Max.)	0.015 (0.006)	0.015 (0.006)	0.017 (0.007)	0.017 (0.007)
Maneuvers	0.020 (0.008)	0.027 (0.011)	0.048 (0.019)	0.071 (0.028)
Whirl	0.010 (0.004)	0.012 (0.005)	0.015 (0.006)	0.015 (0.006)
Bearing Clearance	0.005 (0.002)	0.007 (0.003)	0.007 (0.003)	0.007 (0.003)
Ovalization & Cowl Loads	0.005 (0.002)	0.005 (0.002)	0.005 (0.002)	0.005 (0.002)
Total Mechanical	0.055 (0.022)	0.068 (0.027)	0.093 (0.037)	0.116 (0.046)
Speed & Thermals @ ADP	0.010 (0.004)	0.020 (0.008)	0.020 (0.008)	0.027 (0.011)
Speed & Thermals @ SLTO	0	0	0	0.033 (0.013)
ADP Clearance	0.066 (0.026)	0.088 (0.035)	0.114 (0.045)	0.144 (0.057)
SLTO Clearance	0.055 (0.022)	0.068 (0.027)	0.093 (0.037)	0.149 (0.059)

TABLE 5.6.2-IV

ENERGY EFFICIENT ENGINE LOW-PRESSURE TURBINE
INTERSTAGE SEAL CLEARANCE SUMMARY
(Clearances, cm (in))

TENTH-STAGE ACTIVE CLEARANCE CONTROL SYSTEM AIR

Gap Component	Rotor 2-3 Middle Tooth	Rotor 3-4 Middle Tooth	Rotor 4-5 Front Tooth	Outer Thrust Balance	Inner Thrust Balance
Concentricity (1/2 Max.)	0.012 (0.005)	0.012 (0.005)	0.012 (0.005)	0.012 (0.005)	0.012 (0.005
Maneuvers	0.022 (0.009)	0.038 (0.015)	0.058 (0.023)	0.022 (0.009)	0.022 (0.009
Whirl	0.012 (0.005)	0.012 (0.005)	0.015 (0.006)	0.010 (0.004)	0.010 (0.004
Bearing Clearance	0.007 (0.003)	0.007 (0.003)	0.007 (0.003)	0.005 (0.002)	0.005 (0.002
Ovalization & Cowl Loads	0.005 (0.002)	0.005 (0.002)	0.005 (0.002)	0.005 (0.002)	0.005 (0.002
Total Mechanical	0.060 (0.024)	0.076 (0.030)	0.099 (0.039)	0.055 (0.022)	0.055 (0.022
Speed & Thermals @ ADP	0.045 (0.018)	0.040 (0.016)	0.038 (0.015)	0.007 (0.003)	0.002 (0.00
Speed & Thermals @ SLTO	0	0	0.025 (0.010)	0	0
ADP Clearance	0.106 (0.042)	0.116 (0.046)	0.137 (0.054)	0.063 (0.025)	0.058 (0.023
SLTO Clearance	0.060 (0.024)	0.076 (0.030)	0.124 (0.049)	0.055 (0.022)	0.055 (0.022

5.6.3 Differences Relative to the Flight Propulsion System

There is little difference in the aeromechanical design of the active clearance control system and operating clearances for the flight propulsion system. The only area of significance is in the low-pressure turbine.

In contrast to the integrated core/low spool, the flight engine uses eighth-stage instead of tenth-stage air. Eighth-stage air increases the case closure capability and offers a 0.19 percent efficiency improvement, plus a 0.28 percent advantage in thrust specific fuel consumption. The use of a tenth-stage bleed arrangement in the integrated core/low spool avoids added design and hardware costs.

Also, there are certain related minor design changes. For the flight engine, cooling holes are not drilled in the second-stage vane support hook area or the third-stage vane front support hook, and the cooling passages in these areas are filled with insulation.

5.7 SECONDARY FLOW SYSTEM

5.7.1 General Description

The secondary flow system accomplishes several major functions. It provides the source of air for component cooling, the bearing compartment breather and buffer system , the active clearance control system, rotor thrust balance, and engine/aircraft service bleeds.

The secondary flow system in the integrated core/low spool has several design features, with each exerting partial control over the major coolant sources by setting the operating pressure, flow rate, and/or temperature. These features, as discussed in the following section, are designed to maximize the use of coolant to the hot section components and minimize parasitic gaspath leakage.

5.7.2 Major Design Features

High-Pressure Turbine

The main features of the secondary flow system in the high-pressure turbine are shown in Figure 5.7.2-1. These include a blade coolant supply tangential on-board injection (TOBI) system, a front rim cavity mini tangential on-board injection system, boltless rotor sideplates, and the high-pressure compressor discharge seal. The benefits derived from these features, in conjunction with improved sealing concepts, result in the utilization of only 14.56 percent of the core engine inlet airflow for cooling the disks, blades, vanes, and case.

Tangential On-Board Injection Nozzles -- As discussed earlier in Section 4.6, the high-pressure turbine is designed with both a main and a mini tangential on-board injection system. The main or blade injection nozzle is a high efficiency cascade design. It receives air for blade cooling from the high-pressure compressor inner bleed located forward of the compressor exit vane. This system is pressure balanced to negate the requirement for inner and outer seals. Also, only a small percentage of air (0.1 percent of the total engine inlet flow) is required around the nozzle flow guides at the discharge plane. Since the system is balanced to accommodate the gaspath inner wall pressure, cooling flow is insensitive to rim seal clearance.

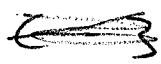

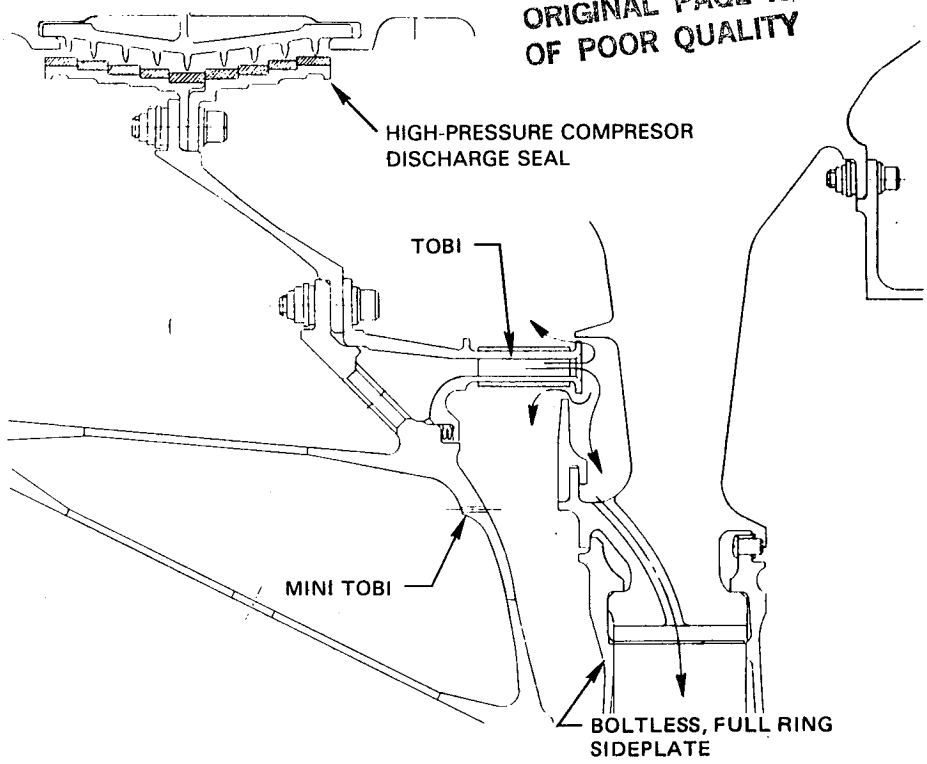

Figure 5.7.2-1 High-Pressure Turbine Secondary Flow System Design Features

The mini tangential on-board injection nozzle preswirls the flow to the front rim cavity to reduce the windage heat up on the front sideplate. This swirl flow field also provides a radial pressure gradient between the main tangential on-board injection nozzle and gas path static pressure. This keeps the ratio of blade supply pressure to gas path inner wall pressure at a fixed level and independent of seal leakage, attachment leakage and blade flow area.

Rotor Sideplates -- The full ring and boltless sideplate configuration considerably reduces leakage and pressure loss in comparison to a conventional segmented design. A diagram of the blade coolant supply system is presented in Figure 5.7.2-2, showing pressure and flow characteristics. The design blade cooling flow is 2.75 percent of the core engine air flow and is supplied to the blade at an inlet pressure of approximately 53 percent of the total pressure at the high-pressure compressor exit. The tangential on-board injection dump pressure of 43.1 percent is increased to 48.2 percent by the free vortex pressure recovery, and up to 53.2 percent by solid body rotation in the disk feed passages.

Compressor Discharge Seal -- The compressor discharge seal is a multi knife edge labyrinth design with an abradable seal land. This seal is designed to operate at a clearance of 0.031 cm (0.0125 in). The calculated leakage rate is 0.4 percent of the total core engine flow.

Seals -- Both "W" seals and feather seals are used extensively in the high-pressure turbine. The "W" seals are used at the interface of the rear plate and blade platform (Figure 5.7.2-2) and at the interface of the vane and inner support. Feather seals are used at various locations in both the inner and outer vane platform to prevent leakage of compressor discharge air into the turbine gaspath. The effectiveness of these sealing techniques was verified under the supporting Leakage Technology Program (Ref. 12).

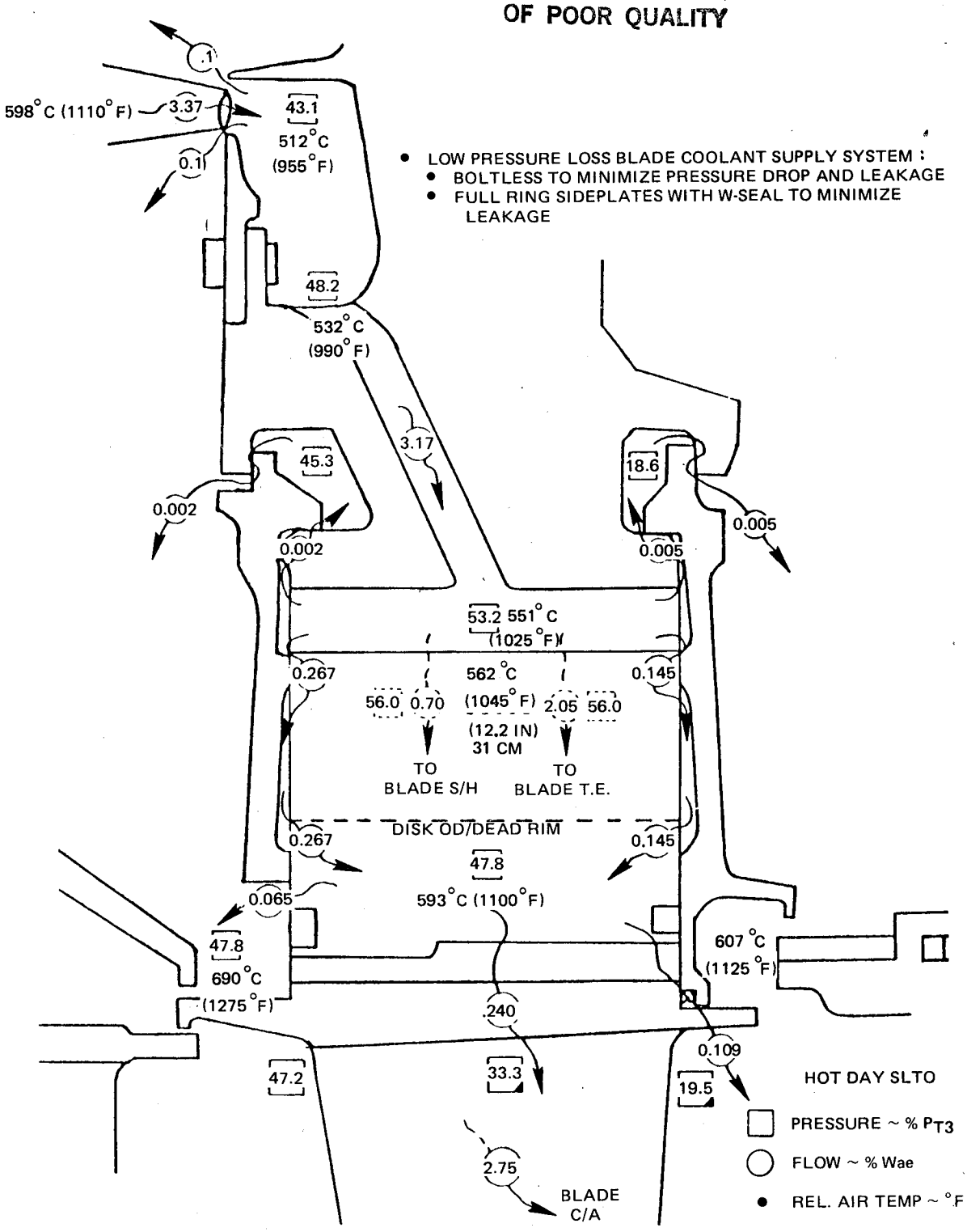

Figure 5.7.2-2 Flow Characteristics of Blade Coolant Supply System

Also, rim seals are positioned at the leading and trailing edge of the blade platform to isolate the gas path from the disk cavity.

A seal at the rear of the high-pressure turbine (refer to Figure 4.7.1-1) is used to provide thrust balance. The net thrust of the high-pressure rotor is calculated at 22,241 N (5000 lb) at sea level takeoff. A buffer seal is located in the proximity of the rear seal and is used to separate cool low-pressure compressor discharge air from the high-pressure turbine bore cooling air for the rear bearing compartment.

Low-Pressure Turbine

The design features in the low-pressure turbine secondary flow system include a pressure-balanced cooling air distribution system, uniform cooling flow to the disk rims, rim shields to thermally isolate disk-blade attachments from the rim cavities, and a combined cooling air and active clearance control system approach to minimize total flow requirements. The low-pressure turbine uses 2.48 percent of the total core engine airflow for cooling and active clearance control

Pressure-Balanced System -- The rotor cooling air distribution system is pressure balanced and independent of rim seal clearances. The main elements of the system are indicated in Figure 5.7.2-3. Holes at the rear of the turbine intermediate case strut meter 0.99 percent of the core engine airflow into a cavity that is defined by the strut, rear thrust balance seal and second-stage disk rim. A portion of this flow (0.46 percent) leaks past the thrust balance seal and is used to cool the turbine bore. 0.33 percent of the remaining air passes through holes in the disk rim shield and serves to cool the blade attachment before being used in the disk rim cavity, where it reduces the temperature in the cavity to less than 732°C (1350°F).

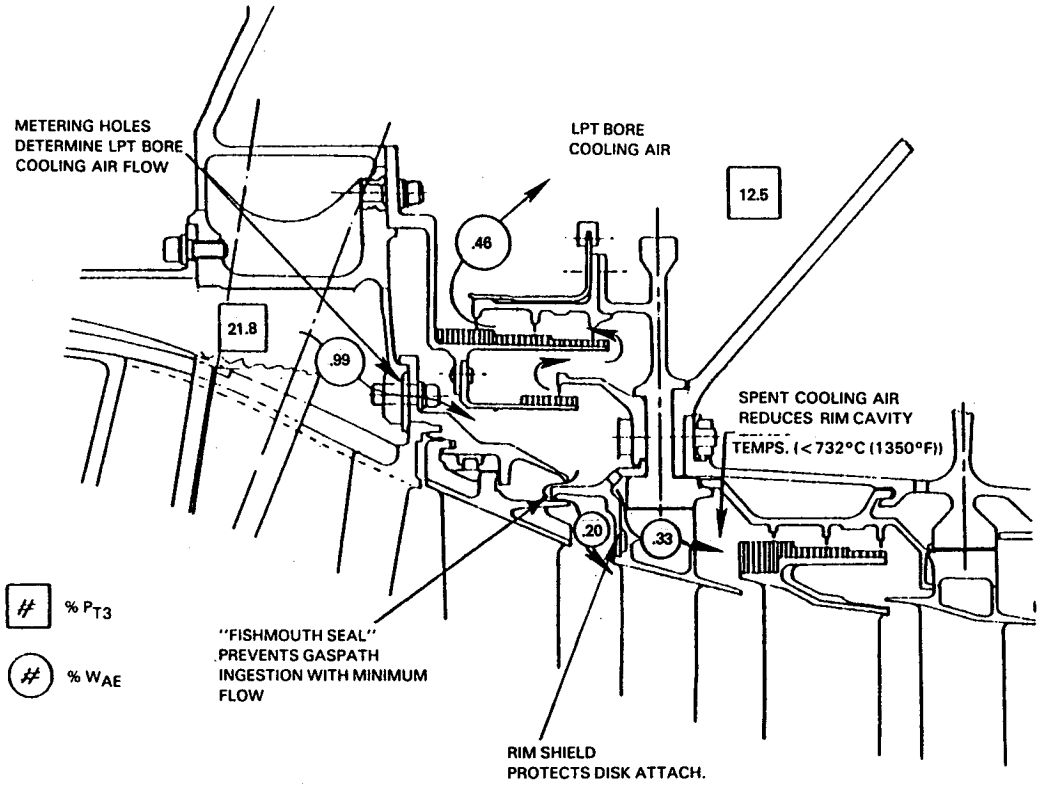

Figure 5.7.2-3 Pressure-Balanced Cooling Air Distribution System

Rotor Cooling Distribution -- The method of distributing secondary cooling air provides uniform flow to the disk rims. A portion of the turbine bore cooling airflow is introduced at the base of the A-frame, as illustrated in Figure 5.7.2-4, and is metered to the third- and fourth-stage disk rims to cool the attachment areas. As the air flows towards the metering holes, a free-vortex flow is established and maintains a positive pressure gradient across the metering holes. The split between the metered flows reflects the temperature exposure of the third- and fourth-stage turbine disks. The used attachment cooling air is exhausted into the downstream rim cavities to reduce the cavity temperatures.

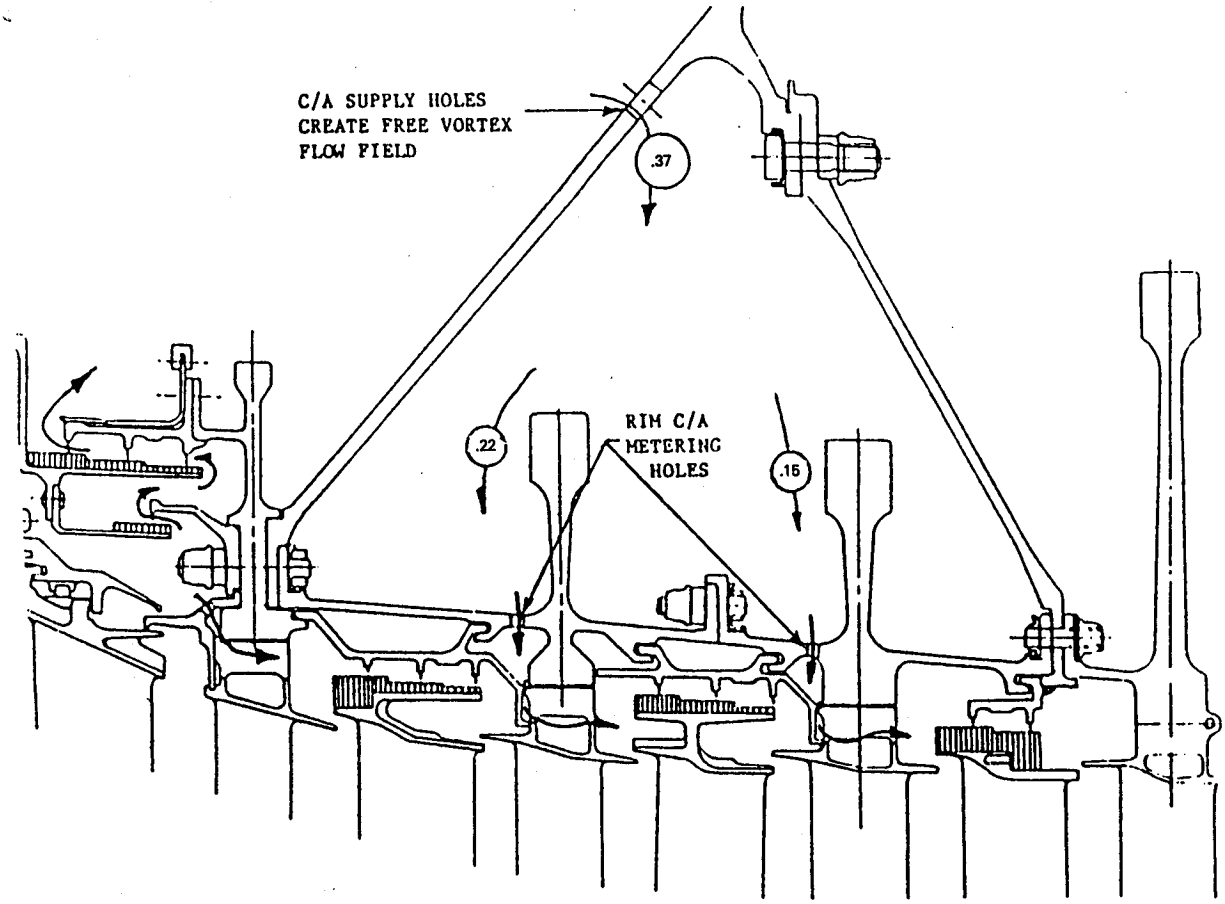

Figure 5.7.2-4 A-Frame Rotor Construction Showing Turbine Rim Cooling Air Flow Distribution

Rim Shields -- Rim shields protect the disk rim from gaspath temperatures. As shown in Figure 5.7.2-3, the rim shield forms a modified "fishmouth" seal to prevent the ingestion of gas flow into the inner cavity. A small amount of flow (0.20 percent of the core engine airflow) is permitted to leak past the seal to maintain the desired pressure differential between the gaspath and inner cavity.

Case Cooling Distribution -- The primary function of the case cooling distribution system is to provide case temperature modulation for blade tip active clearance control. Clearance adjustments are accomplished by controlling the temperatures of the inner case hooks. A double wall case construction facilitates this in as much as the outer case functions as a cooling air manifold from which air is extracted to cool the individual hooks. Figure 5.7.2-5 shows the low-pressure turbine case design as well as the secondary cooling flow rates and key pressure levels.

High-pressure compressor bleed air enters the case manifold and is channeled through a passage created by the inner case and the segmented baffle. This air has a dual function. First, it serves to cool the inner case structure. Second, the air is channeled through metering holes to cool the hooks. With this technique, the cooling airflow distribution becomes independent of part-to-part tolerances.

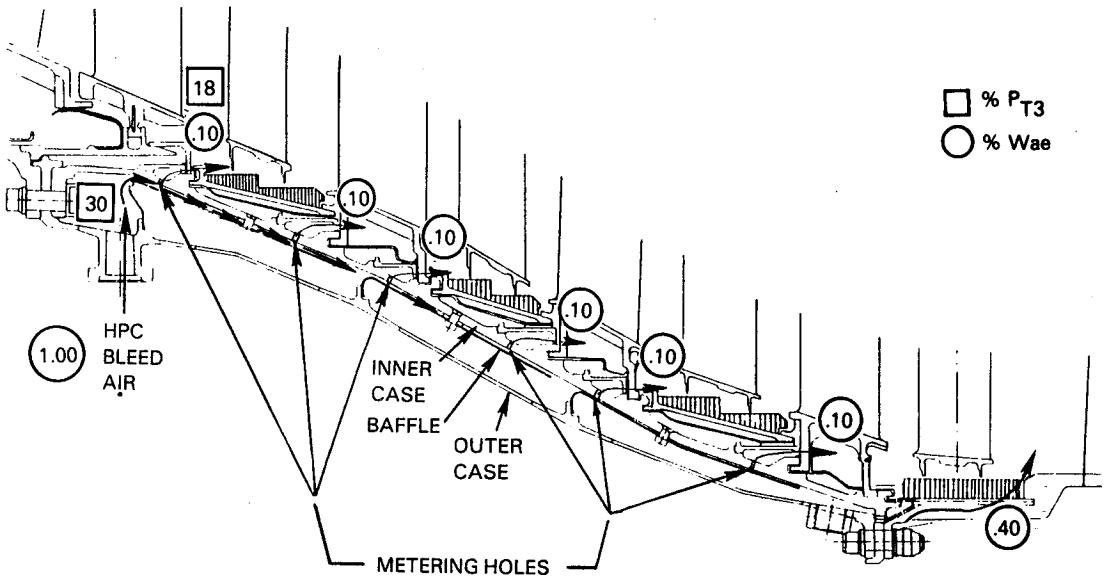

Figure 5.7.2-5 Low-Pressure Turbine Case Cooling Flow Distribution System

5.7.3 Predicted Performance

A detailed map of the integrated core/low spool secondary flow system is shown in Figure 5.7.3-1. This map identifies the predicted flow rates, leakage rates, and static pressures throughout the engine at sea level takeoff conditions. As indicated by the flow summary in Table 5.7.3-I, 17.988 percent of the total core engine airflow is used for cooling.

5.7.4 Differences Relative to the Flight Propulsion System

The secondary flow system in the flight propulsion system retains all of the design features in the integrated core/low spool. However, the flight engine requires 0.67 percent less airflow. This is attributed to the differences in the bleed source for the low-pressure turbine active clearance control system as well as lower leakage rates for the high-pressure turbine vane, outer airseal and intermediate case strut from improved feather seal technology.

ORIGINAL PAGE IS
OF POOR QUALITY

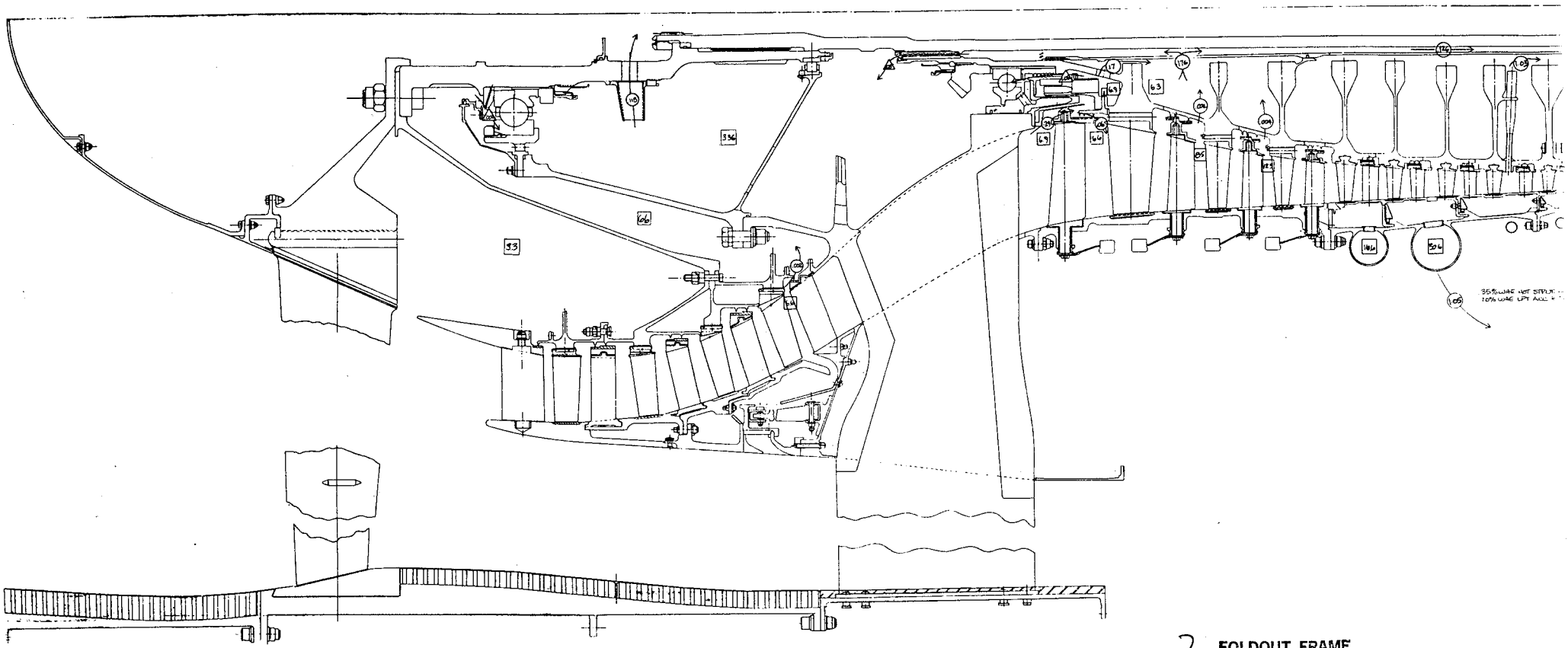

FOLDOUT FRAME

2 FOLDOUT FRAME

ORIGINAL PAGE IS
OF POOR QUALITY

ORIGINAL PAGE IS
OF POOR QUALITY

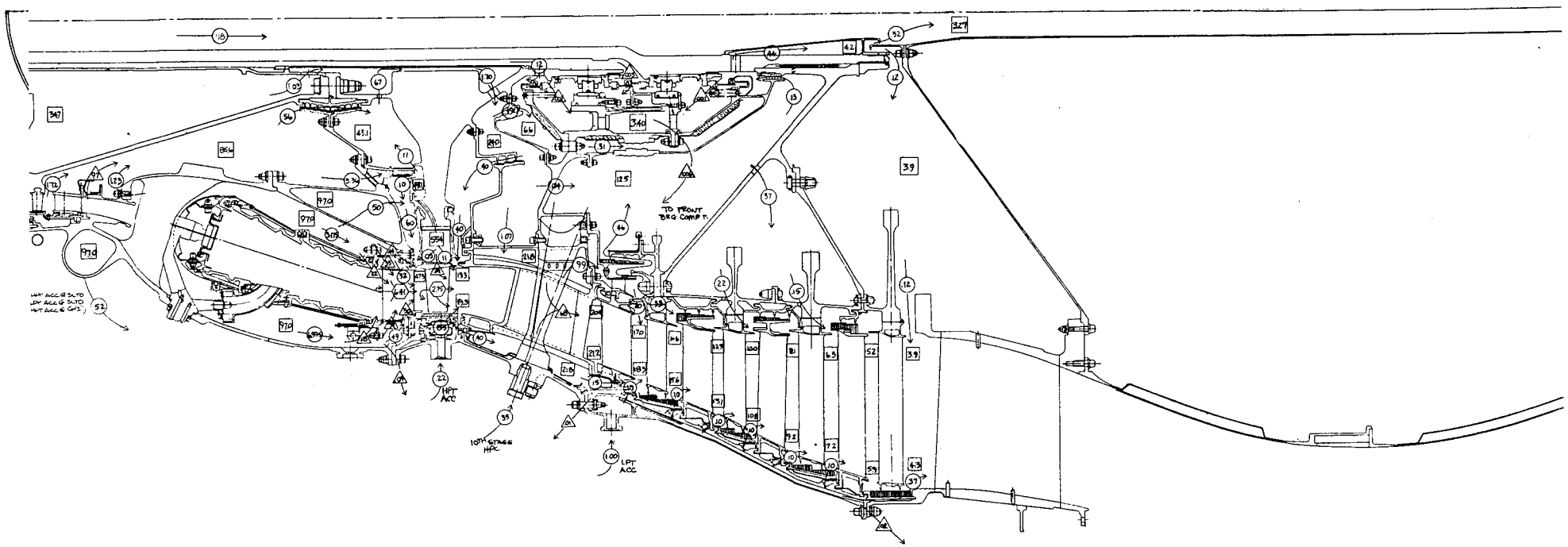

3 FOLDOUT FRAME

4 FOLDOUT FRAME

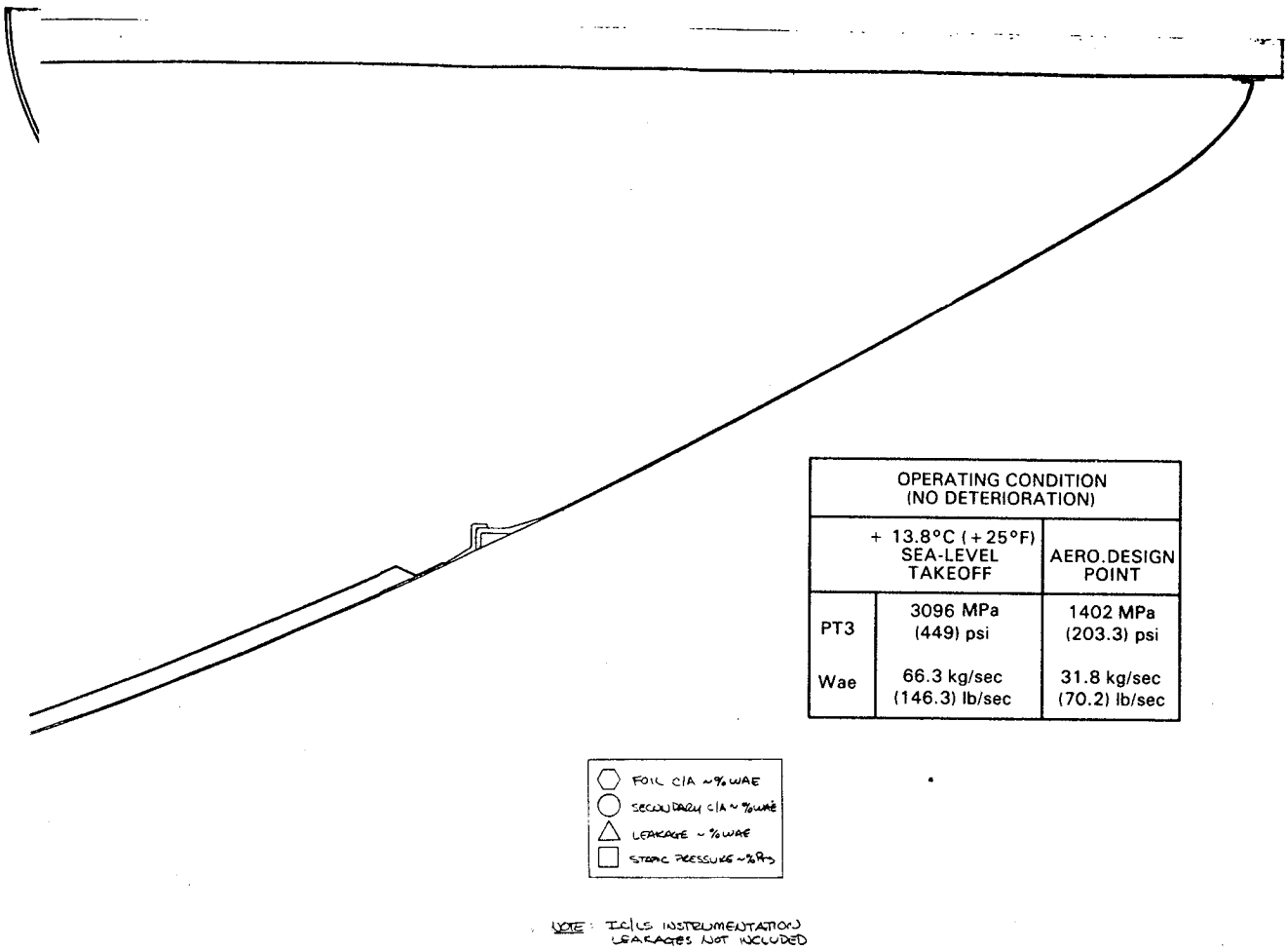

OPERATING CONDITION (NO DETERIORATION)		
	+ 13.8°C (+25°F) SEA-LEVEL TAKEOFF	AERO.DESIGN POINT
PT3	3096 MPa (449) psi	1402 MPa (203.3) psi
Wae	66.3 kg/sec (146.3) lb/sec	31.8 kg/sec (70.2) lb/sec

Figure 5.7.3-1 Integrated Core/Low Spool Secondary Flow System Map At Sea Level Takeoff Conditions

FOLDOUT FRAME

TABLE 5.7.3-I

FLOW SUMMARY
SECONDARY AIRFLOW SOURCES

Low-Pressure Compressor Discharge Inner Diameter	0.292
Seventh-Stage Compressor Front Inner Diameter	0.002
Eighth-Stage Compressor Front Inner Diameter	0.004
Tenth-Stage Compressor Rear Outer Diameter	1.050
Twelfth-Stage Compressor Rear Inner Diameter	1.030
Fifteenth-Stage Compressor Rear Inner Diameter	3.920
Fifteenth-Stage Compressor Rear Outer Diameter	0.520
Combustor Secondary Inner Annulus	3.675
Combustor Secondary Outer Annulus	6.995
	17.488 Percent of Total Core Engine Flow
Fan Discharge Outer Diameter	0.500
Total Cooling Air	17.988 Percent of Total Core Engine Flow

SECTION 6.0
ENGINE TEST INSTRUMENTATION

6.1 INTRODUCTION

The design of the integrated core/low spool included a definition of the test instrumentation to meet the requirements of the planned test program. For a characterization of aerothermal and structural performance, the integrated core/low spool is instrumented with almost 1500 sensors. An instrumentation summary is presented in Table 6.1-I. The type, quantity and placement of this instrumentation is based on analyses, data acquired from supporting technology programs and Pratt & Whitney Aircraft engine development experience. Also, all probes are designed in compliance with Pratt & Whitney Aircraft standards for experimental test instrumentation. A description of the different types of engine instrumentation is presented in the following paragraphs.

6.2. COMPONENT INSTRUMENTATION DESCRIPTION

A detailed instrumentation map of the integrated core/low spool is shown in Figure 6.2-1, identifying the location and type of sensors. Instrumentation wiring from rotating components in the low-pressure spool is routed to a conventional slip ring. The rotor slip ring arrangement is illustrated in Figure 6.2-2 and it accommodates a total of 60 sensors.

Signals from rotating components in the high-pressure spool are transmitted to the static structure by telemetry transmitters. The telemetry package contains 31 transmitters to meet the strain gage and thermocouple requirements for the high-pressure compressor, turbine, and bearings. The transmitters are located near the No. 3 bearing, as shown in Figure 6.2-3. Provisions have been made to supply cooling air in order to maintain a proper operating environment for the transmitters.

6.2.1 Fan

Seven rakes, each containing eight radial sensing elements, are installed at the fan inlet to monitor boundary layer conditions. Seven total/static pressure combination rakes are used to establish the velocity into the fan. During engine operation, four radial locations will be sampled to calibrate the inlet. Also, seven static pressure taps are installed on the outer flowpath wall in the same axial plane as the boundary layer and combination rakes. Three fast-response thermocouples are installed in front of the fan blade to sense a temperature rise associated with an incipient stall condition.

Selected fan blades are instrumented with strain gages at the root, midspan section and tip to monitor vibratory stress. Blade tip clearances are measured by three laser proximity probes equally spaced on the fan containment case. The components of the laser proximity instrumentation are shown in Figure 6.2.1-1.

TABLE 6.1-I

ENERGY EFFICIENT ENGINE INTEGRATED CORE/LOW SPOOL
INSTRUMENTATION REQUIREMENTS

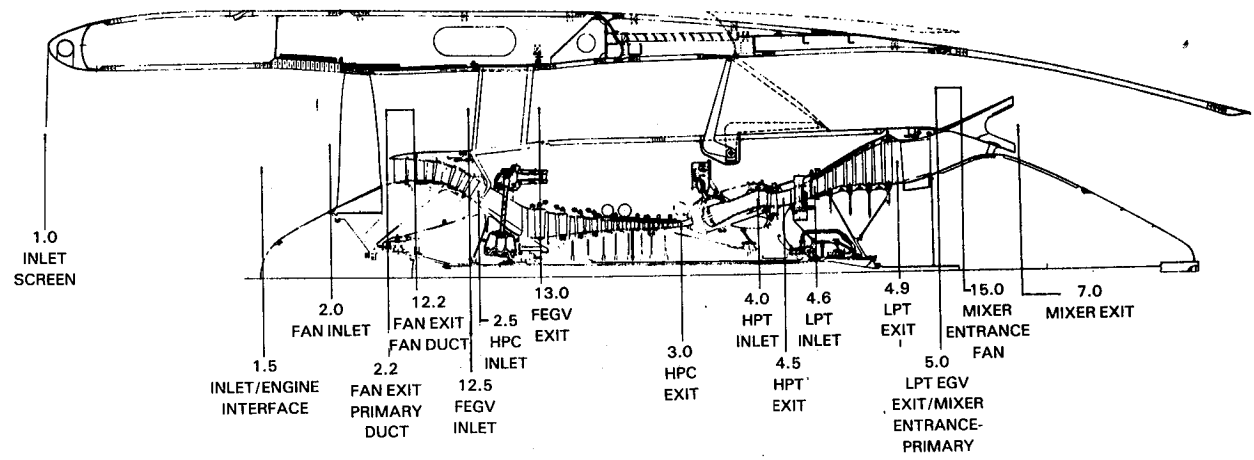

		No. Probes	No. Sensors	Total Sensors	Test* 2
Station 1.0					
Inlet T/C		8	1	8	8
Station 2.0					
Boundary Layer		7	8	56	7
Pitot Static (P)		7	1	7	3
Pitot Static (S)		7	1	7	3
P_T/T_T Fuel Control		2	2	4	
Quick Response T/C		3	2	3	
OD Wall	Static	7	1	7	
Station 2.2					
Pressure		8	1	8	3
High Response	Static	3	1	3	
Temperature		8	1	8	3
Station 2.5					
Pressure Probe		4	10	40	2
Temperature Probe		4	10	40	2
High Response		2	1	2	
ID Wall	Static	4	1	4	
OD Wall	Static	4	1	4	
Station 3.0					
Pressure Probe		6	5	30	2
Temperature Probe		6	5	30	2
ID Wall	Static	4	1	4	
OD Wall	Static	4	1	4	
Diff Bleed Duct	Static	2	1	2	
Diff Bleed Duct	Temp	2	1	2	
Sub Total				273	

*Stream probes retained for mixed flow configuration

TABLE 6.1-I (Cont'd)

ENERGY EFFICIENT ENGINE INTEGRATED CORE/LOW SPOOL
INSTRUMENTATION REQUIREMENTS

		No. Probes	No. Sensors	Total Sensors	Test* 2
Station 4.0					
ID Wall Turb IGV LE	Static	3	1	3	
OD Wall Turb IGV LE	Static	3	1	3	
OD Wall Turb IGV TE	Static	3	1	3	
Station 4.5					
Pressure Probe		8	6	48	3
Temperature Strut LE		6	4	24	
Pyrometer R_1		1	1	1	
Proximity Probe R_1		4	1	4	
ID Wall in Plane of Press Probe	Static	3	1	3	
OD Wall in Plane of Press Probe	Static	3	1	3	
ID Wall Transition Duct	Static	3	1	3	
OD Wall Outer Air Seal SEGM.	Static	3	1	3	
ID Wall Strut Gap	Static	8	3	24	
OD Wall Strut Gap	Static	8	3	24	
Strut Suction Side Root	Static	10	1	30	Suct.
Strut Suction Side Mean	Static	10	1	30	Suct.
Strut Suction Side Tip	Static	10	1	30	Suct.
Strut Pressure Side Root	Static	10	1	30	Press
Strut Pressure Side Mean	Static	10	1	30	Press
Strut Pressure Side Tip	Static	10	1	30	Press
Strut Metal T/C		4	1	4	
Strut Strain Gage		3	1 X	3	
ID Wall Strut TE	Static	3 X	1	3	
OD Wall Strut TE	Static	3 X	1	3	
HPT Case Metal T/C		3 X	1	3	
Strut FWD Compt.	Static	2	1 X	2	
Strut FWD Compt.	Temp	2	1 X	2	
Strut Inner Compt.	Temp	2	1 X	2	
Strut Outer Compt.	Static	2	1 X	2	
Strut Outer Compt.	Temp	2	1 X	2	
Strut Airfoil Metal T/C		4	2	8	
Sub Total				240	

*Stream probes retained for mixed flow configuration

TABLE 6.1-I (Cont'd)

ENERGY EFFICIENT ENGINE INTEGRATED CORE/LOW SPOOL
INSTRUMENTATION REQUIREMENTS

		No. Probes	No. Sensors	Total Sensors	Test* 2
Station 4.9					
Pressure Probe		8	10	80	3
Temperature Probe		8	6	48	3
Air Angle		4	3	12	-
ID Wall	Static	3	1	3	
OD Wall	Static	3	1	3	
Station 5.0					
Wake Traversing		1	17	17	-
Air Angle		4	3	16	-
ID Wall	Static	3	1	3	
OD Wall	Static	3	1	3	
Mixer Strain Gage (Dynamic)		5	1	5	
Station 12.0					
R_1 Proximity Probe		3	1	3	
R_1 Strain Gage- Root		8	1	8	
R_1 Strain Gage- Tip		4	1	4	
R_1 Strain Gage- Shroud (6 Dynamic 2 Static)		8	1	8	
Fan Rotating				20 S/G	
Station 12.2					
Pressure Probe Combination		7	10	70	3
Temperature Probe		7	10	70	3
ID Wall	Static	16	1	16	
OD Wall	Static	16	1	16	
Sub Total				381	

*Stream probes retained for mixed flow configuration

TABLE 6.1-I (Cont'd)

ENERGY EFFICIENT ENGINE INTEGRATED CORE/LOW SPOOL INSTRUMENTATION REQUIREMENTS

		No. Probes	No. Sensors	Total Sensors	Test* 2
Station 13.0					
Pressure Probe		4	8	32	1
FEGV Strain Gage (S/G)	Static	2	1	2	
Fan Exit Case S/G	Static	5	1	5	
Station 15.0					
Pressure Probe		8	10	80	8
LPC					
R4 Inner Cavity	Static	2	1	2	
R4 Inner Cavity	Temp	2	1	2	
R2 Strain Gage-Foil	(Dynamic)	4	1	4	
R3 Strain Gage-Foil	(Dynamic)	4	1	4	
R4 Strain Gage-Foil	(Dynamic)	4	1	4	
R5 Strain Gage-Foil	(Dynamic)	4	1	4	
S2, S3, S4, S5 Strain Gage	Static	4	2	8	
HPC					
R8 Proximity Probe		4	1	4	
R14 Proximity Probe		4	1	4	
IGV Inner Seal Cavity	Static	2	1	2	
IGV Inner Seal Cavity	Temp	2	1	2	
Bleed Duct Case T/C	Temp	4	1	4	
Bleed Duct Case T/C	Temp	4	1	4	
9th Stage Bleed Duct	Static	2	1	2	
9th Stage Bleed Duct	Temp	2	1	2	
10th Stage Bleed Duct	Static	2	1	2	
10th Stage Bleed Duct	Temp	2	1	2	
EGV Inner Cavity	Temp	2	1	2	
Sub Total				177	

*Stream probes retained for mixed flow configuration

TABLE 6.1-I (Cont'd)

ENERGY EFFICIENT ENGINE INTEGRATED CORE/LOW SPOOL
INSTRUMENTATION REQUIREMENTS

		No. Probes	No. Sensors	Total Sensors
HPC (Cont'd)				
R6 Strain Gage-Foil		2	1	2
R7 Strain Gage-Foil		2	1	2
R8 Strain Gage-Foil		1	1	1
R9 Strain Gage-Foil		1	1	1
R10 Strain Gage-Foil		1	1	1
R11 Strain Gage-Foil		1	1	1
R12 Strain Gage-Foil		1	1	1
R13 Strain Gage-Foil		1	1	1
R13 RIM T/C		2	1	2
R13 Bolt Circle T/C		2	1	2
R14 Strain Gage-Foil		1	1	1
R15 Strain Gage-Foil		2	1	2
S0 thru S13 Strain Gage-Foil		8	4	32
S14 Strain Gage-Foil		1	5	5
ACC Supply Tubes	Static	2	1	2
ACC Supply Tubes	Temp	2	1	2
Burner				
Liner Temperature		20	1	20
Liner Static		20	1	20
HPT				
Disk Hub Seal Compt.	Static	2	1	2
Disk Hub Seal Compt.	Temp	2	1	2
Disk Inner Rear Compt.	Static	2	1	2
Disk Inner Rear Compt.	Temp	2	1	2
Disk Outer Rear Compt.	Static	4	1	4
Disk Outer Rear Compt.	Temp	4	1	4
Disk FWD Compt.	Static	2	1	2
Disk FWD Compt.	Temp	2	1	2
TOBI Supply Temp.		2	1	2
Forward Side Plate T/C	(Dynamic)	2	1	2
Rear Side Plate T/C	(Dynamic)	2	1	2
Foil Strain Gage		10	1	
Forward Side Plate Strain Gage	(Dynamic)	2	1	2
Rear Side Plate Strain Gage	(Dynamic)	2	1	2
TOBI Plate Strain Gage	(Dynamic)	1	1	1
Turb IGV Inner Compt.	Static	2	1	2
Turb IGV Inner Compt.	Temp	2	1	2
Interstage Seal Rear Compt.	Static	2	1	2
Interstage Seal Rear Compt.	Temp	2	1	2
TOBI Compt.	Static	2	1	2
TOBI Compt.	Temp	2	1	2
TOBI Supply Comp.	Static	2	1	2
TOBI Supply Comp.	Temp	2	1	2
Sub Total				155

TABLE 6.1-I (Cont'd)

ENERGY EFFICIENT ENGINE INTEGRATED CORE/LOW SPOOL
INSTRUMENTATION REQUIREMENTS

		No. Probes	No. Sensors	Total Sensors
HPT (Cont'd)				
Turb IGV to OAS Compt.	Static	2	1	2
Turb IGV to OAS Compt.	Temp	2	1	2
Turb Support to Rail Compt.	Static	2	1	2
Turb Support to Rail Compt.	Temp	2	1	2
OAS Compt.	Static	2	1	2
Front OAS Rail	Temp	4	1	4
Rear OAS Rail	Temp	4	1	4
Turb IGV Inner Shroud	Static	2	1	2
Turb IGV Inner Shroud	Temp	2	1	2
Turb IGV Outer Shroud	Static	2	1	2
Turb IGV Outer Shroud	Temp	2	1	2
Turb IGV Rear Seal Compt.	Static	2	1	2
Turb IGV Rear Seal Compt.	Temp	2	1	2
Turb IGV Showerhead	Static	2	1	2
Turb IGV Showerhead	Temp	3	1	3
Turb IGV Inner Seal Compt.	Static	3	1	3
Sub Total				40

TABLE 6.1-I (Cont'd)

ENERGY EFFICIENT ENGINE INTEGRATED CORE/LOW SPOOL
INSTRUMENTATION REQUIREMENTS

		No. Probes	No. Sensors	Total Sensors
LPT				
R2 Proximity Probe		4	1	4
R4 Proximity Probe		4	1	4
ID Wall Static 2 V LE	Static	3	1	3
OD Wall Static 2 V LE	Static	3	1	3
ID Compartment 2 V TE	Static	3	1	3
OD Compartment 2 V TE	Static	3	1	3
ID Compartment 3 V LE	Static	3	1	3
OD Compartment 3 V LE	Static	3	1	3
ID Compartment 3 V TE	Static	3	1	3
OD Compartment 3 V TE	Static	3	1	3
ID Compartment 4 V LE	Static	3	1	3
OD Compartment 4 V LE	Static	3	1	3
ID Compartment 4 V TE	Static	3	1	3
OD Compartment 4 V TE	Static	3	1	3
ID Compartment 5 V LE	Static	3	1	3
OD Compartment 5 V LE	Static	3	1	3
ID Compartment 5 V TE	Static	3	1	3
OD Compartment 5 V TE	Static	3	1	3
ID Wall 3 V LE	Temp	2	1	2
R2 Attachment T/C		2	1	2
R4 Attachment T/C		2	1	2
R2, R3, R4, R5, Strain Gage-Foil		4	5	20
R2 Inner Compartment	Static	2	1	2
R2 Inner Compartment	Temp	2	1	2
2 V Inner Compartment	Static	2	1	2
2 V Inner Compartment	Temp	2	1	2
LPT Cooling Air Comp.	Static	2	1	2
LPT Cooling Air Comp.	Temp	2	1	2
2R OAS Case Hook T/C	Temp	4	1	4
3 V Inner Comp. T/C	Temp	2	1	2
3 V OD Attachment T/C	Temp	4	1	4
4 V OD Attachment T/C	Temp	4	1	4
5 V OD Attachment T/C	Temp	4	1	4
EGV Inner Compartment	Static	3	1	3
EGV Inner Compartment	Temp	3	1	3
2 V Foil T/C		4	2	8
2 V Holder T/C	Temp	2	1	2
Sub Total				128

TABLE 6.1-I (Cont'd)

ENERGY EFFICIENT ENGINE INTEGRATED CORE/LOW SPOOL
INSTRUMENTATION REQUIREMENTS

		No. Probes	No. Sensors	Total Sensors
Bearing Compartment				
BRG Support Vibration Pickup			1	10
No.1 BRG Outer race T/C			1	2
No.1 & No.2 Compt.	Static	10	1	2
No.1 & No.2 Compt.	Temp	2	1	2
No.2 BRG Outer Race	Temp	2	1	2
No.3 BRG Outer Race	Temp	2	1	2
No.3 BRG Inner Race	Temp	2	1	2
No.3 BRG Damper Prox Probe		1	1	1
No.3 BRG Spring Strain Gage		3	1	3
No.4 BRG Outer Race	Temp	2	1	2
No.4 BRG Inner Race	Temp	2	1	2
No.4 & 5 BRG Compt.	Static	2	1	2
No.4 & 5 BRG Compt.	Temp	2	2	2
No.4 BRG Spring Strain Gage			1	3
No.5 BRG Outer Race	Temp	3	1	2
No.5 BRG Seal Carrier	Static	2	1	2
No.5 BRG Seal Carrier	Temp	2	1	2
No.5 BRG Rear Seal	Static	2	1	2
No.1 BRG Strain Gage for Thrust Dir.		2	1	2
BRG Compt. ROT. 4 T/C				
Misc.				
N1 Speed Pickup		1	1	1
N2 Speed Pickup		1	1	1
Case Vibration Pickup		3	1	3
Misc. Test				26
Nacelle Cavity	Temp	4	1	4
Center Vent	Static	2	1	2
Tailcone T/C		10	1	10
Tailcone Emissions Probe Probe Center Vent	Temp	2	1	2
Sub Total				98
Total				1492

SUMMARY OF ROTATING INSTRUMENTATION

	Telemetry (High Rotor)			Slip Ring (Low Rotor)	
	S/G	T/C		S/G	T/C
HPC	13	4	Fan	20	-
HPT	15	8	LPC	16	-
BRG	-	4	LPT	20	4
Total	28	16	Total	56	4
Transmittance	28	3			

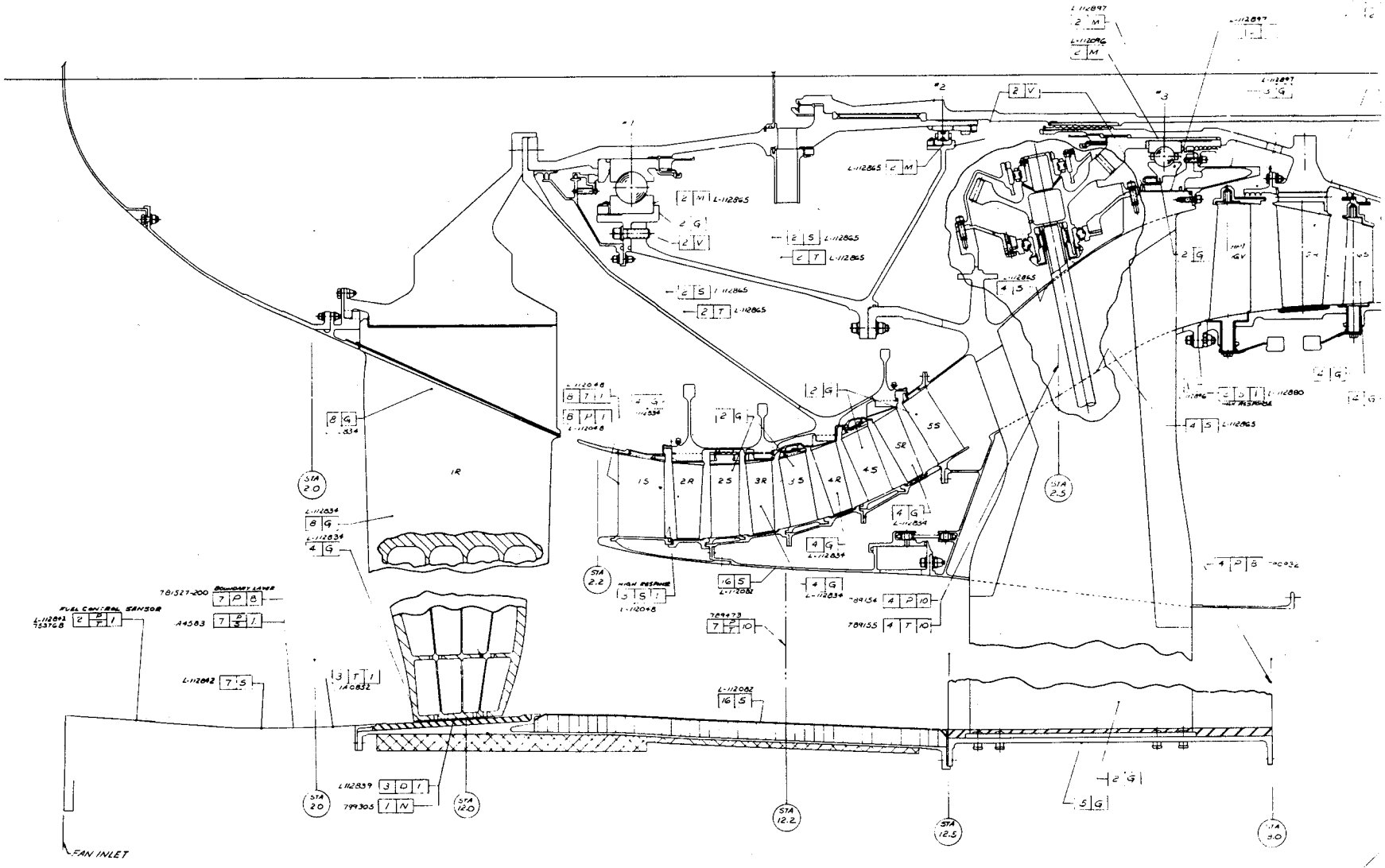

Figure 6.2-1 Integrated Core Low/Spool Instrumentation Roadmap

FOLDOUT FRAME

ORIGINAL PAGE IS
OF POOR QUALITY

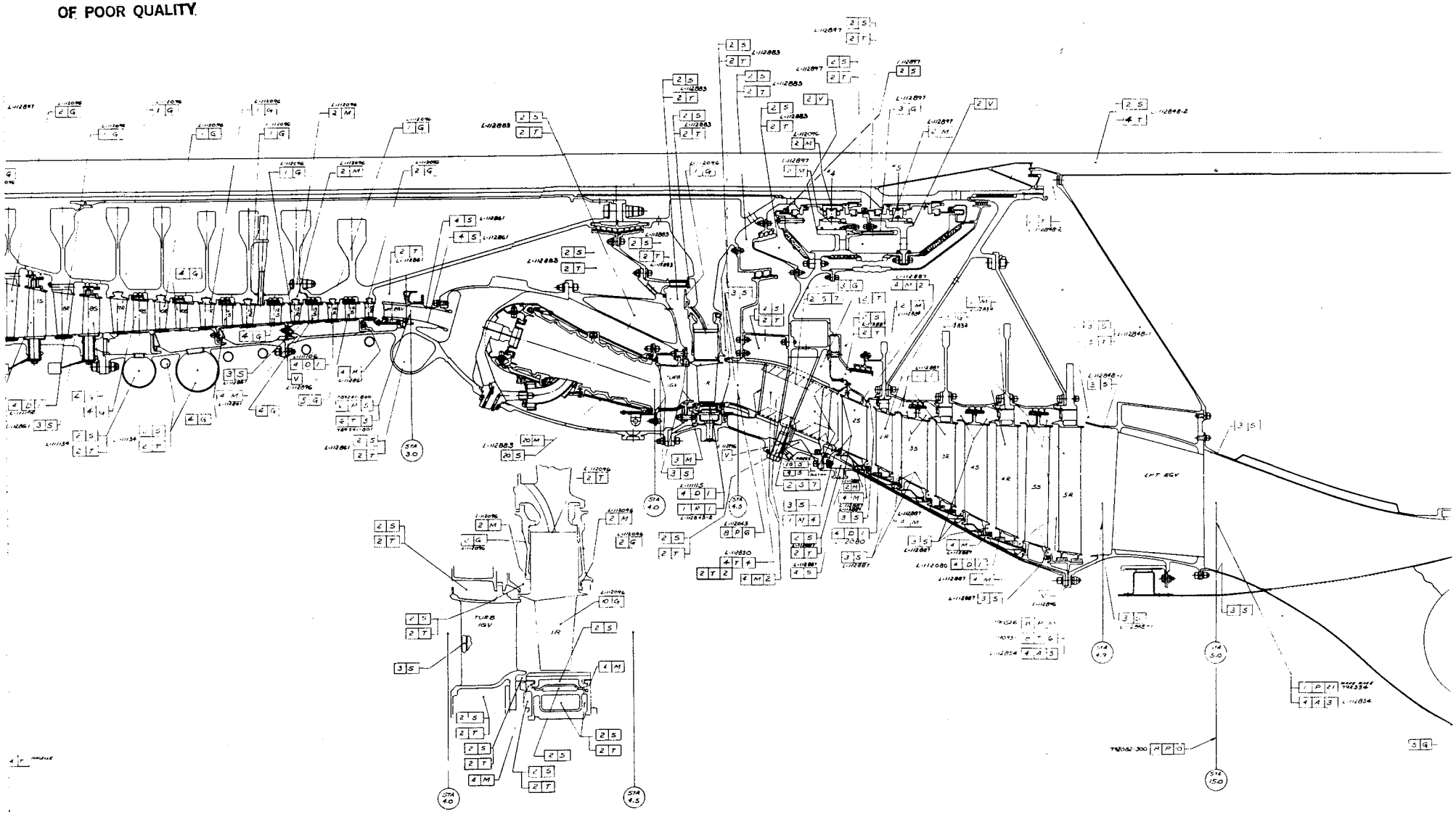

VIEW OF HPT AREA

2 FOLDOUT FRAME

3 FOLDOUT FRAME

4

ORIGINAL PAGE IS
OF POOR QUALITY

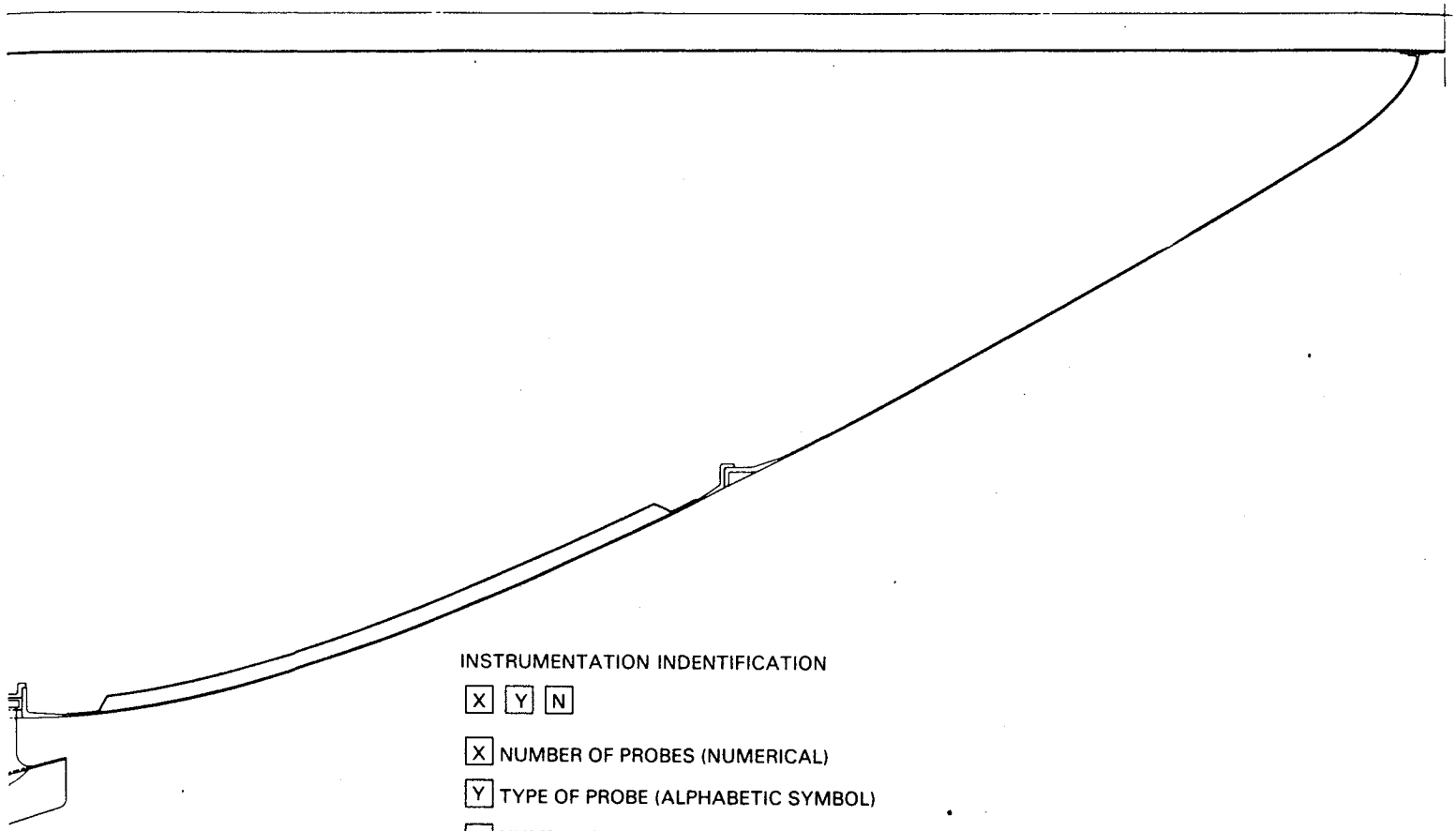

INSTRUMENTATION INDENTIFICATION

[X] [Y] [N]

[X] NUMBER OF PROBES (NUMERICAL)

[Y] TYPE OF PROBE (ALPHABETIC SYMBOL)

[N] NUMBER OF SENSORS (NUMERICAL)

[Y] -TYPE OF PROBE [Y/Y] -COMBINATION PROBE SUCH AS [P/T]

A-AIR ANGLE
B-ACOUSTICS
D-MEASUREMENT (BLADE TIP ETC)
E-EMISSION
F-AIR FLOW
G-STRAIN GAGE
M-METAL TEMPERATURE
N-RPM
P-TOTAL PRESSURE
S-STATIC PRESSURE
T-TEMPERATURE
V-VIBRATION
Z-MISCELLANIOUS
R-PYROMETER

TAILPIPE
10 M

OLDOUT FRAME

5 FOLDOUT FRAME

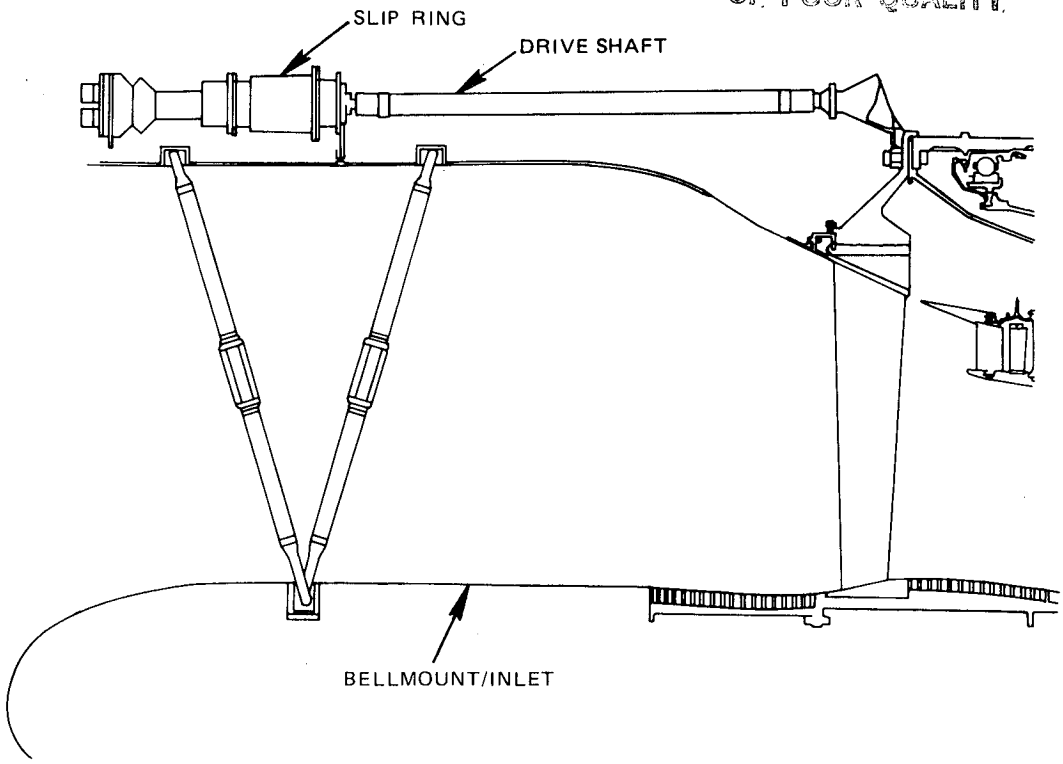

Figure 6.2-2 Low-Pressure Rotor Slip Ring Unit Arrangement

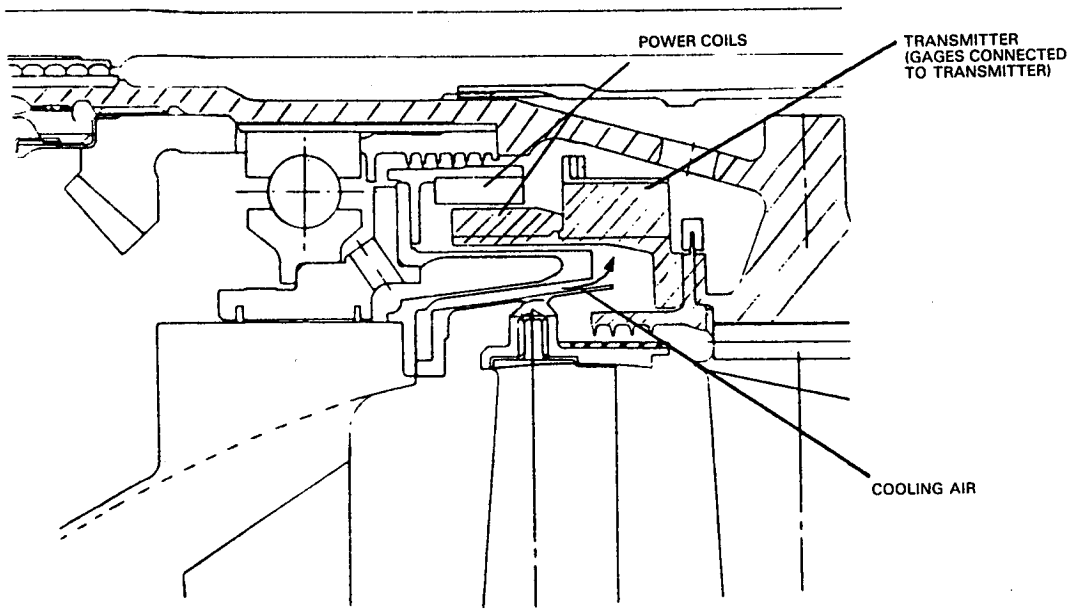

Figure 6.2-3 Build 1 High-Pressure Rotor Rotating Instrumentation Readout

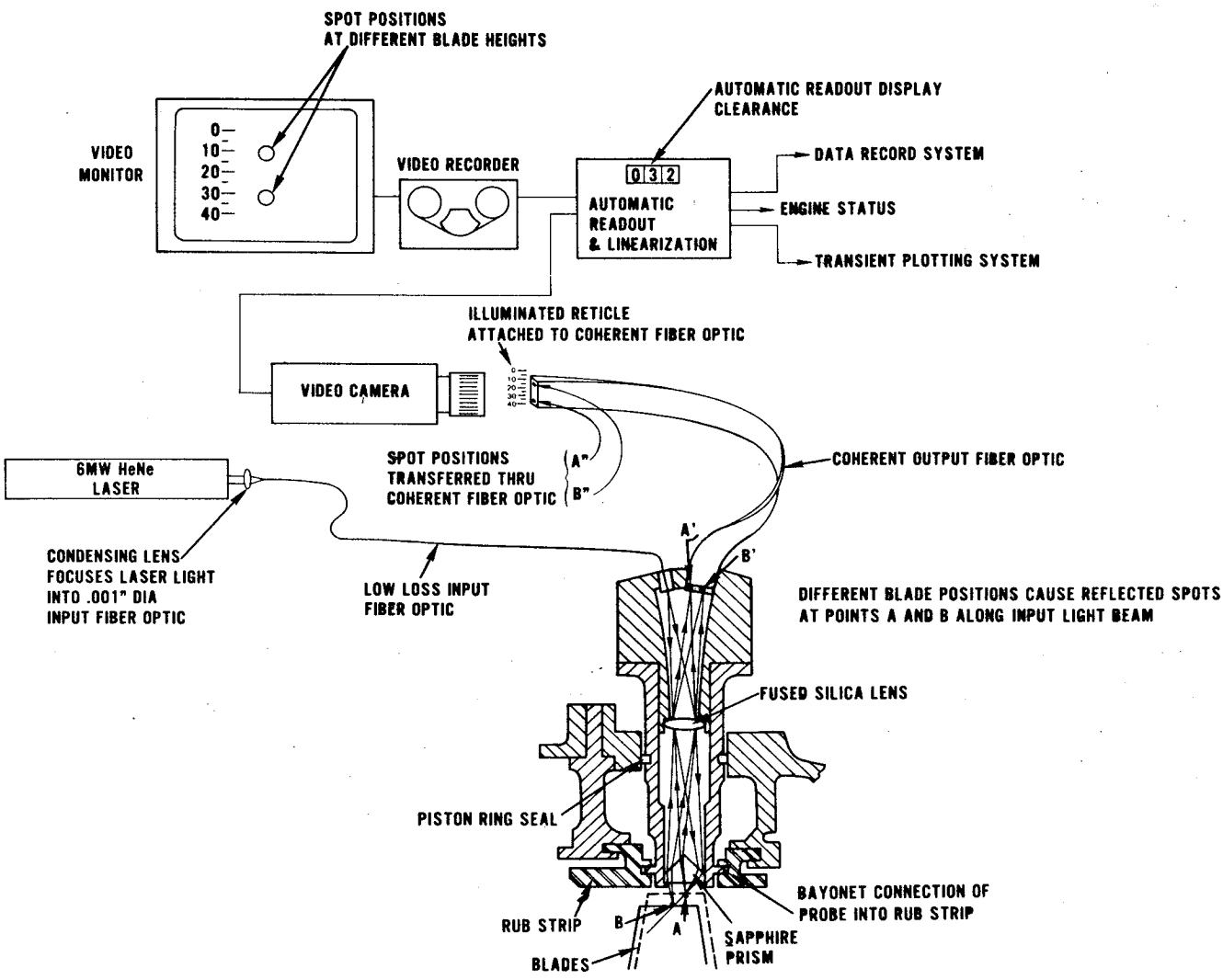

Figure 6.2.1-1 Laser Proximity Probe and System Components for Accurate Measurement of Blade Tip Clearances

In the fan duct stream at the fan exit plane, there are seven combination-type rakes with side by side keil heads to measure total temperature and total pressure. Further downstream, at the trailing edge of the fan exit guide vane, are four total pressure rakes. The circumferential spacing of these rakes has been selected to avoid wake effects from the pylon-matched struts.

6.2.2 Low-Pressure Compressor

The leading edges of eight inlet guide vanes are instrumented with pressure and temperature sensors. To accommodate the sensors, the thin leading edge is machined into the convex side and filled with an epoxy compound to rematch the vane contour. At the mid gap and downstream of the trailing edge of these vanes, three high-response static pressure transducers are installed to detect compressor stall.

Airfoils in all stationary and rotating stages are instrumented with strain gages.

6.2.3 High-Pressure Compressor

Mounted between the compressor intermediate case struts are four total pressure and four total temperature rakes, each with ten radial sampling elements. These rakes are used to monitor the flow conditions entering the high-pressure compressor. Similar instrumentation is used at the compressor exit plane to record combustor inlet conditions. Installed at this plane are six total pressure and six total temperature rakes, each with six radial elements.

Two high-response static pressure transducers are installed in the outer flowpath wall forward of the inlet guide vane to sense compressor stall.

Selected airfoils in all stages of the compressor have strain gages. Also, eighth- and fourteenth-stage blade tip clearances are measured by laser proximity probes. There are four proximity probes at each of these stages. The eighth-, tenth- and fifteenth-stage bleeds as well as the first impingement tube of the active clearance control system are instrumented with temperature and static pressure taps to monitor flow conditions.

6.2.4 Combustor

In the combustor, the outer liner is instrumented with 20 surface metal temperature sensors and 20 static pressure taps. Static pressures are also monitored on the inner and outer diffuser walls.

6.2.5 High-Pressure Turbine

Components in both the flowpath and secondary flow system are extensively instrumented. As indicated in Figure 6.2-1, static pressure taps and thermocouples are installed at numerous locations, including the internal cooling cavity of the first-stage vanes. The blades and sideplates are instrumented with strain gages and surface metal temperature sensors.

An optical pyrometer is also used to record blade surface metal temperatures. The components in the pyrometer system are shown in Figure 6.2.5-1. The maximum blade temperature is calculated to occur on the suction surface of the blade at 50 percent span. A study of various line of sight patterns was conducted to obtain a target at midspan without interference from other blades. Background effects were also studied to ensure that the pyrometer sights only the blade and not infrared signals from the combustor.

Blade tip clearances are measured by four equally spaced laser proximity probes. In the turbine, the probe penetrates through and seals at the turbine case, active clearance control manifold, impingement plate, and seal segment.

6.2.6 Turbine Intermediate Case

Eight total pressure rakes, with each probe containing six sensing elements, are located at the high-pressure turbine exit plane to measure from 0 to 87.5 percent of the inlet guide vane gaps in increments of 12.5 percent.

To reduce turbine blockage, keil head sensors are installed on the leading edge of six strut fairings to measure total temperature. This instrumentation will provide an indication of the inlet conditions to the low-pressure turbine. The sensors are installed on fairings that are not affected by flow disturbances from the pressure probes.

Static pressure taps and surface metal temperature sensors are installed at various locations on the fairing. Static pressure taps are located on two adjacent fairings, one instrumented on the pressure surface and the other on the suction surface at three radial locations. The gap at the root and the tip flowpath surface is also instrumented with static pressure taps located midway across the gap.

Strain gages are installed on the structural strut, bearing compartment support member and strut retention bolt.

6.2.7 Low-Pressure Turbine

Eight total pressure, eight total temperature and four air angle rakes are positioned at the trailing edge of the fifth-stage rotor. The pressure and temperature rakes are located circumferentially to obtain the most representative values from the low-pressure turbine stators based on a particle rotation analysis. The air angle rakes can be used only for the first test of the integrated core/low spool, since the traversing mechanism interferes with the full nacelle duct configuration planned for the second test.

Downstream of the exit guide vane is a traversing total pressure wake rake and four air angle rakes. The wake rake has 17 sensors and spans one gap of the exit guide vane. The air angle probes are located at 20, 40, 60, and 80 percent span of the exit guide vane gap. When the wake rake is used for data acquisition, the adjacent air angle rake and traversing hardware must be removed.

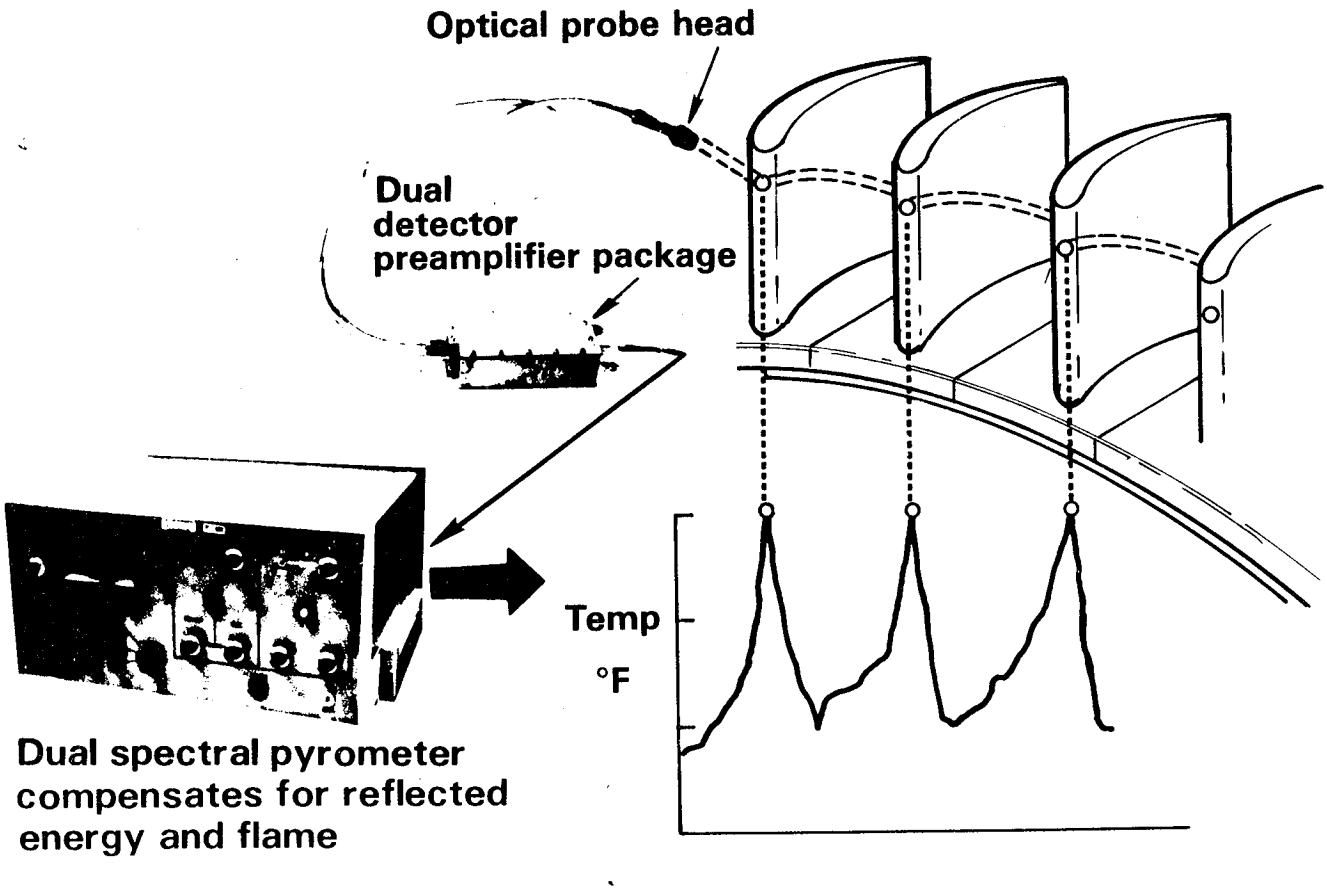

Figure 6.2.5-1 Optical Pyrometer System for Accurate Turbine Blade Temperature Measurement

Laser proximity probes are used to measure blade tip clearances at the second and fourth stages. Four probes can be used at each location for the first test. However, only two of the four probes can be used in the second test because of the nacelle duct.

Selected blades from the four rotor stages are instrumented with strain gages. Static pressure taps and thermocouples are also installed throughout the gas path and secondary flow system, as indicated in Figure 6.2-1.

6.2.8 Mixer

Eight total pressure rakes, each with 10 sensing elements, are located in the fan duct forward of the mixer and radially in-line with the wake rake. Strain gages are on the outer mixer lobe. This instrumentation is planned only for the second test of the integrated core/low spool when the mixer is installed. The mixer itself is instrumented with strain gages.

6.2.9 Bearing Compartment Instrumentation

Each of the five bearings is instrumented with two accelerometers to monitor rotor vibration. These sensors are mounted 90 degrees apart at the same circumferential location in each compartment.

All bearings have thermocouples installed at the bearing housing to outer race interface. The junction is formed with a malleable low temperature silver braze. The Nos. 3 and 4 bearings have similar thermocouple junctions on the inner race, which is part of the high-pressure spool telemetry system. Strain gages are installed on the outer race of the Nos. 1 and 3 ball bearings to provide an indication of rotor thrust direction. Both the front and rear bearing compartments contain air static pressure probes and air thermocouples.

A proximity probe is installed on the No. 3 bearing to measure the oil damper clearance. In addition, strain gages are installed on the Nos. 3 and 4 oil damped bearing springs.

6.2.10 Miscellaneous Instrumentation

Sensors to record low- and high-pressure rotor speeds are located in the fan case and the accessory gearbox, respectively.

In the center vent tube is a series of air thermocouples and static pressure taps. In conjunction with the standard thermocouples is a pair of Platinum Rhodium high temperature capability 1815°C (3300°F) thermocouples, which are used to detect fire.

Engine case vibration is monitored by accelerometers installed on the compressor intermediate case, diffuser case, turbine intermediate case, and turbine exhaust case. Each sensor is located as close to the vertical centerline as allowed by the flange bolt hole pattern and external hardware constraints.

SECTION 7.0
CONCLUDING REMARKS

The design of component test hardware for the integrated core/low spool concludes a major effort under the Energy Efficient Engine Program. This effort has successfully provided the design of a low cost test vehicle that simulates the flight propulsion system.

Design verification has been obtained from the results of analyses and numerous supporting technology programs. On the basis of these tests and analyses, the integrated core/low spool meets nearly all the performance goals and all of the structural goals. Moreover, many of the components meet the goals for the flight propulsion system.

Because of the similarity in design, this effort has also enabled an in-depth analysis of the flight propulsion system. Analyses have verified that program goals for fuel economy, lower operating cost and durability are attainable with the various features in the engine. In addition, the design has provided insight into how refinements might be made to attain additional benefits.

LIST OF ABBREVIATIONS AND SYMBOLS

A	-	Area
act	-	actuation
ADP	-	aerodynamic design point
AMS	-	American Metallurgical Society
avg	-	average
AR	-	area ratio
σB	-	bearing stress
brg	-	bearing
BPR	-	bypass ratio
BX	-	axial cord
CET	-	combustor exit temperature
CEGV	-	compressor exit guide vane
CDA	-	controlled diffusion airfoil
clb	-	climb
cm	-	centimeter
cor	-	corrected
C_p	-	pressure coefficient
cps	-	cycles per second
cr	-	cruise
Cx/U	-	axial velocity-to-wheel speed ratio
D-Factor	-	Individual airfoil aerodynamic loading factor
deg	-	degrees, angle
dia	-	diameter
DWF	-	fuel flow derived
EEC	-	Electronic Engine Control
EGT	-	exhaust gas temperature
EGV	-	exit guide vane
EPR	-	engine pressure ratio
F_N	-	net thrust
FPR	-	fan pressure ratio
FPS	-	flight propulsion system
ft	-	feet
ft/sec	-	feet per second
ΔH	-	specific work
σH	-	hoop stress
HPC	-	high-pressure compressor
HPT	-	high-pressure turbine
IC/LS	-	integrated core/low spool
ID	-	inner diameter
IGV	-	inlet guide vane
in	-	inch
inst	-	installed

LIST OF ABBREVIATIONS AND SYMBOLS (Cont'd)

K	-	spring constant
KEL	-	Knife Edge Labyrinth
kg	-	kilogram
ksi	-	pounds per square inch x 1000
lb	-	pound
lb/sec	-	pounds per second
LE	-	leading edge
LO	-	lead lag
LPC	-	low-pressure compressor
LPT	-	low-pressure turbine
LVDT	-	linial variable differential transducer
M or Mn	-	Mach number
max	-	maximum
MERL	-	Materials Engineering and Research Laboratory
MCA	-	multiple circular arc
min	-	minimum
mm	-	millimeter
N	-	Newton
N_1	-	low-pressure rotor speed
N_2	-	high-pressure rotor speed
NASA	-	National Aeronautics and Space Administration
OAS	-	outer airseal
OD	-	outer diameter
OL	-	operating line
OPR	-	overall pressure ratio
P	-	Pressure
P_2	-	pressure, station 2
P_3	-	pressure, station 3
$\Delta P/P_0$-P	-	airfoil loading parameters
PB	-	burner bressure
PBAC	-	burner pressure at accel
PBDC	-	burner pressure at decel
PLA	-	power lever angle
P-D	-	pressurizing and dump
PR	-	pressure ratio
psi	-	pounds per square inch
psia	-	pounds per square inch absolute
P_S	-	static pressure
P_T	-	total pressure
PWA	-	Pratt & Whitney Aircraft

REF	-	reference
Res	-	resolver
RIT	-	rotor inlet temperature
RPM	-	revolutions per minute
SAE	-	Society of Automotive Engineers
SLS	-	sea level static
SLTO	-	sea level takeoff
s/g	-	strain gage
Std.	-	Standard
T	-	temperature
T/C	-	thermocouple
TLP^R	-	Transient Liquid Phase
Tm	-	torque motor
TO	-	takeoff
TOBI	-	tangential on-board injection
TE	-	trailing edge
TSFC	-	thrust specific fuel consumption
T_T	-	total temperature
U	-	wheel speed
V	-	velocity
W	-	air flow
W_{AE}	-	engine core (stream) airflow
W_{at}	-	total engine airflow
W_f	-	fuel flow
δ	-	corrected pressure
η	-	efficiency, percent
Δ	-	finite change
θ	-	mean turning angle
σ	-	stress

REFERENCES

1. Halle, J. E., and Michael, C. J.: "Energy Efficient Engine Fan Component Detailed Design Report", NASA CR-165466 (PWA-5594-165), September, 1981.

2. Michael, C. J., and Halle, J. E.: "Energy Efficient Engine Low-Pressure Compressor Component Test Hardware Detailed Design Report", NASA CR-165354 (PWA-5594-157), June 1981.

3. Zeisser, M. H., Greene, W., and Dubiel, D. J.: "Energy Efficient Engine Combustor Test Hardware Detailed Design Report", NASA CR-167945 (PWA-5594-197), March, 1982.

4. Dubiel, D. J., Sundt, C. V., Greene, W., and Zeisser, M. H.: "Energy Efficient Engine Sector Combustor Rig Test Program Technology Report", NASA CR-167913 (PWA-5594-180), October 1981.

5. Thulin, R. D., Howe, D. C., and Singer, I. D.: "Energy Efficient Engine High-Pressure Turbine Detailed Design Report", NASA CR-165608 (PWA-5594-171), January 1982.

6. Gardner, W. B.: "Energy Efficient Engine High-Pressure Turbine Uncooled Rig Technology Report", NASA CR-165149, (PWA-5594-92), October, 1979.

7. Leach, K., Thulin, R., and Howe, D.: "Energy Efficient Engine Turbine Intermediate Case and Low-Pressure Turbine Component Test Hardware Detailed Design Report", NASA-CR-167973, (PWA-5594-191), January 1982.

8. Leach, K., and Thulin, R.: "Energy Efficient Engine Turbine Transition Duct Model Technology Report", NASA CR-167996, (PWA-5594-215), August 1982.

9. Sharma, Om, P., et al: "Energy Efficient Engine Low-Pressure Turbine Subsonic Cascade Technology Report", NASA CR-165592, (PWA-5594-167), January 1982.

10. Kozlowski, H., and Larkin, M.: "Energy Efficient Engine Exhaust Mixer Model Technology Report", NASA CR-165459, (PWA-5594-164), June 1981.

11. Gardner, W. B.: "Energy Efficient Engine Flight Propulsion System Preliminary Analysis and Design Report, NASA CR-159487, (PWA-5594-49), April, 1979.

12. Gardner, W. B.: "Energy Efficient Engine High-Pressure Turbine Leakage Technology Report", NASA CR-165202 (PWA-5594-106), December 1980.

DISTRIBUTION LIST

NASA Headquarters
600 Independence Ave. SW
Washington, D. C. 20546
Attention: R/R.S. Colladay RT-6

NASA Headquarters
600 Independence Ave. SW
Washington, D. C. 20546
Attention: RT/C.C. Rosen RTP-6

NASA Headquarters
600 Independence Ave. SW
Washington, D. C. 20546
Attention: RJ/W.S. Aiken RTP-6

NASA-Lewis Research Center
21000 Brookpark Road
Cleveland, Ohio 44135
Attention: RJP/L. Wright

NASA Headquarters
600 Independence Ave. SW
Washington, D. C. 20546
Attention: J. Facey RTP-6

NASA Headquarters
600 Independence Ave. SW
Washington, D. C. 20546
Attention: Library

NASA-Lewis Research Center
21000 Brookpark Road
Cleveland, Ohio 44135
Attention: D.L. Nored MS 301-2

NASA-Lewis Research Center
21000 Brookpark Road
Cleveland, Ohio 44135
Attention: C.C. Ciepluch MS 301-4
20 Copies

NASA-Lewis Research Center
21000 Brookpark Road
Cleveland, Ohio 44135
Attention: P.G. Batterton MS 301-4

NASA-Lewis Research Center
21000 Brookpark Road
Cleveland, Ohio 44135
Attention: G.M. Sievers MS 301-2

NASA-Lewis Research Center
21000 Brookpark Road
Cleveland, Ohio 44135
Attention: Library MS 60-3
2 Copies

NASA-Lewis Research Center
21000 Brookpark Road
Cleveland, Ohio 44135 MS 5-5
Attention: Report Control Office

NASA-Lewis Research Center
21000 Brookpark Road
Cleveland, Ohio 44135
Attention: Tech Utilization Office
MS 3-19

NASA-Lewis Research Center
21000 Brookpark Road
Cleveland, Ohio 44135
Attention: M.J. Hartmann MS 3-7

NASA-Lewis Research Center
21000 Brookpark Road
Cleveland, Ohio 44135
Attention: R.A. Rudey MS 6-8

NASA-Lewis Research Center
21000 Brookpark Road
Cleveland, Ohio 44135
Attention: R.W. Luidens MS 501-10

NASA-Lewis Research Center
21000 Brookpark Road
Cleveland, Ohio 44135
Attention: T.P. Moffitt MS 6-10

NASA-Lewis Research Center
21000 Brookpark Road
Cleveland, Ohio 44135
Attention: J.E. Rohde MS 6-10

NASA-Lewis Research Center
21000 Brookpark Road
Cleveland, Ohio 44135
Attention: R.E. Jones MS 6-31

NASA-Lewis Research Center
21000 Brookpark Road
Cleveland, Ohio 44135
Attention: L.J. Kiraly MS 23-2

NASA-Lewis Research Center
21000 Brookpark Road
Cleveland, Ohio 44135
Attention: D.C. Mikkelson MS 86-1

NASA-Lewis Research Center
21000 Brookpark Road
Cleveland, Ohio 44135
Attention: L.J. Thomas MS 500-305

NASA-Lewis Research Center
21000 Brookpark Road
Cleveland, Ohio 44135
Attention: J.F. Groeneweg MS 77-2

NASA-Lewis Research Center
21000 Brookpark Road
Cleveland, Ohio 44135
Attention: W.M. Braithwaite MS 500-208

NASA-Lewis Research Center
21000 Brookpark Road
Cleveland, Ohio 44135
Attention: R.L. Davies MS 106-1

NASA-Lewis Research Center
21000 Brookpark Road
Cleveland, Ohio 44135
Attention: R. H. Johns MS 49-6

NASA-Lewis Research Center
21000 Brookpark Road
Cleveland, Ohio 44135
Attention: J.F. Sellers MS 100-1

NASA-Lewis Research Center
21000 Brookpark Road
Cleveland, Ohio 44135
Attention: J.R. Mihaloew MS 100-1

NASA-Lewis Research Center
21000 Brookpark Road
Cleveland, Ohio 44135 MS 5-9
Attention: L. Reid

NASA-Lewis Research Center
21000 Brookpark Road
Cleveland, Ohio 44135 MS 86-2
Attention: D.W.Drier

NASA-Lewis Research Center
21000 Brookpark Road
Cleveland, Ohio 44135
Attention: R.W. Niedzwiecki MS 6-11

NASA-Lewis Research Center
21000 Brookpark Road
Cleveland, Ohio 44135 MS 501-3
Attention: AFSC Liaison Office

NASA-Lewis Research Center
21000 Brookpark Road
Cleveland, Ohio 44135 MS 302-2
Attention: Army R&T Propulsion

NASA Ames Research Center
Moffett Field, CA 94035
Attention: 202-7/M. H. Waters
Library (2)

NASA Langley Research Center
Langley Field, VA 23365
Attention: Bob James
Neil Driver (4)
L.J. Williams
Library

NASA Dryden Flight Research Center
P.O. Box 273
Edwards, CA 93523
Attention: J. A. Albers
Library (2)

NASA Scientific and Technical Information Facility
P.O. Box 8757
B.W.I. Airport, MD 21240
Attention: Accessioning Branch (10 copies)

Department of Defense
Washington, D.C. 20301
Attention: R. Standahar 3D1089 Pentagon

Wright-Patterson Air Force Base
Dayton, Ohio 45433
Attention: APL Chief Scientist AFWAL/PS

Wright-Patterson Air Force Base
Dayton, Ohio 45433
Attention: E.E. Abell ASD/YZE

Wright-Patterson Air Force Base
Dayton, Ohio 45433
Attention: H.I. Bush AFWAL/POT

Wright-Patterson Air Force Base
Dayton, Ohio 45433
Attention: E.E. Bailey (NASA Liaison)
AFWAL/NASA

Wright-Patterson Air Force Base
Dayton, Ohio 45433
Attention: R.P. Carmichael ASD/XRHI

Wright-Patterson Air Force Base
Dayton, Ohio 45433
Attention: R. Ellis ASD/YZN

Wright-Patterson Air Force Base
Dayton, Ohio 45433
Attention: W.H. Austin, Jr. ASD/ENF

Eustis Directorate
U.S. Army Air Mobility
R&D Laboratory
Fort Eustis, VA 23604
Attention: J. Lane, SAVDL-EU-Tapp

Navy Department
Naval Air Systems Command
Washington, D. C. 20361
Attention: W. Koven AIR-03E

Navy Department
Naval Air Systems Command
Washington, D. C. 20361
Attention: J.L. Byers AIR-53602

Navy Department
Naval Air Systems Command
Washington, D. C. 20361
Attention: E.A. Lichtman AIR-330E

Navy Department
Naval Air Systems Command
Washington, D. C. 20361
Attention: G. Derderian AIR-5362C

NAVAL AIR Propulsion Test Center
Trenton, NJ 08628
Attention: J. J. Curry
A. A. Martino (2)

USAVRAD Command
PO Box 209
St. Louis, MO 63166
Attention: Ropbert M. Titus (ASTIO)

Department of Transportation
NASA/DOT Joint Office of Noise Abatement
Washington, D.C. 20590
Attention: C. Foster

Federal Aviation Administration
12 New England Executive Park
Burlington, MA 18083
Attention: Jack A. Sain, ANE-200

Curtiss Wright Corporation
Woodridge, NJ 07075
Attention: S. Lombardo
S. Moskowitz (2)

Detroit Diesel Allison Div. G.M.C.
P.O. Box 894
Indianapolis, IN 46206
Attention: W. L. McIntire

Cummins Engine Co.
Technical Center
500 S. Poplar
Columbus, IN 47201
Attention: J. R. Drake

AVCO/Lycoming
550 S. Main Street
Stratford, CT 06497
Attention: H. Moellmann

Detroit Diesel Allison Div. G.M.C.
333 West First Street
Dayton, Ohio 45402
Attention: F. H. Walters

The Garrett Corporation
AIResearch Manufacturing Co.
Torrance, CA 90509
Attention: F. E. Faulkner

The Garrettt Corportion
AIResearch Manufacturing Co.
402 S. 36 Street
Phoenix, AZ 85034
Attention: Library

General Electric Co./AEG
One Jimson Road
Evendale, Ohio 45215
Attention: R.W. Bucy (3 copies)
T. F. Donohue (4)
D. Bahr

Pratt & Whitney Aircraft Group/UTC
Government Products Division
P.O. Box 2691
West Palm Beach, Fl 33402
Attention: B. A. Jones

The Garrettt Corportion
AIResearch Aviation Co.
19201 Susana Road
Compton, CA 90221
Attention: N. J. Palmer

AIResearch Manufacturing Co.
111 South 34th Street
P.O. Box 5217
Phoenix, AZ 85010
Attention: C. E. Corrigan
(93-120/503-4F)

Williams Research Co.
2280 W. Maple Road
Walled Lake, MI 48088
Attention: R. VanNimwegen
R. Horn
Library

Teledyne CAE, Turbine Engines
1330 Laskey Road
Tolendo, Ohio 43612
Attention: R. H. Gaylord

General Electric Co./AEG
1000 Western Ave.
Lynn, MA 01910
Attention: R. E. Neitzel

Pratt & Whitney Aircraft Group/UTC
Commercial Products Division
East Hartford, Ct 06108
Attention: I. Mendelson
MS-162-31

Pratt & Whitney Aircraft Group/UTC
Commercial Products Division
East Hartford, Ct 06108
Attention: D. Gray
MS-118-26

Boeing Commercial Airplane Co.
P.O. Box 3707
Seattle, WA 98124 (2)
Attention: P. E. Johnson MS 9H-46
D. C. Nordstrom MS 73-01

Boeing Aerospace Co.
P.O. Box 3999
Seattle, Wa 98124
Attention: D. S. Miller MS 40-26
H. Higgins (2)

The Boeing Co., Wichita Division
Wichita, KS 67210
Attention: D. Tarkelson

Douglas Aircraft Company
McDonnell Douglas Corp.
3855 Lakewood Boulevard
Long Beach, CA 90846
Attention: R. T. Kawai Code 36-41
M. Klotzsche (2)

Lockheed California Co.
Burbank, CA 91502
Attention: J. F. Stroud, Dept. 75-42
R. Tullis, Dept. 75-21
J. I. Benson (3)

General Dynamics Convair
P. O. Box 80847
San Diego, CA 92138
Attention: S. Campbell, MZ 632-00

North American Aircraft Operations
Advanced Systems Design, R & D
P.O. Box 92098
Los Angeles, CA 90009
Attention: John C. Sargent, Code GB12

Gates Learjet Corp.
P. O. Box 7707
Wichita, KS 67277
Attention: P. Manousos

McDonnell Aircraft Co.
McDonnell Douglas Corp.
P. O. Box 516
St. Louis, MO 63166
Attention: F. C. Claser Dept. 243

Lockheed Georgia Co.
Marietta, GA 30060
Attention: H. S. Sweet

Grumman Aerospace Corp.
South Oyster Bay Road
Bethpage, New York 11714
Attention: C. Hoeltzer

American Airlines
Maint. & Engr. Center
Tulsa, OK 74151
Attention: W. R. Neeley

Eastern Airlines
International Airport
Miami, FL 33148
Attention: A. E. Fishbein

Delta Airlines, Inc.
Hartsfield-Atlanta International Airport
Atlanta, GA 30320
Attention: C. C. Davis

TransWorld Airlines
605 Third Avenue
New York, NY 10016
Attention: A. E. Carrol

Pan American World Airways, Inc.
JFK International Airport
Jamica, NY 11430
Attention: A. MacLarty

United Airlines
San Francisco International Airport
Maint. Operations Center
San Francisco, CA 94128
Attention: J. J. Overton

Hamilton Standard
Bradley Field
Windsor Locks, CT 06096 (2)
Attention: P. J. Dumais, MS 1A-3-1
A. T. Reiff, MS 1-2-2

FluiDyne Engineering Corp.
5900 Olson Memorial Highway
Minneapolis, MN 55422
Attention: J. S. Holdhusen

Rohr Corporation
P.O. Box 878
Foot & H Street
Chula Vista, CA 92012
Attention: Library

Solar Division
International Harvester
2200 Pacific Highway
San Diego, CA 92112
Attention: Library

Gas Dynamics Laboratories
Aerospace Engineering Building
University of Michigan
Ann Arbor, MI 48109
Attention: Dr. C. W. Kaufmann

Massachusetts Inst. of Technology
Dept. of Astronautics & Aeronautics
Cambridge, MA 02139
Attention: Library

Massachusetts Inst. of Technology
Dept. of Structural Mechanics
Cambridege, MA 02139
Attention: James Mar
A. Epstein (2)

Westinghouse Electric Corp.
P.O. Box 5837
Beulah Road
Pittsburgh, PA 15236
Attention: Library

University of Tennessee
Space Institute
Tullahoma, TN 37388
Attention: Dr. V. Smith

TRW Equipment Group
TRW Inc.
23555 Euclid Ave.
Cleveland, OH 44117
Attention: I. Toth

DISTRIBUTION LIST (Cont'd)

Aerospace Corporation
R & D Center
Los Angeles, CA 90045
Attention: Library

George Shevlin
P.O. Box 1925
Washington, D.C. 20013

Brunswick Corporation
2000 Brunswick Lane
Deland, Fl 32720
Attention: A. Erickson

Drexel University
College of Engineering
Philadelphia, PA 19104
Attention: A. M. Mellor

Pennsylvania State University
Dept. of Aerospace Engineering
233 Hammond Bldg.
University Park, PA 16802
Attention: B Lakshminarayana

Iowa State University
Dept. of Mechanical Engineering
Ames, IA 50011
Attention: P. Kavanagh